

SMART MODELING OF OPTIMAL INTEGRATION OF HIGH PENETRATION OF PV – SMOOTH PV

APPENDIX TO THE FINAL REPORT

Thomas Ackermann
Stanislav Cherevatskiy
Tom Brown
Robert Eriksson
Afshin Samadi
Mehrdad Ghandhari
Lennart Söder
Dietmar Lindenberger
Cosima Jägemann
Simeon Hagspiel
Vladimir Ćuk
Paulo F. Ribeiro
Sjef Cobben
Henrik Bindner
Fridrik Rafn Isleifsson
Lucian Mihet-Popa

Supported by:



Project Partners:

Energynautics GmbH, Germany
University of Cologne, Germany
KTH Royal Institute of Technology, Sweden
DTU Technical University of Denmark
TUE Eindhoven University of Technology, Netherlands

THE CONSORTIUM



Energynautics GmbH, Germany
Project Manager: Thomas Ackermann
t.ackermann@energynautics.com



University of Cologne, Chair of Energy
Economics, Cologne, Germany
Contact: Dietmar Lindenberger
dietmar.lindenberger@uni-koeln.de



Royal Institute of Technology (KTH)
Electric Power Systems, Stockholm, Sweden
Contact: Prof. Lennart Söder
lennart.soder@ekc.kth.se

Robert Eriksson
robbaner@kth.se



Risø National Laboratory for Sustainable Energy (DTU), Technical University of Denmark,
Copenhagen, Denmark
Contact: Henrik Binder hwbi@risoe.dtu.dk



Eindhoven University of Technology (TUE),
Electrical Power Systems, Eindhoven, The
Netherlands
Contact: Prof. Will Kling w.l.kling@tue.nl

8

APPENDIX



8 APPENDIX

The appendix at hand contains the scientific papers and reports that include detailed description of the methodologies applied and results achieved by the participating parties within the Smooth PV project. To jump to the paper, click on the corresponding title.

| Paper / Report | Participant | Milestone | Reference in the report |
|---|--------------------|-----------|-------------------------|
| Transporting Renewables: Systematic Planning for Long-Distance HVDC Lines | Energynautics | 2 | App01 |
| Determining the Maximum Feasible Amount of Photovoltaics in the European Transmission Grid Under Optimal PV Utilization | Energynautics | 4 | App02 |
| The economic inefficiency of grid parity: The case of German photovoltaics in scenarios until 2030 | UoC | 6 | App03 |
| Cost-optimal Power System Extension Under Flow-based Market Coupling and High Shares of Photovoltaics | UoC, Energynautics | 4, 8 | App04 |
| Development of Tools for DER Components in a Distribution Network | DTU | 10 | App05 |
| Simulation Model developed for a Small-Scale PV System in Distribution Networks | DTU | 10 | App06 |
| Development of Tools for Simulation Systems in a Distribution Network and Validated by Measurements | DTU | 11 | App07 |
| Development, Improvements and Validation of a PV System Simulation Model in a Micro-Grid | DTU | 11 | App08 |
| Model Predictive Controller for Active Demand Side Management with PV Self-consumption in an Intelligent Building | DTU | 12 | App09 |
| Characterisation of the rapid fluctuation of the aggregated power output from distributed PV panels | DTU | 12 | App10 |
| Comparison of a Three-Phase Single-Stage PV System in PSCAD and PowerFactory | KTH | 14, 15 | App11 |
| Comparison of a Three-Phase Single-Stage PV System in PSCAD and PowerFactory (Master Thesis, provided as a separate file on the website) | KTH | 14, 15 | App12 |
| Improving the Photovoltaic Model in PowerFactory (Master Thesis, provided as a separate file on the website) | KTH | 14, 15 | App13 |
| Coordinated Droop Based Voltage Control among PV Systems in Distribution Grids | KTH | 16 | App14 |
| Equivalent modelling of several PV power plants | KTH | 16 | App15 |

| Paper / Report | Participant | Milestone | Reference in the report |
|--|------------------------------|------------------|--------------------------------|
| Evaluation of Reactive Power Support Interactions Among PV Systems Using Sensitivity Analysis | KTH | 16 | App16 |
| Modeling the Frequency Response of Photovoltaic Inverters | TUE | 18 | App17 |
| Dynamic behavior of grid-connected inverters during voltage dips (Traineeship report, provided as a separate file on the website) | TUE | 18 | App18 |
| Modeling of photovoltaic inverters for power quality studies (Master Thesis, provided as a separate file on the website) | TUE | 19 | App19 |
| Considerations on Harmonic Impedance Estimation in Low Voltage Networks | TUE | 20 | App20 |
| Aspects of a generic photovoltaic model examined under the German Grid Code for Medium Voltage | Energynautics | Additional | App21 |
| Evaluating the Impact of PV Module Orientation on Grid Operation | Energynautics | Additional | App22 |
| Considerations on the Modeling of Photovoltaic Systems for Grid Impact Studies | TUE, DTU, KTH, Energynautics | Additional | App23 |
| Variability and smoothing effects of PV power production | KTH | Additional | App24 |

Transporting Renewables: Systematic Planning for Long-Distance HVDC Lines

Tom Brown, Stanislav Cherevatskiy, Eckehard Tröster
Energynautics GmbH
Mühlstraße 21, 63225 Langen, Germany
Email: t.brown@energynautics.com

Abstract—The planning and operation of high voltage direct current (HVDC) lines within synchronous alternating current (AC) transmission networks has become an important topic, particularly with the integration of remote renewables into the grid. The optimal dispatch of particular fixed AC-DC networks has already been studied in the literature; we focus in this paper on optimizing the initial positioning of the DC network within the AC network and how it should be optimally sized. The problem is challenging because the optimization criteria (such as reducing congestion, overloading and losses) are non-linear while the optimization space of possible connection points of the DC terminals is discrete. Techniques are presented here based on a linearized version of the AC load-flow equations known as power transfer distribution factors (PTDFs). Examples are calculated for Germany in the year 2030 and for the European network up to the year 2050, with renewable power plants built out to provide 90% of electrical energy.¹

Keywords: HVDC, HVDC planning, PTDF, optimization, AC/DC interaction

1. INTRODUCTION

The integration of large amounts of renewable energy into the power system requires new power corridors to transfer the energy to where it is needed. For example, good wind resources are often geographically remote, on coastlines or in the sea, and thus can be far away from load centres; in addition, the balancing effects of aggregating multiple wind sites can best be leveraged when very wide areas are interconnected.

For the transmission of power over long distance high voltage direct current (HVDC) has several advantages over high voltage alternating current (HVAC): lower losses over long distances and therefore lower costs; higher power transmission for the same mast height and ground clearance; no need for reactive power compensation along the line; as a result, it is feasible to put underground or in the sea; much better controllability and hence greater ease of allocating the cost of the transmission assets; and, in the case of voltage source converter (VSC) HVDC technology, the stabilization of weak grids (see for example [1]).

A further advantage of HVDC is the ability to connect different synchronous AC networks and thus enable power transfers between them. The majority of HVDC lines that have thus far been built have been between grids that are not synchronous; exceptions are

mostly lines under bodies of water, such as Fenno-Skan between Finland and Sweden and the connection between Italy and Greece. However this is now changing, as the need for long distance power transmission, particularly to accommodate renewables, has led to plans for HVDC lines within meshed synchronous AC zones. Examples in Europe include the currently under construction Inelhe line between Spain and France [2] and planned lines between Belgium and Germany [3] and within Germany itself [4].

A high voltage DC network running parallel to an AC network presents several challenges, many of which have been tackled in the literature. The effects on stability and voltage control during disturbances have been widely studied for different technologies (see for example [5] and [6] for recent operation and control strategies). Interactions between several nearby HVDC systems where the subject of, for example, [7]. From a more economic perspective, optimal power flow strategies for mixed AC-DC systems with fixed topology were considered in [8] and [9], while hourly scheduling of HVDC with VSC was discussed in [10].

From a planning point of view, the optimal expansion of AC transmission systems is already a highly developed field, with various strategies being employed depending on the size of the network, the time horizon, whether generation assets are also included in the optimization and what kind of objective function is used. The optimization problem is non-linear because the load-flow equations and computation of losses are non-linear; it is constrained by the various characteristics of the assets; it is in general non-convex; and it is a mixed integer problem, since transmission and generation assets can only be built out in discrete steps. Usually the topology of the network is assumed to be fixed. To enable computation in reasonable times simplifications are often made, such as the linearization of the load-flow equations, neglecting losses, forcing convexity of the solution space or allowing expansion of the network in arbitrarily-sized steps. Literature surveys can be found in [11], [12], [13].

Some optimal planning studies have also incorporated HVDC systems alongside AC networks [14], [15] but they assume that the location and topology of the HVDC line is fixed and only optimize its capacity. DC lines are built out in preference to the AC grid to enable longer distance power flows and thus cheaper

¹Presented with peer review at EWEA 2013 in Vienna.

generation technologies to be dispatched. By allowing more controllable power transfers, they can also relieve large parts of the AC grid, although they may require the AC grid to be strengthened at the connection points. Overdimensioning of the DC line must also be avoided, to prevent parallel flows in the opposite direction on the AC network.

In this paper we introduce and investigate some algorithms for choosing not just the size but also the optimal placing of HVDC lines within an AC network. They can be located to relieve congestion in the AC network, to reduce overloading of AC lines, to reduce power losses or to reduce overall network expansion costs. To simplify the problem we linearize the load-flow equations using Power Transfer Distribution Factors (PTDFs), a strategy already used in other studies [16], [17]. However the optimization problem remains non-linear since the objective functions are non-linear. The problem is also by nature discrete, since particular nodes must be selected for attaching the DC network.

Case studies are presented for the European transmission system, with a particular focus on Germany. An aggregated grid model is used for the power flow calculations, while the scenario for installed capacities and dispatch of generation technology is taken from the SmoothPV project [18], in which generation and transmission assets were jointly optimized for social welfare up to the year 2050 with a 90% reduction in CO₂ emissions. Germany was chosen as the main focus because the need for HVDC links within Germany is already known (to carry wind from the North to the South of the country to replace shut-down nuclear capacity) and because studies already exist against which we can compare our results, such as the German Network Development Plan 2012 [4].

The remainder of the paper is structured as follows: Section II presents the methodology. The algorithms are applied to Germany in Section III. Section IV expands the analysis to the rest of Europe. Section V concludes. In the Appendix a flow-allocation algorithm for detecting long distance flows in AC networks is presented which is related to the other algorithms presented here.

2. METHODOLOGY

The basic methodology is to minimize an objective function which gives each HVDC configuration within the AC network a score based on how much it reduces losses, congestion, costs or overloading in the AC network. Load-flow equations are incorporated into the objective function so that the effect of the HVDC network on every AC line is taken into account. Each different HVDC configuration (i.e. the different connection points, including simple multiterminal examples) is optimized separately and then the results are compared.

2.1. The PTDF representation of the load-flow equations

To simplify the problem, linearizations of the load-flow equations are used called Power Transfer Distribution Factors (PTDFs), which are essentially the same as

what is known as a ‘DC load flow’ calculation. It is a linearized relation between the net power imbalances at each node and the active power flows on the lines, based only on series reactances of the lines and the voltage angles.

The non-linear AC load-flow equations can be linearised if we assume that: all voltages are set to 1 p.u.; reactive power is neglected; losses are neglected; line series reactance is always bigger than the resistance $X \gg R \approx 0$; voltage angles between busses are small enough to make the approximation $\sin(\delta_i - \delta_j) \approx \delta_i - \delta_j$.

If $i, j \in \{1, \dots, n\}$ label the nodes, then let P_{ij} represent the real power flow along the branch between nodes i and j , δ_i the voltage angle at each node with respect to some reference and x_{ij} the reactance of the branch. Then the load-flow equation for each branch simplifies to

$$P_{ij} = \frac{1}{x_{ij}}(\delta_i - \delta_j) \quad (1)$$

Combining this equation with the fact that the power transfers in each branch incident at each node must add up to the power balance at that node, the branch flows can be related linearly to the nodal balances

$$\mathbf{P}_{\text{branch}} = \mathbf{PTDF} \cdot \mathbf{P}_{\text{nodal}} \quad (2)$$

The elements of the matrix \mathbf{PTDF} are the power transfer distribution factors, constituting the linear relationship between the load flows on the lines and nodal power balances. They can also be calculated by choosing a slack bus within the network and measuring the change in power flow on each line for an additional power transfer between a chosen node in the network and the slack bus (this is where the name PTDF comes from).

2.2. Optimization and objective functions

A variety of different objective functions were tested, each with different advantages and disadvantages that should be taken into account when planning an HVDC line.

For each topology (e.g. single HVDC line, two HVDC lines, multiterminal configurations) the different possible locations of the connection nodes were enumerated and then the power flow for each configuration was optimized separately. The optimization space is the power transfers $\{\mathbf{x}\}$ between nodes connected by the HVDC network, represented as power injections at the nodes. For a single line connecting two nodes there is one variable; for three nodes in a multi-terminal configuration there are two variables.

For the non-linear optimization the quasi-Newton algorithm of Broyden, Fletcher, Goldfarb and Shanno (BFGS) as implemented in the Python library SciPy [19] was used, which offered good performance for the problems under consideration.

The optimization is highly dependent on the generation dispatch data, which determines the power flows in the AC network. The data will be discussed shortly. The optimization was performed separately for each

dispatch snapshot and then the scores were summed across the snapshots to get the optimal configuration for a variety of load flow situations.

The objective functions considered here were:

1) *Power losses reduction*: The power-loss objective function optimizes for the reduction in losses in all branches b of the AC network with and without the HVDC lines

$$f_{\text{losses}}(\mathbf{x}) = \sum_b \left[P_{b,\text{before}}^2 - P_{b,\text{after}}^2(\mathbf{x}) \right] * \frac{R_b}{V_b^2} \quad (3)$$

This is only an approximation of the actual losses on the line, since by simplifying the load flow equations we have neglected reactive power flows and losses, but it serves as a reasonably accurate proxy, where R_b is the resistance of the line and V_b the (constant) voltage. The losses incurred in the HVDC lines, assuming a rate of 3% for every 1000km [20], are small in comparison to the losses reduction on the AC network, so we neglect them here.

2) *Congestion reduction*: The congestion reduction function measures the reduction in power flow on each line multiplied by its length ℓ_b

$$f_{\text{MWkm}}(\mathbf{x}) = \sum_b \left[|P_{b,\text{before}}| - |P_{b,\text{after}}(\mathbf{x})| \right] * \ell_b \quad (4)$$

This function is particularly sensitive to parallel loop flows in the AC network where power spreads out in the network, travelling over long indirect routes to get to where it is used. It is also useful for deciding how much power to dispatch in the DC network $\{\mathbf{x}\}$ so that it doesn't cause backward flows in the reverse direction in the AC network (which would worsen the score).

3) *Cost reduction*: The congestion function can be adapted to optimize the cost of building the DC network versus the AC network

$$f_{\text{Cost}}(\mathbf{x}) = \sum_b \left[|P_{b,\text{before}}| - |P_{b,\text{after}}(\mathbf{x})| \right] * \ell_b * c_{\text{OHL}} - \sum_h |x_h| * (\ell_h * c_{\text{OHL}} + c_{\text{Converter}}) \quad (5)$$

The first term is the cost saved by reduced flows on the AC lines, while the second term is the cost of the DC lines h and converters. c_{OHL} is the cost per MW per kilometre of overhead lines (assumed to be the same for AC and DC) and $c_{\text{Converter}}$ is the cost per MW of the AC-DC converters required at the connection points of the DC network to the AC grid. We have taken cost values $c_{\text{OHL}} = \text{€}400/\text{MW}/\text{km}$ and $c_{\text{Converter}} = \text{€}150,000/\text{MW}$ from [18], but neglected the terrain factors used there.

This function is not perfect, since one would only build out transmission capacity in discrete parts. It also gives positive scores to power reductions within the thermal limits of existing infrastructure, which wouldn't provide a cost benefit. In addition, it does not take into account costs incurred by the higher losses and reactive power compensation in the AC network, so it must be treated with caution.

4) *Loading reduction*: For the loading reduction the score is weighted according to whether the DC lines helps reduce the loading on AC lines which are already loaded over 70% of their thermal limit (70% was chosen as a safety margin following n-1 security criteria and also to allow flexibility for future increases in load and generation)

$$f_{\text{thermal}}(\mathbf{x}) = \sum_b \left[\text{reduction of loadings above 70\%} \right] * \ell_b \quad (6)$$

Let the loading be $L_b = P_b/P_{b,\text{thermal limit}}$. If the loadings before and after the introduction of the HVDC system are below 70%, the score is zero. If the loading before is less than 70% but the HVDC system has increased the loading above 70% then the score is the negative of the difference between the new loading and 70%. If the loading before is more than 70% then the score corresponds to how much the HVDC system has decreased (positive score) or increased (negative score) the loading. Reductions below 70% are ignored.

This function is perhaps more relevant than the congestion MWkm function from a planning perspective, since it is sensitive to reductions only on overloaded AC lines. The MWkm function may reward configurations that reduce loading on lines that are already well below their thermal limits, which are not of concern to planners.

2.3. Network model

To analyse the power flows in the European transmission network, a detailed model of the high voltage grid is used. This model was developed with DlgSILENT's power system calculation tool PowerFactory and covers all ENTSO-E members. It consists of over 200 nodes, representing generation and load centers within Europe, 450 high voltage AC (HVAC) lines and all the high voltage DC (HVDC) lines within the ENTSO-E area (see Figure 1 for the German part of the network). The grid model is built for AC load flow calculations, but in this paper only DC load flow was used.

The model includes load and generation allocation keys, which distribute generation per technology across the nodes within each market region. The network and distribution keys were validated by comparing cross-border flows in the model against publicly available data from ENTSO-E, after which the impedances and allocation keys were optimized to ensure good agreement across several snapshots of the network.

The model covers four points in time: 2011, based on the current network; 2020, including all mid-term planning projects from ENTSO-E's Ten Year Network Development Plan [3] (constituting 82 GVA of extra AC and 13 GW of extra DC capacity compared to 2011); and 2030 and 2050 based on the optimal generation and transmission expansion taken from the SmoothPV project [18]. The 2030 and 2050 networks include a fixed HVDC overlay grid which connect the major load centres in each market region (see Figure 4). The initial motivation for the study presented in this paper was to determine where HVDC lines should be placed

in the SmoothPV network, since the linear optimization algorithms used for that project needed fixed line topologies before they could optimize for the size of the transmission assets.

For the Germany case study the 2020 network was used with the 2030 dispatch data, so that the stresses on the network in 2030 could be seen from the perspective of a present-day planner.

For the European case study a slightly different approach was used: the overlay grid in 2030 and 2050 was assumed to be in fixed locations (but the capacity was free to be optimized), while HVDC lines were then optimized in each country but forced to be connected to the overlay grid landing point in each market region.

2.4. Generation dispatch scenario to 2050

The load, generation and transmission system expansion scenario up to 2050 was taken from the SmoothPV project [18], which jointly optimized generation and both AC and DC network infrastructure using similar PTDF-based methods (the methodology is discussed in [17]) based on a 90% CO₂ reduction target compared to 1997. The grid model was the same as that presented above; the electricity market model was developed at the Institute of Energy Economics in Cologne [22].

For the years 2011, 2020, 2030 and 2050 the dispatch was calculated for eight typical days per year on an hourly basis, representing variations in electricity demand as well as in solar and wind resources [23]. Extreme events that particularly stress the power system, such as periods of low wind and high demand, were also covered. For the case studies in this paper we have focused on snapshots with high wind, to model situations when the network is put under strain by large wind power inflows.

For the study of Germany, 42 GW of onshore wind were installed by 2030 along with 44 GW of offshore wind (28 GW in the North Sea and 16 GW in the Baltic Sea), assuming cost-optimal development. (In the Network Development Plan of 2012 by contrast, 64 GW of onshore wind and only 28 GW of offshore are foreseen in the lead scenario by 2032.) All the nuclear plants are assumed to have been taken off-line.

For the entire ENTSO-E area the installed capacities for onshore wind were 264 GW in 2030 and 266 GW in 2050, and for offshore wind 166 GW in 2030 and 497 GW in 2050. Big cost reductions were assumed and predictions this far ahead should obviously be treated with caution.

2.5. Simplifications and assumptions

The use of DC load flow, a simplification necessary to reduce computation complexity, means that we cannot take account of reactive power flows, voltage stability or reactive power compensation in the AC network.² No account was taken of fault behaviour either.

We have made no assumptions about the HVDC technology used; the HVDC line is modelled with a

static generator taking up active power in one place and another delivering it somewhere else. We assume by 2050 VSC or similar technology will be available for large power transfers and will be favoured due to its ability to provide reactive power and hence contribute towards system stability.

3. TEST CASE: GERMANY IN 2030

Germany was chosen as a test case for these algorithms both because the aggregated network model is most detailed for Germany and because there are already existing plans for HVDC capacity in Germany [4] with which we can compare our results.

For each topology all possible nodes within Germany were considered in the optimization for the connection of the HVDC terminals. For the changes in power flows on the network measured by the objective functions, all branches in Germany and the bordering countries were included. The network capacities from 2020 were used with the dispatch data predicted for 2030, as explained above. This means that in the base case, without HVDC lines, there are already a significant number of AC lines which are overloaded (see Figure 2).

For each optimization we have taken an average across 8 winter snapshots with high wind levels; a maximum score is also included for comparison. The nodal dispatch in the windiest snapshot is indicated graphically in Figure 1.

3.1. Optimizing for a single line

The results for a single HVDC line are displayed in Tables I to IV. The highest scoring lines for losses reduction and congestion reduction are in agreement: a line with capacity around 20 GW is recommended from Hamburg (DE03), in between the offshore wind parks in the North and Baltic seas, and load centres in the very south of Germany, around Ulm (DE34), Augsburg (DE30) and Munich (DE35). With such a line one can save around 4 GW of losses in the AC network under windy winter conditions, around 14000 GWkm of loading on the AC network and reduce the number of overloaded lines by a factor of 3. The line between Hamburg and Ulm is marked on the map in Figure 1.³

The graphic in Figure 1 shows the extent to which the loading on the AC network is reduced by the introduction of the HVDC line. All routes going from north to south have their burden reduced, including loop flows that go through the Netherlands, Belgium and France and on the other side through Poland and the Czech Republic. Some lines near the connection points have increased loading, particularly in the south, as the connection point stresses the network locally delivering the power.

These capacities agree broadly with the German Network Development Plan 2012 (NEP) [4], which foresees capacity of 20 GW from the North Sea to southern Germany in its scenario for 2032. In the NEP strain

²A study of these issues for several HVDC configurations in the network of the German TSO Amprion can be found in [21].

³The background image in this figure and others is courtesy of ENTSO-E.

on the AC network is avoided by splitting the capacity into four separate corridors⁴ across the country with multiple terminals in each corridor, although one must bear in mind that this also increases the costs by adding converter stations. We will explore simpler versions of such multiterminal solutions in the next section.

The avoided losses in Table I appear quite high, but there are several reasons for this. Firstly, the 2020 version of the network was used for this study, so the capacities of the AC lines are under-sized; as you can see from Figure 2 many of the lines are overloaded, so their losses will be higher than in a properly-dimensioned network. Secondly, there is a very large amount of power (50 GW including Denmark) being injected in the north, enough to cover most of Germany's demand at its lowest point and around 60% of its peak demand, therefore a significant amount of power is being transported over long distances. From Figure 1 it is clear that many lines, including those far away, are affected by this power flow. And thirdly, since the losses go quadratically with the power, reducing the power from higher values has a very large effect on the losses reduction.

The scores in saved costs from Table III are roughly in agreement for location, with the exception of a high-scoring line going from North (DE03, Hamburg) to the East (DE18, Chemnitz), which appears because of a lack of West-East capacity dating back to the Reunification of Germany and because the shorter length of the HVDC line leads to a lower cost.

The optimized capacities are noticeably lower than for the other objective functions, between 3 GW and 8 GW. For reasons discussed before, the cost savings for the AC network are most likely a significant underestimate, since it doesn't take account of the discrete steps in which transmission capacity is built out and it doesn't take account of the cost of losses and reactive compensation in the network.

The scores for reducing overloading on lines loaded over 70% can be found in Table IV. In contrast to the losses and congestion scores, the highest scoring are delivering power to the East. This is because around half the overloaded lines are in this eastern region, so there is a strong bias towards reducing the loading there. Because the distances there are not so great and the losses in the AC network correspondingly lower, it may be better to build out the AC network here, and then use HVDC for the longer routes.

An example of the change in loading profile for the AC network is depicted in Figure 2 for a 17 GW line from DE03 to DE32. The single DC line has reduced the number of overloaded lines by a factor of three, reducing the total which are over their thermal capacity from 39% to 13%. (That so many lines are overloaded shouldn't be alarming, since we've used the 2020 network.)

Given the discrepancies between the other scores, it is surprising that the losses and congestion scores

TABLE I
SCORES FOR LOSSES REDUCTION

| Line | Averaged score (MW) | Averaged power (GW) | Max score (MW) | Power max (GW) |
|-------------|---------------------|---------------------|----------------|----------------|
| DE03 → DE34 | 4458 | 18 | 6250 | 21 |
| DE03 → DE30 | 4362 | 17 | 6005 | 20 |
| DE03 → DE35 | 4268 | 17 | 5829 | 20 |
| DE03 → DE32 | 4122 | 16 | 6046 | 20 |
| DE03 → DE18 | 3957 | 20 | 5263 | 23 |
| DE03 → DE33 | 3876 | 15 | 5639 | 18 |
| DE03 → DE31 | 3791 | 15 | 5183 | 17 |

TABLE II
SCORES FOR CONGESTION REDUCTION

| Line | Averaged score (GWkm) | Averaged power (GW) | Max score (GWkm) | Power max (GW) |
|-------------|-----------------------|---------------------|------------------|----------------|
| DE03 → DE34 | 13864 | 19 | 18123 | 23 |
| DE03 → DE30 | 13495 | 19 | 17402 | 23 |
| DE03 → DE35 | 13326 | 20 | 17065 | 23 |
| DE03 → DE18 | 12347 | 22 | 14916 | 26 |
| DE03 → DE31 | 12287 | 19 | 15823 | 22 |
| DE03 → DE29 | 12126 | 19 | 15529 | 22 |
| DE03 → DE32 | 12082 | 18 | 17336 | 22 |

TABLE III
SCORES FOR REDUCED COST

| Line | Averaged score (million €) | Averaged power (GW) | Max score (m€) | Power max (GW) |
|-------------|----------------------------|---------------------|----------------|----------------|
| DE03 → DE18 | 362 | 8 | 495 | 11 |
| DE03 → DE35 | 201 | 3 | 209 | 5 |
| DE03 → DE31 | 136 | 2 | 112 | 3 |
| DE03 → DE34 | 128 | 4 | 289 | 8 |
| DE03 → DE30 | 118 | 2 | 178 | 2 |
| DE07 → DE35 | 109 | 3 | 93 | 3 |
| DE03 → DE23 | 98 | 4 | 203 | 8 |

TABLE IV
SCORES FOR REDUCING OVERLOADED LINES

| Line | Averaged score (%) | Averaged power (GW) | Max score (%) | Power max (GW) |
|-------------|--------------------|---------------------|---------------|----------------|
| DE03 → DE18 | 3116 | 19 | 3992 | 22 |
| DE03 → DE19 | 2871 | 18 | 3670 | 21 |
| DE03 → DE32 | 2617 | 15 | 3855 | 17 |
| DE03 → DE30 | 2569 | 14 | 3393 | 16 |
| DE03 → DE11 | 2567 | 18 | 3309 | 21 |
| DE03 → DE35 | 2564 | 14 | 3344 | 16 |
| DE03 → DE34 | 2535 | 15 | 3397 | 18 |

are in such close accord. They show good agreement on recommended locations and for the recommended capacities the congestion method recommends lines about 10% bigger. A possible explanation is that the length of each line ℓ_b in equation (4) is a good enough proxy for the resistance in (3) and for large currents the quadratic relation of losses to current is flat enough that it is sufficient to model the losses as linearly dependent on the power.⁵ The congestion method is significantly faster computationally, so presents a good compromise when the size of the potential solution space grows large.

⁵In equations, we are saying that for large I , we can approximate the loss function $P = RI^2$ with $P = A + BI$. Since the losses score (3) is a subtraction of losses, the constant A disappears.

⁴The line DE03 to DE34 most resembles Corridor C in the NEP.

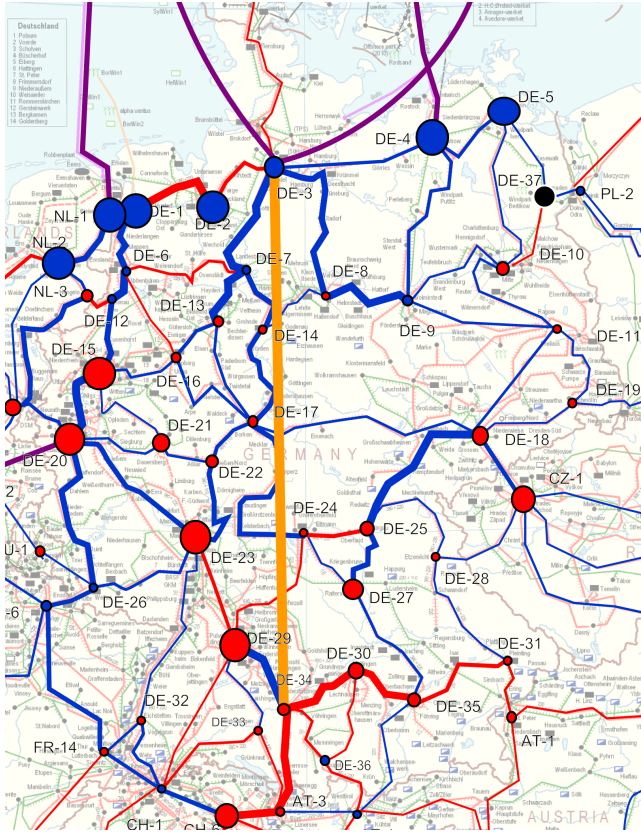


Fig. 1. The aggregated network model for Germany. For this windy winter snapshot, blue nodes have net generation, red net load, while their radii are in proportion to their power. The orange line is the HVDC, carrying 20 GW. Blue AC lines have their loading reduced by the HVDC line; for red lines the loading increases (in both cases proportional to the width of line).

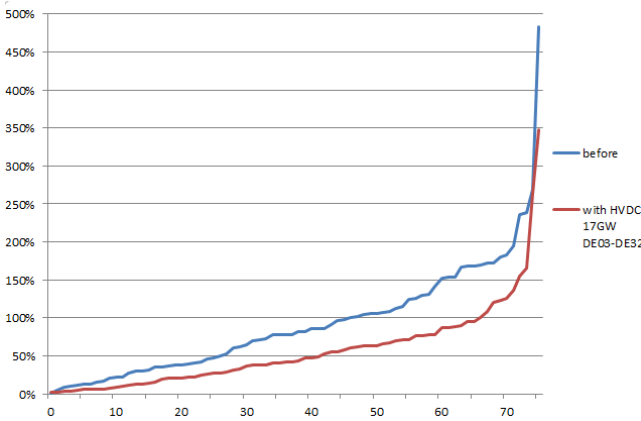


Fig. 2. Loading as a percentage of the thermal limits of the 76 lines in Germany on a windy winter day, with and without an HVDC line carrying 17 GW from Hamburg (DE03) to Freiburg (DE32).

3.2. Optimizing for a multiterminal three-node network

In this section we consider a multiterminal topology which connects three nodes with HVDC lines. To simplify the problem we treat this configuration as two HVDC lines with a common connection node, although in reality the lines would split at a fourth point, see the examples drawn in Figure 3. Results are calculated for the losses-reduction and congestion objective functions in Tables V and VI, since these methods gave the

TABLE V
LOSSES SCORES FOR THREE-NODE NETWORK

| Lines | Averaged score (MW) | Averaged power (GW) | Max score (MW) | Power max (GW) |
|-----------|---------------------|---------------------|----------------|----------------|
| DE03→DE18 | 5299 | 10 | 6817 | 11 |
| DE03→DE34 | | 12 | | 15 |
| DE01→DE34 | 5269 | 11 | 6997 | 13 |
| DE03→DE34 | | 13 | | 16 |
| DE03→DE32 | 5052 | 9 | 6835 | 12 |
| DE03→DE35 | | 10 | | 11 |

TABLE VI
CONGESTION SCORES FOR THREE-NODE NETWORK

| Lines | Averaged score (GWkm) | Averaged power (GW) | Max score (GWkm) | Power max (GW) |
|-----------|-----------------------|---------------------|------------------|----------------|
| DE03→DE18 | 16425 | 12 | 20760 | 12 |
| DE03→DE34 | | 13 | | 16 |
| DE01→DE34 | 15296 | 12 | 21196 | 16 |
| DE03→DE34 | | 15 | | 19 |
| DE03→DE32 | 14847 | 12 | 19941 | 16 |
| DE03→DE35 | | 9 | | 8 |

best indications in the previous section for long-distance power transfers. For interest's sake and to save space, we have left out some configurations which were very similar to the others.

The three highest scoring configurations are a line from North to South that branches off to the East (DE18, Chemnitz), a line from the North that splits when it gets to the South, and lines from the Northwest (DE01) and the North (DE03) that join and then go down to the South. Two of these configurations are show in Figure 3.

Compared to single line configurations, the amount of losses that can be avoided in such configurations rises by around 24% and the congestion score by 18%. The amount of power being transported away from the coast has also been increased by just over 20%, which is enabled because the power is able to be dispatched more evenly around the network, avoiding strain around the connection points.

3.3. Optimizing for two HVDC lines

From the previous multiterminal solutions it is clear that HVDC lines connecting the big power injection points in the Northwest (DE01) and North (DE03) are preferred. Therefore in this section we consider two lines, one from each of these points, and optimize for the positions of the other ends of the two lines. The results for the losses-reduction and congestion metric are in Tables VII and VIII (again we have not repeat configurations that are very similar).

The optimal connections are from the North-East to the South and then from the North to Chemnitz in the East. The top-scoring result is drawn in Figure 3. Comparing the optimal solutions with the three-terminal case, the losses avoided increases only 7% and the congestion reduction by 10%. However the amount of power transferred increases by 41%, which is significant. This increase in power is because the two lines

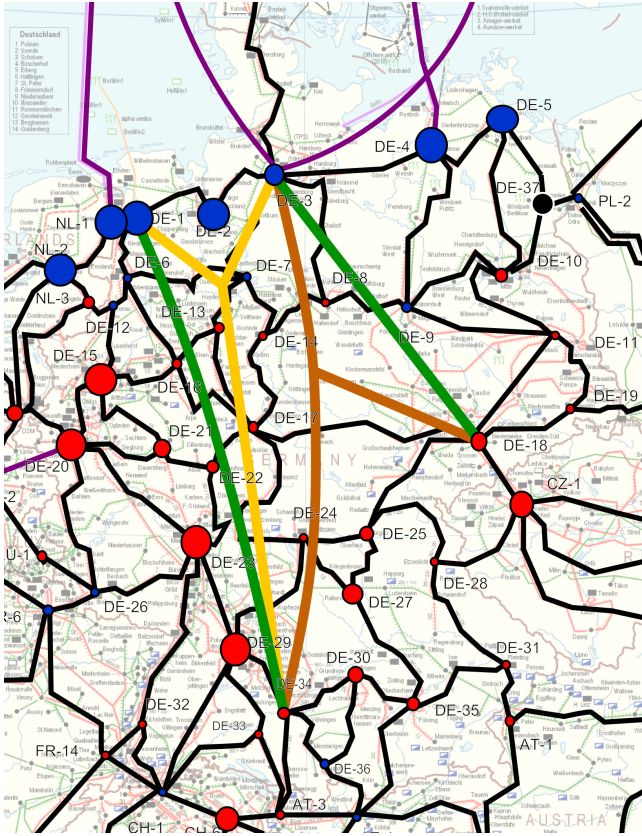


Fig. 3. Two different 3-node multiterminal solutions (in yellow and brown) and one two-line solution (in green). The branching points in the middle for the 3-node solutions are indicative only and have not been optimized.

TABLE VII
LOSSES SCORES FOR TWO LINES

| Lines | Averaged score (MW) | Averaged power (GW) | Max score (MW) | Power max (GW) |
|-----------|---------------------|---------------------|----------------|----------------|
| DE01→DE34 | 5666 | 16 | 7594 | 19 |
| DE03→DE18 | | 15 | | 18 |
| DE01→DE32 | 5550 | 13 | 7653 | 17 |
| DE03→DE18 | | 16 | | 19 |
| DE01→DE32 | 5471 | 12 | 7692 | 15 |
| DE03→DE30 | | 14 | | 16 |

can be far enough apart that the strain induced at the connection points is spread out.

It's also interesting to note that these results are not fully in accordance with the NEP, in which all the HVDC lines bring power to the South and not to the East. An explanation is that the NEP assumes more onshore wind expansion in the East, which would cover the load there, while from Figure 3 it is clear that there is a big load centre in the Czech Republic being served.

Also interesting is that the single HVDC line solution from DE03 to DE34 doesn't appear high in the list. This means if we'd taken the single solution and then tried to add a second line separately, we would have missed the optimal two-line solution. Solutions with multiple terminals need to be considered jointly for optimal results.

TABLE VIII
MWKM SCORES FOR TWO LINES

| Lines | Averaged score (GWkm) | Averaged power (GW) | Max score (GWkm) | Power max (GW) |
|-----------|-----------------------|---------------------|------------------|----------------|
| DE01→DE34 | 18141 | 16 | 22870 | 20 |
| DE03→DE18 | | 17 | | 20 |
| DE01→DE32 | 17433 | 15 | 23404 | 19 |
| DE03→DE18 | | 18 | | 21 |
| DE01→DE34 | 17059 | 17 | 21737 | 24 |
| DE03→DE28 | | 15 | | 16 |

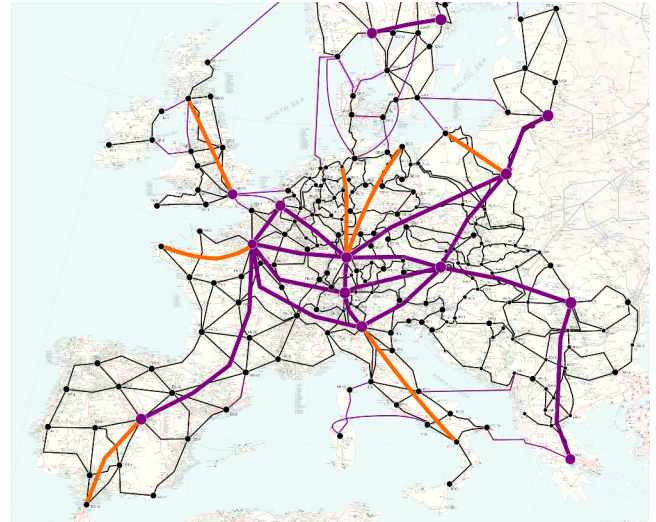


Fig. 4. European model with an overlay HVDC grid between regional load centres in purple and internal HVDC lines in orange.

4. EUROPE TO 2050

In this section we present results computed for the SmoothPV project [18], a project to optimize generation and transmission capacity for the whole of Europe up to 2050 with 90% CO₂ reductions. For computational reasons it was decided to first fix the topology of an overlay HVDC grid connecting the major load centres (in purple in Figure 4), whose capacities were set by the main optimization algorithm along with the AC transmission capacities and the generation distribution. The HVDC lines internal to each market region (in orange in Figure 4) were then selected using the algorithms presented above, with the condition that they connect directly to the overlay grid.

The resulting locations and capacities of the internal lines are presented in Table IX. With the exception of Spain, every line was necessitated by the development of offshore wind. Very large installed capacities far from load centres meant that such lines scored highly.

Note that the capacities in Germany for 2030 are lower than those presented above, since the locations on the coast were fixed based on the 2050 dispatch, which sees a proportionally bigger expansion of offshore wind in the Baltic Sea. In addition the other ends of the lines were forced to connect to the overlay grid landing point in the load centre of Stuttgart.

TABLE IX
DOMESTIC HVDC LINES CONNECTING TO THE OVERLAY GRID

| Country | From (Optimized) | To (Fixed) | Capacity 2030 (GW) | Capacity 2050 (GW) |
|---------|---------------------|---------------|-----------------------|-----------------------|
| DE | Bremerhaven | Stuttgart | 13 | 25 |
| DE | Greifswald | Stuttgart | 3 | 10 |
| ES | Algeciras | Madrid | 4 | 7 |
| FR | Cherbourg | Paris | 2 | 6 |
| GB | Glasgow | London | 3 | 6 |
| IT | Naples | Milan | 1 | 8 |
| PL | Gdansk | Warsaw | 2 | 16 |

5. CONCLUSIONS

In this paper we have developed four algorithms to optimize the placement of HVDC networks within AC transmission systems. They allow HVDC lines to be planned in a systematic way in a variety of configurations, which we hope will be useful not just for roadmap studies with aggregated network models, but also for real-life network planners.

In a case-study for Germany we found our predictions for necessary HVDC capacity agreed broadly with the scenario for 2032 from the German Network Development Plan [4], which calls for significant capacity in a North-South direction, although we also found a need for lines connecting to the central eastern part of the country. Results for a European HVDC supergrid were also presented.

From a methodological point of view the losses- and congestion-reducing objective functions worked well in identifying the need for long-distance power transfers. Since they largely agreed and the congestion function was computationally quicker, for larger studies we would recommend the congestion function for quick and accurate results. We also found that for more complicated topologies, multiple lines and terminals must be optimized jointly to obtain the best results.

For future studies it would be very interesting to increase the scope of the optimizations by working with network models that have not been aggregated, and to consider more complicated topologies. It would also be useful to incorporate planning for the entire network, including generation assets and AC capacity built out in discrete steps. Some of the simplifications outlined in Section II-E could be avoided, but at the expense of significantly higher computation times.

ACKNOWLEDGMENT

This research was funded through the Smart Modelling of Optimal Integration of High Penetration of PV (SmoothPV) project with grant number 0325272 by the German Federal Ministry for the Environment, Nature Conservation and Nuclear Safety and by the federal state of North-Rhine Westphalia. Responsibility for the contents of this publication lies with the authors.

REFERENCES

- [1] J. Pan et al., "AC Grid with Embedded VSC-HVDC for Secure and Efficient Power Delivery," *IEEE Energy 2030*, November 2008.
- [2] Inelfe project website, <http://www.inelfe.eu/>.
- [3] ENTSO-E, "Ten Year Network Development Plan 2012," European Network of Transmission System Operators for Electricity (ENTSO-E), Tech. Rep., 2012.
- [4] "Netzentwicklungsplan Strom 2012, 2. Entwurf," <http://www.netzentwicklungsplan.de>, 2012.
- [5] J. Paulinder, "Operation and Control of HVDC links embedded in AC systems," Licenciate Thesis, Chalmers University of Technology, 2003.
- [6] Y. Phulpin, J. Hazra, and D. Ernst, "Model predictive control of HVDC power flow to improve transient stability in power systems," Wide-Area Monitoring, Control & Protection (IEEE SmartGridComm).
- [7] D.L.H. Aik, and G. Andersson, "Voltage stability analysis of multi-infeed HVDC systems," *IEEE Transactions on Power Delivery*, Vol. 12, Issue 3, pp. 1209–1318, 1997.
- [8] U. De Martinis, F. Gagliardi, A. Losi, V. Mangoni, and F. Rossi, "Optimal load flow for electrical power systems with multiterminal HVDC links," *IEEE Proceedings*, Vol. 137, Pt. C, No. 2, 1990.
- [9] M. Baradar, M.R. Hesamzadeh, and M. Ghandhari, "Second-Order Cone Programming for Optimal Power Flow in VSC-type AC-DC Grids," *IEEE PES Transactions on Power Systems*, 2012.
- [10] A. Loffjou, M. Shahidehpour, and Y. Fu, "Hourly Scheduling of DC Transmission Lines in SCUC With Voltage Source Converters," *IEEE Transactions on Power Delivery*, vol. 26, no. 2, 2001.
- [11] G. Latorre, "Classification of publications and models on transmission expansion planning," *IEEE Transactions on Power Systems*, vol. 18, pp. 938–946, 2003.
- [12] F. Wu, F. Zheng, and F. Wen, "Transmission investment and expansion planning in a restructured electricity market," *Energy*, vol. 31, pp. 954–966, 2006.
- [13] M. Groschke, A. Eßer, D. Möst, and W. Fichtner, "Neue Anforderungen an optimierende Energiesystemmodelle für die Kraftwerkseinsatz- und Zubauplanung bei begrenzten Netzkapazitäten," *ZfE Zeitschrift für Energiewirtschaft*, vol. 33, pp. 14–22, 2009.
- [14] M. Fürsch et al., "Roadmap 2050: Cost-efficient RES-E penetration and the role of grid extensions," 2011.
- [15] J. Boldt et al., "Renewables in the Grid Modeling the German Power Market of the Year 2030", 2012.
- [16] W. Hogan, J. Rosellón, and I. Vogelsang, "Toward a combined merchant-regulatory mechanism for electricity transmission expansion," *Journal of Regulatory Economics*, vol. 38, pp. 113–143, 2010.
- [17] S. Hagspiel et al., "Cost-optimal Power System Extension Under Flow-based Market Coupling and High Shares of Photovoltaics," 2nd International Workshop on Integration of Solar Power into Power Systems, Lisbon, 2012.
- [18] Smooth PV Study, to be published early 2013, see <http://www.smooth-pv.info/> for more information.
- [19] SciPy implementation of BFGS optimization, see <http://docs.scipy.org/doc/scipy/reference/generated/scipy.optimize.minimize.html>.
- [20] Siemens promotional literature for Ultra HVDC Transmission System, <http://www.energy.siemens.com/hq/en/power-transmission/hvdc/hvdc-ultra/>.
- [21] A. Wasserrab, M. Fleckenstein, F. Balzer, "Integration of Wind Power in Germany's Transmission Grid by using HVDC Links," 12th Conference on Wind Integration, 2012.
- [22] J. Richter. (2011) Electricity market model description (Working Paper) Institute of Energy Economics at the University of Cologne.
- [23] EuroWind, "Database for hourly wind speeds and solar radiation from 2006-2010 (not public)." EuroWind GmbH, Tech. Rep., 2011.
- [24] Consentec, Frontier Economics, Institute of Power Systems and Power Economics (RWTH Aachen), "Analysis of cross-border congestion management methods for the european internal electricity market," Consentec, Frontier Economics, Institute of Power Systems and Power Economics (RWTH Aachen), Tech. Rep., 2004.
- [25] Frontier Economics and Consentec, "Study on the further issues relating to the inter-TSO compensation mechanism," commissioned by the European Commission Directorate-General Energy and Transport, 2006.

APPENDIX: DETECTING LONG-DISTANCE FLOWS WITH MARGINAL PARTICIPATION

In this section we present a method to allocate the power flow on a particular line to the different producing and consuming nodes in the network. There is *a priori* no unique way to do this allocation; we borrow a method called Marginal Participation that has been suggested for calculating the compensation to transmission system operators owed for the use of each other's assets [25] (it has also been used in South America). By allocating flows to particular nodes, we can detect whether power is flowing over long distances through the network, and therefore whether there is a need for long distance HVDC transmission.

We use a variant of Marginal Participation using a 'virtual' slack bus, as described in [25]. The PTDF in equation (2) already defines an allocation of flows to the nodes, but the results depend very strongly on the choice of slack bus. We can get around this problem by adding a constant to each row of the PTDF (corresponding to each branch), which has the effect of distributing the slack 'virtually' around the network. This might seem arbitrary but we can choose the constant with a particular goal in mind: in our case, following [25], we choose the constant so that for each branch the contribution to the flows from generators and loads is equal (we could have chosen any ratio between the contributions of generators and loads, but we want to detect when consumers and producers are far away from each other, so 50-50% makes sense). In this way the results are completely independent of the choice of slack bus.

With this allocation in place we can take any line we suspect is overloaded due to long-distance power transfers and see whether this is indeed the case. For example, in a windy snapshot the line DE18 → DE25 in eastern Germany from Chemnitz to Bamberg was loaded at 113%. The decomposition of this flow into contributions from specific nodes is in Table X along with the distance of the nodes from the line.

TABLE X
MARGINAL PARTICIPATION ALGORITHM FOR LINE DE18→DE25

| Node | Type | Fraction of flow (%) | Distance (km) |
|------|----------|----------------------|---------------|
| DE01 | producer | 2 | 569 |
| DE02 | producer | 3 | 568 |
| DE03 | producer | 4 | 443 |
| DE04 | producer | 9 | 300 |
| DE05 | producer | 12 | 420 |
| DE09 | producer | 6 | 100 |
| DE18 | producer | 12 | 0 |
| DE25 | consumer | 3 | 0 |
| DE27 | consumer | 3 | 93 |
| DE32 | consumer | 6 | 603 |
| DE33 | consumer | 8 | 449 |
| DE34 | consumer | 10 | 449 |
| DE35 | consumer | 14 | 280 |
| DE36 | consumer | 6 | 536 |

The biggest contributors are indeed far away: the coastal nodes where there is a lot of wind injection (particularly on the Baltic sea at the node DE05 nearest to Chemnitz) and the load centres in the far south (particularly DE35, Munich). The average distance to the producers is 343km and to the consumers is 344km, so it would make sense to build a DC link between these two groups given the likely losses over such a distance.

Determining the Maximum Feasible Amount of Photovoltaics in the European Transmission Grid Under Optimal PV Utilization

Stanislav Cherevatskiy, Ekehard Tröster
Energynautics GmbH
Langen, Germany
s.cherevatskiy@energynautics.com

Abstract—In the past few years a significant growth of the number of photovoltaic (PV) systems has been observed worldwide and particularly in Europe. Increasing maturity of this technology and growing manufacturing capacities have led to a considerable decline in prices. Looking at a future possible development of installed PV capacities in Europe, the paper at hand investigates how well the available PV energy is made use of when the installed capacity of PV reaches nearly 2000 gigawatt-peak (GWp). A methodology is presented that aims at optimal placement of PV plants taking into consideration region-specific irradiation conditions in Europe and restrictions imposed by the transmission network. Additionally, a method for optimized placement and dimensioning of storage systems along with their best possible operation strategy is applied for assessment of the effect on PV utilization.

Keywords: photovoltaics utilization, European transmission grid, storage, DIGSILENT PowerFactory

I. INTRODUCTION

Recent developments in prices for photovoltaic (PV) systems have demonstrated that grid parity for this electricity source might be reached sooner than expected even in regions with less favorable irradiation conditions. Germany alone currently accommodates around 30 GWp of installed PV capacity taking the leading position worldwide [1]. This development has been largely stimulated by increasing manufacturing capacities, feed-in tariffs and growing retail electricity prices. Assuming further price decline of PV systems and growing electricity prices along with the governmental goals towards a considerable reduction of greenhouse gas emissions, a big increase in the number of PV installations can be anticipated in Europe. Therefore, this renewable electricity source has the potential to cover a substantial amount of load in the upcoming decades.

So far grid-connected PV installations in Europe have taken place predominantly on the low and medium voltage levels distributed quite homogeneously, leading to a situation where electricity produced by PV is consumed for the most part in the vicinity of the producers without having to be transported over large distances utilizing the transmission system. However, with increasing PV capacity at certain

locations this situation will at some point change as PV-generated electricity will be able to cover the complete regional demand in certain hours and even provide excess PV generation. Assuming that such a region is coupled to the interregional transmission system this excess energy can either be transported away over large distances to supply consumers in other regions, be stored for later use or be curtailed. Clearly the former two options would require the availability of transmission capacity and storage systems as prerequisites, which, if not existent or existent to insufficient degree, would require investments in the corresponding infrastructure. The curtailment of PV, on the other hand, requires no additional infrastructure but decreases the number of full load hours and may decrease economical attractiveness of PV, let alone wasting a valuable source of renewable electricity, which, although not usable locally, could replace fossil generation elsewhere. Already today lack of adequate transmission system capacity leads to curtailment of wind power in Northern Germany as described in [2]. Although issues associated with PV systems currently predominate on the distribution system level, large expansion of PV could lead to similar effects as for wind power, especially if current postponements of grid expansion measures are taken into account. Large-scale storage limitations are currently given by location scarcity for e.g. pumped hydro storage plants, limited maturity of certain technologies and their high price. The latter two have a large improvement potential whereas the former has only limited potential for additional exploitation, partly due to environmental aspects and resistance by the population.

In the light of restrictions imposed by the transmission network and storage options described above, utilization of electricity produced by an increasing number of PV plants in the future may suffer setbacks leading to a decreasing number of full load hours. In order to assess the influence of the mentioned factors, simulations using Energynautics' European transmission grid model were carried out in DIGSILENT PowerFactory looking at future utilization of grid-connected PV in Europe while taking into consideration possible restrictions imposed by the electricity network and storage infrastructures. Optimal placement of PV generation capacities is determined by means of optimal power flow simulations allowing for diverse solar insolation properties

of different European regions and transmission network limitations. Several possible projections of future PV capacity growth were then developed, starting with the amount required to supply the complete European load on a sunny summer weekend, then increasing this amount linearly. Furthermore, the effect of optimally placed and operated storage on PV utilization was investigated in several scenarios representing various amounts of storage. The results for each investigated case present the annual load coverage through PV and the amount of curtailed PV energy and offer reflections on the maximum feasible amount of installed PV capacity in Europe aimed at maximizing load coverage through PV on the one hand and minimizing curtailed PV energy on the other.

It should be emphasized here that distribution system issues associated with large amounts of installed PV generating capacities, such as inadmissible voltage increase and overloading of power systems equipment, are not taken into consideration. Similarly, issues concerning power system operation based on large amounts of nonsynchronous generation are assumed to be solvable, permitting the operation of the power system on the basis of inverter-coupled generation.

Section II details the approach taken for modeling and calculations while section III presents calculations results. Conclusions are drawn in section IV.

II. METHODOLOGY

The principal question aimed to be answered in this study is how efficiently power available from PV installations can be utilized on the European level. This depends on how much power generated by PV is consumed locally, how much of the excess power can be transported to other locations and how much power can be stored provided storage capabilities are in place. Several projections concerning the installed capacity are considered with the goal to increase PV's share in supply of the demand. Simultaneously, more PV capacity may lead to large amounts of local excess PV power at certain locations in the system in certain hours in relation to demand on the same nodes. The limitations for power exchange between distant regions by means of the transmission system given by the limited thermal capacity of transmission lines lead to curtailment of PV power. It is assumed that sufficient reactive power compensation for the transmission network is in place so that neither voltage stability nor voltage angle stability are an issue. When PV is curtailed at one location due to transmission grid restrictions other generating capacities need to be present to supply load at another location if there is not enough PV to cover demand locally. These generating capacities could be constituted by other renewable resources, fossil fuel plants and storage systems. The present study focuses on photovoltaics and system planning defined by its behavior. No correlation with other volatile resources of renewable energy, such as wind power, is considered.

The calculations that are described subsequently were carried out using a detailed model of the European transmission grid, which is described in section II.A. In the first step, suitable locations and appropriate amounts of PV installations are identified under the assumption of demand supplied completely by PV for a specific hour as explained in section II.B. Next, section II.C describes the methodology applied for calculations of a complete year for determination of utilized and curtailed PV energy while considering different scenarios in terms of available storage capacity.

A. European transmission grid model

Calculations were conducted with Energynautics' high voltage transmission network model, which was developed with the power system calculation tool DIGSILENT PowerFactory. The model covers all ENTSO-E member countries and is designed for calculations of load flow and optimal load flow. Having over 200 nodes the model represents the load and generation centers in Europe in an aggregated fashion. The load across the nodes is distributed using a dedicated distribution key which is based on factors such as population density and the location of heavy industry. Aggregated transmission routes between and inside the individual countries are mostly modeled as 380 kV high voltage AC lines. In addition, high voltage DC lines are present as well summing up to 450 lines in total for both technologies. Although the model is capable of AC load flow calculations and can determine losses, reactive power flows and the necessary compensation, optimal power flow calculations (OPF) were conducted on DC basis for this study owing to the fact that the principal interest here lies in the active power balancing of PV power on the European level.

This study deals with large amounts of installed PV capacity in Europe that could be reached at a certain point in time in the future. As the exact time point depends on a variety of factors it cannot be predicted with certainty. Hence, the year 2050 was chosen as a rough target for estimating the development of electricity consumption. Moreover, a prediction concerning the expansion of the transmission network was made. It is based on the assumption that all projects in a mid-term planning horizon from the ENTSO-E's Ten Year Network Development Plan (TYNDP) [3] will be built. The transmission system model was upgraded by implementing most of these projects. In total 82 GVA of additional capacity were added to account for new HVAC lines and 13 GVA for new HVDC lines representing the state of year 2020. From this point onwards no further expansion of the transmission grid is considered until the year 2050. This setting will provide understanding of the role that the transmission grid plays in terms of curtailment of PV. For a joint optimization of transmission and generation systems please refer to a companion paper [4]. The model's aggregated nodes and lines are shown in Figure 1 having the predicted year-2020 status. It is furthermore assumed that Europe is able to fully cover its electricity needs without importing solar-generated power from North Africa.



Figure 1: Aggregated model of the European high-voltage transmission grid (Source: Energynautics)

B. Determination of minimum PV capacity

The study at hand aims to determine the upper reasonable limit for installed capacity with regard to utilized PV energy. However, before calculations of PV usage are conducted, a starting point for the installed PV capacity needs to be found. This has been done using the methodology that is described in the following.

PV is set to supply 100% of demand in all modeled countries (EU27 excluding Malta and Cyprus, including Norway and Switzerland) on a clear-sky summer weekend day at noon. The rationale behind this approach is that the power produced by PV plants at this hour is at its maximum while the demand in the system is relatively low compared to, for example, a winter weekday. If PV were set to supply a certain hour on a day that bears the highest demand in a year, such as a winter weekday, there would be a large number of hours in a year with excess PV generation, i.e. lots of hours when total European demand is smaller than total PV produced. This setting would lead to inefficient PV sizing from the outset. Dimensioning PV according to the light-load day, in contrast, implies that none or only little curtailment is expected throughout the year. Some curtailment might still take place due to inhomogeneous weather situation in different European regions and local grid congestion. By setting the time point to noon, the resulting PV capacity thus corresponds to one of the day's load peaks.

As mentioned previously, load assumptions are made for 2050 serving as the reference year and were developed by EWI based on ENTSO-E data for 2011 weighted according to region-specific GDP growth.

PV generation capacities determined using the described approach were not set equal to the demand at the nodes in the model they are installed at. Instead, in order to have PV benefit from locations with best irradiation conditions placement of generation capacities was carried out in accordance with region-specific average annual solar insolation data. To this end, generators on all nodes in the grid model were assigned one of six possible production costs representing six solar regions of distinct average annual insolation amount. Essentially, those regions with better irradiation properties were set to have lower production cost and those exhibiting less irradiation were assigned higher production cost. These regions are shown in Figure 2. The segmentation was done by the Institute of Energy Economics at the University of Cologne (EWI) and is based on [5]. Darker regions represent locations with high solar irradiation whereas the lighter ones stand for regions with a smaller yield.

In the next step, after this cost setting was fed into the model by allocating the production cost to all generators, a DC optimal power flow (OPF) calculation with the objective function set to minimization of generation costs was performed. This optimization mode maximizes the power output of those generators that are able to produce at lower cost, which are in our case situated in areas with high irradiation.

The transmission system limitations play a key role in cross-border long-distance balancing of PV and demand. Hence, the OPF was configured to respect the thermal limits of the lines while still prioritizing generation at sunny locations. With grid restrictions in place this yields a distribution of PV similar to that of demand totaling 770 GWp in installed capacity. This number represents the base case to be used for simulations of the complete year. PV plants could be made up by both small and large PV systems situated at all voltage levels underlying the corresponding node in the transmission network. Table I summarizes the relative distribution of PV and demand per country.

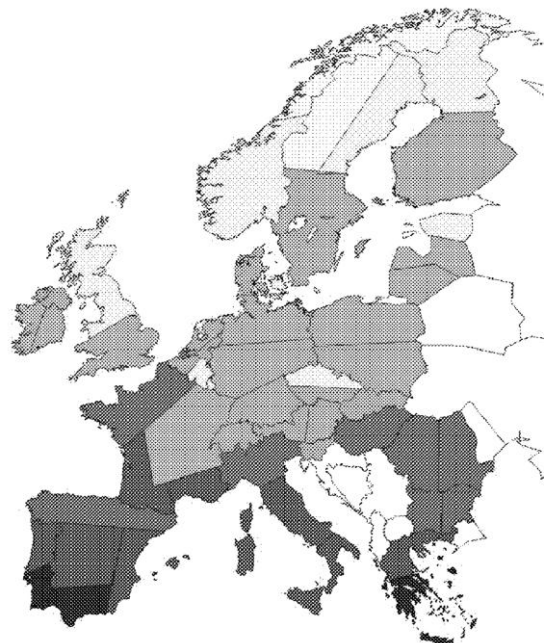


Figure 2: Solar regions (Source: EWI)

TABLE I RELATIVE DISTRIBUTION OF INSTALLED PV CAPACITY AND DEMAND IN EUROPE

| Country | Installed PV, % | Demand, % |
|----------------|-----------------|------------|
| Austria | 1.6 | 1.9 |
| Belgium | 1.3 | 2.7 |
| Bulgaria | 1.1 | 1.1 |
| Czech Republic | 0.9 | 2.3 |
| Denmark | 0.7 | 0.9 |
| Estonia | 0.0 | 0.3 |
| Finnland | 2.1 | 2.1 |
| France | 13.4 | 14.1 |
| Germany | 11.8 | 12.7 |
| Great Britain | 9.0 | 9.5 |
| Greece | 2.7 | 2.4 |
| Hungary | 2.8 | 1.5 |
| Ireland | 1.0 | 0.9 |
| Italy | 12.9 | 11.7 |
| Latvia | 0.6 | 0.3 |
| Lithuania | 0.0 | 0.4 |
| Luxembourg | 0.0 | 0.2 |
| Netherlands | 5.4 | 3.2 |
| Norway | 1.3 | 2.5 |
| Poland | 6.4 | 5.6 |
| Portugal | 2.5 | 2.1 |
| Romania | 1.9 | 2.4 |
| Slovakia | 0.9 | 1.0 |
| Slovenia | 0.0 | 0.4 |
| Spain | 13.1 | 12.9 |
| Sweden | 4.6 | 3.7 |
| Switzerland | 2.1 | 1.3 |
| Total | 100 | 100 |

C. Whole-year calculation scenarios

With the determined amount of installed PV in Europe in the base case, simulations of the complete year can be started. Under several different scenarios each of these calculations yields relevant quantities concerning the utilization and curtailment of available PV energy. These calculations comprise hourly OPF simulations using hourly demand and irradiation data for Europe for model input.

Hourly irradiation data were taken from the Satel-Light database [6] that offers access to solar radiation data all over Europe based on measurements from a geostationary satellite and estimations of cloud cover. As the exact locations of the aggregated nodes in the model are known, corresponding irradiation data were applied on the installed PV capacity yielding PV power available hourly at each network node. The data used here is based on irradiation measurements for the year 2000. The 2050 load data were extrapolated from 8 typical days to represent a complete year.

Next, the PV power and demand data were fed into the model for each node of the transmission network and for each hour. An OPF calculation series of the complete year was then performed, whose output showed how much PV power was actually used at each node, how much needed to be curtailed due to grid restrictions or excess PV generation and how much power needed to be provided by other sources of electricity in order to ensure that entire demand is supplied. This process was applied a number of times to allow for three scenario settings. Each of the scenarios contained four options in terms of installed PV capacities, which started with the base case and assumed proportional increases in steps of 385 GWp (being 50% of the base case) until the maximum of 1925 GWp. In scenario 1 no storage was considered that would enable capturing PV power that was curtailed owing to restrictions imposed by the thermal

capability of the lines or if excess PV power was being generated at a certain hour in the complete system. This is the most pessimistic scenario and leads to highest amount of curtailed PV.

In scenario 2 storing PV energy was allowed in today's pumped hydro power plants, whose locations are known and are placed on the corresponding nodes in the model. In addition, some extra storage was added at nodes that exhibited PV curtailment after simulations according to scenario 1 with installed PV capacity in Europe corresponding to that determined in the base case (770 GWp). Dimensioning was carried out based on the amount of energy curtailed in spring as this represents a compromise between winter when only a small amount of storage would be needed due to low PV irradiation and summer when the needed storage would be too large for other seasons. The determined amount of required storage capacity totals to around 290 GWh. These strategically placed units could be constituted both by small and large units dispersed throughout the sub-transmission and distribution level underlying the corresponding transmission node. A prominent representative of a small unit is an electric vehicle (EV). EV are expected to be present in large numbers in the future of mobility and power systems. These storage systems would absorb PV power that could neither be consumed locally nor transported through the transmission system to other locations and inject it back into the network whenever required at a later time point.

Last, scenario 3 incorporated storage that was dimensioned and placed in accordance with PV curtailment as seen in the year calculated in scenario 1 having around 1155 GWp PV in the system. Clearly, the resulting amount of storage capacity of about 1540 GWh is substantially higher than the one derived from calculations with 770 GWp PV installed in Europe. Table II gives an overview of the considered scenario settings. As can be seen from the table the number of conducted whole-year calculations adds up to 12.

TABLE II CALCULATION SCENARIOS

| Installed PV, GWp | Total storage capacity in Europe in GWh | | |
|-----------------------|---|------------|------------|
| | Scenario 1 | Scenario 2 | Scenario 3 |
| 770; 1155; 1540; 1925 | none | 290 | 1540 |

The calculation of quantities associated with storage operation implemented in the model takes place according to the rules described in the following. In the equations below $P_{i,h}$ stands for the active power dispatched by the OPF algorithm at a particular node i on a particular hour h . $P_{PV,i,h}$ denotes residual PV power after netting of PV power available a priori with the demand. This a priori netting ensures that as much PV power as possible is consumed by the demand in the network at the corresponding transmission node. $P_{N,STOR,i}$ denotes the nominal power of the aggregated storage unit at node i whereas $SOC_{i,h}$, $SOC_{i,h-1}$ and $SOC_{MAX,i}$ stand for current state of charge (SOC), SOC in the previous simulated hour and the nominal storage capacity of the storage unit at node i , respectively. The hourly time resolution means that hourly power and energy values are mutually interchangeable. Consider the case where dispatched power on a particular hour and node is below the available PV power:

$$SOC_{i,h} = \min\{SOC_{i,h-1} + \min(P_{N,STORi}, (P_{PVi,h} - P_{i,h})), SOC_{MAXi}\} \quad (1)$$

if $P_{i,h} \leq P_{PVi,h}$

Here the following applies for PV power stored $P_{PVSTORi,h}$, utilized $P_{UTILi,h}$ and curtailed $P_{CURTi,h}$:

$$P_{PVSTORi,h} = SOC_{i,h} - SOC_{i,h-1} \quad (2)$$

$$P_{UTILi,h} = P_{i,h} + P_{PVSTORi,h} \quad (3)$$

$$P_{CURTi,h} = P_{PVi,h} - P_{UTILi,h} \quad (4)$$

Hence, if only a part of available PV power is dispatched by the OPF algorithm, the remaining part will be stored by a unit at the same node if within the limits imposed by storage's nominal power and capacity.

For the case that power dispatched by the OPF algorithm at a particular node on a particular hour exceeds the available PV power, storage is dispatched to discharge and free up capacity, so that when PV is in excess again sometime later it can be stored again instead of being curtailed due to the fact that the storage is full. This also means that storage is prioritized over other plants, which is surely a reasonable operation strategy when a lot of PV is present in the system. Weather forecasts will definitely play an important role when deciding how to operate storage in the future power system management. For the described case the following equations apply:

$$SOC_{i,h} = \max\{SOC_{i,h-1} - \min(P_{N,STORi}, (P_{i,h} - P_{PVi,h})), SOC_{MINi}\} \quad (5)$$

if $P_{i,h} > P_{PVi,h}$

where SOC_{MINi} stands for the minimum allowed storage state and

$$P_{PVSTORi,h} = 0 \quad (6)$$

$$P_{UTILi,h} = P_{PVi,h} \quad (7)$$

$$P_{CURTi,h} = 0 \quad (8)$$

Last, in the case that no PV but only residual load is present at a node, storage is set to cover the load limited by its nominal power and remaining capacity. If the load could be completely covered, remaining storage capacity is made available to the rest of the system.

III. WHOLE-YEAR CALCULATION RESULTS

This section presents results obtained after calculations of complete years in accordance with the distribution of PV installations given in Table I and scenarios described in section II.C.

A. Scenario 1: no storage

In scenario 1 no storage was considered to be available meaning that PV power that is present in abundance at one node can only be transported by means of the transmission grid to other locations up until the thermal limits of the lines are hit. Relevant quantities can be seen in dependence of total installed PV capacity in Europe in Figure 3.

Starting with 770 GWp of installed PV, less than 1% of annual PV energy available in abundance at certain nodes cannot reach other locations to be utilized solely due to grid restrictions, as there is not a single hour in the year when total power available from PV exceeds the total demand in the system. This is the result of PV dimensioning for a light-load day in summer as described in section II.B. In this case PV is able to supply around 17% of the yearly

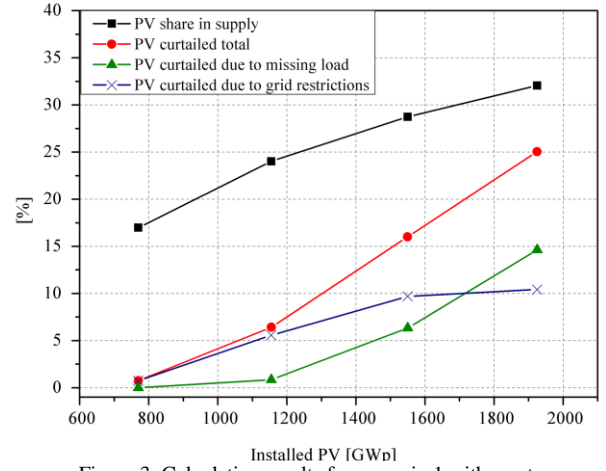


Figure 3: Calculation results for scenario 1 with no storage

load. As the installed PV capacity increases by 50% to 1155 GWp, curtailment can be seen to have increased to over 6% in total, and the largest part of it is still caused by the grid restrictions. However, there are some hours in a year now where the total energy available from PV exceeds the total amount of load in the system such that the surplus amount could not be consumed even if the grid were not the limiting factor and is therefore ascribed to missing load. This quantity grows further with increasing PV capacity and at some point shortly after 1700 GWp, PV curtailed due to missing load exceeds the amount of curtailed energy caused by grid restrictions. The latter share exhibits a saturation behavior staying relatively constant at 10% of total available PV energy from about 1550 GWp on. This means that up to this amount of curtailed PV could be saved by enforcing the grid appropriately.

The results of this scenario show that if the installed capacity of grid-connected PV systems should reach 1925 GWp without any grid enforcement after 2020 or storage options, 25% of available PV energy would be wasted. The PV's share in load coverage does not follow the proportionality of increasing installed capacity and thus only supplies about 32% of demand with 1925 GWp installed as compared to 17% being supplied by a 2.5 times smaller capacity of 770 GWp.

B. Scenario 2: 290 GWh storage

Storage simultaneously fixes the two factors that influence the amount of curtailed PV energy, namely the grid restrictions and excess of PV energy in relation to demand in the system in certain hours. The wasted energy caused by the latter factor can only be reduced through storage, while the effect of the former, in contrast, can be rectified either through storage or through grid enforcement. Hence, in the evaluation of annual curtailment figures the difference between the curtailed PV energy and excess PV energy on a particular hour is attributed to inadequate grid resources rather than to excess PV amount.

Figure 4 illustrates the quantities related to PV usage in this scenario. As can be seen, storage introduced into the system is now able to reduce the amount of curtailed PV energy to around 23% compared to 25% seen in scenario 1 for 1925 GWp of installed PV. This seems to be a modest number, however the absolute amount of avoided curtailed energy still adds up to nearly 51000 GWh per year, which

corresponds to electricity consumed by Portugal in 2011 [8]. Storage essentially shifts the curtailment curves to larger values of installed PV capacity by a certain degree.

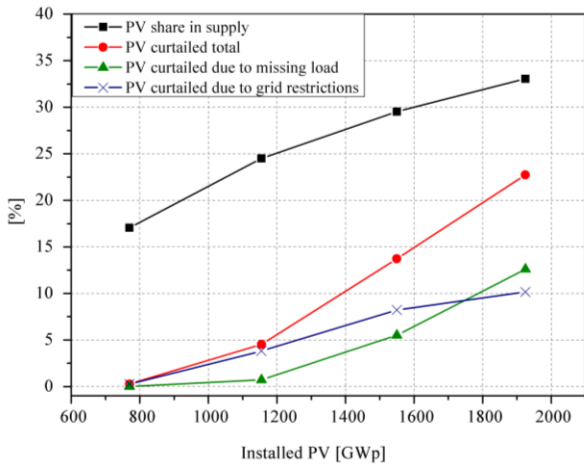


Figure 4: Calculation results for scenario 2 with 290 GWh of storage

C. Scenario 3: 1540 GWh storage

The effect of a larger storage than the one considered in the previous scenario is visible in Figure 5.

Up until 1155 GWp the storage which has been dimensioned to attend this very amount of PV installed in the system is able to capture almost the complete excess PV energy on all nodes and inject it into the system at a later time thus effectively keeping the curtailment down at well below 1%. It also significantly contributes to reduction of curtailed PV energy caused by grid restrictions. With 1540 GWp PV in the system the curtailment totals to 5%. In the end, with 1925 GWp present in the system the PV's share in load supply adds up to about 38% under a curtailment of about 12% which is mostly attributed to grid restrictions. In the present case appropriate grid enforcement would contribute significantly to reduction of the total curtailed PV energy.

The results show that even about 2000 GWp of PV in the system could be feasible provided that the grid is expanded in appropriate locations so as to enable transport of abundant PV energy at some nodes to others where this resource is scarce. A large damping effect is provided by storage with a total capacity across Europe of 1540 GWh, which is equivalent to the full capacity of nearly 31 Mio.

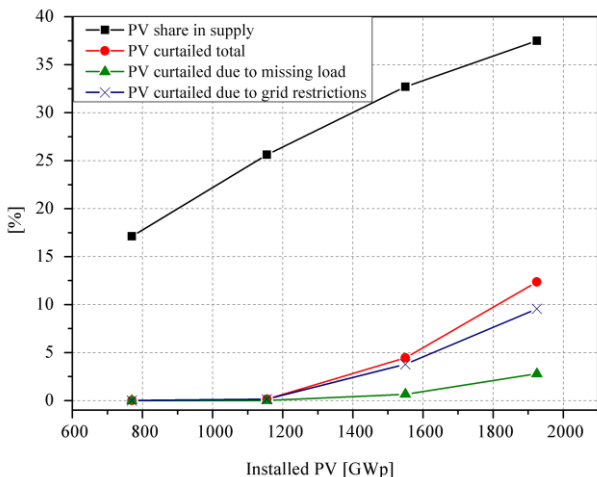


Figure 5: Calculation results for scenario 3 with 1540 GWh of storage

electric vehicles, which is a quite significant number although it could underlie significant variations considering possible breakthroughs in terms of higher energy density of future batteries¹. Besides, Germany alone plans to have 6 Mio. electric vehicles rolling on its streets by 2030 as stated in [7] such that the above number of 31 Mio. in total for the whole of Europe appears to be a realistic number by 2050. In addition, other storage technologies, such as compressed air energy storage could be available on a wide scale by then.

Figure 6 compares the number of annual average full loads hours reached by PV in all Europe for the three considered storage scenarios. Compared to scenarios 1 and 2 storage dimensioned for 1155 GWp of installed PV in the European power system in scenario 3 is able to increase PV usage substantially, even for larger installed capacities.

Summarizing, it has been shown in the present study that curtailment of PV energy can be reduced significantly if storage is dimensioned and placed strategically on specific nodes in the transmission system. It can be thus concluded that around 30 to 40% of annual demand in Europe can be feasibly covered by PV. That is, the amount of curtailed PV energy is acceptable in relation to the amount of storage that needs to be built. Any further expansion of PV capacity is likely to represent a high economic burden owing to the disproportionately high amount of required storage capacity.

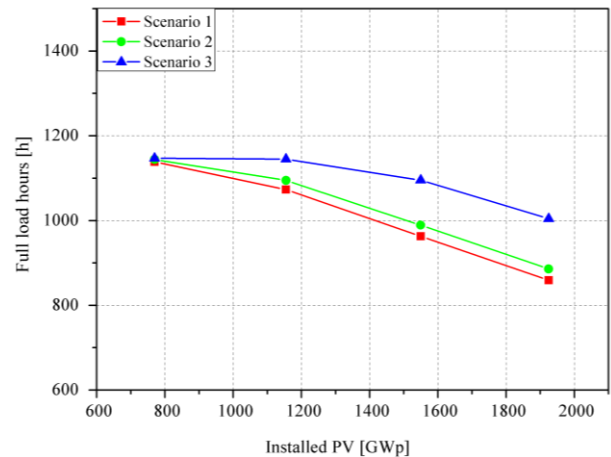


Figure 6: Comparison of full load hours of PV in Europe for different scenarios

¹ 50 kWh per EV were assumed with reference to the Tesla Roadster

IV. CONCLUSIONS

In this work a methodology is presented that aims at an optimal placement of a large amount of grid-connected photovoltaic installations according to the solar irradiation potential in Europe and under consideration of restrictions imposed by the European transmission network.

The transmission restrictions lead to a well-distributed placement of PV capacities to match the distribution of the demand. The resulting distribution is kept while the total installed capacity is increased proportionally up until nearly 2000 GWp of installed PV while conducting optimal power flow simulations of a complete year in order to assess the curtailment of PV associated with excess PV energy and insufficient transmission capacity. The influence of strategically placed and dimensioned storage capacities is determined in several simulations scenarios demonstrating a potential for significant reduction of curtailed PV energy in the interconnected European grid under a large-scale deployment of distributed storage systems. With 1540 GWh storage capacity in the system, which could be constituted by, for example, electric vehicles, compressed air energy storage and others, approximately 1550 GWp of PV covering about 33% of the annual demand can be accommodated by the system with a 5% annual curtailment of PV energy. Demand side management could provide for a shift in diurnal load cycle helping to keep the PV power and demand in the system well-correlated. Appropriate grid enforcement could further reduce the amount of curtailed PV energy. For example, PV's share in load coverage could be increased to 38%, which however would lead to 12% curtailment unless necessary grid extension or additional storage capacity is provided. Further expansion of installed PV capacity aimed at increasing PV's share in load supply would necessitate disproportionately high storage and grid extension to keep the amount of curtailed energy low.

ACKNOWLEDGMENT

This research was funded through the Smart Modelling of Optimal Integration of High Penetration of PV (SmoothPV) project with grant number 0325272 by the German Federal Ministry for the Environment, Nature Conservation and Nuclear. Responsibility for the contents of this publication lies with the authors.

REFERENCES

- [1] German Federal Network Agency, September 2012, monthly statistics available online at:
http://www.bundesnetzagentur.de/DE/Sachgebiete/Elektrizitaet/Gas/ErneuerbareEnergienGesetz/VerguetungssaetzePVAnlagen/VerguetungssaetzePhotovoltaik_Basepage.html
- [2] J. Bömer, Ecofys, "Abschätzung der Bedeutung des Einspeisemanagements nach EEG 2009", report in German, October 2011
- [3] ENTSO-E Ten-Year Network Development Plan 2012, July 2012, available online at:
<https://www.entsoe.eu/system-development/tyndp/tyndp-2012/>
- [4] S. Hagspiel, C. Jägemann, D. Lindenberger, S. Cherevatskiy, E. Tröster, T. Brown „Cost-optimal Power System Extension Under Flow-based Market Coupling and High Shares of Photovoltaics“, to be presented at the 2nd International Workshop on Integration of Solar Power into Power Systems, November 2012, Lisbon, Portugal
- [5] EuroWind, 2011. Database for hourly wind speeds and solar radiation from 2006-2010 (not public). Tech. rep., EuroWind.

- [6] S@tel-Light, an online database, available at:
<http://www.satel-light.com/>
- [7] Federal Ministry for the Environment, Nature Conservation and Nuclear Safety "Energy Concept 2050 – Milestones and Assessments", October 2010, available online at:
https://www.bmu.de/english/energy_efficiency/doc/46721.php
- [8] ENTSO-E's consumption database, available online at:
<https://www.entsoe.eu/resources/data-portal/consumption/>

The economic inefficiency of grid parity: The case of German photovoltaics in scenarios until 2030

Cosima Jägemann, Simeon Hagspiel, Dietmar Lindenberger
Institute of Energy Economics, University of Cologne
Vogelsanger Strasse 321, 50827 Cologne, Germany
Email: cosima.jaegemann@ewi.uni-koeln.de

Abstract—Due to massive reductions in the price for photovoltaic (PV) systems, PV grid parity has recently been reached for German households. As PV system prices continue to decrease, the gap between the levelized costs of electricity (LCOE) of PV and the retail electricity tariff will grow and trigger investments in residential PV systems for captive electricity generation – even in the absence of any direct financial incentives such as solar power feed-in tariffs. However, while the single household can lower its annual electricity costs through investments in rooftop PV systems for captive electricity generation, the partial optimization of the single household is inefficient from an economic perspective. Households optimize their PV investment by comparing the LCOE of PV to the residential electricity tariff that includes network tariffs, taxes, levies and other surcharges that can be avoided when consuming self-produced PV electricity instead of purchasing electricity from the grid. Therefore, private investments in rooftop PV systems receive an indirect financial incentive in the current regulatory environment.

This paper analyzes the consequences of PV grid parity in Germany until 2030 from both the single household and the wholesale market perspective. We find that exempting self-consumed PV electricity from all additional charges induces significant investments in rooftop PV systems and small scale storage systems, allowing for high shares of in-house PV electricity consumption. From the single household perspective, the optimal PV and storage system capacities increase with the number of residents living in the household, enabling households to cover on average 72 % of their annual electricity demand by self-produced PV electricity. The single household's optimization behavior entails direct consequences for the wholesale market, as it changes the residual load both in volume and structure. The inefficiency caused by the partial optimization of single households (induced by PV grid parity) leads to significant excess costs of 7.1 bn €₂₀₁₁ compared to the cost-optimal solution achieved under a total system optimization which ensures the cost-efficient development of Germany's electricity generation mix up to 2030.

I. INTRODUCTION

The photovoltaic (PV) market in Germany has seen unprecedented growth over the last years. Since 2009, installed capacity rose by approximately 7.5 GW per year, reaching 25 GW at the end of 2011. This massive expansion was due to a combination of generous solar power feed-in tariffs – guaranteed to PV electricity producers by the German Renewable Energy Sources Act (EEG) – and decreasing PV system prices, which over the last 6 years have fallen at a faster rate than the solar power feed-in tariffs.¹

¹PV system prices have fallen by over 65 % from 2006 to 2012 [1].

In order to slow down the expansion of PV capacities and the associated costs of supporting PV electricity – which are added to the electricity price and hence passed on to the electricity consumers via the so called 'EEG' surcharge – the federal government agreed to further cut the feed-in tariffs for photovoltaics and to stop the direct financial incentives once a cumulative capacity of 52 GW is reached.² However, due to the fact that PV grid parity has recently been achieved for households in Germany [2], investments in rooftop PV systems are expected to become a compelling option for residential electricity consumers in the near future, even in the absence of any direct financial incentives such as solar power feed-in tariffs.

PV grid parity for households is defined as the threshold at which the levelised costs of electricity (LCOE) - including initial investment and operations and maintenance costs - of the PV system over its lifetime reach parity with the residential electricity tariff. Hence, PV grid parity marks the point in time at which households can lower their annual electricity costs by consuming self-produced PV electricity rather than purchasing electricity from the grid.

Due to the fact that households avoid network tariffs, taxes,

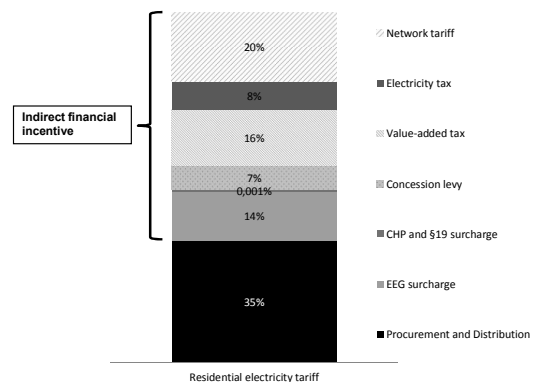


Fig. 1. Composition of Germany's residential electricity tariff in 2012 based on [3]

levies and other surcharges for the amount of PV electricity consumed in-house, the grid parity calculus depicts an indirect financial incentive for PV electricity generation granted to residential PV electricity consumers (see Figure 1). How-

²Germany's National Renewable Energy Action Plan foresees a target value of 52 GW for PV in 2020

ever, the expenditure savings on the side of the residential PV electricity consumers go along with revenue shortfalls on the side of the government, municipalities and system operators, which will need to be somehow compensated. For example, the costs for operating, maintaining and upgrading the grid do not decrease with the amount of PV electricity consumed in-house but rather increase due to necessary investments in the distribution grid. Hence, system operators will need to either increase the network tariffs or change the tariff structure - e.g. from energy-related to capacity-related tariffs - to be able to cover the costs. Moreover, households save electricity tax payments for the share of in-house PV electricity consumption, which contribute to public funds (e.g. pension funds) in Germany. Hence, an increased share of in-house PV electricity consumption induced by PV grid parity results in a reallocation of financial resources: it lowers the burden to be borne by households that consume a part of their PV electricity generation and increases the burden to all other electricity consumers. Moreover, society is faced with significant excess costs under such a scenario, due to the fact that investments in rooftop PV and small scale storage capacities do not depict a cost-efficient investment option in Germany before 2030. Specifically, the partial optimization on the household level leads to an inefficient electricity generation mix from the total system perspective. The potential cost savings from the single household per-

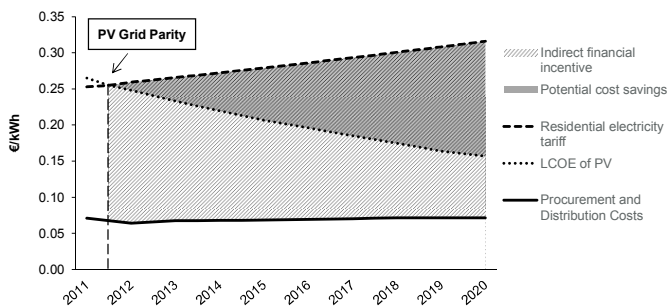


Fig. 2. Potential costs savings from the single household perspective induced by PV grid parity

spective correspond to the difference between the residential electricity tariff and the LCOE of PV. The greater the difference between the residential electricity tariff and the LCOE of PV increases, the larger the potential cost savings achievable by households become, as shown in Figure 2.³ However, potential cost savings are limited to the amount of PV electricity that is consumed by the residents.

The rapidly growing gap between the residential electricity tariff and the LCOE of PV is expected to lead to considerable investments in rooftop PV systems for in-house electricity consumption in the near future.⁴ However, given the prevalent mismatch of sunshine hours and residential electricity consumption behavior, supplementary investments in storage

³The residential electricity tariff is assumed to increase by 3 % per year and PV system prices to decrease by approximately 3.3 % per year until 2020.

⁴The greater the gap between residential electricity tariffs and LCOE of PV, the higher the return on investment. To depict a compelling investment option, the return on investment will at least need to exceed the capital market interest rates for fiscal investments with a comparable investment risk.

capacities could increase the potential cost savings, allowing for higher shares of in-house PV electricity consumption. At present, studies have primarily focused on the identification of the point in time at which PV grid parity will be reached ([4], [2]) as well as on the analysis of factors influencing this point of time ([5],[6],[7]). The potential consequences of PV grid parity, in contrast, have hardly been analyzed.

An adequate assessment of the potential impact of PV grid parity on the total electricity system requires a profound analysis of the single household's cost minimization behavior. In the absence of any direct financial incentive such as solar power feed-in tariffs, the single household's decision concerning the installation and the dimensioning of a PV and storage system depends on the gap between the residential electricity tariff and the LCOE of PV, the household's electricity consumption profile and the market value of the non-consumed PV electricity that is fed into the grid. The single household's cost minimization behavior entails direct consequences for the wholesale market. This is because increased shares of in-house PV electricity consumption cause changes in the residual load, both in volume and structure, and in turn effect the provision and operation of power plants.⁵

In this paper, we analyze the consequences of PV grid parity in Germany after 2020 - both from the single household and the wholesale market perspective - by iterating a household optimization model with an electricity system optimization model. Within this framework, the following questions will be answered:

- What are the optimal PV and storage system capacities - from the single household perspective - induced by PV grid parity?
- What is the share of total PV electricity generation that can be consumed in-house by a single household (given the optimal dimensioning of PV and storage system capacities)?
- What is the share of a single household's annual electricity demand that can be supplied by self-produced PV electricity (given the optimal dimensioning of PV and storage system capacities)?
- What are the consequences for the wholesale market?
- What are the excess costs induced by PV grid parity?

The remainder of the paper is structured as follows: Section II presents the scenario definition and the methodology developed to analyze the consequences of indirect financial incentives for PV electricity generation - induced by PV grid parity in Germany until 2030. Section III summarizes the model results and analyzes their implications for Germany's power sector up to 2030. Section IV concludes and provides an outlook on further possible research.

II. METHODOLOGY

In this section, the scenarios are defined and the models are presented that are used to analyze the effects of indirect

⁵In the analysis, the residual load corresponds to Germany's total electricity demand (load) without the accumulated in-house PV electricity consumption of the single households.

financial incentives – induced by PV grid parity – both from the single household and the wholesale market perspective.

A. Scenario definition

For the analysis of the grid parity effects, two scenarios are defined. As seen in Table I, which lists the main settings of the scenario simulations, the difference between the scenarios refers to the deployment of PV systems in Germany after 2020. While in scenario A the expansion of PV systems is based on the single household's optimization behavior (induced by PV grid parity), scenario B simulates a cost-efficient development of Germany's electricity generation mix up to 2030. All other assumptions regarding political targets or the expansion of interconnector capacities are identical in both scenarios. Germany (and its neighboring countries) are assumed to achieve their national renewable energy targets stated in the National Renewable Energy Action Plans (NREAP's) by 2020 and the European CO₂ reduction target, which increase linearly up to 60 % until 2030 (compared to 1990 levels). Moreover, the interconnector capacities between Germany and its neighboring countries are assumed to be expanded according to planned projects according to the ENTSO-E's 10-Year Network Development Plan 2012 (TYNDP) [8].

The scenarios described above are simulated with two op-

TABLE I
SCENARIO DEFINITION

| | A | B |
|---|-------------------------------|---------------------|
| Deployment of PV systems after 2020 | Household optimization | System optimization |
| Expansion of renewables until 2020 | Realization of NREAP targets | |
| Expansion of interconnector capacities until 2030 | Realization of TYNDP projects | |
| Reduction of CO ₂ emissions until 2030 | 60 % (compared to 1990) | |

timization models: a household optimization model and an electricity system optimization model. The following sections introduce these two models and describe the iterative approach used in the analysis to quantify the effects of PV grid parity from the single household and the wholesale market perspective in scenario A.⁶

B. Household optimization model

In the first step, a linear optimization model is developed to minimize the annual electricity costs of households, given yearly solar irradiance and electricity consumption profiles, PV and storage system investment costs, residential electricity tariffs and hourly market values of PV electricity generation. The model in turn determines the optimal PV and storage system capacities from the single household perspective – depending on the number of residents living in the house (i) and the location of the house (r) – as well as hourly system performance statistics, including hourly PV

⁶Note that the cost-efficient development of Germany's electricity generation mix in scenario B is simulated by using the electricity system optimization model. In specific, no iteration with the household optimization model is conducted.

TABLE II
MODEL SETS, PARAMETERS AND VARIABLES

| Sets | |
|------------------|--|
| $h \in H$ | Hour of the year |
| $i \in I$ | Number of residents living in the household |
| $r \in R$ | Region |
| Parameters | |
| $a_{h,r}$ | Solar irradiance on tilted PV cell [W/m ²] |
| c^{PV} | PV investment costs [€/kW] |
| c^{ST} | Storage investment costs [€/kW] |
| $d_{h,i,r}$ | Electricity demand [kWh] |
| η | Efficiency of the storage [%] |
| m^{ST} | PV O&M costs [€/kW] |
| m^{ST} | Storage O&M costs [€/kWh] |
| p^R | residential electricity tariff [€/kWh] |
| p_h^W | Market value of PV electricity [€/kWh] |
| u | Discount rate [%] |
| ω | PV Performance ratio [%] |
| \bar{a} | Solar irradiance under STC [W/m ²] |
| t^{PV} | PV lifetime [years] |
| t^{ST} | Storage lifetime [years] |
| Variables | |
| $C_{i,r}$ | Total costs [€] |
| $C_{i,r}^{PV}$ | Annualized PV investment costs [€] |
| $C_{i,r}^{ST}$ | Annualized storage investment costs [€] |
| $E_{h,i,r}^{PU}$ | Electricity purchased from the grid [kWh] |
| $E_{h,i,r}^{PV}$ | Electricity supplied by PV system [kWh] |
| $E_{h,i,r}^{SA}$ | Electricity sold to the grid [kWh] |
| $E_{h,i,r}^{ST}$ | Electricity supplied by storage system [kWh] |
| $G_{h,i,r}^{PV}$ | Total PV electricity generation [kW] |
| $K_{i,r}^{PV}$ | Capacity of PV system [kW] |
| $K_{i,r}^{ST}$ | Capacity of storage system [kWh] |
| $L_{h,i,r}^{ST}$ | Storage level [kWh] |
| $M_{i,r}$ | O&M cost [€] |
| $P_{i,r}$ | Costs of purchasing electricity [€] |
| $R_{i,r}$ | Revenue from selling electricity [€] |
| $S_{h,i,r}$ | Storage input [kWh] |

electricity self-consumption and grid feed-in profiles.

The annual electricity costs of a household are defined as the sum of the annualized PV system investment costs ($C_{i,r}^{PV}$), the annualized storage system investment costs ($C_{i,r}^{ST}$), the annual operation and maintenance costs ($M_{i,r}$) and the annual costs for the amount of electricity purchased from the electricity grid ($P_{i,r}$). In addition, annual electricity costs are decreased by the revenue acquired from selling PV electricity to the grid ($R_{i,r}$), which is assumed to be remunerated by the market value of PV electricity in the specific hour (p_h^W). The annual electricity costs are minimized subject to several techno-economic constraints. Equation (7) depicts the power balance of supply and demand that needs to be achieved for each point in time. The electricity generation of the household's PV system in a specific hour and region ($G_{h,i,r}^{PV}$) can either be directly consumed by the household ($E_{h,i,r}^{PV}$), sold to the electricity grid ($E_{h,i,r}^{SA}$) or stored in the battery system ($S_{h,i,r}$). At the same time, however, the household's electricity demand in a specific hour and region ($d_{h,i,r}$) needs to be met by electricity supplied by the PV system ($E_{h,i,r}^{PV}$), the storage system ($E_{h,i,r}^{ST}$) or the electricity grid ($E_{h,i,r}^{PU}$) (Eq. (8)). As stated in Equation (9), the power output of a household's PV system in a specific hour and region ($G_{h,i,r}^{PV}$) depends on the solar irradiance on the tilted PV cells in

the specific hour and region ($a_{h,r}$) and on the performance ratio of the PV cells (ω). The maximum storage level of a household's battery system ($L_{h,i,r}^{ST}$) is determined by the storage capacity ($K_{i,r}^{ST}$) (Eq. (10)), while the hourly change in the storage level of a household's battery system depends on the storage operation in the specific hour and the losses during the charging process (Eq. (11)).

$$\min C_{i,r} = C_{i,r}^{PV} + C_{i,r}^{ST} + M_{i,r} + P_{i,r} - R_{i,r} \quad (1)$$

s.t.

$$C_{i,r}^{PV} = c^{PV} \cdot K_{i,r}^{PV} \cdot \left[1 - \frac{1}{(1+u)^{t^{PV}}} \right] \quad (2)$$

$$C_{i,r}^{ST} = c^{ST} \cdot K_{i,r}^{ST} \cdot \left[1 - \frac{1}{(1+u)^{t^{ST}}} \right] \quad (3)$$

$$M_{i,r} = m^{PV} \cdot K_{i,r}^{PV} + m^{ST} \cdot K_{i,r}^{ST} \quad (4)$$

$$P_{i,r} = \sum_{h \in H} \left[p^R \cdot E_{h,i,r}^{PU} \right] \quad (5)$$

$$R_{i,r} = \sum_{h \in H} \left[p_h^W \cdot E_{h,i,r}^{SA} \right] \quad (6)$$

$$G_{h,i,r}^{PV} = E_{h,i,r}^{PV} + E_{h,i,r}^{SA} + S_{h,i,r} \quad (7)$$

$$d_{h,i,r} = E_{h,i,r}^{PV} + E_{h,i,r}^{ST} + E_{h,i,r}^{PU} \quad (8)$$

$$G_{h,i,r}^{PV} = K_{i,r}^{PV} \cdot \omega \cdot \left[\frac{a_{h,r}}{\bar{a}} \right] \quad (9)$$

$$L_{h,i,r}^{ST} \leq K_{i,r}^{ST} \quad (10)$$

$$L_{h+1,i,r}^{ST} - L_{h,i,r}^{ST} = \left[S_{h,i,r} \cdot \omega \right] - E_{h,i,r}^{ST} \quad (11)$$

Given that the focus of the analysis is on the German electricity market, all country-specific input parameters of the household optimization model – such as the residential electricity tariff, the household's electricity consumption profile and the solar irradiance profile – have been defined according to German levels.

The single households' electricity consumption profiles were derived with the model of domestic electricity use developed in [9], which creates synthetic electricity demand data for 24 hours (with one-minute resolution) through the simulation of domestic appliance use – depending on the number of residents living in the house, the day of the week and the month of the year.⁷ The domestic electricity demand model was configured to the use of domestic appliances in Germany based on data from [10], [11], [12] and [13] and run for 8760 hours of the year. Overall, 250 annual electricity consumption profiles were simulated, each differing with regard to the number of residents living in the dwelling (1-5) and the amount of domestic appliances.

The hourly solar irradiance profiles for three different regions in Germany were taken from [14] and converted from a horizontal to a tilted surface.

All other input parameters of the household optimization model are listed in Table III. The input parameters are set to the expected values achievable between the years 2025

TABLE III
ASSUMPTIONS OF THE HOUSEHOLD OPTIMIZATION MODEL IN
SCENARIO A

| Parameter | |
|-----------|-----------------------------------|
| \bar{a} | 1000 [W/m ²] |
| c^{PV} | 1250 [€ ₂₀₁₁ /kWp] |
| c^{ST} | 500 [€ ₂₀₁₁ /kWh] |
| η | 95 [%] |
| m^{PV} | 11 [€ ₂₀₁₁ /kWp p.a.] |
| m^{ST} | 7.5 [€ ₂₀₁₁ /kWh p.a.] |
| p^R | 0.378 [€ ₂₀₁₁ /kWh] |
| t^{PV} | 30 [years] |
| t^{ST} | 15 [years] |
| u^R | 3 [%] |
| ω | 75 [%] |

and 2030, at which time any direct financial incentives such as solar power feed-in tariffs are assumed to be abolished. However, at this time, the gap between the residential electricity tariff and the LCOE of PV is assumed to have increased to a level resulting in an attractive rate of return from investments in PV and storage system capacities. In specific, PV system investment costs (c^{PV}) are assumed to amount to 1,250 €₂₀₁₁/kWp (incl. VAT of 19 %) and the technical lifetime of PV systems (t^{PV}) is assumed to amount to 30 years. Moreover, storage systems are assumed to exhibit investment costs (c^{ST}) of 500 €₂₀₁₁/kWh and to have a technical lifetime (t^{ST}) of 15 years.⁸ In contrast to the residential electricity tariff (p^R), which is derived by linear extrapolation of current values and assumed to amount to 0.378 €₂₀₁₁/kWh,⁹ the market value of PV electricity (p_h^W) is endogenously determined with the electricity system optimization model, which is presented in the next section.

C. Iteration with an electricity system optimization model

From a wholesale market perspective, a large PV penetration and a high share of self-consumed PV electricity generation on the household level causes changes in the load and the provision and operation of power plants. As a result, there is a change in the marginal value of excess (not self-consumed) PV electricity that is fed into the electricity grid. To account for this interdependent relationship, the household optimization model is iterated with an electricity system optimization model.

The electricity system optimization model used in this analysis is an extended version of the long-term investment and dispatch model for conventional, renewable, storage and transmission technologies as presented in [15]. It covers 29 countries (EU27 plus Norway and Switzerland), which can be aggregated to larger market regions to reduce the computational time. The model determines the cost-efficient development of generation and storage capacities and their operation for the time period up to 2030. The objective of the model is to minimize accumulated discounted total system costs while being subject to several techno-economic restrictions, such as the hourly matching of supply and demand, fuel availabilities and potential space for renewable

⁸The assumptions regarding the storage system reflect expectations for Lithium-Ion batteries.

⁹The residential electricity tariff is assumed to increase by 3 % per year until 2025.

⁷The domestic electricity demand model is distributed under <http://hdl.handle.net/2134/5786> and documented in [9].

energies as well as politically implemented restrictions such as EU-wide CO₂ emission reduction targets and limited nuclear power deployment.¹⁰

The simulation of the European electricity markets is carried out as a two-stage process: In the first step, investments in generation and storage capacities are simulated in 5-year time steps until 2030. For each of the years, the model determines both investments in new capacities and decommissionings of existing capacities.¹¹ The dispatch of capacities is calculated for eight typical days per year on an hourly basis (scaled to 8760 hours), representing variations in electricity demand as well as in solar and wind resources along with their multivariate interdependencies. In the second step, the capacity mix in 2030 is fixed and a high-resolution dispatch is simulated. Instead of typical days, the dispatch is simulated on the basis of hourly load profiles as well as hourly electricity generation profiles of wind and solar power technologies for 8760 hours of the year (based on historical hourly wind and solar radiation data from [14]). Due to computational time constraints the simulation is run for 9 European market regions, which are considered most relevant for dispatch and investment decisions in Germany. The simulated market regions are depicted in Figure 3.

The results of the electricity system optimization model

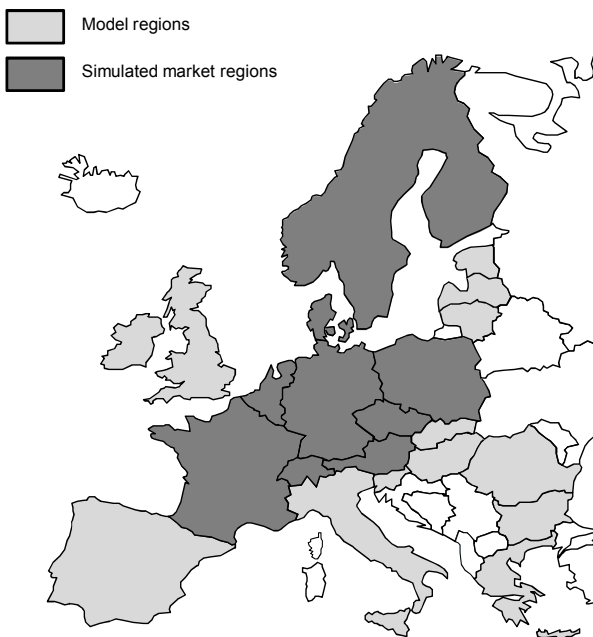


Fig. 3. Simulated model regions

encompass the commissioning and decommissioning of conventional, renewable and storage capacities until 2030, the electricity generation of all technologies and the marginal costs of electricity generation in each hour of the year 2030.

Since the optimal PV and storage system capacities from the single household perspective directly depend on the

¹⁰Total system costs are defined by investment costs, fixed operation and maintenance costs, variable production costs and costs due to ramping thermal power plants.

¹¹All assumptions regarding techno-economic parameters, fossil fuel prices and investment costs of conventional, storage and renewable technologies are based on [16].

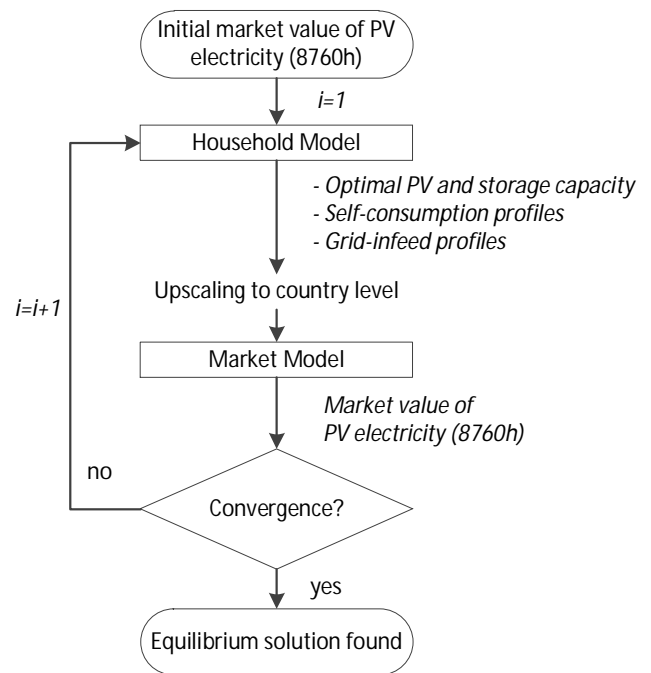


Fig. 4. Schematic representation of the iterative process

marginal value of excess (not self-consumed) PV electricity, the results of the household optimization model are iterated with the results of the electricity system optimization model. Figure 4 shows a schematic representation of the iterative process. Based on an initial market value of PV electricity in 2030 (which was assumed to amount to 0.055 €/kWh in all hours of the year) the household optimization model determines the optimal PV and storage capacities (depending on the number of residents living in the house and the location in Germany), as well as hourly system performance statistics, including the single household's hourly electricity self-consumption and grid feed-in profiles.

To analyze the impact of the single household's optimization behavior on the German electricity market, the results are scaled up to the country level by multiplying the model results with the number of one- and two-family-houses located in Germany (differentiated by the number of residents and the location of the houses). The procedure assumes complete rational behavior and abstracts from the so-called 'landlord-tenant' problem ([17]). Hence, scenario A can be said to depict a situation of 'unconstrained grid parity' in Germany up until 2030.

The upscaled results of the household optimization model – i.e. the household's optimal PV and storage capacities, self-consumption and grid-infeed profiles – serve as input parameters for the electricity system optimization model, which in turn determines the marginal costs of electricity generation in each hour of the year 2030. Given the fact that the marginal costs of electricity generation reflect the market value of excess (not self-consumed) PV electricity generation, the marginal costs of electricity generation are in turn taken as an input parameter for the household optimization model. Specifically, the household's PV electricity generation that is not self-consumed, but rather fed into the electricity

grid, is assumed to be remunerated by the marginal costs of electricity generation – which are determined by the electricity system optimization model.

Based on the new marginal costs of electricity generation – which reflect the market value of PV electricity – the household optimization model determines the optimal PV and storage capacities from the single household perspective. This iterative process is continued until the convergence of results is achieved.

III. RESULTS

Figure 5 presents the development of optimal PV capacities during the iterative process in scenario A, depending on the numbers of residents (1-5) and the location (Southern, Central, Northern Germany) of the household. Optimal PV capacities reach stable levels after only three iteration steps. On average, optimal PV capacities change by less than 1 % in the last iteration step. Other quantities that are subject to change while iterating the two models – such as the optimal storage capacities and the market value of PV electricity – show the same convergent behavior.

Table IV shows the optimal PV and storage system ca-

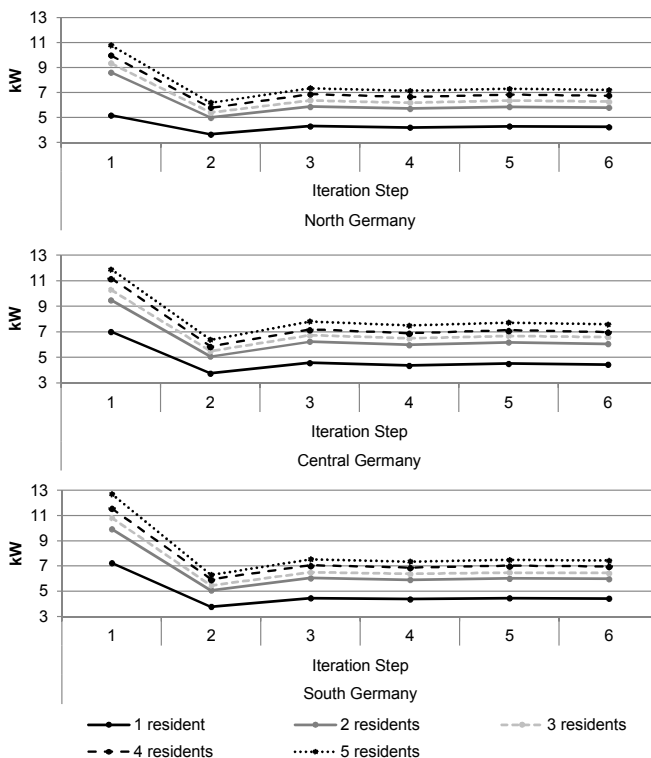


Fig. 5. Development of optimal PV capacities during the iteration in scenario A

pacities, the share of the household's annual PV electricity generation that is consumed in-house and the share of the household's annual electricity demand that is covered by self-produced PV electricity in scenario A after convergence has been reached (i.e. for iteration step 6). Both optimal PV and storage system capacities increase with the number of residents living in the household. However, the shares of in-house PV electricity consumption (i.e. the share of the household's annual PV electricity generation that is

consumed in-house and not fed into the electricity grid) lie within a relatively low and narrow range between 43 % and 46 % for all configurations. Interestingly, households are able to cover 67 % to 77 % of their annual electricity demand by self-produced PV electricity in scenario A, given the optimized PV and storage capacities.

Figure 6 shows the average share of the (daily) household

TABLE IV
OVERVIEW OF MODEL RESULTS

| | North Germany | Central Germany | South Germany |
|--|---------------|-----------------|---------------|
| Optimal PV capacity [kW] | | | |
| 1 Resident | 4.2 | 4.4 | 4.4 |
| 2 Residents | 5.8 | 6.1 | 6.0 |
| 3 Residents | 6.3 | 6.6 | 6.4 |
| 4 Residents | 6.8 | 7.0 | 7.0 |
| 5 Residents | 7.2 | 7.6 | 7.4 |
| Optimal storage capacity [kWh] | | | |
| 1 Resident | 3.3 | 3.4 | 3.9 |
| 2 Residents | 4.4 | 4.5 | 5.1 |
| 3 Residents | 4.9 | 5.1 | 5.7 |
| 4 Residents | 5.2 | 5.5 | 6.1 |
| 5 Residents | 5.5 | 5.7 | 6.4 |
| Share of in-house PV electricity consumption [%] | | | |
| 1 Resident | 45% | 43% | 45% |
| 2 Residents | 45% | 43% | 45% |
| 3 Residents | 45% | 43% | 45% |
| 4 Residents | 45% | 44% | 45% |
| 5 Residents | 46% | 44% | 45% |
| Household demand coverage by PV electricity [%] | | | |
| 1 Resident | 67% | 71% | 75% |
| 2 Residents | 67% | 71% | 76% |
| 3 Residents | 68% | 72% | 76% |
| 4 Residents | 68% | 72% | 77% |
| 5 Residents | 68% | 73% | 77% |

electricity demand that can be covered by self-produced PV electricity during summer and winter in scenario A. On average, households are able to cover up to 96 % of their daily electricity demand by self-produced PV electricity in the summer, and up to 80 % in the winter. After having

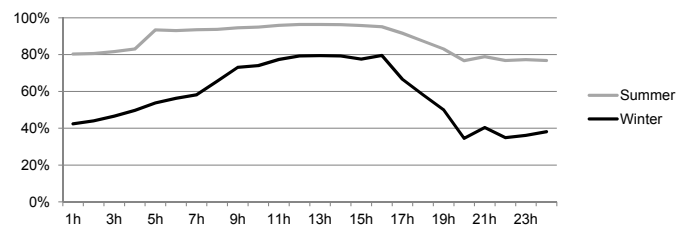


Fig. 6. Average daily residential electricity demand coverage by self-produced PV electricity in Germany in 2030

determined the optimal PV and storage system capacities for each single household, results are scaled to the country level by multiplying the optimal residential capacities with the number of one- and two-family-houses located in Germany, differentiated by the number of residents and the location of the houses (Table V) – based on data from [18] and [19].¹² In total, 82 GW of rooftop PV capacities are installed by 2030 in scenario A – in addition to the 52 GW of PV capacities foreseen in 2020 by Germany's NREAP.

¹²To account for the fact that part of the rooftop potential of one- and two-family-houses will already be used to achieve commitment with Germany's NREAP target for photovoltaic in 2020 (52 GW) only 90 % of the one- and two-family-houses have been used for the upscaling.

TABLE V
NUMBER OF ONE- AND TWO-FAMILY-HOUSES LOCATED IN GERMANY

| | North Germany | Central Germany | South Germany |
|-------------|---------------|-----------------|---------------|
| 1 Resident | 927,873 | 2,019,445 | 130,7012 |
| 2 Residents | 1,401,861 | 2,736,602 | 1,736,486 |
| 3 Residents | 587,329 | 1,129,975 | 714,979 |
| 4 Residents | 545,935 | 1,047,263 | 662,260 |
| 5 Residents | 190,168 | 362,654 | 229,064 |

Storage capacities built in combination with these rooftop PV facilities amount to 65 GWh, corresponding to 160 % of currently installed pump storage capacities in Germany (40 GWh in the year 2010).

As shown in Figure 7 and Figure 8, high shares of in-

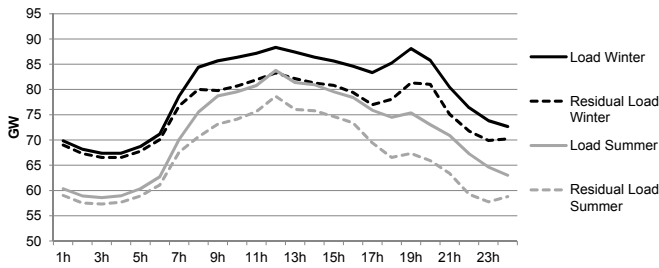


Fig. 7. Average (residual) load on weekdays in the summer and the winter in Germany in 2030

house PV electricity consumption on the single household level cause significant changes in the load supplied by the wholesale electricity market (residual load) in scenario A.¹³ On average, the load supplied by the wholesale electricity market on weekdays decreases by up to 12 % in the summer, and by up to 8 % in the winter due to in-house PV electricity consumption. Interestingly, the highest load reduction on weekdays occurs in the evening hours – due to the in-house consumption of PV electricity that was stored in the battery system during the day. However, since Figure 7 and Figure 8 show the average load reduction on weekdays during summer and wintertime, it cannot be concluded that peak load is reduced. For such a conclusion, specific instances in time would need to be analyzed in detail. This is subject to further research.

The partial optimization of the single households (induced

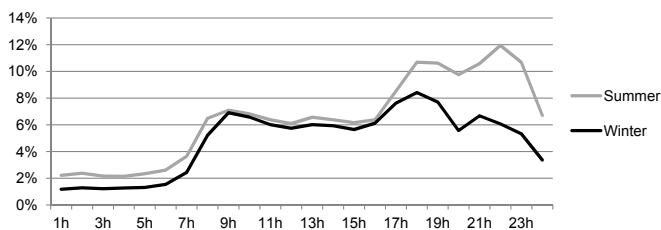


Fig. 8. Average load reduction on weekdays through in-house PV electricity consumption in the summer and the winter in Germany in 2030

by PV grid parity) in scenario A leads to significant excess costs. In comparison to scenario B – which assumes no partial optimization of the single households but instead

¹³In this analysis, the term ‘residual load’ corresponds to Germany’s total electricity demand (load) without the accumulated in-house PV electricity consumption on the household level.

a total system optimization – accumulated and discounted total system costs increase by 7.1 bn €₂₀₁₁ up until 2030. This massive increase in total system costs is caused by the fact that investments in rooftop PV systems and small scale storage technologies (such as lithium-ion batteries) on the single household level do not depict a cost-efficient investment option in Germany before 2030. Instead of rooftop PV and small scale storage systems, wind onshore (plus 7 GW) and gas capacities (plus 9 GW) are deployed in scenario B up until 2030. Furthermore, 11 GW of ground-mounted PV systems are installed as a cost-efficient option in Southern Germany after 2025 in scenario B.¹⁴

IV. CONCLUSIONS

Our model-based analysis has shown that the rapidly growing gap between the residential electricity tariff and the LCOE of PV may lead to considerable investments in rooftop PV systems and storage capacities for in-house PV electricity consumption in Germany up until 2030. Given our scenario assumptions, 82 GW of rooftop PV systems are installed by 2030 in addition to the 52 GW of PV capacities foreseen by the German NREAP for 2020. Accumulated household storage capacities built in combination with these PV facilities amount to 65 GWh, corresponding to 160 % of currently installed pump storage capacities in Germany. The optimal dimensioning of the PV and storage capacities from the single household perspective allows on average 72 % of the household’s annual electricity demand to be covered by self-produced PV electricity.

The single household’s optimization behavior entails direct consequences for the wholesale market, as it changes the residual load both in volume and structure. In terms of volume, residential demand for electricity decreases dramatically, thus leading to significant revenue shortfalls for conventional power plants. In addition, more than half of the total PV electricity generation on the household level is fed into the electricity grid.

Overall, the indirect financial incentive induced by PV grid parity leads to massive excess costs of 7.1 bn €₂₀₁₁ until 2030, due to the fact that rooftop PV and small scale storage systems are not a cost-efficient investment option from a total system perspective until 2030.

Further research will check the robustness of the results by performing sensitivity analyses, specifically with respect to both residential electricity prices and investment costs (of both PV and storage systems). Moreover, specific effects of increased in-house PV electricity consumption will be investigated in more detail, such as the impact of PV generation on peak demand levels or on the future development of the capacity mix. It would be particularly interesting to analyze the consequences of PV grid parity for other EU member states where solar resources as well as electricity pricing systems are different than those in Germany.

ACKNOWLEDGMENT

This research was funded through the Smart Modelling of Optimal Integration of High Penetration of PV (SmoothPV)

¹⁴Note that the ground-mounted PV systems are assumed to have 10 % lower investment costs than roof-mounted PV systems due to economies of scale.

project by the federal state of North-Rhine Westphalia. Responsibility for the contents of this publication lies with authors.

REFERENCES

- [1] BSW Solar. (2012, September) Preisindex Photovoltaik. BSW Solar. [Online]. Available: <http://www.solarwirtschaft.de/preisindex>
- [2] M. Bost, B. Hirschl, and A. Aretz, "Effekte von eigenverbrauch und netzparität bei der photovoltaik - beginn der dezentralen energierevolution oder nischeneffekt," Institut für kologische Wirtschaftsforschung (Auftraggeber: Greenpeace Energy eG, Hamburg), Tech. Rep., 2011.
- [3] BDEW, "Bdew-strompreisanalyse mai 2012 - haushalte und industrie," 2012.
- [4] R. Bhandari and I. Stadler, "Grid parity analysis of solar photovoltaic systems in germany using experience curves," *Solar Energy*, vol. 83, p. 16341644, 2009.
- [5] K. Branker, M. Pathak, and J. Pearce, "A review of solar photovoltaic leveled cost of electricity," *Renewable and Sustainable Energy Reviews*, vol. 15, pp. 4470–4482, 2011.
- [6] C. J. Yang, "Reconsidering solar grid parity," *Energy policy*, vol. 38, pp. 3270–3273, 2010.
- [7] P. Lund, "Boosting new renewable technologies towards grid parity - economic and policy aspects," *Renewable Energy*, vol. 36, pp. 2776–2784, 2011.
- [8] ENTSO-E, "10-Year Network Development Plan 2012," European Network of Transmission System Operators for Electricity, Tech. Rep., 2012.
- [9] I. Richardson, M. Thomson, D. Infield, and C. Clifford, "Domestic electricity use: A high-resolution energy demand model," *Energy and Buildings*, vol. 42, p. 18781887, 2010.
- [10] DESTATIS. (2012, September) Ausstattung privater Haushalte mit elektrischen Haushalts- und sonstigen Geräeten - Deutschland. [Online]. Available: https://www.destatis.de/DE/ZahlenFakten/GesellschaftStaat/EinkommenKonsumLebensbedingungen/AusstattungGebrauchsgueterm/Tabellen/Haushaltsgeraete_D.html
- [11] ——. (2012, September) Ausstattung privater Haushalte mit Informations- und Kommunikationstechnik - Deutschland. [Online]. Available: https://www.destatis.de/DE/ZahlenFakten/GesellschaftStaat/EinkommenKonsumLebensbedingungen/AusstattungGebrauchsgueterm/Tabellen/Infotechnik_D.html
- [12] ——. (2012, September) Ausstattung privater Haushalte mit Unterhaltungselektronik - Deutschland. [Online]. Available: https://www.destatis.de/DE/ZahlenFakten/GesellschaftStaat/EinkommenKonsumLebensbedingungen/AusstattungGebrauchsgueterm/Tabellen/Unterhaltungselektronik_D.htm
- [13] Statistika. (2012, September) Ausstattung mit kleineren Haushaltsgerten. [Online]. Available: <http://de.statista.com/statistik/daten/studie/174770/umfrage/bestand-an-kleineren-haushaltsgeraeten/>
- [14] EuroWind, "Database for hourly wind speeds and solar radiation from 2006-2010 (not public)." EuroWind GmbH, Tech. Rep., 2011.
- [15] J. Richter. (2011) Electricity market model description (Working Paper) Institute of Energy Economics at the University of Cologne.
- [16] M. Frsch, S. Hagspiel, C. Jgemann, S. Nagl, D. Lindenberger, and E. Trster, "The role of grid extensions in a cost-efficient transformation of the European electricity system until 2050," *EWI Working Paper, No. 12/04*, pp. URL <http://www.ewi.uni-koeln.de/publikationen/working-papers/>, 2012.
- [17] A. Jaffe and R. N. Stavins, "The energy efficiency gap. what does it mean?" *Energy Policy*, vol. 22(10), pp. 804–810, 1994.
- [18] DESTATIS, "Haus- und Grundbesitz sowie Wohnverhältnisse privater Haushalte - Fachserie 15 Sonderheft 1," Tech. Rep., 2008, https://www.destatis.de/DE/Publikationen/Thematisch/EinkommenKonsumLebensbedingungen/EinkommenVerbrauch/EVS_HausGrundbesitzprivaterHaushalte2152591089005.xls?__blob=publicationFile.
- [19] ——. "Bestand und Struktur der Wohneinheiten - Fachserie 5 Heft 1 - Mikrozensus-Zusatzerhebung 2010," Tech. Rep., 2010, https://www.destatis.de/DE/Publikationen/Thematisch/EinkommenKonsumLebensbedingungen/Wohnen/WohnsituationHaushalte2055001109005.xls?__blob=publicationFile.

Cost-optimal Power System Extension Under Flow-based Market Coupling and High Shares of Photovoltaics

Simeon Hagspiel, Cosima Jägemann, Dietmar Lindenberger
 Institute of Energy Economics, University of Cologne
 Vogelsanger Strasse 321, 50827 Cologne, Germany
 Email: simeon.hagspiel@ewi.uni-koeln.de

Stanislav Cherevatskiy, Eckehard Tröster, Tom Brown
 Energynautics GmbH
 Mühlstraße 21, 63225 Langen, Germany
 Email: s.cherevatskiy@energynautics.com

Abstract—Electricity market models, implemented as dynamic programming problems, have been applied widely to identify possible pathways towards a cost-optimal and low carbon electricity system. However, the joint optimization of generation and transmission remains challenging, mainly due to the fact that different characteristics and rules apply to commercial and physical exchanges of electricity in meshed networks. This paper presents a methodology that allows to optimize power generation and transmission infrastructures jointly through an iterative approach based on power transfer distribution factors (PTDFs). As PTDFs are linear representations of the physical load flow equations, they can be implemented in a linear programming environment suitable for large scale problems such as the European power system. The algorithm iteratively updates PTDFs when grid infrastructures are modified due to cost-optimal extension and thus yields an optimal solution with a consistent representation of physical load flows. The method is demonstrated on a simplified three-node model where it is found to be stable and convergent. It is then scaled to the European level in order to find the optimal power system infrastructure development under the prescription of strongly decreasing CO₂ emissions in Europe until 2050 with a specific focus on photovoltaic (PV) power.

I. INTRODUCTION

Motivated by ambitious emission reduction and renewable energy integration targets, the European power system is expected to undergo substantial changes. Electricity market models, implemented as a dynamic programming problem, have been applied widely to identify possible pathways. However, these models mostly lack an appropriate representation of the physical grid which represents the backbone of today's power system. Specifically, a joint optimization of generation and transmission is difficult, mainly due to the fact that different characteristics and rules apply to commercial and physical exchanges of electricity in meshed networks.

This is specifically true when dealing with an intermeshed alternating current (AC) transmission network as the European power system. According to Kirchhoff's circuit law, multiple paths are taken by the physical flows when settling trades from one point to another via the intermeshed grid (so

called loop flows), such that a large number of lines may be impacted.

Many studies have dealt with the problem of transmission system expansion. Comprehensive literature surveys for the general problem of transmission system expansion and corresponding modelling issues are provided in [1], [2]. As stated in [1], the problem comprises economic and engineering considerations, which can easily be confirmed when analysing the corresponding fields of research.

From an engineering perspective, early approaches to transmission system expansion can be found in [3] or [4] that both formulate linear load flow equations in order to find overloaded lines, however only considering snapshots of the future power system. Besides linear programming, later works also deploy various other optimization methods, such as non-linear programming, mixed-integer programming or artificial intelligence methods [5].

The second stream of analysing transmission system extensions is mostly based on economic considerations: In [6] the analytical model uses PTDF in order to integrate loop flows that were previously found to have a significant impact on the efficiency of the market outcome in meshed networks [7]. They assume an invariant PTDF matrix and furthermore do not address social welfare effects. A very similar modelling framework is applied in [8] to analyse an incentive mechanism for transmission expansion with a profit-maximizing transmission system company and a competitive wholesale market based on nodal pricing, and in [9] to specifically analyse the impact of different cost functions.

This paper presents a methodology that couples an electricity market model with a power flow model to jointly optimize both power generation and transmission grid infrastructures under flow-based market coupling using an iterative approach based on power transfer distribution factors (PTDFs). The objective of the proposed method is to find the overall cost-optimal solution for serving electricity to the consumers, and thus to optimize social welfare. PTDFs are linear representations of the load flow equations which

can be used to calculate physical active power flows in the power network given market transactions. As such, they can be implemented in a linear programming environment determining the cost-optimal development of power system infrastructures under certain restrictions. However, a set of given PTDFs is only valid as long as certain criteria are met, such as no reactive power flows and no losses. Furthermore the PTDFs change with each change of grid configuration, so we suggest a method whereby the PTDFs are updated and fed back every time the grid is modified. The method is demonstrated on a simplified three-node model where the iterative optimization algorithm is found to be stable and convergent.

The paper then provides an outlook on a large-scale application that is currently being implemented in order to find the optimal power system infrastructure development under the prescription of strongly decreasing CO₂ emissions in Europe until 2050 with a specific focus on photovoltaic (PV) power. The following two main questions shall be answered within this framework:

- What does a cost-optimized European power system (both generation and grid) look like in 2030 (medium term) and 2050 (long term)?
- How does an optimized grid extension help to cost-optimally deploy power from photovoltaic (PV) installations in Europe?

The results of this large-scale application will be published in a separate paper.

The remainder of the paper is structured as follows: Section II presents the methodology developed to jointly optimize power generation and transmission grid infrastructures in an iterative manner based on PTDFs. The algorithm is applied to a simple three node network in Section III. Section IV presents an outlook on the modelling framework of the large-scale application to the European power system with large shares of photovoltaics. Section V concludes.

II. METHODOLOGY

This section is subdivided into two parts. First, starting from the most general formulation of the load flow equations in an intermeshed AC grid, a linear PTDF representation is derived suitable for being integrated in a large scale linear optimization problem. Then, a model is presented focusing on the problem of integrating load flow calculations in an economic optimization framework with the objective to find the cost-optimal grid infrastructure in a multi-node network with different load and generation characteristics.

A. Load flow equations and PTDF representation

As noted in most electrical engineering books (e.g. refer to [10]), the most general form of the network equations in

an AC power system can be written as follows:

$$\begin{aligned} P_i &= U_i \sum_{j \in I} U_j (g_{ij} \cos(\delta_i - \delta_j) + b_{ij} \sin(\delta_i - \delta_j)) \\ Q_i &= U_i \sum_{j \in I} U_j (g_{ij} \sin(\delta_i - \delta_j) - b_{ij} \cos(\delta_i - \delta_j)) \\ P_{ij} &= U_i^2 g_{ij} - U_i U_j g_{ij} \cos(\delta_i - \delta_j) - U_i U_j b_{ij} \sin(\delta_i - \delta_j) \\ Q_{ij} &= -U_i^2 (b_{ij} + b_{ij}^{sh}) + U_i U_j b_{ij} \cos(\delta_i - \delta_j) \\ &\quad - U_i U_j g_{ij} \sin(\delta_i - \delta_j) \end{aligned} \quad (1)$$

In the above equations, P_i and Q_i represent the active and reactive power injected at node i , whereas P_{ij} and Q_{ij} stand for the active and reactive power flow on line ij connecting node i and j , respectively. I is the set of nodes the network consists of. As can be seen, voltage levels U and phase angles δ of the nodes as well as series conductances g and series susceptances b of the transmission lines are determining active and reactive power flows.

There are two well-known algorithms to solve this set of equations, namely the Gauss-Seidel and the Newton-Raphson methods [10]. These algorithms are capable of dealing with the non-linearities in the above equations. Noticeably, both methods are iterative and need an initial guess for all unknown variables. For the purpose of implementing load flow calculations in a linear optimization environment, as presented in this paper, a linear representation of the above equations has to be found. To this end, the following assumptions can be made:

- All voltages are set to 1 p.u., meaning that there is no voltage drop.
- Reactive power is neglected, i.e. Q_i and Q_{ij} is set to zero.
- Losses are neglected, and line reactance is by far larger than the resistance: $X \gg R \approx 0$.
- Voltage angle differences are small, such that $\sin(\delta_i - \delta_j) \approx \delta_i - \delta_j$.

By making these assumptions, the AC load flow equations can be simplified to a linear relationship:

$$P_{ij} = b_{ij}(\delta_i - \delta_j) = \frac{x_{ij}}{x_{ij}^2 + R_{ij}^2}(\delta_i - \delta_j) \approx \frac{1}{x_{ij}}(\delta_i - \delta_j) \quad (2)$$

According to Kirchoff's power law, the active power injection at bus i is then given by

$$P_i = \sum_{j \in \Omega_i} \frac{1}{x_{ij}}(\delta_i - \delta_j) = \left(\sum_{j \in \Omega_i} \frac{1}{x_{ij}} \right) \delta_i + \sum_{j \in \Omega_i} \left(-\frac{\delta_j}{x_{ij}} \right) \quad (3)$$

with Ω_i being the set of buses adjacent to i . For a system with multiple (N) branches, (3) can be written in matrix form as

$$\mathbf{P}_{nodal} = \mathbf{B} \cdot \boldsymbol{\Theta} \quad (4)$$

where \mathbf{P}_{nodal} is the vector containing the net active power injections P_i , $\boldsymbol{\Theta}$ the vector of phase angles and \mathbf{B} is the nodal admittance matrix with the following entries:

$$B_{ij} = -\frac{1}{x_{ij}} \quad (5)$$

$$B_{ii} = \sum_{j \in \Omega_i} \frac{1}{x_{ij}} \quad (6)$$

Due to the fact that \mathbf{B} is singular, the row and column belonging to the reference bus is deleted (thus assuming a zero reference angle at this bus). The resulting vectors and matrix are named \mathbf{B}' , $\mathbf{\Theta}'$ and \mathbf{P}'_{nodal} . We can now solve (4) for $\mathbf{\Theta}'$:

$$\mathbf{\Theta}' = \mathbf{B}'^{-1} \cdot \mathbf{P}'_{nodal} \quad (7)$$

Next, we consider the dependency between the load flow on line ij and the phase angle over the same line according to 2 and find the matrix representation to be:

$$\mathbf{P}_{branch} = \mathbf{H} \cdot \mathbf{\Theta}' \quad (8)$$

with \mathbf{P}_{branch} the vector of the net active power flows P_{ij} and $H_{ki} = 1/x_{ij}$, $H_{kj} = -1/x_{ij}$ and $H_{km} = 0$ for $m \neq i, j$ (note that k runs over the branches ij). $\mathbf{\Theta}'$ can then be inserted in (8) to give:

$$\mathbf{P}_{branch} = \mathbf{H} \cdot \mathbf{\Theta}' = \mathbf{H} \cdot \mathbf{B}'^{-1} \cdot \mathbf{P}'_{nodal} = \mathbf{PTDF} \cdot \mathbf{P}'_{nodal} \quad (9)$$

The elements of \mathbf{PTDF} are the power transfer distribution factors, constituting the linear relationship between the load flows on the lines and nodal power balances.

In the next step, a market model will be introduced that simulates the dispatch of different power plants in different market regions and thus nodal power balances in a cost-minimizing manner. Power flows can then be calculated using the PTDF approach that was introduced in this section, and an additional restriction ensures that line flows stay below thermal limits. Furthermore, the model will be implemented such that thermal limits (i.e. transmission capacity) can be increased when contributing to the cost-optimal solution.

B. Model for the cost optimal expansion of grid infrastructures

The goal of the study presented in this paper is to determine the cost-optimal extension of AC and DC grid infrastructures. To this end, the above deduced linear power flow representation can be embedded in an electricity market model. Herein, an exogenously given demand shall be supplied at least cost by the various technological options of generation and transmission. Market models are commonly modeled as linear optimization problem which is well suited for most applications, especially when large systems with high technological, spatial and temporal resolution shall be analysed. With the methodology deduced in the previous section, load flow calculations and grid extensions can explicitly be included in such a linear program.

Moreover, the methodology presented in this section is also able to account for possible DC grid extensions. Compared to the AC system, flows on the DC lines are easier to deal with due to the fact that all lines are assumed to be point-to-point connections that are equipped with converter stations. This technical equipment makes it possible to perfectly control the flows on the corresponding line, such that trades can directly be settled via those lines (in other words, trades directly translate into physical flows).

Suppose that the level of demand in market i at time t , D_i^t is an exogenous parameter entering the optimization problem. The power that can be generated in market i at

time t by technology a at costs of $c_{i,a}^t$ is denoted by $G_{i,a}^t$. Furthermore, transmission capacities between i and j are denoted in vector-form by \mathbf{P}_{max} and can be built up at costs of λ . All quantities are possibly different with respect to space and time.

Within this framework, the following linear program formalizes the optimization problem for the cost-efficient supply of electricity including generation as well as AC and DC transmission expansion.

$$\min C_{tot} = \sum_{i \in I} \sum_{a \in A} \sum_{t \in T} G_{i,a,t} c_{i,a,t} + \lambda^{AC} \cdot \mathbf{P}_{max}^{AC} + \lambda^{DC} \cdot \mathbf{P}_{max}^{DC} \quad (10)$$

s.t.

$$\sum_{a \in A} G_{i,a,t} + \sum_{j \in J} T_{j,i,t} = D_{i,t} \quad (11)$$

$$T_{i,j} = T_{i,j}^{AC} + T_{i,j}^{DC} \quad (12)$$

$$\mathbf{P}^{AC} = \mathbf{PTDF} \cdot \mathbf{T}^{AC} \quad (13)$$

$$\mathbf{P}^{DC} = \mathbf{T}^{DC} \quad (14)$$

$$-\mathbf{P}_{max}^{AC} \leq \mathbf{P}^{AC} \leq \mathbf{P}_{max}^{AC} \quad (15)$$

$$-\mathbf{P}_{max}^{DC} \leq \mathbf{P}^{DC} \leq \mathbf{P}_{max}^{DC} \quad (16)$$

(10), being the objective function, states that total costs for electricity supply shall be minimized. Costs arise from producing electricity on the one hand and costs related to transmission grid extensions on the other (note that for the sake of simplicity the expansion of generation capacity is not included at this stage. This condition can easily be relaxed, as done in the large-scale application presented in Section IV). The equilibrium condition (11) ensures that supply equals demand in each market region i at every instant in time t . Electricity can be supplied either by generation in the local market or by imports from other markets. Trades can be settled via AC or DC grid infrastructures, as stated in (12). Once trade flows are set, the resulting physical flows can be calculated: For the AC grid, we use the methodology based on PTDFs as introduced in section II-A and recaptured in (13). For the DC grid, trades directly translate into physical flows (14). The last two Equations (15) and (16) restrict the resulting flows to the line capacities \mathbf{P}_{max} that are currently installed. Line capacities in turn are subject to optimization.

As shown in section II-A, the PTDF matrix depends on the physical characteristics of the AC grid, especially on line reactances. When AC grid capacities change, the PTDF matrix will also change. Thus, whenever the optimal solution includes increasing line capacities, the underlying PTDF matrix that was used to deduce the optimum is no longer a valid one for the resulting system. Consequently, a new PTDF matrix is calculated based on the new grid infrastructure, and updated within the above optimization problem. The problem therefore has to be solved iteratively while updating the PTDF matrix every time the market model has found an optimal solution. A schematic representation of the resulting process is shown in Figure 1.

Note that an alternative approach to the process described in Figure 1 would be the calculation of the PTDF matrix directly in the market model according to (9). However, as the elements of \mathbf{PTDF} depend on the line capacities

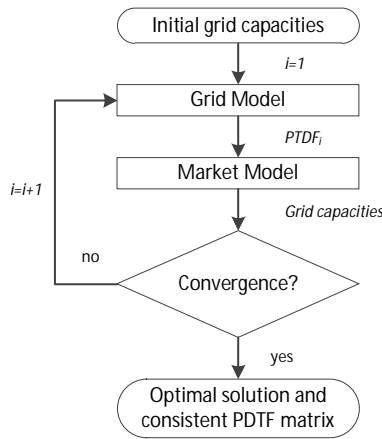


Fig. 1. Schematic representation of the iterative process

P_{max}^{AC} , this would make (13) non-linear and the optimization problem difficult to solve, especially in large-scale applications. In fact, there are very effective methods for solving linear programming problems, such as the Simplex algorithm (see e.g. [11], [12]), whereas algorithms for non-linear optimization problems are either inefficient or only find a local instead of the global optimum (see e.g. [13]).

III. THREE NODE NETWORK

In this section the methodology developed in Section II shall be applied to a simple example. A three node network was chosen as this is the easiest setting for which loop flows play a role.

With a given demand as well as fixed available generation capacities and costs, the cost-optimal solution for a full electricity supply shall be found that potentially involves transmission grid extensions.

A. Setting of the three node network example

The setting of the three node network considered in this part of the analysis is shown in Figure 2.

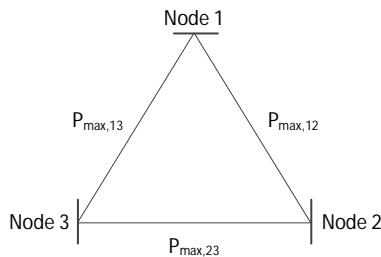


Fig. 2. Three-node network considered in this section

With (9), the transaction-based PTDF matrix for this network can be calculated as in the following equation. Each entry of the matrix is labeled with the corresponding transaction $T_{i,j}$ and impact on line $L_{i,j}$ in order to facilitate reading.

$$PTDF = \frac{1}{x_{12} + x_{13} + x_{23}} \begin{bmatrix} L_{13} & T_{13} & T_{23} & T_{12} \\ L_{12} & x_{12} + x_{23} & x_{23} & x_{12} \\ L_{23} & x_{13} & -x_{23} & x_{13} + x_{23} \\ & x_{13} & x_{13} + x_{12} & -x_{12} \end{bmatrix} \quad (17)$$

As in [6], we assume additional line capacity is added in parallel, such that the reactances' dependency on line capacity takes the following form:

$$x_{ij} = \frac{x_{ij,0}}{P_{max,ij}/P_{ij,0}}. \quad (18)$$

Note that the algorithm needs a starting point for the iteration. Starting from an initial guess for line capacities and corresponding line reactances the algorithm iteratively searches for optimal grid capacities while updating line reactances according to (18).

We assume different generation and load levels at each node that are exogenous and constant. We then consider a 10 year planning horizon for which the grid shall be optimized. Generation costs at node 1 and 2 are 20 Eur/MWh or 1.752 Mio. Eur per MW supplied for 10 years, and 15 Eur/MWh or 1.314 Mio. Eur/(MW*10a) at node 3. Costs for grid upgrades amount to 1000 Eur per MW and km, with distances of 300 km between all nodes. Furthermore we assume that for security reasons a minimum of 50 MW shall be built on each line which adds an additional restriction to the optimization problem formulated in Equations 10 to 16.

Table I summarizes load level P_{load} , available generation capacity P_{gen} and generation costs C_{gen} at each of the three nodes, as well as the costs for grid upgrades.

TABLE I
ASSUMPTIONS FOR THE THREE NODE NETWORK EXAMPLE

| Parameter | Unit | Node 1 | Node 2 | Node 3 |
|-----------------|------------------|----------|----------|----------|
| P_{load} | MW | 800 | 300 | 200 |
| P_{gen} | MW | 300 | 300 | 800 |
| C_{gen} | Mio.Eur/(MW*10a) | 1.752 | 1.752 | 1.314 |
| | | Line 1-2 | Line 1-3 | Line 2-3 |
| C_{tran}^{AC} | Mio.Eur/MW | 0.3 | 0.3 | 0.3 |
| C_{tran}^{DC} | Mio.Eur/MW | 1.5 | 1.5 | 1.5 |

B. Results of the three node network example

Based on the assumptions listed in the previous Section we run the model as it was presented in Section II in order to determine necessary grid extensions when all three nodes shall be connected through an AC and/or DC transmission grid. The results are presented in Figures 3 to 5 that capture all endogenous system properties that are subject to change when running the iterative simulation. Noticeably, in this example DC grid extensions are not part of the optimal solution due to higher investment costs compared to AC transmission grids.

For the initial guess all line capacities and reactances were set to 100 MW and 1 Ohm, respectively. Consequently, a power transfer of x from Node A to B results in power flows of $2/3*x$ on line A-B and $1/3*x$ on lines A-C and C-B. Node 1 is lacking 500 MW of power generation that needs to be imported from outside. Due to lower generation costs and availability, the missing 500 MW are supplied by Node 3. Transmission lines are extended such that these 500 MW can be transported from Node 3 to Node 1, hence $2/3*500$ MW flow on line 1-3 and $1/3*500$ MW via node 2 (i.e. on line 1-2 and line 2-3). Furthermore, the optimal solution includes the usage of the full capacity available at lower costs in Node 3.

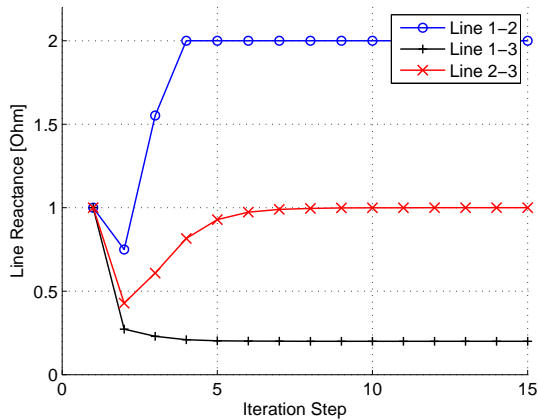


Fig. 3. Development of transmission line reactances during the iteration

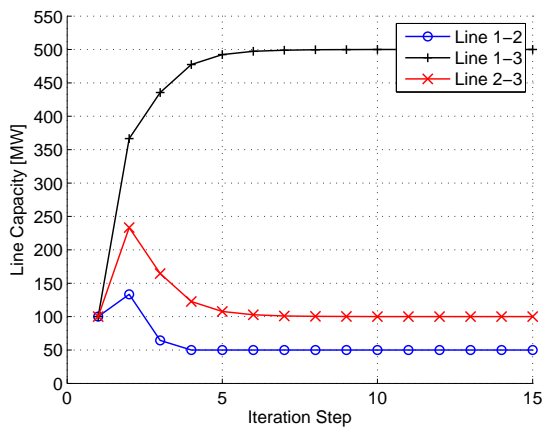


Fig. 4. Development of transmission line capacities during the iteration

The inherent advantage is that the flows on line 1-2 resulting from the trade between nodes 3 and 2 counteract the flow from 3 to 1 via 2, thus leading to a situation where less grid extensions are needed on this particular line. Necessary grid extensions in iteration step 1 then amount to 133 1/3 MW on line 1-2, 366 2/3 MW on line 1-3 and 233 1/3 on line 2-3. Total costs sum up to 2.1472 Mio. Euros.

In the next iteration step, line reactances are updated according to (18) and previously optimized line capacities, thus changing the PTDFs, power flows and optimized line capacities. As can be seen in Figure 4, necessary upgrades on line 1-3 further increase. This is caused by the following sequence of events: capacity extension on this line is highest, and therefore, line reactance decreases the furthest. As more power flows on lines with low reactance, larger transmission capacities are needed on line 1-3 in order to handle the increasing power flows. Following the same logic, necessary transmission capacities on lines 1-2 and 2-3 decrease. Noticeably, as only one line is affected by increasing transmission capacities whereas the capacities of two lines are reduced, total system costs are lowered during the iteration as can be observed in Figure 5. The reactance of line 1-2 increases sharply in the third iteration step since only moderate capacity upgrades were found to be cost-optimal. During the next iterations, capacity of line 1-2 further

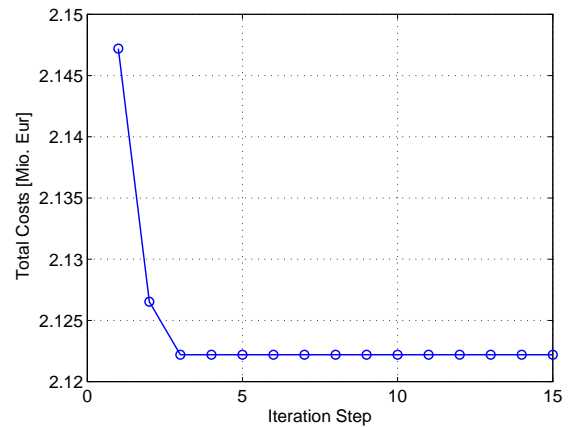


Fig. 5. Development of total system costs during the iteration

decreases and rapidly approaches the minimum extension capacity of 50 MW with corresponding line reactance of 2 Ohm.

During the iterative process, all endogenous system properties reach stable levels after only a few iteration steps. Optimized line capacities, for instance, change by less than 0.1% after iteration step 10.

IV. LARGE-SCALE APPLICATION

This section presents an outlook on further work that applies the previously developed method to a large-scale problem. Specifically, an electricity market model and a power flow model both covering the European power system are coupled via PTDFs in order to find the optimal power system infrastructure development under the prescription of strongly decreasing CO₂ emissions in Europe until 2050 with a specific focus on photovoltaic (PV) power. The following two main questions shall be answered within this framework:

- What does a cost-optimized European power system (both generation and grid) look like in 2030 (medium term) and 2050 (long term)?
- How does an optimized grid extension help to cost-optimally deploy power from PV installations in Europe?

The two models are introduced in Sections IV-B and IV-A, whereas the iteration between them is described in Section IV-C. Please note that the results of the large-scale application are still being finalized and will be published in a separate paper.

A. Power flow model

To analyse the power flows in the European transmission network, a detailed model of the high voltage grid is used. This model was developed with DIGSILENT's power system calculation tool PowerFactory and covers all ENTSO-E members. It consists of a total of over 200 nodes, representing generation and load centers within Europe, 450 high voltage AC (HVAC) lines and all the high voltage DC (HVDC) lines within the ENTSO-E area. The grid model is built for AC load flow calculations and thus can be used not just for active power flows, but also to calculate losses

within the network, reactive power flows and the necessary compensation to maintain network stability.

As a starting point for the iterations two versions of the grid model were prepared: one representing the European grid as it was in 2011 and another for the predicted state of the network in 2020. For the future projection, it was assumed that all projects in mid-term planning from ENTSO-E's Ten Year Network Development Plan will be built. In total 82GVA of extra capacity was added for new HVAC lines and 13GVA for new HVDC lines between 2011 and 2020.

Whereas in the market model all the load and generation is aggregated for each market region (i.e. assuming a copper plate with no internal power transfers), the grid model consists of multiple nodes per market region.¹ The distribution of demand and generation assets across the nodes within each market region are set using allocation keys, which are based on factors such as population density, siting of heavy industry, location of thermal power plants and the availability of renewable energy resources.

The network and distribution keys were validated by comparing cross-border flows in the model against publicly available data from ENTSO-E, after which the impedances and allocation keys were optimized to ensure good agreement across several snapshots of the network.

In 2011 and 2020 the majority of DC lines lie between the different synchronous zones of the ENTSO-E area, such as the undersea connection between France and Great Britain. To allow the economic model the choice of extending the HVDC network, an Overlay Network of DC lines was constructed for 2030 and 2050 with DC connections permitted between all neighboring market regions, including those within the same AC network. To take account of the effect of DC transfers on the AC grid, a PTDF for DC transactions was calculated, in addition to the AC PTDF for transactions inside the AC network. This DC PTDF linearizes the effect of DC transfers on the AC network, capturing for example the power flows to and from the DC connection points.

An additional challenge was presented by the fact that each market region spans several nodes within the grid model. To accurately capture the flows between the nodes inside each region, which change depending on the dispatch of generation technologies at any given time, the node allocation keys (K) were directly incorporated into the PTDF. In this way the nodal power balances within the model can be determined for any dispatch situation, with the power flows then following directly from the usual PTDF. Thus (13) is reformulated as follows:

$$P^{AC} = PTDF \cdot (K^D \cdot D - K^G \cdot G - K^{DC} \cdot T^{DC}) \quad (19)$$

B. Electricity market model

The market model used in this analysis is an extended version of the long term investment and dispatch model for conventional, renewable, storage and transmission technologies as presented in [14]. It covers 29 countries (EU27

¹Note that this could be overcome by simulating a nodal pricing regime where each node of the transmission grid is its own market region. However, this would call for a market model that is even more complex than the one that is currently used and could thus not be solved in a reasonable time.

plus Norway and Switzerland) at an aggregated level (i.e. 18 market regions).²

The model determines possible paths of how the installed capacities will develop and how they are operated until 2050 under different assumptions, assuming that the European markets will achieve the cost-minimizing mix of different technologies - a market result that is set in full competition. The objective of the model is thus to minimize accumulated discounted total system costs while being subject to several techno-economic restrictions, such as the hourly matching of supply and demand, fuel availabilities or potential space for renewable energies, and politically implied restrictions, such as an EU-wide CO₂ emission reduction target or limited nuclear power deployment. The dispatch is calculated for eight typical days per year on an hourly basis (scaled to 8760 hours), representing variations in electricity demand as well as in solar and wind resources along with their multivariate interdependencies. Extreme events that particularly stress the power system, e.g. periods of low wind and high demand, are also covered. To account for local weather conditions, the model considers several wind and solar power regions (subregions) within market regions based on hourly meteorological wind speed and solar radiation data [15]. For the study presented in this paper, the grid optimization has been implemented in the electricity market model as in equations (10) to (16) and (19).

An important assumption concerns the congestion management, i.e. the restriction of electricity transactions between market regions: As opposed to NTC-based market coupling which is still the predominant method for congestion management in the European power system, our calculations are all based on a flow-based market coupling regime. The reason for this is two-fold:

- Flow-based market coupling is implemented in the market model in order to optimize thermal limits of the transmission grid directly and without having to calculate Net Transfer Capacities (NTC) every time the grid infrastructure is changed. This results in a clearly defined interface between the market model and the power flow model, namely the PTDF matrix.
- Previous studies have shown that flow-based market coupling increases market efficiency, and should thus be chosen in order to determine the cost-efficient electricity supply while optimizing social welfare.³

C. Iteration between the models

Years of reference included in the analysis are 2011, 2020, 2030, 2050. As described in Section II, the interface for the power system optimization is the PTDF matrix. It is initially calculated from the flow model for the years 2011 and 2020 for which the grid infrastructure is not optimized; we argue that for the year 2020 optimized grid extensions would not be realistic within this timeframe, due to long planning and

²The aggregation was done due to very long computational times

³For a general discussion of flow-based transmission rights and congestion management see [16]. Analyses of different congestion management regimes in the European power system and possible increases in market efficiency were published in [17], [18], [19], [20], [21]. Practical feasibility of the concept is currently proven in the Central Western European (CWE) Region, as discussed in [22].

permission procedures of such projects. For the year 2011, the model represents current line capacities while for 2020 a number of mid-term grid extensions are included as reported in the Ten Year Network Development Plan (TYNDP) [23].

For later years, however, optimal grid extensions are allowed leading to variations in line capacities. These extensions alter the impedances within the network model, which in turn change the PTDF. Since the way the PTDF changes is non-linear, it cannot be incorporated directly into the linear optimization problem, so instead the PTDF is updated iteratively until it converges on the optimal consistent solution. As a starting point for the 2030 and 2050 networks, the 2020 PTDF is used. Note that in the electricity market model, generation capacities are optimized starting from 2011.

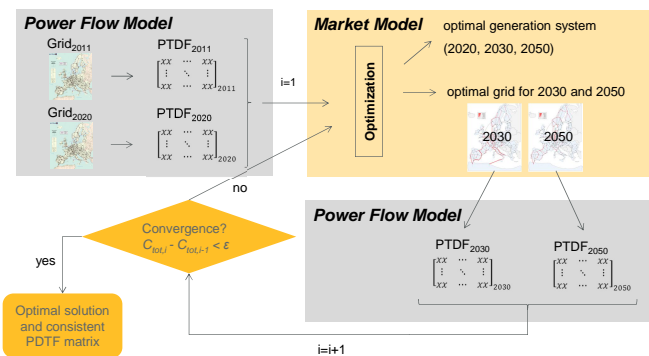


Fig. 6. Iteration between the market and the power flow model of the European power system

V. CONCLUSIONS

Joint optimization of generation and transmission is an extremely important yet difficult task, mainly due to the fact that different characteristics and rules apply to commercial and physical exchanges of electricity in meshed networks. In this paper a method is developed based on an iterative PTDF calculation that is suitable for determining the cost-optimal extension of large-scale power systems - such as the European interconnected network - including generation as well as grid facilities. An interface is implemented based on PTDF matrices that couples market and grid models and combines the inherent advantages of both model types. Specifically, the algorithm is formulated as a linear optimization problem that can be solved efficiently. It is tested for a simple three node network where it is found to be stable and convergent.

The method is currently implemented for a large-scale case study to find an optimal power system infrastructure development under the prescription of large shares of photovoltaics in Europe until 2050 by using a linear European Electricity Market Model and a European Transmission Network Model. Within this framework, it is analysed how the cost-optimal European power system develops until 2030 (medium term) and 2050 (long term), and how enhanced grid extensions help to cost-optimally deploy power from photovoltaic (PV) installations in Europe. First results indicate that - as expected - without grid extensions electricity needs to be supplied more locally. However, the costs savings

enabled by optimal grid extensions is not as pronounced due to strongly decreasing costs of renewable energy technologies that diminish the importance of local resource quality (namely wind and solar radiation). Furthermore, it can be observed that large-scale PV deployment calls for storage devices in order to balance out the diurnal variations.

The approach presented in this paper could be further developed in various directions, specifically with respect to the market model that could be formulated as a different class of optimization problem. The most interesting ones would be:

- A mixed integer problem in order to formulate that only multiples of available line configurations can be added.
- A non-linear optimization problem in order to avoid the iteration.
- Further spatial disaggregation towards a nodal-pricing regime in order to overcome the difficulty of having an unequal number of nodes in the power flow and market model.

Furthermore, it could be analysed numerically how gains in social welfare can be created when switching from NTC to flow-based market coupling all over Europe.

ACKNOWLEDGMENT

This research was funded through the Smart Modelling of Optimal Integration of High Penetration of PV (SmoothPV) project with grant number 0325272 by the German Federal Ministry for the Environment, Nature Conservation and Nuclear Safety and by the federal state of North-Rhine Westphalia. Responsibility for the contents of this publication lies with authors.

REFERENCES

- [1] F. Wu, F. Zheng, and F. Wen, "Transmission investment and expansion planning in a restructured electricity market," *Energy*, vol. 31, pp. 954–966, 2006.
- [2] M. Groschke, A. Eßer, D. Möst, and W. Fichtner, "Neue Anforderungen an optimierende Energiesystemmodelle für die Kraftwerkseinsatz- und Zubauplanung bei begrenzten Netzkapazitäten," *ZfE Zeitschrift für Energiewirtschaft*, vol. 33, pp. 14–22, 2009.
- [3] L. L. Garver, "Transmission network estimation using linear programming," *IEEE Transactions on Power Apparatus and Systems*, vol. 89, pp. 1688–1697, 1970.
- [4] R. Villasana, L. Garver, and S. Salon, "Transmission network planning using linear programming," *IEEE Transactions on Power Apparatus and Systems*, vol. 104, pp. 349–356, 1985.
- [5] G. Latorre, "Classification of publications and models on transmission expansion planning," *IEEE Transactions on Power Systems*, vol. 18, pp. 938–946, 2003.
- [6] W. Hogan, J. Rosellón, and I. Vogelsang, "Toward a combined merchant-regulatory mechanism for electricity transmission expansion," *Journal of Regulatory Economics*, vol. 38, pp. 113–143, 2010.
- [7] J. B. Bushnell and S. E. Stoft, "Improving private incentives for electric grid investment," *Resource and Energy Economics*, vol. 19, pp. 85–108, 1997.
- [8] J. Rosellón and H. Weigt, "A dynamic incentive mechanism for transmission expansion in electricity networks - theory, modeling and application," *The Energy Journal*, vol. 32, pp. 119–148, 2011.
- [9] J. Rosellón, I. Vogelsang, and H. Weigt, "Long-run cost functions for electricity transmission," *The Energy Journal*, vol. 33, pp. 131–160, 2012.
- [10] G. Andersson, *Power System Analysis*. Eidgenössische Technische Hochschule Zürich (ETH), 2011.
- [11] K. G. Murty, *Linear Programming*. John Wiley & Sons, 1983.
- [12] M. J. Todd, "The many facets of linear programming," *Mathematical Programming*, vol. 91, pp. 417–436, 2002.

- [13] S. P. Boyd, *Convex Optimization*. Cambridge University Press, New, 2004.
- [14] J. Richter. (2011) Electricity market model description (Working Paper) Institute of Energy Economics at the University of Cologne.
- [15] EuroWind, "Database for hourly wind speeds and solar radiation from 2006-2010 (not public)." EuroWind GmbH, Tech. Rep., 2011.
- [16] H.-P. Chao, S. Peck, S. Oren, and R. Wilson, "Flow-based transmission rights and congestion management," *The Electricity Journal*, vol. 13, pp. 38–58, 2000.
- [17] A. Ehrenmann and Y. Smeers, "Inefficiencies in european congestion management proposals," *Utilities Policy*, vol. 13, pp. 135–152, 2005.
- [18] C. Jullien, V. Pignon, S. Robin, and C. Staropoli, "Coordinating cross-border congestion management through auctions: An experimental approach to european solutions," *Energy Economics*, vol. 34, pp. 1–13, 2012.
- [19] K. Neuhoff, R. Boyd, T. Grau, J. Barquin, F. Echabarren, J. Bialek, C. Dent, C. von Hirschhausen, B. F. Hobbs, F. Kunz, H. Weigt, C. Nabe, G. Papaefthymiou, and C. Weber. (2011) Renewable electric energy integration - quantifying the value of design of markets for international transmission capacity. Deutsches Institut für Wirtschaftsforschung (DIW).
- [20] K. Neuhoff, B. F. Hobbs, and D. Newbery. (2011) Congestion management in european power networks - criteria to assess the available options. Deutsches Institut für Wirtschaftsforschung (DIW).
- [21] Consentec, Frontier Economics, Institute of Power Systems and Power Economics (RWTH Aachen), "Analysis of cross-border congestion management methods for the european internal electricity market," Consentec, Frontier Economics, Institute of Power Systems and Power Economics (RWTH Aachen), Tech. Rep., 2004.
- [22] M. Aguado, R. Bourgeois, J. Bourmaud, J. V. Casteren, M. Ceratto, M. Jäkel, B. Malfliet, C. Mestda, P. Noury, M. Pool, W. van den Reek, M. Rohleder, P. Schavemaker, S. Scolari, O. Weis, and J. Wolpert. (2012) Flow-based market coupling in the central western european region - on the eve of implementation. Cigre.
- [23] ENTSO-E, "Ten Year Network Development Plan 2012," European Network of Transmission System Operators for Electricity (ENTSO-E), Tech. Rep., 2012.

Development of Tools for DER Components in a Distribution Network

L. Mihet-Popa, C. Koch-Ciobotaru, F. Isleifsson and H. Bindner

Abstract – The increasing amount of Distributed Energy Resources (DER) components into distribution networks involves the development of accurate simulation models that take into account an increasing number of factors that influence the output power from the DG systems. This paper presents two simulation models: a PV system model using the single-diode four-parameter model based on data sheet values and a Vanadium Redox Battery (VRB) system model based on the efficiency of different components and the power losses. The unit models were implemented first in MATLAB/Simulink and the simulation results have been compared with the data sheet values and with the characteristics of the units. To point out the strong dependency on ambient conditions and to validate the simulation models a complex data processing subsystem model has also been developed. A PV and a VRB inverter models have also been developed and implemented in PowerFactory to study load flow, steady-state voltage stability and dynamic behavior of a distribution system.

Index Terms—distributed energy resources-DER; distributed generation-DG; incidence and tilt angle; micro-grid; PV panels; solar radiation; state of charge (SOC);vanadium redox battery-VRB;

I. NOMENCLATURE

A : diode quality factor; G_a : solar irradiance; I_0 , I_{sc} : open circuit and short circuit currents; I_{mpp} , P_{mpp} , V_{mpp} : maximum power point of current, power and voltage; NOCT: nominal operating conditions; n_{ps} , n_s , n_{sp} : no. of panels in series, no of cells in series in one panel and no. of strings in parallel; R_s : series resistance; T_a , T_{cell} : ambient and cell temperature; V_{oc} , V_T : open circuit and junction thermal voltage; W_s : wind speed; α : solar altitude angle; α_s : solar azimuth angle; α_w : azimuth angle; β : panel tilt angle; β_t : temperature coefficient for change in I_{sc} ; φ : location latitude; δ : solar declination angle; ω : mounting coefficient.

II. INTRODUCTION

Renewable energy systems are expanding due to not only environmental aspect but also due to social, economical and political interest. The European Union is aiming at a specific CO₂ reduction in the electricity sector in the near future (20% reduction by 2020). This will involve a significant growth of PV installation all over Europe resulting in a few hundred GW of capacity [1].

The increased PV capacity will influence power system operation and design. Power supplied from a PV array depends mostly on present ambient conditions such as:

irradiation and temperature [2-5].

PV output voltage changes mainly with temperature while PV output current changes mainly with irradiation. Therefore in order to develop a very precise simulation model the local wind speed and the solar radiation incidence angle, in terms of the slope and surface azimuth, should be considered [5]-[8].

In order to determine the hourly incident radiation on a surface of any orientation it is necessary to evaluate the ratio of incident radiation on the tilted surface to that on a horizontal surface considering beam, sky diffuse and ground reflected radiation separately [3], [6], [9].

Increased distributed generation is becoming more important in the current power system and in the future it will rely more on distributed energy resources and micro-grids. The flexible micro-grid has to be able to import/export energy from/to the grid, control the active and reactive power flows and manage of the storage energy [7], [10].

The battery package is an interesting option for storing excess energy from the hybrid grid (wind intermittency) for later use. It may also act as a peak shaving unit and thereby contribute to a stronger grid [13], [15]-[17].

This paper proposes the development of simulation tools to analyze and simulate power systems with renewable energy sources and electricity storage devices. The tools are based on models implemented first in MATLAB-Simulink and validated by measurements. The paper focuses on simulation models of a small-scale PV System and on a VRB system connected to a micro-grid and on improvements and validating it using experimental facility of an active and distributed power systems laboratory called SYSLAB. In order to find out the differences between DER components in power systems and to study the impact on bus voltage and frequency the systems have also been implemented in DIgSILENT PowerFactory.

III. DISTRIBUTED ENERGY SYSTEM ARCHITECTURE. EXPERIMENTAL FACILITY-SYSLAB

SYSLAB is a laboratory for research in distributed control and smart grids with a high share of renewable energy production. Its experimental facility is a Wind/PV/Diesel Hybrid Mini-Grid with local storage and a novel control infrastructure. The facility is spread across three sites located several hundred meters apart, as can be seen in Fig. 1a).

It includes two wind turbines (11kW and 55kW), a PV-plant (7.8 kW), a diesel gen-set (48kW/60kVA), an intelligent office building with controllable loads (20kW), a number of loads (75kW, 3*36kW) and a Vanadium Battery of 15 kW/190 kWh. At each of the three sites there is a switchboard that allows the components installed at the site to be connected to either of two bus bars. The two bus bars at each site are connected to a crossbar switchboard allowing the flexible setup of the system(s) to be studied. The bus bars can be either connected to the national grid or can be part of

This work was supported in part by the E.U. Project-Smooth PV, No. 10580/2011-2012 and also partially supported by the strategic grant POSDRU/88/1.5/S/50783 of the Ministry of Labor, Family and Social Protection, Romania, co-financed by the EU Social Fund – Investing in people.

L. Mihet-Popa, F. Isleifsson and H. Bindner are with the Department of Electrical Engineering, Danish Technical University-DTU, 4000 Roskilde, Denmark (e-mail: lmih@elektro.dtu.dk).

C. Koch-Ciobotaru is with POLITEHNICA University of Timisoara, Romania (e-mail: cosmin.koch@aut.upt.ro).

an isolated system. It allows components and systems to be in grid connected operation, island operation, or operation in parallel with wind turbine or PV-plant, as it is shown in Fig. 1b).

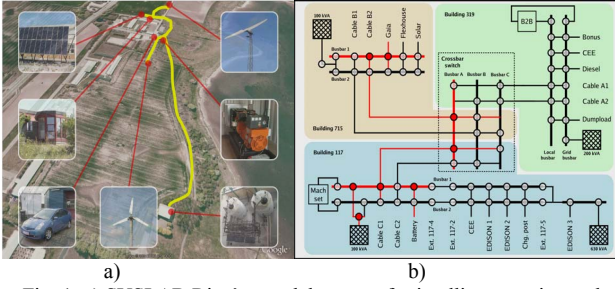


Fig. 1. a) SYSLAB Risø's new laboratory for intelligent, active and distributed power systems and b) details about SYSLAB Micro-Grid architecture.

The components are all connected in one distributed control and measurement system that enables very flexible setup with respect to experimental configuration.

A. PV Panel System

The PV panels are mounted in three strings: two strings having 18 panels of 165 W each, and another one containing 12 panels of 100 W [19]. The strings are connected to the SYSLAB grid through a three-phase PV inverter (SMA Sunny Tripower).

From PV system two sets of data are provided. The first set consists of the ambient measurements from the weather station: solar irradiance on the horizontal, ambient temperature, and wind speed. The second set represents the electric measurements taken from the inverter: the AC output power to the grid, and on each PV string the DC power, voltage, and current. The two sets of data are read at different sampling frequencies: 1 Hz for the electrical and 0.1 Hz for the ambient. These large sets of data are used to develop an accurate model of the existing PV setup and to validate it.

B. Energy Storage System

The vanadium redox battery system installed in SYSLAB is connected to the grid via a four quadrant power converter and can deliver 15 kW on the AC side and the nominal storage capacity is 190 kWh. The battery can operate in two modes: P-Q mode (where the active and reactive power of the battery is set by the user) and U-f mode where the power is set according to the grid voltage and frequency and the pre-defined droop-curves [15].

C. Data Acquisition and Control System

The data acquisition and control system (hardware and software) is responsible for the supervision and control of the research platform for distributed intelligent energy systems with a high penetration of renewable energy. The supervisory software code was written in Java and is able to manage the data acquisition, processes the data and executes the control loop and outputs the control variables. The sensors outputs are connected to a signal conditioning board, which in turn is connected to the data acquisition (DAQ) board based on a PC (SCADA System).

IV. PV PANEL AND ARRAY MODELING

A. Modeling of the PV Panel

To be able to develop an accurate PV panel model it is necessary to define the right equivalent circuit. This paper uses a single diode equivalent circuit for the PV model, described by a simple exponential function:

$$i = I_{sc} - I_0 \cdot \left(e^{(v+iR_s)/n_s V_T} - 1 \right) \quad (1)$$

Manufacturers typically provide limited operational data for photovoltaic panels. These data are available only at standard rating conditions, for which the irradiance is 1000 W/m² and the cell temperature is 25 °C, except for the NOCT which is determined at 800 W/m² and an ambient temperature of 20 °C.

Equations for the short circuit current and the open circuit voltage as a function of absolute temperature ΔT include temperature coefficients that provide the rate of change with respect to temperature of the PV performance parameters, can be express as:

$$\begin{aligned} I_{sc} &= I_{sc25} \cdot (1 + \beta_I \cdot \Delta T) \\ V_{oc} &= V_{oc25} \cdot (1 + \chi \cdot \Delta T) \\ \Delta T &= T_{cell} - T_a \end{aligned} \quad (2)$$

To complete the model it is also necessary to take into account the variation of the parameters with respect to irradiance:

$$I_{sc} = I_{sc25} \cdot (G_a / 1000) \quad (3)$$

Using a four parameters model of a single diode equivalent circuit, the v-i characteristics for a solar panel string depending on irradiance and temperature has the following expressions:

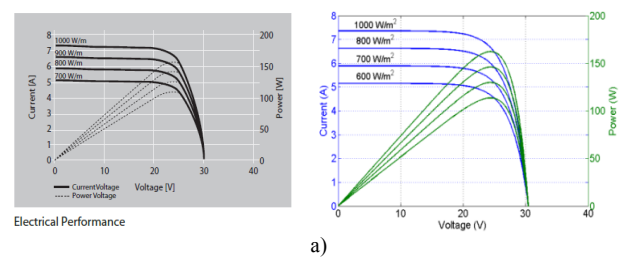
$$v = n_{ps} \cdot V_{oc} + n_{ps} \cdot n_s \cdot V_T \cdot \ln \left(1 - i / (n_{sp} \cdot I_{sc25} \cdot G_a / 1000) \right) \quad (4)$$

$$i = n_{sp} \cdot I_{sc} \cdot \left(1 - e^{(v - n_{ps} \cdot V_{oc} + R_s \cdot i) / (n_{ps} \cdot n_s \cdot v)} \right) \quad (5)$$

The equations (4) and (5) can be used to calculate the voltage and current over a string of panels.

The model used to obtain the static characteristics of the PV panels has been developed in MATLAB using the equations presented above. The model was developed for one panel, as a function of irradiance and temperature. The model has as inputs G_a and T_{cell} on the panel and it sweeps the voltage range of the PV panel in order to calculate the output current and power. PV cells have nonlinear i-v and p-v characteristics. Its output voltage and power change according to temperature and irradiation.

Fig. 2 shows the typical characteristics for a PV model and also a comparison between PV technical characteristics from datasheet (on the left) and simulation results for one panel.



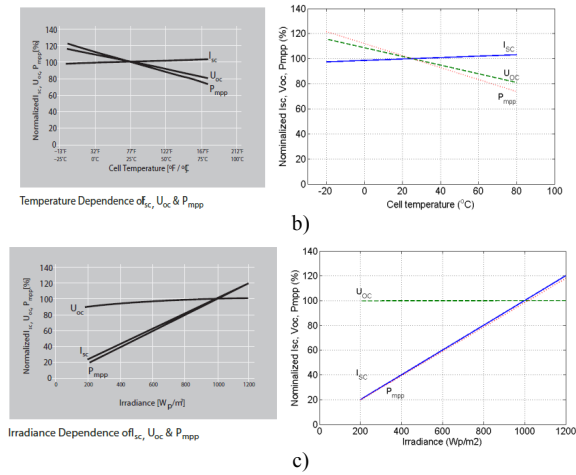


Fig. 2. Comparison between PV technical characteristics from datasheet (on the left) and simulation results for one panel.

B. Modeling of the PV Array

A Matlab/Simulink model has been developed, based on the equations presented in the last section, in order to reproduce the electrical behavior of the existing PV strings at the SYSLAB experimental facility. The model has the temperature and the solar radiance on the panel as inputs and the AC power at the inverters' grid side as output.

For obtaining the maximum power of the panel strings, the condition $(dp/dv=0)$ should be fulfilled.

The block diagram implemented in Simulink that was developed to implement this model is depicted in Fig. 3.

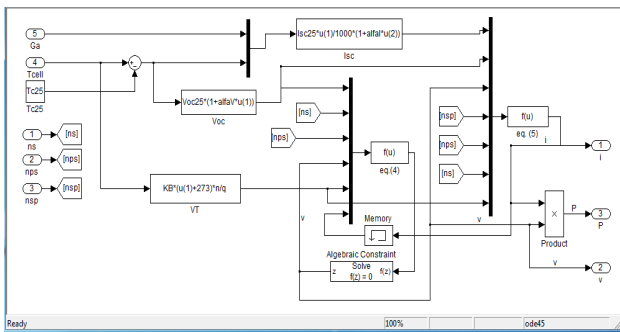


Fig. 3. PV string model implemented in Simulink.

C. Improvements and Validation of the Model

Two types of measurements are taken from the experimental facility: ambient measurements from the weather station and electrical measurements taken from the inverter. All these measurements are implemented into our model using a subsystem called "Measurements", as can be seen in Fig. 4.

The three ambient measurements: ambient temperature, horizontal solar radiation, and wind speed are fed to a module/subsystem (called *Data Processing* in Fig. 4) that calculates the cell temperature of the PV panels and the solar radiation on them, which are the inputs for the PV models together with the number of panels in series, the number of cells in series and the number of strings in parallel.

The simulation model, developed before in MATLAB/Simulink for one PV panel (Fig. 3), has been improved and modified for a PV array with three strings. A block diagram of the model can also be seen in Fig. 4.

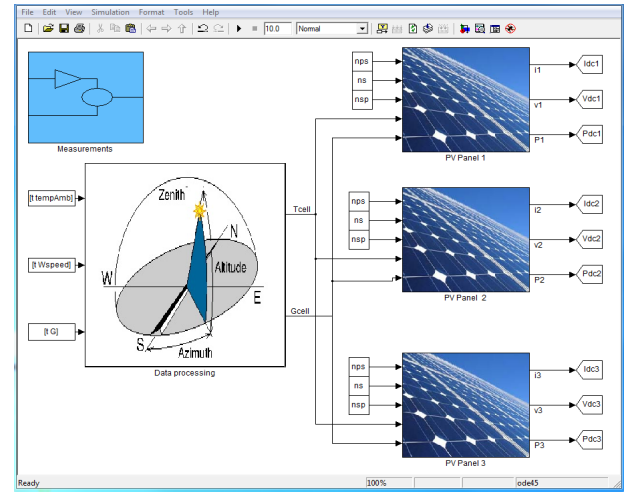


Fig. 4. Block diagram of the simulation model for PV array.

1) Cell Temperature

The cell temperature T_{cell} can be very different from the ambient temperature T_a and it depends on the solar irradiation G_a , T_a and also on the wind speed W_s . Solar irradiation acts on increasing T_{cell} and the wind speed has a cooling effect and lowers T_{cell} [3], [5].

If the PV panels are mounted in the regions with high wind potential (as in our case), the wind speed must be considered. The forced (wind) convection is large for high wind speeds and the cell temperature function takes the following form [5]:

$$T_{cell} = T_a + \omega \cdot (0.32 / (8.91 + 2 \cdot W_s / 0.67)) \cdot G_a \quad (6)$$

Where W_s is the wind speed measured on horizontal plane and ω is the mounting coefficient, which depends on the mounting conditions of the PV panels and can be expressed as:

$$\omega = 15^0 \cdot (SolarNoon - \Delta T) \quad (7)$$

The wind that produces the cooling effect through forced convection is the wind parallel to the panel surface; that is why the transformation $W_{parallel} = W_s / 0.67$ is used.

For a better understanding on the influence of solar irradiance and wind speed on the cell temperature, a graphical representation of these values is depicted in Fig. 5. The differences in temperature of the PV cells according to different considerations are also presented.

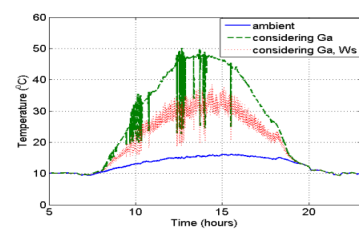


Fig. 5. Ambient measurements and their effect on the PV cell temperature.

The solar irradiance has a high heating effect, at noon it can be seen a 30°C increase of cell temperature. Considering also the wind effect, the cell temperature is lowered, at noon, with 12°C. This change in temperature has an effect on the output power; as shown also in Fig. 2b). At each degree change in temperature, the efficiency modifies with approximately 0.44%: That means that if the temperature rises, the efficiency decreases and vice versa [20, 21].

2) Solar irradiance on the PV panel

As shown in Fig. 2c), the solar radiance has influence

only on the current and implicitly on the output power of the PV panel, so the plots contain the effect of the change in the input solar irradiance, according to the ‘adaptation’ of the horizontal solar irradiance to the real case of the PV panel. The solar irradiance input to the model is the horizontal value measured from the weather station. This translates into substantial differences as can also be seen in Fig 5.

a) *Considering the tilt angle of the PV panels*

The PV panels from SYSLAB are tilted at $\beta=60^\circ$. For introducing this factor into the model, the declination angle (δ) has to be defined. The declination angle is the angular position of the sun at solar noon with respect to the plane of the equator. Its value is given by [6]:

$$\delta = 23.45 \cdot \sin(360 \cdot (284 + n / 365.25)) \quad (8)$$

Where 23.45 is the Tropic of Cancer latitude. For this equation, the days are numbered from the spring equinox (day 81) and using the fact that \sin is a periodic function, $365-81=284$.

The relation between solar irradiance on horizontal plane G_{horiz} and the solar irradiance on a tilted panel, facing south is [6]:

$$G_{panel} = (G_{horiz} \cdot \sin(\alpha + \beta)) / \sin(\alpha) \quad (9)$$

In which $\alpha = 90-\varphi+\delta$.

From this equation it is clear that the ratio between the solar irradiance on the PV panel and the one on the horizontal changes during the year, as the earth orbits the sun and the declination angle changes with every day. The day number of the considered day for the simulation has to be an input for the model [20].

b) *Considering the orientation of the PV panels*

For estimating the solar irradiance for a non facing south PV panel from a facing south PV, which the model calculates at this stage, some additional relations have to be introduced, such as: solar hour angle, equation of time and daylights saving time [3]. For calculating the solar irradiation on the PV panels from the solar radiation on a tilted panel, calculated at stage 2 (Fig. 6b), a correction factor was defined as:

$$G_{corr} = \cos(\omega) / \cos(\omega - deviation) \quad (10)$$

In addition to the day’s number in the year, the model has to be provided with the local time, as of this 13° deviation, the solar irradiance on the PV panel has a nonlinear variation from the measured horizontal solar irradiation according to the position of the sun on the sky in each moment of the day (Fig. 6c).

In Fig. 6 are presented the simulation results versus measurements at different stages of the modeling. These Figures also shows the importance of several factors that have to be taken in consideration, especially PV panel tilt angle and orientation.

In Fig. 6 a) is shown a comparison between measured and simulated output power without considering wind speed effect or any improvements.

Fig. 6 b) shows the same wave form for output power, with the same peak values, and the same changes in power due to shading effect in a synchronous manner. The simulation has a delay of around 50 minutes. This is the effect of the PV panels’ orientation, which have a 13° deviation from the E-W axis.

Considering the tilt angle and orientation, the influence of solar irradiance and wind speed on the cell temperature the measurements and simulations are almost identically, as can

be seen in Fig. 6 c).

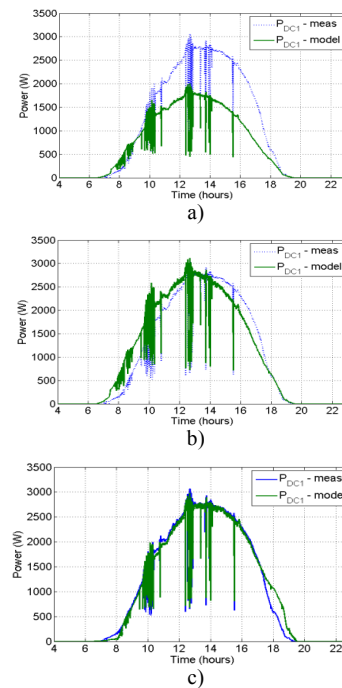


Fig. 6. Solar irradiance adaptation steps.

V. VRB MODEL IMPLEMENTED IN MATLAB-SIMULINK AND VALIDATED BY MEASUREMENTS

A. VRB Modeling and Implementation

The VRB model has been developed in MATLAB/Simulink and is based on the power balance between the input and the stored power considering the efficiency of different components and the power losses, as it is shown in Fig. 7. These characteristics of the battery have been computed based experiments by measuring different electric values at different loads and SOC levels [15].

The simulation model of the battery system contains four subsystems: the power converter, the cell stacks, the energy storage, voltage limitation and the auxiliaries, as it is depicted in Fig. 7 b).

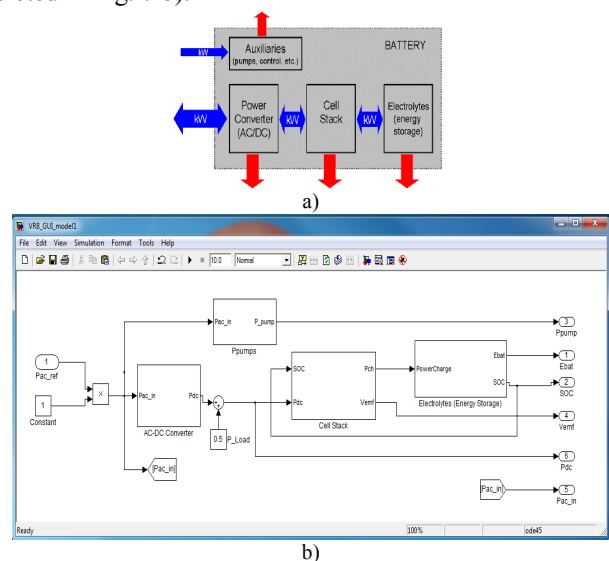


Fig. 7 a) Schematic drawing of the battery system (the red arrows indicate losses from the different parts of the system) and b) Simulink implementation.

The power converter was modeled using a look-up table with the efficiency of the AC-DC converter in charge and

discharge operation modes.

The efficiency of the cell stacks was implemented as a function of the DC power at different SOC levels, when the battery was running in stable conditions during charge/discharge modes.

The total power available is related to the electrode area in the cell stacks and the total energy stored in the VRB depends on both the SOC and the amount of active chemical substances. The actual energy stored in the battery is defined as:

$$E_{batt} = E_{batt0} + \int P_{cell} \cdot dt \quad (11)$$

Where E_{batt0} is the initial energy stored in the battery and P_{cell} is the charge/discharge power at the electrolyte side.

The state of charge (SOC) is defined as the amount of energy stored in the battery (E_{batt}) divided by the total energy capacity E_T :

$$SOC = E_{batt} / E_T \quad (12)$$

The energy storage subsystem was implemented based on (11) and (12) having as output E_{bat} and SOC.

For a vanadium battery the auxiliary power consumption is significant since the electrolyte has to be circulated for the battery to be operational. The power of the auxiliaries (control system, pumps, etc.) can be derived from the measured AC power of the battery and the total power flow over the bus (when only the battery is connected). When the battery is off, the power consumption (for the control PC and the displays) is 235W. When the battery is on and the pumps are running the power consumption is between 1.1 and 1.6 kW depending on the AC power. The auxiliary block has also been modeled by a look-up table considering experimental data from [15].

The voltage limitation block has two functionalities: to calculate the DC side voltage of the converter and to calculate the AC limit power according to the SOC. The power input is physically limited and at high SOC values, the converter is not able to receive the prescribed power, but a limited one. Also the subsystem contains an empirical relation between the SOC and the voltage across the electrolyte (V_{cell}), also implemented by a look-up table based on experiments.

B. Comparison between simulation and measurements

In order to validate the simulation model, measurements were taken from the DAQ board of the VRB, fed into the model and verifying the output values of the battery and of the model.

The following experiment for a time scale of 36 hours was considered: starting from a SOC=93.5% the battery was discharged with a constant power $P_{AC}=15kW$, until SOC=18%. Then a charge sequence was considered from SOC=14% until the level of SOC=87% at $P_{AC}=10kW$.

A comparison between simulations and measurements of SOC level and DC Voltage is presented in Fig. 8. As can be seen it is a very small difference between graphics, which means that the simulation model developed can be an accurate tool for studying and analyzing the characteristics of the energy storage system in a distributed network.

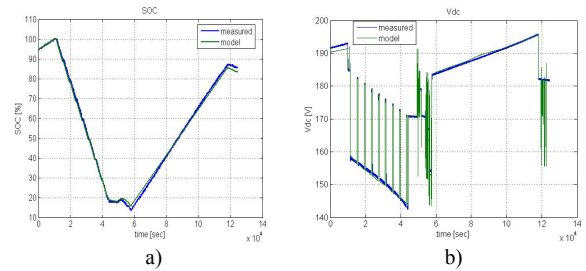


Fig. 8. Comparison between simulations and measurements: a) State of Charge sequence-SOC and b) DC Voltage- V_{dc} versus time.

VI. SIMULATION MODEL OF DER COMPONENTS DEVELOPED IN POWERFACTORY FOR DISTRIBUTION NETWORKS

Computer models of power systems are widely used by power system utilities to study load flow, steady-state voltage stability and dynamic and transient behavior of power system.

DIgSILENT PowerFactory has been chosen because provides the ability to simulate load flow, RMS fluctuations in the same software environment. It provides a comprehensive library of models for electrical components in the power system [18].

The dynamic models of the PV System and VRB system implemented in PowerFactory has been built with standard components library and are based on the same equations used for MATLAB/Simulink models presented before.

The blocks of the PV system (Fig. 9b), such as: PV model, DC-Link and controller of the Static Generator and of the VRB system (Fig. 9c), such as: battery model, charge and P-Q controllers are implemented in the dynamic simulation language DSL of DIgSILENT. DSL allows the user to implement specific models that are not standard in the DIgSILENT library and thus to create own developed blocks either as modifications of existing models or as completely new models. The internal simulation language DSL has also been used to define the PV and VRB characteristics and to initialize the parameters and variables of the models.

Fig. 9 a) shows a single line diagram of the SYSLAB architecture implemented in PowerFactory. For load flow analysis, also shown in Fig. 9 a), the local voltage controller could be set to three different modes: $\cos\phi$, V and $droop$. For RMS and EMT simulations the static generator supports two different models: current source and voltage source models. In our case we use a current source model which has as inputs d-q axis reference current coming from the controller and $\cos\phi_{ref}$ and $\sin\phi_{ref}$ signals from a PLL model.

Fig. 9 b) shows the schematic structure of the PV System model, developed for time-domain simulations where a DSL model is required, including Photovoltaic Model, DC-Link Model, PLL block and Static Generator with its Controller. The Static Generator is an easy to use model of any kind of static (non rotating) generators. Applications are PV Generators, Storage devices, wind generators etc. The PV system frame also contains the measurements blocks used as inputs for different components of the model. For instance, the Photovoltaic Model has as inputs irradiation G and cell temperature $temp_{Cell}$, obtained from MATLAB-Simulink model considering the tilt angle, orientation and the influence of solar irradiation and wind speed on the cell temperature, implemented as a look-up table, as can be seen in Fig. 10a). Also the MPP of current, power and voltage as a function of time for one module are shown.

In Fig. 9 c) it is shown the VRB system block diagram developed for time-domain simulations (RMS and EMT). The battery energy storage system contains the model of VRB, developed in DSL using the same equations like in Simulink model presented in the last section and the charge/discharge controller which takes in consideration the SOC level of the battery, DC current and voltage of the cell stacks and provides the current set-point for the inverter. Also, to study the system stability the frequency and power controllers have been implemented.

In order to validate the simulation model developed in PowerFactory and to compare the results with MATLAB-Simulink model, the same measurements have been used like in the last section when we compare the results of Simulink model with experiments (Fig. 8).

As can be seen in Fig. 11 a) the simulation results of DC Voltage and Power for different SOC level are similar. Also, to point out the accuracy of the simulation model developed in PowerFactory in Fig. 11 b) is depicted a comparison between simulated and measured SOC level.

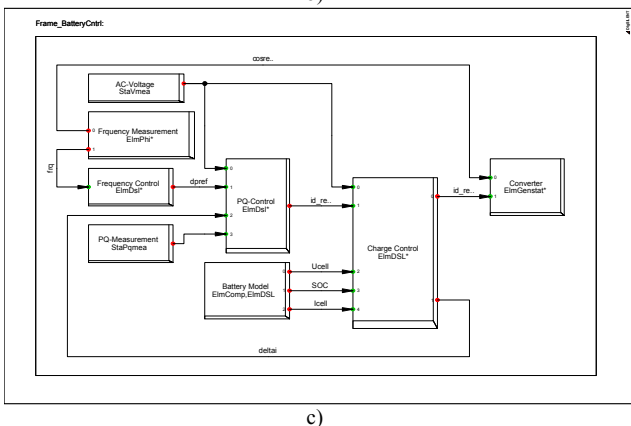
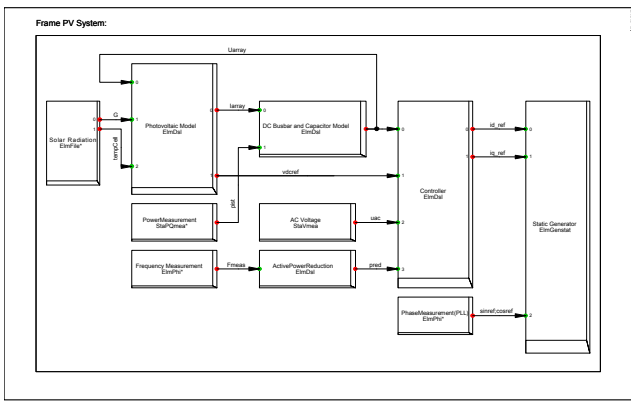
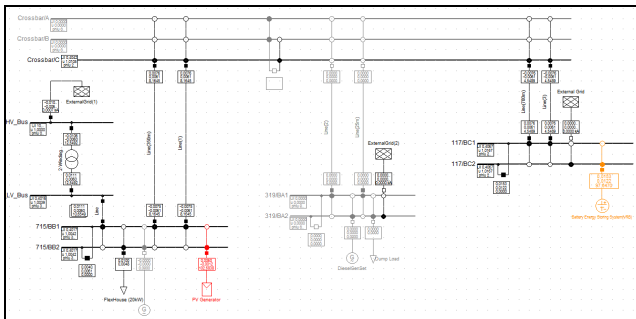


Fig. 9. a) Single line diagram of SYSLAB configuration, b) schematic block diagram of the PV system model and c) VRB system implemented in PowerFactory.

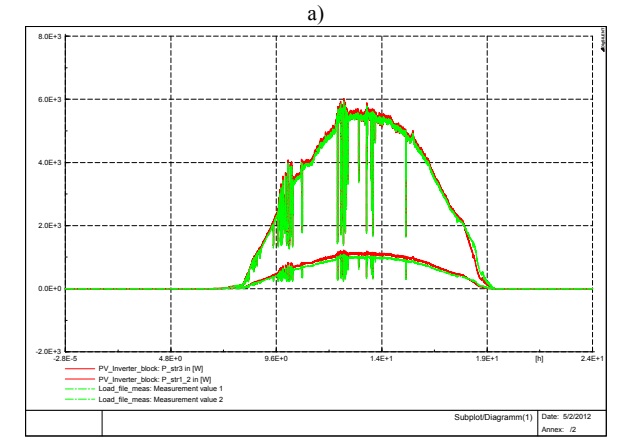
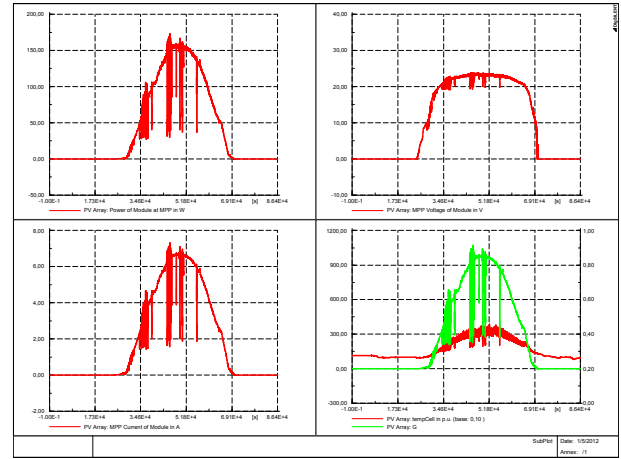


Fig. 10. Simulation results of the PV system model, a) and a comparison between simulations and measurements, b).

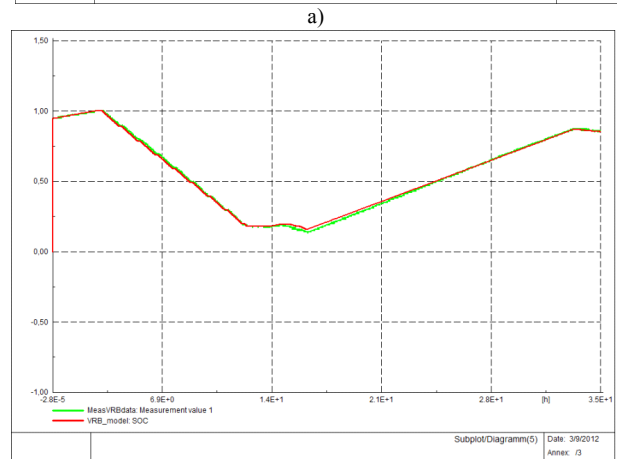
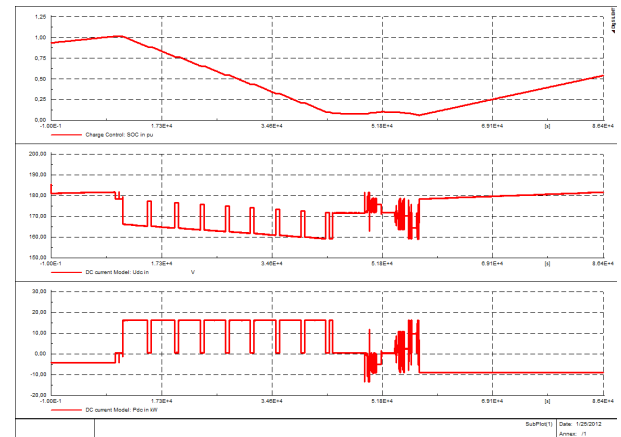


Fig. 11. Simulation results of the VRB system model, a) and a comparison between simulated and measured SOC level, b).

VII. CONCLUSIONS

This paper proposes the development and implementation of simulation tools to analyze and simulate power systems with renewable energy sources and electricity storage. The tools are based on models validated by measurements.

A four-parameter model of a PV panel and a PV system, implemented in MATLAB/Simulink, using data provided by the manufacturer with semi-empirical equations to predict the PV characteristics for any condition. The PV characteristics are modeled according to a single diode four parameter equivalent circuit and according to PV parameters values taken from the manufacturer technical data.

The paper also proposes a data processing simulation model that relies on ambient data from a local weather station, like most common in a real situation, not from sensors mounted on the PV panels. The model calculates the cell temperature and the solar irradiance on the PV panels considering, among others, the tilt angle, the orientation of the panels, and the wind cooling effect. The paper shows that these factors significantly influence the power output from the PV panels.

The VRB system model has been developed and implemented first in MATLAB-Simulink considering the efficiency and the power losses of different components. The characteristics of the battery have been computed based on experiments by measuring electrical parameters at different loads and SOC levels.

Comparison with experimental data, acquired by SCADA system and processed by MATLAB, and with the characteristics of the PV panels and VRB, provided by manufacturers, has shown that the models implemented in MATLAB/Simulink can be an accurate simulation tool to study and analyze the characteristics of individual units and for the prediction of energy production with energy storage systems.

A PV system model and a VRB system model, using the same equations and parameters as in MATLAB/Simulink has also been developed and implemented in PowerFactory to study load flow, steady-state voltage stability and dynamic behavior of a distributed power system. Also, the simulation results have shown a good similarity between both tools.

VIII. REFERENCES

- [1] Energynautics GmbH, Longen, Germany, 2010. Available: www.energynautics.com
- [2] S. Seme, G. Stumberg, and J. Vorsic, "Maximum efficiency trajectories of a two-axis sun tracking system determined considering tracking system consumption," *IEEE Trans. On Power Electronics*, vol. 26, no. 4, pp. 1280-1290, Apr. 2011.
- [3] W. De. Soto, S. A. Klein, and W. A. Beckman, "Improvement and validation of a model for photovoltaic array performance," *ELSEVIER Solar Energy*, vol. 80, pp. 78-88, 2006.
- [4] Y. Riffonneau, S. Bacha, S. Baruel and S. Ploix, "Optimal Power Management for grid connected PV Systems with batteries", *IEEE Transaction on Sustainable Energy*, vol. 2, no. 3, pp. 309-320, July 2011.
- [5] J. E. Skoplaki, A. G. Boudouvis and J. A. Polyvos, "A simple correlation for the operating temperature of photovoltaic modules of arbitrary mounting", *ELSEVIER Solar Energy Materials*, pp. 1393-1402, 2008.
- [6] K. Murat, S. Mehmet, B. Yunus, D. Sedat, "Determining optimum tilt angles and orientations of photovoltaic panels in Saliurfa", *IEEE Transaction on Renewable Energy*, vol. 29, issue 8, pp. 1265-1275, 2004.
- [7] H. Jiayi, J. Chuanwen, and X. Rong, "A review on distributed energy resources and MicroGrid", *ELSEVIER Renewable & Sustainable Energy Reviews*, vol. 12, pp. 2472-2483, 2008.

- [8] M. G. Villalva, J. R. Gazoli, E. R. Filho, "Comprehensive Approach to Modelling and Simulation of Photovoltaic Arrays", *IEEE Transaction on Power Electronics*, vol. 24, issue: 5, pp. 1198-1208, 2009.
- [9] D. Y. Goswami, *Principles of Solar Engineering*, (2nd ed.), Philadelphia: Taylor & Francis, 2000, p. 81-98.
- [10] M. Jansen, R. Louie, M. E. Amoli and F. Sami, "Model and simulation of a 75 kW PV solar array", in *Proc. 2010 IEEE PES Transmission and Distribution Conference and Exposition*, pp. 1-5.
- [11] S. Dezso, R. Teodorescu and P. Rodriguez, "PV panel model based on datasheet values", in *Proc. 2007 IEEE International Symposium on Industrial Electronics*, pp. 2392-2396.
- [12] H. Liu, L. Jin, D. Le and A. A. Chowdhury, "Impact of high penetration of solar photovoltaic generation on power system small signal stability", in *Proc. 2010 POWERCON*, pp. 1-7.
- [13] A.D. Hansen, P. Sørensen, L.H. Hansen, H. Bindner, "Models for a Stand-Alone PV System", Risø National Laboratory, Roskilde, Risø-R-1219 (EN) / SEC-R-12, Dec. 2000.
- [14] *IEEE Standard for Interconnecting Distributed Resources with Electric Power Systems*, IEEE Standard 1547-2008.
- [15] H. Bidner, C. Ekman, O. Gehrke and F. Isleifsson, "Characterization of Vanadium Flow Battery", Risø-R-1753 Report, Roskilde, Denmark, October 2010.
- [16] L. Barote, R. Weissbach, R. Teodorescu, C. Marinescu, M. Cirstea, "Stand-Alone Wind System with Vanadium Redox Battery Energy Storage", IEEE, International Conference on Optimization of Electrical and Electronic Equipments, OPTIM'08, pp. 407-412, 22-24 May 2008, Brasov, Romania.
- [17] W. Wang, B. Ge, D. Bi and D. Sun, "Grid-Connected Wind Farm Power Control using VRB-based Energy Storage System", *IEEE Transaction on Energy Conversion*, pp.3772-3777, 2010.
- [18] DiGSILENT PowerFactory, User's Manual and Tutorial-Version 14.1, Gomaringen-Germany, November 2011.
- [19] Schuco S 165-SPU, Data sheet and technical data of the Photovoltaic Module.
- [20] L. Mihet-Popa, C. Koch-Ciobotaru, F. Isleifsson and H. Bindner, "Development of tools for simulation systems in a distribution network and validated by measurements", the 13th International Conference on Optimisation of Electrical and Electronic Equipment, OPTIM 2012, May 24-26, Brasov-Romania, pp. 1022-1031.
- [21] F. Genduso, R. Miceli and G. Ricco-Galluzzo, "Flexible Power Converters for the Fault Tolerant Operation of Micro-Grids", XIX International Conference on Electrical Machines-ICEM 2010, Rome.

IX. BIOGRAPHIES

Lucian Mihet-Popa received the B.S. degree, M.S. degree and Ph.D. degree from the POLITEHNICA University of Timisoara, Romania, in 1999, 2000 and 2003, respectively, all in electrical engineering. He is currently working as a Scientist with the Department of Electrical Engineering-DTU since 1st March 2011. He is also an Associate Professor in the Department of Electrical Engineering at POLITEHNICA University of Timisoara. Dr. Mihet-Popa received in 2005 the second prize paper award of the IEEE Industry Applications Society. His research interest includes control and modeling of DER components in micro grids, electrical machines and drives, detection and diagnosis of faults, especially for wind turbine applications.

Cosmin Koch-Ciobotariu was born in Arad, Romania, in 1985. He received the B.E. degree in Automation and Computer Science at Politehnica University of Timisoara in 2009. He is currently working towards the Ph.D. degree. His interests include control systems, renewable energy, and energy storage.

Fridrik Rafn Isleifsson received the M.sc. degree in electrical engineering from the Technical University of Denmark in 2006. He is currently a Ph.D. student with the Intelligent Energy System Programmed at the Technical University of Denmark. His research focuses on demand side participation in providing ancillary services to the power system and implementation of control strategies in laboratory demonstrations.

Henrik W. Bindner was born on 30 June 1964 in Copenhagen, Denmark. He received his master in electrical engineering from the Technical University of Denmark in 1988. Since 1990 he has been with Risø DTU National Laboratory for Sustainable Energy in the Wind Energy Division, currently as a Senior Scientist. He has mainly been working on integration of wind energy into power system. Currently, he is researching how distributed energy resources can be applied to increase penetration of wind energy.

Simulation Model developed for a Small-Scale PV System in Distribution Networks

C. Koch-Ciobotaru*, L. Mihet-Popa*** F. Isleifsson** and H. Bindner**

* POLITEHNICA University/Automation and Computer Science, Timisoara, Romania

** Denmark Technical University/Electrical Engineering, Roskilde, Denmark
cosmin.koch@aut.upt.ro; lmih@elektro.dtu.dk

Abstract—This paper presents a PV panel simulation model using the single-diode four-parameter model based on data sheet values. The model was implemented first in MATLAB/Simulink, and the results have been compared with the data sheet values and characteristics of the PV panels in standard test conditions. Moreover to point out the strong dependency on ambient conditions and its influence on array operation and to validate simulation results with measured data a complex model has also been developed. A PV inverter model, using the same equations and parameters as in MATLAB/Simulink has also been developed and implemented in PowerFactory to study load flow, steady-state voltage stability and dynamic behavior of a distributed power system.

I. INTRODUCTION

Renewable energy systems are expanding due to not only environmental aspect but also due to social, economical and political interest. The European Union is aiming at a specific CO₂ reduction in the electricity sector in the near future (20 % reduction by 2020). This will involve a significant growth of PV installation all over Europe resulting in a few hundred Giga watts of capacity [1].

The increased PV capacity will influence power system operation and design. Power supplied from a PV array depends mostly on present ambient conditions such as: irradiation and temperature [2-5].

PV output voltage changes mainly with temperature while PV output current changes mainly with irradiation. Therefore in order to develop a very precise simulation model the local wind speed and the solar radiation incidence angle, in terms of the slope and surface azimuth, should be considered [5-8].

In order to determine the hourly incident radiation on a surface of any orientation it is necessary to evaluate the ratio of incident radiation on the tilted surface to that on a horizontal surface considering beam, sky diffuse and ground reflected radiation separately [3], [6], [9].

Increased distributed generation is becoming more important in the current power system and in the future it will rely more on distributed energy resources and micro-grids. The flexible micro-grid has to be able to import/export energy from/to the grid, control the active and reactive power flows and manage of the storage energy [7, 10, and 14].

This paper focuses on the simulation models of a small-scale PV System connected to a distributed network and on improvements and validating it using experimental

facility of an active and distributed power systems laboratory. In order to find out the differences between DER components in power systems and to study the impact on bus voltage and frequency the system has also been implemented in PowerFactory.

II. DISTRIBUTED ENERGY SYSTEM ARCHITECTURE. EXPERIMENTAL FACILITY

The experimental system is a laboratory for research in distributed control and smart grids with a high share of renewable energy production. Its experimental facility is a Wind/PV/Diesel Hybrid Mini-Grid with local storage and a novel control infrastructure. The facility is spread across three sites located several hundred meters apart.

It includes two wind turbines (11kW and 55kW), a PV-plant (7.8 kW), a diesel gen-set (48kW/60kVA), an intelligent office building with controllable loads (up to 20kW), a number of loads (75 kW, 3*36 kW) and a Vanadium Battery of 15 kW/190 kWh.

At each of the three sites there is a switchboard that allows the components installed at the site to be connected to either of two bus bars. The two bus bars at each site are connected to a crossbar switchboard allowing the flexible setup of the system(s) to be studied. The bus bars can be either connected to the national grid or can be part of an isolated system. It allows components and systems to be in grid connected operation, island operation, or operation in parallel with wind turbine or PV-plant.

A. PV Panels

The PV panels are mounted in three strings: two strings having 18 panels of 165 W each, and another one containing 12 panels of 100 W. The strings are connected to the grid through a three-phase PV inverter.

B. Data Acquisition and Control System

The data acquisition and control system (hardware and software) is responsible for the supervision and control of the research platform for distributed intelligent energy systems with a high penetration of renewable energy. The supervisory software code was written in Java and is able to manage the data acquisition, processes the data and executes the control loop and outputs the control variables. The sensors outputs are connected to a signal conditioning board, which in turn is connected to the data acquisition (DAQ) board based on a PC (SCADA System).

III. PV PANEL AND ARRAY MODELING

A. Modeling of the PV Panel

This paper uses a single diode equivalent circuit for the PV model, described by a simple exponential function:

$$i = I_{sc} - I_0 \cdot \left(e^{(v+iR_s)/n_s \cdot V_T} - 1 \right) \quad (1)$$

In which I_{sc} and I_0 are the short-circuit and open-circuit currents, R_s is the cell series resistance, n_s is the number of cells in the panel connected in series and V_T represents the junction thermal voltage which includes the diode quality factor, the Boltzmann's constant, the temperature at STC and the charge of the electron.

Manufacturers typically provide limited operational data for photovoltaic panels. These data are available only at standard rating conditions, for which the irradiance G_a is 1000 W/m^2 and the cell temperature T_{cell} is $25 \text{ }^\circ\text{C}$, except for the NOCT which is determined at 800 W/m^2 and an ambient temperature T_a of $20 \text{ }^\circ\text{C}$.

Equations for the short circuit current I_{sc} and the open circuit voltage V_{oc} as a function of absolute temperature ΔT include temperature coefficients that provide the rate of change with respect to temperature of the PV performance parameters, can be express as:

$$\begin{aligned} I_{sc} &= I_{sc25} \cdot (1 + \beta_I \cdot \Delta T) \\ V_{oc} &= V_{oc25} \cdot (1 + \chi \cdot \Delta T) \end{aligned} \quad (2)$$

$$\Delta T = T_{cell} - T_a$$

To complete the model it is also necessary to take into account the variation of the parameters with respect to irradiance:

$$I_{sc} = I_{sc25} \cdot (G_a / 1000) \quad (3)$$

Using a four parameters model of a single diode equivalent circuit, the v-i characteristics for a solar panel string depending on irradiance and temperature has the following expressions:

$$v = n_{ps} \cdot V_{oc} + n_{ps} \cdot n_s \cdot V_T \cdot \ln \left(1 - i / (n_{sp} \cdot I_{sc25} \cdot G_a / 1000) \right) \quad (4)$$

$$i = n_{sp} \cdot I_{sc} \cdot \left(1 - e^{(v - n_{ps} \cdot V_{oc} + R_s \cdot i) / (n_{ps} \cdot n_s \cdot v)} \right) \quad (5)$$

The equations (4) and (5) can be used to calculate the voltage and current over a string of panels.

The model used to obtain the static characteristics of the PV panels has been developed in MATLAB using the equations presented above. The model was developed for one panel, as a function of irradiance and temperature. The model has as inputs G_a and T_{cell} on the panel and it sweeps the voltage range of the PV panel in order to calculate the output current and power. PV cells have nonlinear i-v and p-v characteristics. Its output voltage and power change according to temperature and irradiation.

Fig. 1 shows the typical characteristics for a PV model and also a comparison between PV technical characteristics from datasheet (on the left) and simulation results for one panel.

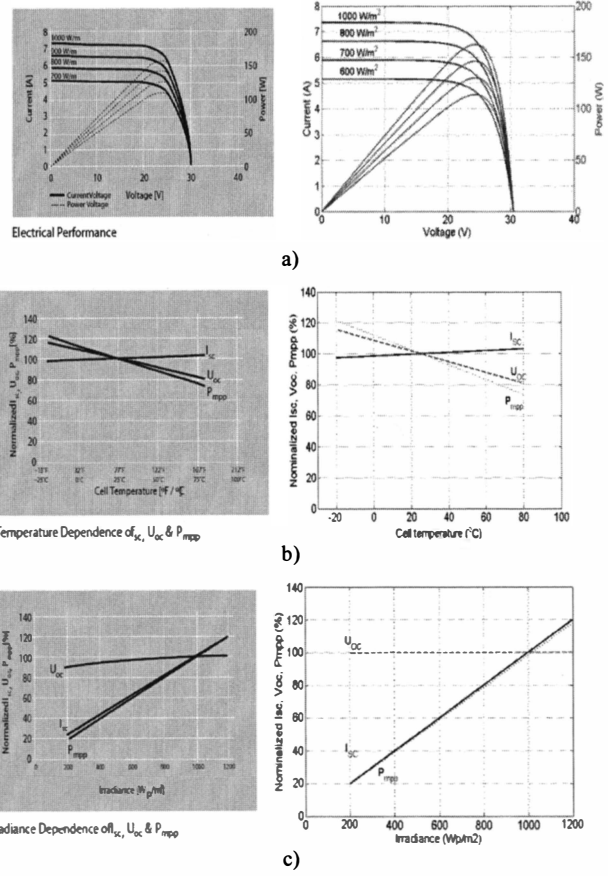


Fig. 1. Comparison between PV technical characteristics from datasheet (on the left) and simulation results for one panel.

B. Modeling of the PV Array

A MATLAB/Simulink model has been developed, based on the equations presented in the last section, in order to reproduce the electrical behavior of the existing PV strings at the experimental system. The model has the temperature and the solar radiance on the panel as inputs and the AC power at the inverters' grid side as output.

For obtaining the maximum power of the panel strings, the condition $(dp/dv=0)$ should be fulfilled.

The block diagram implemented in Simulink that was developed to implement this model is depicted in Fig. 2.

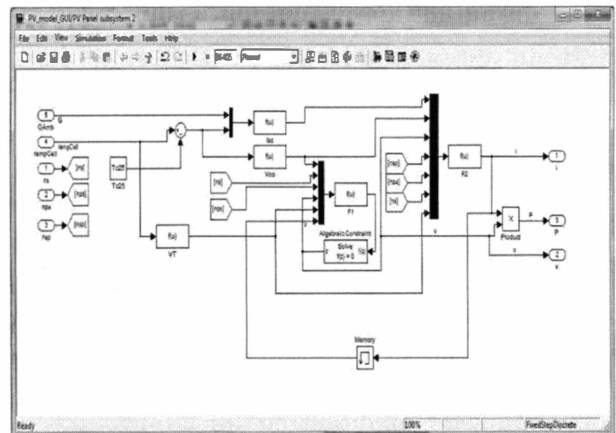


Fig. 2. PV string model implemented in Simulink

C. Improvements of the Model

Two types of measurements are taken from the experimental facility: ambient measurements from the weather station and electrical measurements taken from the inverter.

The three ambient measurements: ambient temperature, horizontal solar radiation, and wind speed are fed to a module that calculates the cell temperature of the PV panels and the solar radiation on them.

1) Cell Temperature

The cell temperature T_{cell} can be very different from the ambient temperature T_a and it depends on the solar irradiation G_a , T_a and also on the wind speed W_s . Solar irradiation acts on increasing T_{cell} and the wind speed has a cooling effect and lowers T_{cell} [3], [5].

If the PV panels are mounted in the regions with high wind potential (as in our case), the wind speed must be considered. The forced (wind) convection is large for high wind speeds and the cell temperature function takes the following form [5]:

$$T_{cell} = T_a + \omega \cdot (0.32 / (8.91 + 2 \cdot W_s / 0.67)) \cdot G_a \quad (6)$$

Where ω is the mounting coefficient, which depends on the mounting conditions of the PV panels and W_s is the wind speed measured on horizontal plane.

The wind that produces the cooling effect through forced convection is the wind parallel to the panel surface; that is why the transformation $W_{parallel} = W_s / 0.67$ is used.

For a better understanding on the influence of solar irradiance and wind speed on the cell temperature, a graphical representation of these values is depicted in Fig. 3. The differences in temperature of the PV cells according to different considerations are also presented.

2) Solar irradiance on the PV panel

The solar radiance has influence only on the current and implicitly on the output power of the PV panel, so the plots contain the effect of the change in the input solar irradiance, according to the ‘adaptation’ of the horizontal solar irradiance to the real case of the PV panel.

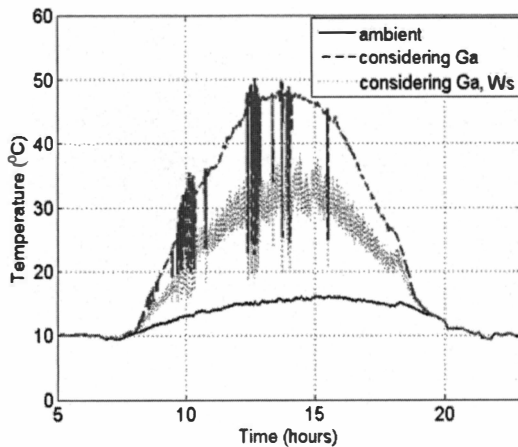


Fig. 3. Ambient measurements and their effect on the PV cell temperature.

The solar irradiance input to the model is the horizontal value measured from the weather station. This translates into substantial differences as can also be seen in Fig 3.

D. Simulation and validation of the array model

The simulation model, developed before in MATLAB/Simulink for one PV panel, has been improved and modified for a PV array with three strings. A block diagram of the model can be seen in Fig. 4.

The PV array model is based on the equations (1-3). These equations represent the PV characteristics taking into account the no. of strings in parallel and the no. of panels in series.

In Fig. 5 are presented the simulation results versus measurements at different stages of the modeling. These Figures also shows the importance of several factors that have to be taken in consideration, especially PV panel tilt angle and orientation.

Fig. 5 b) shows the same wave form for output power, with the same peak values, and the same changes in power due to shading effect in a synchronous manner. The simulation has a delay of around 50 minutes. This is the effect of the PV panels’ orientation, which have a 13° deviation from the E-W axis.

Considering the tilt angle and orientation, the influence of solar irradiance and wind speed on the cell temperature the measurements and simulations are almost identically, as can be seen in Fig. 5 c).

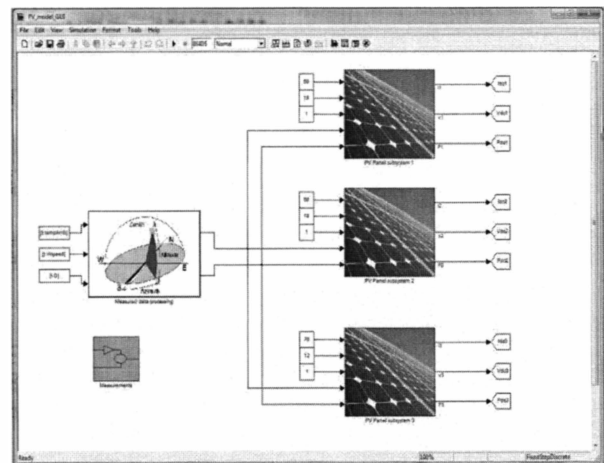
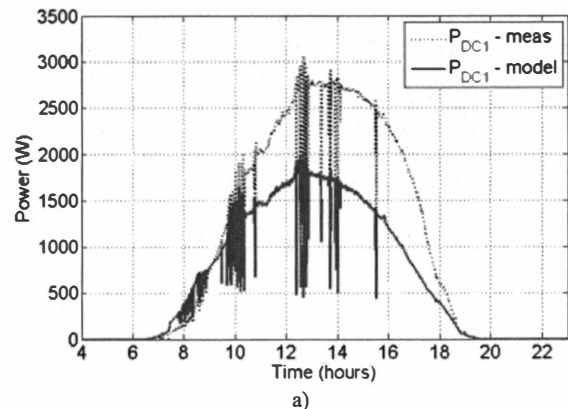


Fig. 4. Block diagram of the simulation model for PV array.



a)

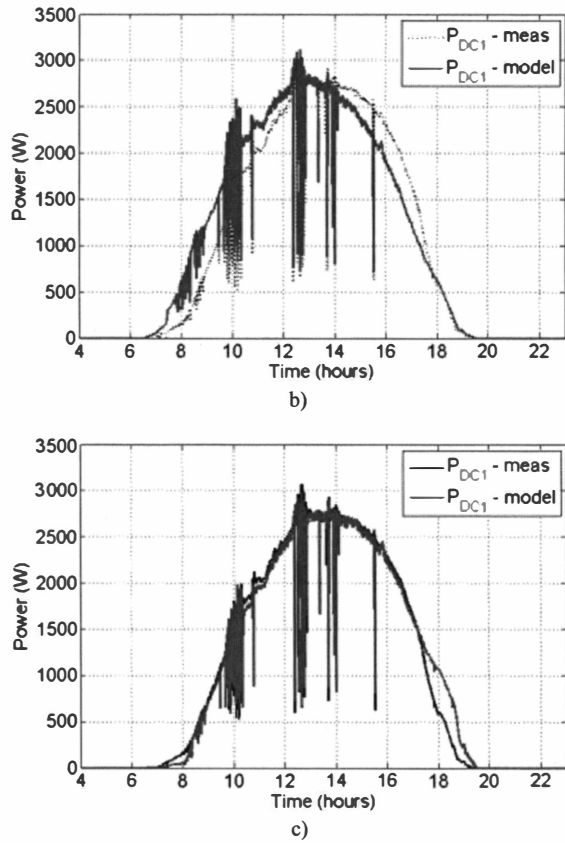


Fig. 5. Solar irradiance adaptation steps.

IV. SIMULATION MODEL OF THE PV SYSTEM DEVELOPED IN POWERFACTORY FOR DISTRIBUTION NETWORKS

Computer models of power systems are widely used by power system utilities to study load flow, steady-state voltage stability and dynamic and transient behavior of power system.

DIgSILENT PowerFactory has been chosen because provides the ability to simulate load flow, RMS fluctuations in the same software environment. It provides a comprehensive library of models for electrical components in the power system [14].

The dynamic model of the PV System implemented in PowerFactory has been built with standard components library and is based on the same equations used for MATLAB/Simulink model presented before.

The blocks of the PV model, DC-Link and controller of the Static Generator are implemented in the dynamic simulation language DSL of DIgSILENT. DSL allows the user to implement specific models that are not standard in the DIgSILENT library and thus to create own developed blocks either as modifications of existing models or as completely new models. The internal simulation language DSL has also been used to define the PV characteristics and to initialize the parameters and variables of the model.

Fig. 6 a) shows a single line diagram of the laboratory architecture implemented in PowerFactory.

Fig. 6 b) shows the schematic structure of the PV System model, developed for time-domain simulations

where a DSL model is required, including Photovoltaic Model, DC-Link Model, PLL block and Static Generator with its Controller. The Static Generator is an easy to use model of any kind of static (non rotating) generators. The common characteristic of these generators is that they are all connected to the grid through a static converter. Applications are PV Generators, Storage devices, wind generators etc.

On the basic data tab of the single line diagram it is possible to set up the number of parallel generators and the power ratings of one PV panel.

For load flow analysis, also shown in Fig. 6 a), the local voltage controller could be set to three different modes: $\cos\phi$, V and droop.

For RMS and EMT simulations the static generator supports two different models: controlled current and voltage source models. In our case we use a controlled current source model which has as inputs d-q axis reference current coming from the controller and d-q reference angles ($\cos\theta_{ref}$ and $\sin\theta_{ref}$) from a PLL built-in model.

Photovoltaic Model has as inputs irradiation G and cell temperature $temp_{Cell}$, obtained from MATLAB-Simulink model considering the tilt angle, orientation and the influence of solar irradiation and wind speed on the cell temperature (Fig. 4), implemented as a look-up table, as can be seen in Fig. 7. Also the MPP of current, power and voltage as a function of time for one module are shown.

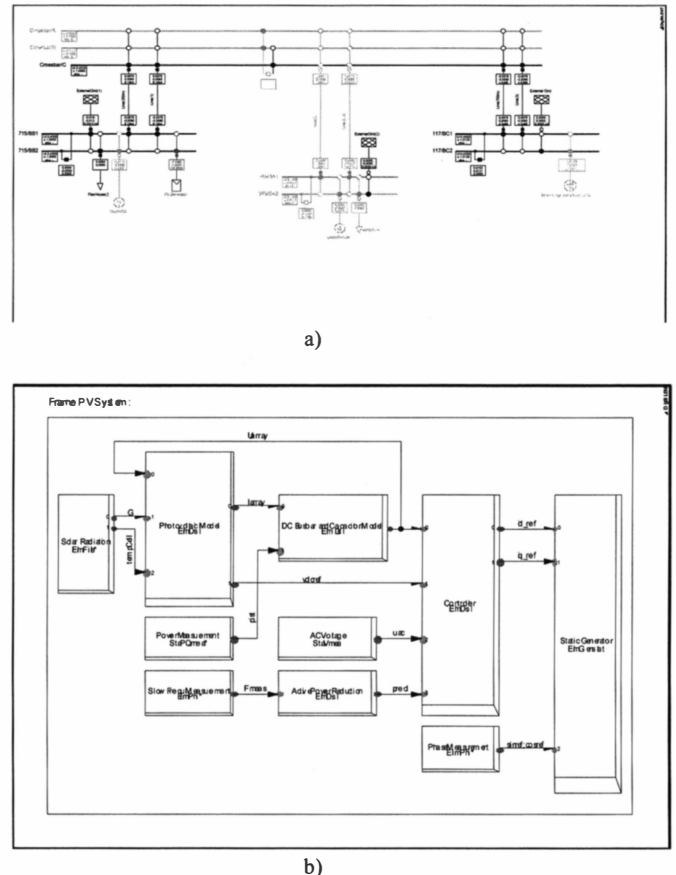


Fig. 6. a) Single line diagram of SYSLAB configuration implemented in PowerFactory and b) schematic block diagram of the PV system model.

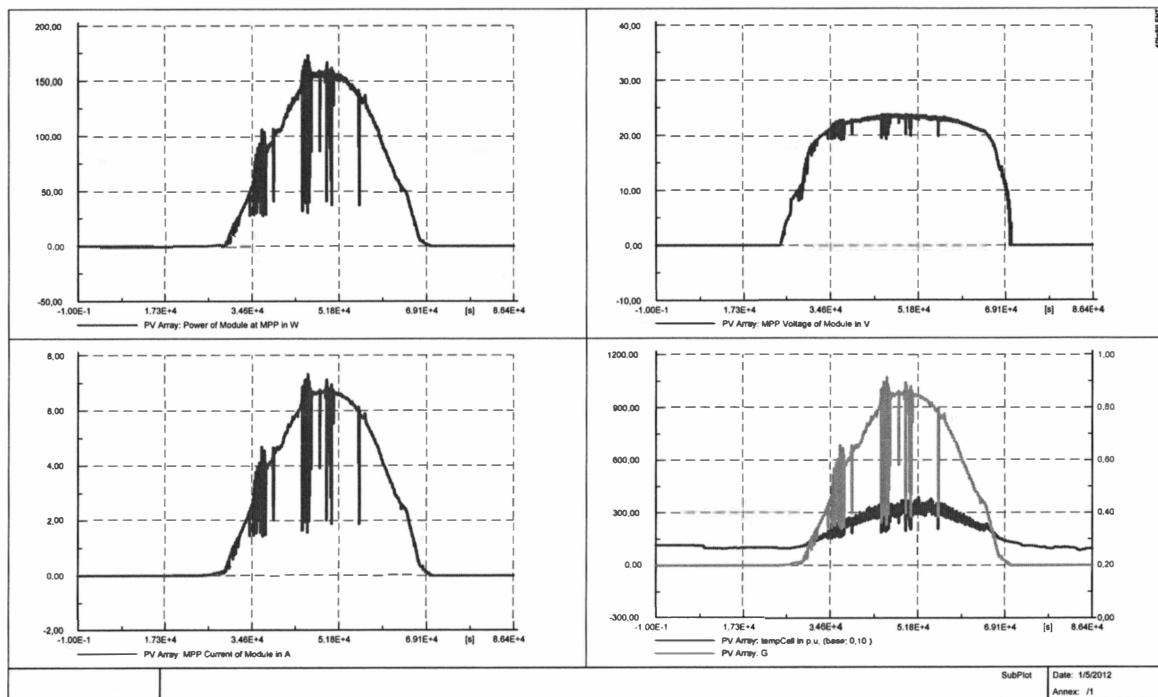


Fig. 7. Simulation results of the PV system model implemented in PowerFactory

V. CONCLUSIONS

This paper proposes a four-parameter model of a PV panel and a PV system, implemented in MATLAB/Simulink, using data provided by the manufacturer with semi-empirical equations to predict the PV characteristics for any condition. PV characteristics are modeled according to a single diode four parameter equivalent circuit and PV parameters values taken from the manufacturer technical data.

The paper also proposes a model that relies on ambient data from a local weather station, like most common in a real situation, not from sensors mounted on the PV panels. The model calculates the cell temperature and the solar irradiance on the PV panels considering, among others, the tilt angle, the orientation of the panels, and the wind cooling effect. The paper shows that these factors significantly influence the power output from the PV panels.

Comparison with experimental data, acquired by SCADA system and processed by MATLAB, and with the characteristics of the PV panels, provided by manufacturers, has shown that the model implemented in MATLAB/Simulink can be an accurate tool for the prediction of energy production.

A PV system model, using the same equations and parameters as in MATLAB/Simulink to define the PV module and characteristics, has also been developed and implemented in PowerFactory to study load flow, steady-state voltage stability and dynamic behavior of a distributed power system.

A comparison between both simulation models, implemented in MATLAB/Simulink and PowerFactory, has shown a good similarity. That means that this work can be used for further development of tools for DER components in a distributed network.

ACKNOWLEDGMENT

This work was supported in part by the E.U. Project-Smooth PV, No. 228449/2011 and also partially supported by the strategic grant POSDRU/88/1.5/S/50783 (2009) of the Ministry of Labor, Family and Social Protection, Romania, co-financed by the European Social Fund – Investing in people.

REFERENCES

- [1] *** www.energynautics.com, Energynautics GmbH, Longen, Germany, 2010.
- [2] S. Seme, G. Stumberg, and J. Vorsic, "Maximum efficiency trajectories of a two-axis sun tracking system determined considering tracking system consumption", *IEEE Trans. On Power Electronics*, vol. 26, no. 4, pp. 1280-1290, Apr. 2011.
- [3] W. De. Soto, S. A. Klein, and W. A. Beckman, "Improvement and validation of a model for photovoltaic array performance", *ELSEVIER Solar Energy*, vol. 80, pp. 78-88, 2006.
- [4] Y. Riffonneau, S. Bacha, S. Barruel and S. Ploix, "Optimal Power Management for grid connected PV Systems with batteries", *IEEE Transaction on Sustainable Energy*, vol. 2, no. 3, pp. 309-320, July 2011.
- [5] E. Skoplaski, A. G. Boudouvis and J. A. Polyvos, "A simple correlation for the operating temperature of photovoltaic modules of arbitrary mounting", *ELSEVIER Solar Energy Materials*, pp. 1393-1402, 2008.
- [6] K. Murat, S. Mehmet, B. Yunus, D. Sedat, "Determining optimum tilt angles and orientations of photovoltaic panels in Saliurfa", *IEEE Transaction on Renewable Energy*, vol. 29, issue 8, pp. 1265-1275, 2004.
- [7] H. Jiayi, J. Chuanwen, and X. Rong, "A review on distributed energy resources and MicroGrid", *ELSEVIER Renewable & Sustainable Energy Reviews*, vol. 12, pp. 2472-2483, 2008.
- [8] M. G. Villalva, J. R. Gazoli, E. R. Filho, "Comprehensive Approach to Modelling and Simulation of Photovoltaic Arrays", *IEEE Transaction on Power Electronics*, vol. 24, issue: 5, pp. 1198-1208, 2009.
- [9] D. Y. Goswami, *Principles of Solar Engineering*, (2nd ed.), Philadelphia: Taylor & Francis, 2000, p. 81-98.

- [10] M. Jansen, R. Louie, M. E. Amoli and F. Sami, "Model and simulation of a 75 kW PV solar array", in Proc. 2010 IEEE PES Transmission and Distribution Conference and Exposition, pp. 1-5.
- [11] S. Dezso; Teodorescu R.; and Rodriguez P., "PV panel model based on datasheet values", in Proc. 2007 IEEE International Symposium on Industrial Electronics, pp. 2392-2396.
- [12] H. Liu, L. Jin, D. Le and A. A. Chowdhury, "Impact of high penetration of solar photovoltaic generation on power system small signal stability", in Proc. 2010 POWERCON, pp. 1-7.
- [13] A.D. Hansen, P. Sørensen, L.H. Hansen, H. Bindner, "Models for a Stand-Alone PV System", Risø National Laboratory, Roskilde, Risø-R-1219(EN) / SEC-R-12, Dec. 2000.
- [14] DIGSILENT PowerFactory, Digsilent gmbh, November 2010.

Development of Tools for Simulation Systems in a Distribution Network and Validated by Measurements

L. Mihet-Popa^{1,2}, C. Koch-Ciobotaru², F. Isleifsson¹ and H. Bindner¹
 Technical University of Denmark¹, POLITEHNICA University of Timisoara²
lmih@elektro.dtu.dk, cosmin.koch@aut.upt.ro

Abstract- The increasing amount of DER components into distribution networks involves the development of accurate simulation models that take into account an increasing number of factors that influence the output power from the DG systems. This paper presents two simulation models: a PV panel model using the single-diode four-parameter model based on data sheet values and a VRB system model based on the efficiency of different components and the power losses. The models were implemented first in MATLAB/Simulink and the results have been compared with the data sheet values and with the characteristics of the units. Moreover to point out the strong dependency on ambient conditions and its influence on array operation and to validate simulation results with measured data a complex model has also been developed. A PV inverter model and a VRB inverter model, using the same equations and parameters as in MATLAB/Simulink, has also been developed and implemented in PowerFactory to study load flow, steady-state voltage stability and dynamic behavior of a distribution power system.

I. INTRODUCTION

Renewable energy systems are expanding due to not only environmental aspect but also due to social, economical and political interest. The European Union is aiming at a specific CO₂ reduction in the electricity sector in the near future (20% reduction by 2020). This will involve a significant growth of PV installation all over Europe resulting in a few hundred Giga watts of capacity [1].

The increased PV capacity will influence power system operation and design. Power supplied from a PV array depends mostly on present ambient conditions such as: irradiation and temperature [2-5].

PV output voltage changes mainly with temperature while PV output current changes mainly with irradiation. Therefore in order to develop a very precise simulation model the local wind speed and the solar radiation incidence angle, in terms of the slope and surface azimuth, should be considered [5-8].

In order to determine the hourly incident radiation on a surface of any orientation it is necessary to evaluate the ratio of incident radiation on the tilted surface to that on a horizontal surface considering beam, sky diffuse and ground reflected radiation separately [3], [6], [9].

Increased distributed generation is becoming more important in the current power system and in the future it will rely more on distributed energy resources and micro-grids. The flexible micro-grid has to be able to import/export energy from/to the grid, control the active and reactive power flows and manage of the storage energy [7], [10].

The battery package is an interesting option for storing excess energy from the hybrid grid (wind intermittency) for later use. It may also act as a peak shaving unit and thereby contribute to a stronger grid [13], [15-17].

This paper proposes the development of simulation tools to analyze and simulate power systems with renewable energy sources and electricity storage devices. The tools are based on models implemented first in MATLAB-Simulink and validated by measurements. The paper focuses on simulation models of a small-scale PV System and on a VRB system connected to a micro-grid and on improvements and validating it using experimental facility of an active and distributed power systems laboratory. In order to find out the differences between DER components in power systems and to study the impact on bus voltage and frequency the systems have also been implemented in PowerFactory.

II. DISTRIBUTED ENERGY SYSTEM ARCHITECTURE. EXPERIMENTAL FACILITY-SYSLAB

SYSLAB is a laboratory for research in distributed control and smart grids with a high share of renewable energy production. Its experimental facility is a Wind/PV/Diesel Hybrid Mini-Grid with local storage and a novel control infrastructure. The facility is spread across three sites located several hundred meters apart, as can be seen in Fig. 1a).

It includes two wind turbines (11kW and 55kW), a PV-plant (7.8 kW), a diesel gen-set (48kW/60kVA), an intelligent office building with controllable loads (20kW), a number of loads (75kW, 3*36kW) and a Vanadium Battery of 15 kW/190 kWh. At each of the three sites there is a switchboard that allows the components installed at the site to be connected to either of two bus bars. The two bus bars at each site are connected to a crossbar switchboard allowing the flexible setup of the system(s) to be studied. The bus bars can be either connected to the national grid or can be part of an isolated system. It allows components and systems to be in grid connected operation, island operation, or operation in parallel with wind turbine or PV-plant, as it is shown in Fig. 1b).

The components are all connected in one distributed control and measurement system that enables very flexible setup with respect to experimental configuration.

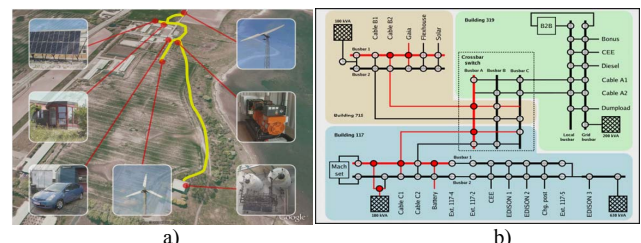


Fig. 1. a) SYSLAB Risø's new laboratory for intelligent, active and distributed power systems and b) details about SYSLAB Micro-Grid architecture.

PV Panel System

The PV panels are mounted in three strings: two strings having 18 panels of 165 W each, and another one containing 12 panels of 100 W. The strings are connected to the SYSLAB grid through a three-phase PV inverter (SMA Sunny Tripower).

Two sets of data are provided by PV system. The first set consists of the ambient measurements from the weather station: solar irradiance on the horizontal, ambient temperature, and wind speed. The second set represents the electric measurements taken from the PV inverter: the AC output power to the grid, and on each PV string the DC power, voltage, and current. The two sets of data are read at different frequencies: 1 Hz for the electrical and 0.1 Hz for the ambient. These large sets of data are used to develop an accurate model of the existing PV setup and to validate it.

Energy Storage System

The Vanadium Redox Battery (VRB) system installed in SYSLAB is connected to the grid via a four quadrant power converter and can deliver 15 kW on the AC side and the nominal storage capacity is 190 kWh.

The battery can operate in two modes: P-Q mode (where the active and reactive power of the battery is set by the user) and U-f mode where the power is set according to the grid voltage and frequency and the pre-defined droop-curves.

A. Data Acquisition and Control System

The data acquisition and control system (hardware and software) is responsible for the supervision and control of the research platform for distributed intelligent energy systems with a high penetration of renewable energy. The supervisory software code was written in Java and is able to manage the data acquisition, processes the data and executes the control loop and outputs the control variables. The sensors outputs are connected to a signal conditioning board, which in turn is connected to the data acquisition (DAQ) board based on a PC (SCADA System).

III. PV PANEL AND ARRAY MODELING

A. Modeling of the PV Panel

To be able to develop an accurate PV panel model it is necessary to define the right equivalent circuit. This paper uses a single diode equivalent circuit for the PV model as it is shown in Fig. 2, and which is described by a simple exponential function:

$$i = I_{ph} - I_0 \left(e^{\frac{v+iR_s}{n_s V_T}} - 1 \right) \quad (1)$$

The double diode model is considered, by many researchers, to be more accurate than the single diode model; the latter one is blamed for being imprecise particularly at low irradiance levels.

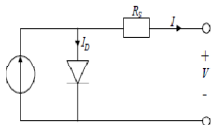


Fig. 2. Equivalent circuit of a PV cell.

However, it has been found out that when it was used for modeling the behavior of many interconnected modules, the single diode model is preferred by many of the authors in the literature [5], [11].

A solar cell can be characterized by the following fundamental parameters:

a) Short circuit current: $I_{ph}=I_{sc}$. It is the greatest value of the current generated by a cell. It is produced under short circuit conditions when $V=0$.

b) Open circuit voltage corresponds to the voltage drop across the diode (p-n junction), when it is traversed by the photocurrent I_{ph} (namely $ID=I_{ph}$), namely when the generated current is $I=0$. It reflects the voltage of the cell and it can be mathematically expressed as:

$$V_{oc} = \frac{k_B T_c A}{q} \ln \left(\frac{I_{ph}}{I_0} \right) = V_T \ln \left(\frac{I_{ph}}{I_0} \right) \quad (2)$$

c) Maximum power point is the operating point, at which the power dissipated in the resistive load is maxim: $P_{max}=I_{max}U_{max}$.

d) Maximum efficiency is the ratio between the maximum power and the incident light power:

$$\eta = \frac{P_{max}}{P_{in}} = \frac{I_{max}V_{max}}{AG_a} \quad (3)$$

e) Fill factor is the ratio of the maximum power that can be delivered to the load and the product of I_{sc} and V_{oc} :

$$FF = \frac{P_{max}}{V_{oc}I_{sc}} = \frac{V_{max}I_{max}}{V_{oc}I_{sc}} \quad (4)$$

Manufacturers typically provide limited operational data for photovoltaic panels. These data are available only at standard rating conditions, for which the irradiance is 1000 W/m^2 and the cell temperature is 25°C , except for the NOCT which is determined at 800 W/m^2 and an ambient temperature of 20°C . It is known that the temperature and irradiance play a central role in PV conversion process since it affects basic electrical parameters, such as the voltage and the current of the PV generator. As a consequence, the operating temperature of a PV device represents a fundamental variable which directly affects the electrical power output of the device and its efficiency.

Equations for the short circuit current and the open circuit voltage as a function of absolute temperature include temperature coefficients that provide the rate of change with respect to temperature of the PV performance parameters, can be express as:

$$\begin{aligned} I_{sc} &= I_{sc25}(1 + \beta \Delta T) \\ V_{oc} &= V_{oc25}(1 + \chi \Delta T) \\ \Delta T &= T^c (\text{C}) - 25^\circ \end{aligned} \quad (5)$$

To complete the model it is also necessary to take into account the variation of the parameters with respect to irradiance:

$$I_{sc} = I_{sc25} \frac{G_a}{1000} \quad (6)$$

Using a four parameters model of a single diode equivalent circuit, the v-i characteristics for a solar panel string depending on irradiance G_a and temperature T_c , has the following expressions:

$$v = n_{ps} V_{oc} + n_{ps} n_s V_T \ln \left(1 - \frac{i}{n_{sp} I_{sc25} \frac{G_a}{1000}} \right) \dots (7)$$

$$i = n_{sp} I_{sc} \left(1 - e^{-\frac{v - n_{ps} V_{oc} + R_s i}{n_{ps} n_s V_T}} \right) \quad (8)$$

These equations can be used to calculate the voltage and current over a string of panels.

The model used to obtain the static characteristics of the PV panels has been developed in MATLAB using the equations presented above. The model was developed for one panel, as a function of irradiance and temperature. The model has as inputs the solar irradiance G_a and the cell temperature T_c on the panel and it sweeps the voltage range of the PV panel in order to calculate the output current and power.

PV cells have nonlinear i-v and p-v characteristics. Its output voltage and power change according to temperature and irradiation.

Fig. 3 shows the typical characteristics for a PV model and also a comparison between PV technical characteristics from datasheet (on the left) and simulation results for one panel.

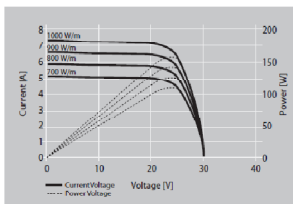
B. Modeling of the PV Array

A Matlab/Simulink model has been developed, based on the equations presented in the last section, in order to reproduce the electrical behavior of the existing PV strings at the SYSLAB experimental facility. The temperature and the solar radiance on the panel are the inputs of the model and the AC power at the inverters' grid side is the output of the model. For obtaining the maximum power of the panel strings, the condition (9) should be fulfilled:

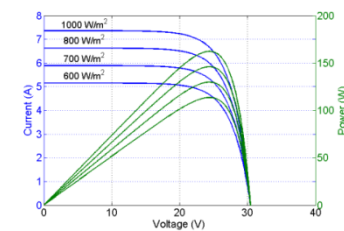
$$\frac{dP}{dV} = 0 \quad (9)$$

That means:

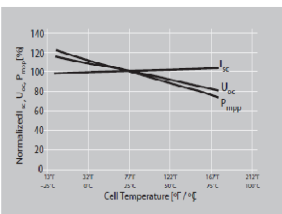
$$n_{sp} I_{sc} \left[1 - e^{-\frac{v - n_{ps} V_{OC} + R_s i}{n_{ps} n_s V_T}} - \frac{v}{n_{ps} n_s V_T} e^{-\frac{v - n_{ps} V_{OC} + R_s i}{n_{ps} n_s V_T}} \right] = 0 \quad (10)$$



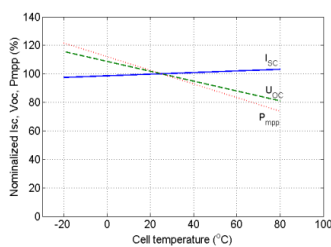
Electrical Performance



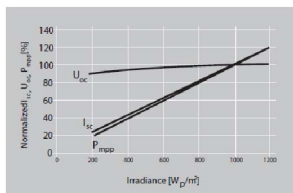
a)



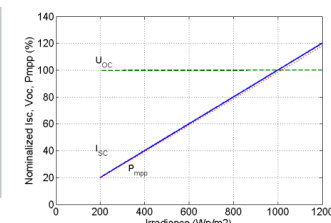
Temperature Dependence of I_{sc} , U_{oc} & P_{mpp}



b)



Irradiance Dependence of I_{sc} , U_{oc} & P_{mpp}



c)

Fig. 3. Comparison between PV technical characteristics from datasheet (on left) and simulation results for one panel.

The block diagram implemented in Simulink that is developed to implement this model is depicted in Fig. 4.

In order to solve the implicit function expressed above with the voltage as the unknown, the “algebraic constraints” block was used.

An additional assumption was made in this case because the equation also requires the current value, which is computed from the voltage value; in order to break the loop, the current value is taken from the last simulation step. This assumption relies on the fact that the electric measurements have a sample time of 1 second and the environment measurements have a sample time of 10 seconds; thus the system changes states each 10 seconds, and only once in this 10 seconds interval the model takes the current value from the previous state.

However, if the parameters mentioned in Appendix are provided, a more simple way of calculating the maximum power, with highly accurate results, can be considered by using (5) and (6):

$$P_{mpp} = FFI_{sc} V_{OC} (1 + \alpha \Delta T) \quad (11)$$

For the model input values, the measurements from the weather station had to be translated via additional function that were implemented, in order to reproduce the values on the actual PV panel conditions.

C. Improvements and Validation of the Model

As stated before, two types of measurements are taken from the experimental facility: ambient measurements from the weather station and electrical measurements taken from the PV inverter.

The three ambient measurements: ambient temperature, horizontal solar radiation and wind speed are fed to an additional simulation module that calculates the cell temperature of the PV panels and the solar radiation on them.

1. Cell temperature

The cell temperature can be very different from the ambient temperature and it depends on the solar irradiation G_a , ambient temperature T_a and also on the wind speed W_s (Fig. 5). Solar irradiation acts on increasing T_{cell} and the wind speed has a cooling effect and lowers T_{cell} .

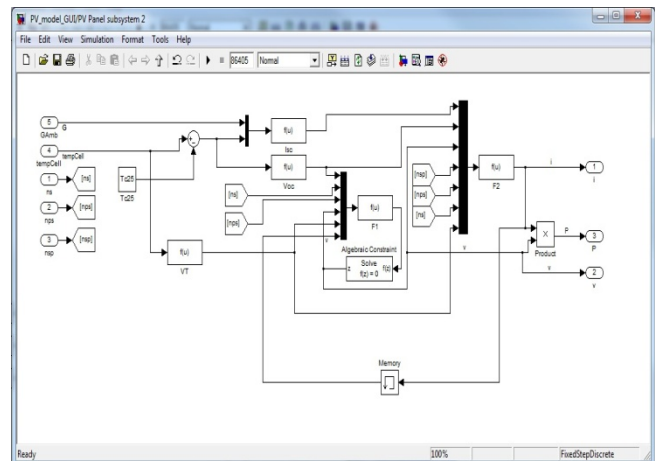


Fig. 4. The PV string model implemented in Simulink.

The simplest relation for the steady state operating cell temperature T_c and the ambient temperature T_a , considering only the influence of the solar irradiance G_a is [13]:

$$T_c = T_a + kG_a \quad (12)$$

The values for k are usually in the range of 0.02-0.04. The value for this coefficient can be obtained from the data sheet, considering the NOCT values:

$$k = \frac{NOCT - T_{aNOCT}}{G_{aNOCT}} \quad (13)$$

Usually, in low wind speed areas, the effect of the wind on the PV cells is negligible, the free convection and the radiation term having very small values [3], [5].

If the PV panels are mounted in regions with high wind potential (as in our case), the wind speed must be considered because it has a large influence. The forced (wind) convection is large for high wind speeds and the cell temperature function takes the following form [5]:

$$T_c = T_a + \omega \left(\frac{0.32}{8.91 + 2 \frac{W_s}{0.67}} \right) G_a \quad (14)$$

Where ω is the mounting coefficient, which depends on the mounting conditions of the PV panels and W_s is the wind speed measured on horizontal plane.

The wind that produces the cooling effect through forced convection is the wind parallel to the panel surface; that is why the transformation $W_{\text{parallel}} = W_s/0.67$ is used.

For a better understanding on the influence of solar irradiance and wind speed on the cell temperature, a graphical representation of these values is depicted in Fig. 5.

The differences in temperature of the PV cells according to different considerations are also presented in Fig. 5.

The solar irradiance has a high heating effect, at noon it can be seen a 30°C increase of cell temperature. Considering also the wind effect, the cell temperature is lowered, at noon, with 12°C. This change in temperature has an effect on the output power; as it has been shown in Fig. 3b). For instance, at each degree change in temperature, the efficiency modifies with approximately 0.44 %, if the temperature rises, the efficiency decreases and vice versa.

2. Solar irradiance on the PV panel

The major advantage of the SYSLAB experimental facility is the multitude of measurements that can be used to identify phenomenon or causes and to include them accurately into the model.

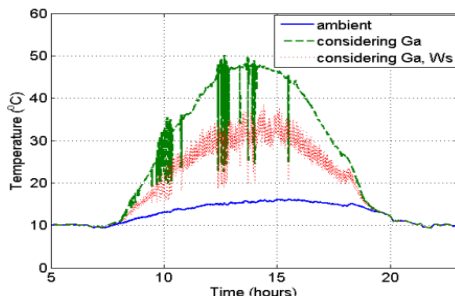


Fig. 5. Ambient measurements and their effect on the PV cell temperature.

As shown in Fig. 3c), the solar irradiance has influence only on the current and implicitly on the output power of the PV panel, so the plots contain the effect of the change in the input solar irradiance, according to the 'adaptation' of the horizontal solar irradiance to the real case of the PV panel. The solar irradiance input to the model is the horizontal value measured from the weather station. This translates into substantial differences.

3. Considering the tilt angle of the PV panels

The PV panels from SYSLAB, shown in Fig. 1a) are tilted at 60°. For introducing this factor into the model, the declination angle has to be defined:

The declination angle is the angular position of the sun at solar noon with respect to the plane of the equator. Its value is given by [6]:

$$\delta = 23.45 \sin \left(360 \frac{284+n}{365.25} \right) \quad (15)$$

Where 23.45 is the Tropic of Cancer latitude.

For this equation, the days are numbered from the spring equinox (day 81) and using the fact that \sin is a periodic function, $365-81=284$.

The relation between solar irradiance on horizontal plane and the solar irradiance on a tilted panel, facing south is:

$$S_{\text{panel}} = \frac{S_{\text{horiz}} \sin(\alpha+\beta)}{\sin \alpha} \quad (16)$$

In which $\alpha = 90-\varphi+\delta$.

From this equation it is clear that the ratio between the solar irradiance on the PV panel and the one on the horizontal changes during the year, as the earth orbits the sun and the declination angle changes with every day. The day number of the considered day has also to be considered as input for the simulation model.

4. Considering the orientation of the PV panels

For estimating the solar irradiance for a non facing south PV panel from a facing south PV, which the model calculates at this stage, some additional definitions and relations have to be introduced.

Solar hour angle – the geometrical angle between the sun's sky position projected on the ground in each moment of the day and the projection at solar noon; each hour, the sun travels 15° on the sky. It has a negative value before solar noon, zero at solar noon and positive after.

$$\omega = 15^\circ(\text{SolarNoon} - T) \quad (17)$$

Equation of time – is an astronomical term accounting for changes in the time of solar noon for a given location over the course of a year. Earth's elliptical orbit and Kepler's law of equal areas in equal times are the culprits behind this phenomenon. The equation describing this difference (in minutes) is given below [3]:

$$M = 2\pi \frac{M_{\text{day}}}{365.25} \quad (18)$$

$$\Delta_{\text{noon}} = (-7.65 \sin M + 9.86 \sin(2M + 3.6)) \quad (19)$$

$$\text{SolarNoon} = 12(\text{hours}) + \Delta_{\text{noon}}(\text{minutes}) \quad (20)$$

The daylight saving time has to be considered also: in summer hour, the solar noon is at 12+1=13 hours. For calculating the solar irradiation on the PV panels from the solar radiation on a tilted panel, calculated at stage 2 (Fig. 7b), a *correction factor* is defined as:

$$F_{\text{corr}} = \frac{\cos \omega}{\cos(\omega - \text{deviation})} \quad (21)$$

In addition to the day's number in the year, the model has to be provided with the local time, as of this 13° deviation, the solar irradiance on the PV panel has a nonlinear variation from the measured horizontal solar irradiation according to the position of the sun on the sky on each moment of the day.

The simulation model, developed before in MATLAB/Simulink for one PV panel, has been improved and modified for a PV array with three strings. A block diagram of the model can be seen in Fig. 6.

The PV array model is based on the equations (7-9). The equations (7-9) represent the PV characteristics taking into account the no. of strings in parallel and the no. of panels in series.

Solving the equation (11) we can determine the maximum power point, which the inverter should track precisely, because in the PV systems there are no mechanical parts involved, and thus, the time constants are very small, being all electrical in nature (e.g. compared to wind turbine systems).

In Fig. 7 are presented the simulation results versus measurements at different stages of the modeling. These figures also show the importance of several factors that have to be taken in consideration, especially PV panel tilt angle and orientation.

In Fig. 7 a) is shown a comparison between measured and simulated output power without considering wind speed effect or any improvements, such as: the orientation and the tilt angle of the PV panels.

Fig. 7 b) shows the same waveform for output power, with the same peak values, and the same changes in power due to shading effect in a synchronous manner. The simulation has a delay of around 50 minutes. This is the effect of the PV panels' orientation, which have a 13° deviation from the E-W axis.

Considering the tilt angle and orientation, the influence of solar irradiance and wind speed on the cell temperature the measurements and simulations are almost identically, as can be seen in Fig. 7 c).

5. VRB MODEL IMPLEMENTED IN MATLAB-SIMULINK AND VALIDATED BY MEASUREMENTS

A. VRB Modeling and Implementation

The VRB model has been developed in Matlab/Simulink and is based on the power equilibrium between the input and the stored power considering the efficiencies of different components and the power losses, as can be seen in Fig. 8. These characteristics of the battery have been computed based on experiments by measuring different electric values at different loads and SOC levels [15].

The simulation model of the battery system contains five subsystems: the power converter, the cell stacks, the energy

storage, voltage limitation and the auxiliaries, as it is depicted in Fig. 8 b).

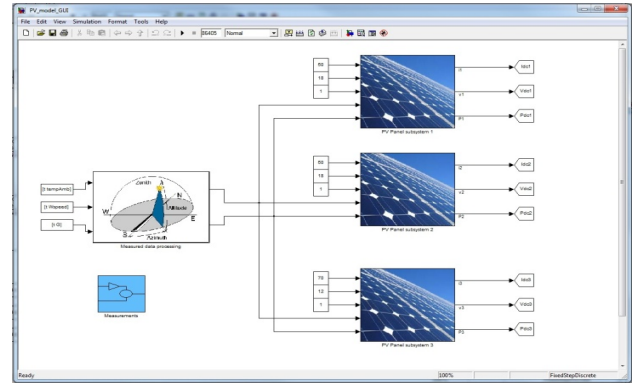


Fig. 6. Block diagram of the simulation model for PV array.

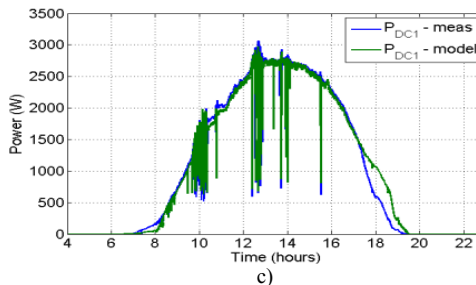
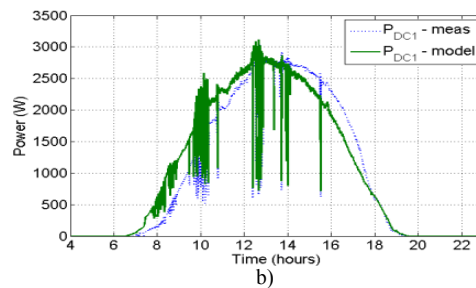
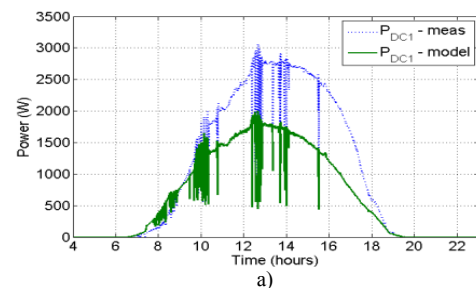
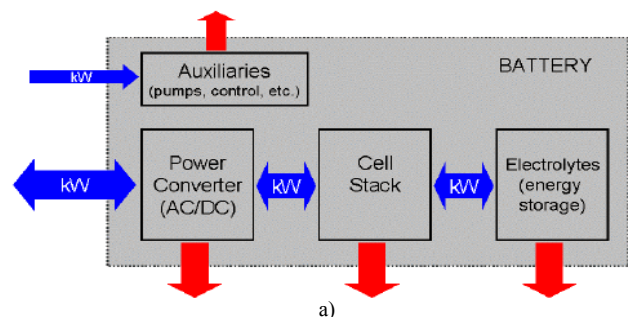


Fig. 7. Solar irradiance adaptation steps.



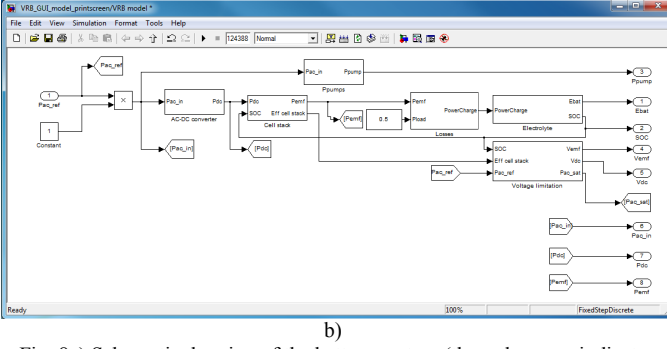


Fig. 8a) Schematic drawing of the battery system (the red arrows indicate losses from the different parts of the system) and b) Simulink implementation.

The power converter was modeled using a look-up table with the efficiency of the AC-DC converter in charge and discharge operation modes.

The efficiency of the cell stacks was implemented as a function of the DC power at different SOC levels, when the battery was running in stable conditions during charge/discharge modes, and can be described by:

$$\text{eff} = \left(1 + \frac{\text{eff}_{\text{SOC}100} - 1}{15}\right) (\pm P_{\text{DC}}) \left(1 - \left(1 - \frac{\text{eff}_{\text{SOC}0}}{\text{eff}_{\text{SOC}100}}\right) \text{SOC}\right) \quad (22)$$

In which the efficiency $\text{eff}_{\text{SOC}0}$ was considers at $P_{\text{DC}}=15 \text{ kW}$ and $\text{SOC}=0 \%$ and $\text{eff}_{\text{SOC}100}$ at $P_{\text{DC}}=15 \text{ kW}$ and $\text{SOC}=100 \%$. The total power available is related to the electrode area in the cell stacks and the total energy stored in the VRB depends on both the SOC and the amount of active chemical substances. The actual energy stored in the battery is defined as:

$$E_{\text{batt}} = E_{\text{batt}0} + \int P_{\text{cell}} dt \quad (23)$$

Where $E_{\text{batt}0}$ is the initial energy stored in the battery and P_{cell} is the charge/discharge power at the electrolyte side. The state of charge (SOC) is defined as the amount of energy stored in the battery (E_{batt}) divided by the total energy capacity E_T :

$$\text{SOC} = \frac{E_{\text{batt}}}{E_T} \quad (24)$$

The energy storage subsystem was implemented based on (23) and (24) having as output E_{bat} and SOC .

For a vanadium battery the auxiliary power consumption is significant since the electrolyte has to be circulated for the battery to be operational. The power of the auxiliaries (control system, pumps, etc.) can be derived from the measured AC power of the battery and the total power flow over the bus (when only the battery is connected). When the battery is off, the power consumption (for the control PC and the displays) is 235W. When the battery is on and the pumps are running the power consumption is between 1.1 and 1.6kW depending on the AC power [15]. The auxiliary block has also been modeled by a look-up table considering experimental data from [15].

The voltage limitation block has two functionalities: to calculate the DC side voltage of the converter and to calculate the AC limit power according to the SOC. The power input is physically limited and at high SOC values, the converter is not

able to receive the prescribed power, but a limited one. Also the subsystem contains an empirical relation between the SOC and the voltage across the electrolyte (V_{cell}) implemented by a look-up table based on experiments.

B. Comparison between simulation and measurements

In order to validate the simulation model, measurements were taken from the DAQ board of the VRB, fed into the model and verifying the output values of the battery and of the model.

The following experiment for a time scale of 36 hours was considered: starting from a SOC=93.5% the battery was discharged with a constant $P_{\text{AC}}=15\text{kW}$, until SOC=18%. Then a charge sequence from SOC=14% until SOC=87% at $P_{\text{AC}}=10\text{kW}$ was considered. A comparison between simulations and measurements is presented in Fig. 9.

6. SIMULATION MODEL OF DER COMPONENTS DEVELOPED IN DIGSILENT POWERFACTORY FOR DISTRIBUTION NETWORKS

In the distribution network a high share of PV may require new approaches for voltage control as the power output of PV system can change rapidly if clouds pass very fast over the PV system. New control approaches may include active P/Q control from the PV system, changed design of the embedded distribution system control as well as active demand-side control [14].

Computer models of power systems are widely used by power system utilities to study load flow, steady-state voltage stability and dynamic and transient behavior of power system.

DIGSILENT PowerFactory has been chosen because provides the ability to simulate load flow, RMS fluctuations in the same software environment. It provides a comprehensive library of models for electrical components in the power system [18].

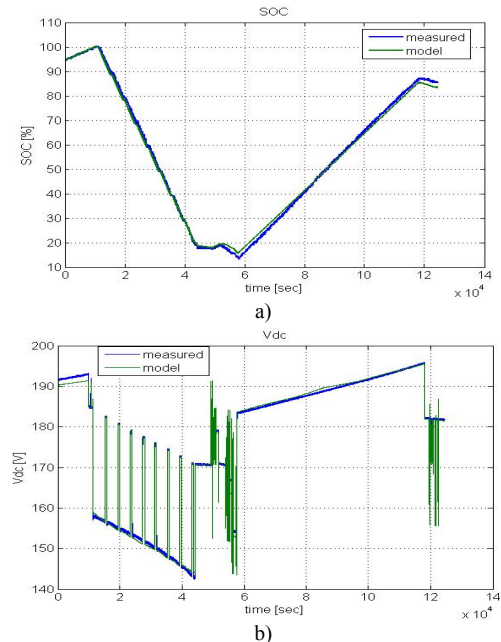


Fig. 9. Comparison between simulations and measurements: a) State of Charge sequence-SOC and b) DC Voltage- V_{dc} .

The dynamic models of the PV System and VRB system implemented in PowerFactory has been built with standard components library and are based on the same equations used for MATLAB/Simulink models presented before.

The blocks of the PV system (Fig. 10b), such as: PV model, DC-Link and controller of the Static Generator and of the VRB system (Fig. 10c), such as: battery model, charge and P-Q controllers are implemented in the dynamic simulation language DSL of DiGSILENT. DSL allows the user to implement specific models that are not standard in the DiGSILENT library and thus to create own developed blocks either as modifications of existing models or as completely new models. The internal simulation language DSL has also been used to define the PV and VRB characteristics and to initialize the parameters and variables of the models.

Fig. 10 a) shows a single line diagram of the SYSLAB architecture implemented in PowerFactory. For load flow analysis, also shown in Fig. 10 a), the local voltage controller could be set to three different modes: $\cos\phi$, V and $droop$. For RMS and EMT simulations the static generator supports two different models: current source and voltage source models. In our case we use a current source model which has as inputs d-q axis reference current coming from the controller and $\cos\phi_{ref}$ and $\sin\phi_{ref}$ signals from a PLL model.

Fig. 10 b) shows the schematic structure of the PV System model, developed for time-domain simulations where a DSL model is required, including Photovoltaic Model, DC-Link Model, PLL block and Static Generator with its Controller. The Static Generator is an easy to use model of any kind of static (non rotating) generators. Applications are PV Generators, Storage devices, wind generators etc. The PV

system frame also contains the measurements blocks used as inputs for different components of the model. For instance, the Photovoltaic Model has as inputs irradiation G and cell temperature $temp_{Cell}$, obtained from MATLAB-Simulink model considering the tilt angle, orientation and the influence of solar irradiation and wind speed on the cell temperature, implemented as a look-up table, as can be seen in Fig. 11a). Also the MPP of current, power and voltage as a function of time for one module are shown.

In Fig. 10 c) it is shown the VRB system block diagram developed for time-domain simulations (RMS and EMT). The battery energy storage system contains the model of VRB, developed in DSL using the same equations like in Simulink model presented in the last section and the charge/discharge controller which takes in consideration the SOC level of the battery, DC current and voltage of the cell stacks and provides the current set-point for the inverter. Also, to study the system stability the frequency and power controllers have been implemented.

In order to validate the simulation model developed in PowerFactory and to compare the results with MATLAB-Simulink model, the same measurements have been used like in last section when we compare the results of Simulink model with experiments (Fig. 9). The data were acquired by SCADA system with a sampling time of 1 sec and process by MATLAB. The simulations sample-time in PowerFactory was the same like in measurements. As can be seen in Fig. 11 b) the simulation results of DC Voltage and Power for different SOC level are similar.

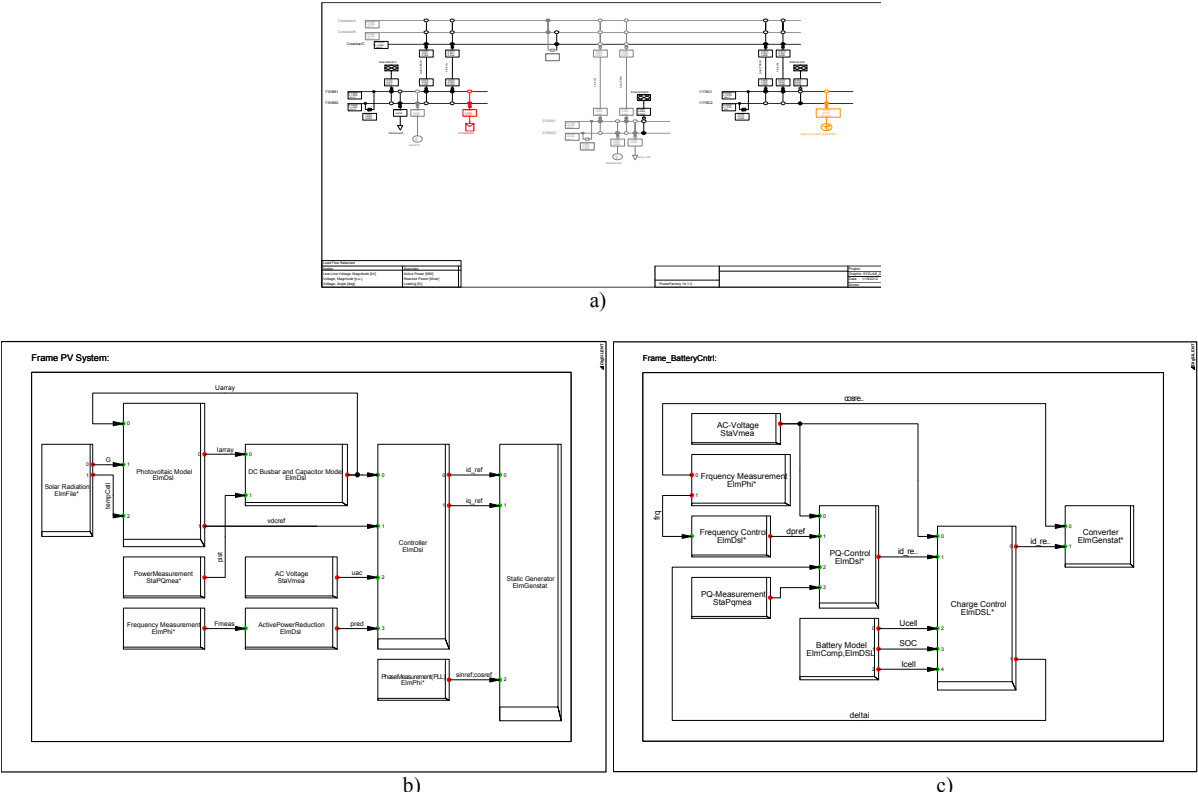
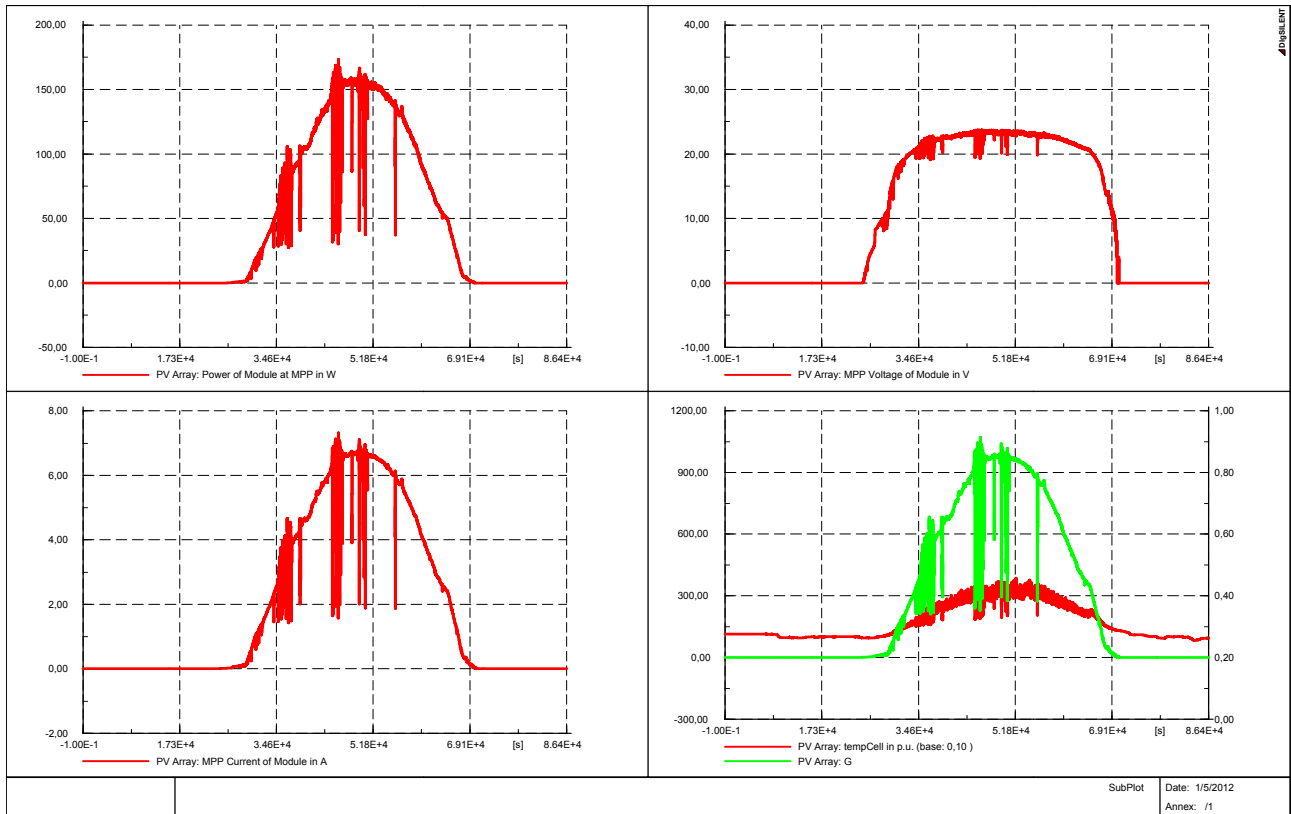
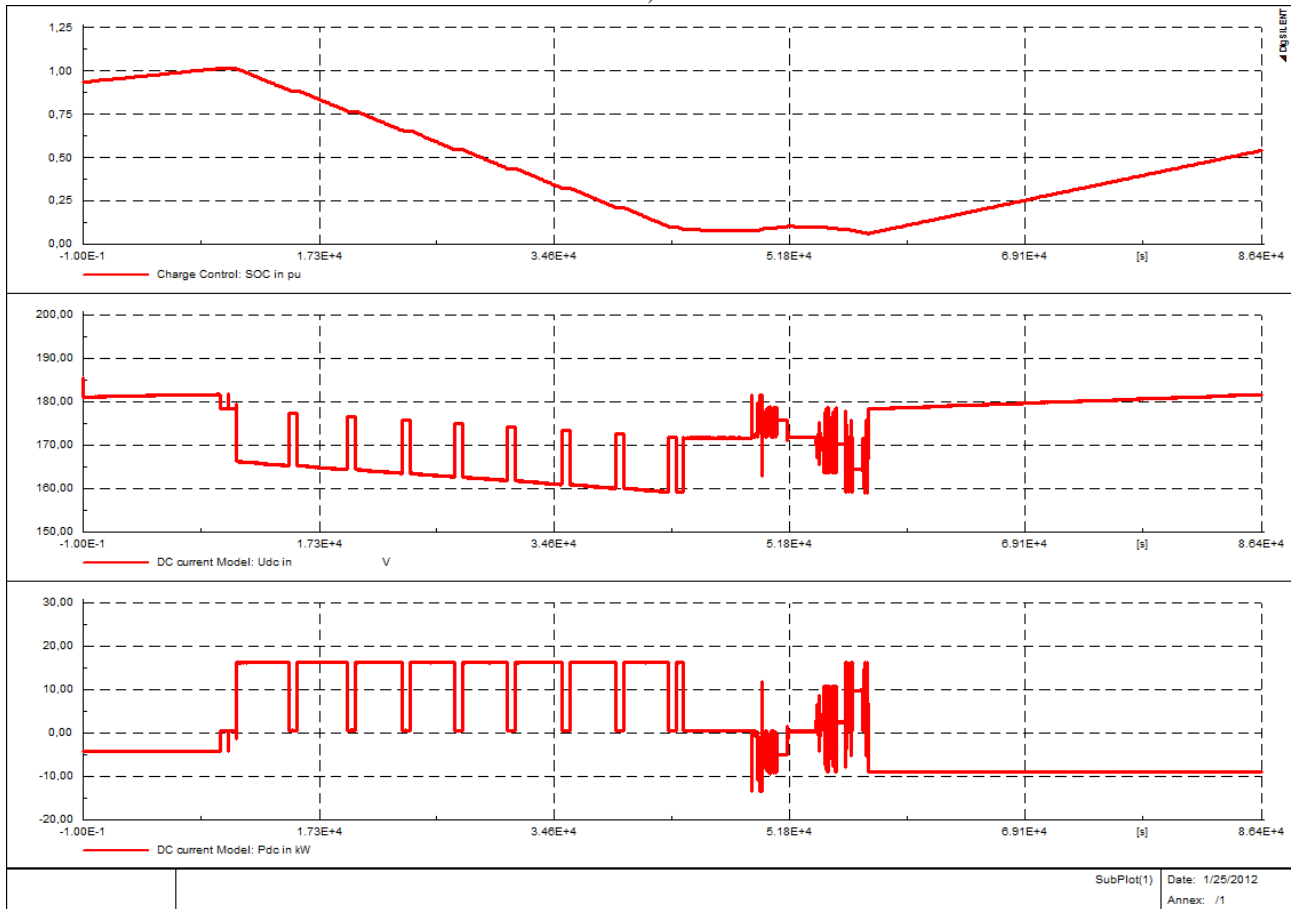


Fig. 10. a) Single line diagram of SYSLAB configuration, b) schematic block diagram of the PV system model and c) VRB system implemented in PowerFactory.



a)



b)

Fig. 11. Simulation results of the PV system model, a) and of the VRB system model, b) in DIgSILENT PowerFactory.

CONCLUSIONS

This paper proposes the development of simulation tools to analyze and simulate power systems with renewable energy sources and electricity storage. The tools are based on models validated by measurements.

A four-parameter model of a PV panel and a PV system, implemented in MATLAB/Simulink, using data provided by the manufacturer with semi-empirical equations to predict the PV characteristics for any condition. PV characteristics are modeled according to a single diode four parameter equivalent circuit and according to PV parameters values taken from the manufacturer technical data.

The paper also proposes a model that relies on ambient data from a local weather station, like most common in a real situation, not from sensors mounted on the PV panels. The model calculates the cell temperature and the solar irradiance on the PV panels considering, among others, the tilt angle, the orientation of the panels, and the wind cooling effect. The paper shows that these factors significantly influence the power output from the PV panels.

The VRB model has been developed and implemented first in MATLAB-Simulink considering the efficiency and the power losses of different components. The characteristics of the battery have been computed based experiments by measuring electrical parameters at different loads and SOC levels.

Comparison with experimental data, acquired by SCADA system and processed by MATLAB, and with the characteristics of the PV panels and VRB, provided by manufacturers, has shown that the models implemented in MATLAB/Simulink can be an accurate simulation tool to study and analyze the characteristics of individual units and for the prediction of energy production with energy storage systems.

A PV system and a VRB system model, using the same equations and parameters as in MATLAB/Simulink has also been developed and implemented in PowerFactory to study load flow, steady-state voltage stability and dynamic behavior of a distributed power system. Also, the simulation results have shown a good similarity between both tools.

APPENDIX

TABLE I.

OPERATIONAL DATA FOR PV PANEL FROM DATA SHEET

| Parameter (unit) | Value | Description |
|---|--------|---|
| for STC – solar irradiance (G_s)=1000W/m ² , cell temperature(T_c)=25°C, wind speed 1m/s | | |
| P_{mpp} (W) | 165 | Rated output power |
| V_{mpp} (V) | 24.2 | Nominal voltage |
| I_{mpp} (A) | 6.83 | Nominal current |
| V_{oc25} (V) | 30.4 | Open circuit voltage |
| I_{sc25} (A) | 7.36 | Short circuit current |
| α (%/°C) | -0.478 | Temperature coefficient for change in (P_{mpp}) |
| β (%/°C) | 0.057 | Temperature coefficient for change in |

| | | (I_{sc}) |
|---|--------|---|
| χ (%/°C) | -0.346 | Temperature coefficient for change in (U_{oc}) |
| δ (%/°C) | -0.004 | Temperature coefficient for change in (I_{mpp}) |
| ε (%/°C) | 50 | Temperature coefficient for change in (U_{mpp}) |
| for NOCT – solar irradiance(G_{aNOCT})=800W/m ² , ambient air temperature(T_{aNOCT})=20°C, wind speed 1m/s | | |
| NOCT (°C) | 46.2 | Cell temperature on the above mentioned conditions |

TABLE II.

VRB MODEL PARAMETERS

| PARAMETER | VALUE |
|---|---------|
| SERIES RESISTANCE, R_s [Ω] | 0.25 |
| DC NOMINAL CURRENT, I_{dc} [A] | 136 |
| AC NOMINAL CURRENT, I_{ac} [A] | 30 |
| DC VOLTAGE(OPERATING RANGE), V_{dc} [V] | 130-190 |
| AC VOLTAGE(OPERATING RANGE), V_{ac} [V] | 360-440 |
| MAXIMUM OPERATING APARENT POWER, S[kVA] | 20 |
| MAXIMUM OPERATING ACTIVE POWER, P[kW] | 20 |
| MAXIMUM REACTIVE POWER, Q[kVAR] | 12 |

ACKNOWLEDGMENT

This work was supported in part by the E.U. Project No. 228449/2010-2012 and also partially supported by the strategic grant POSDRU/88/1.5/S/50783 (2009) of the Ministry of Labor, Family and Social Protection, Romania, co-financed by the European Social Fund – Investing in people.

REFERENCES

- [1] *.www.energynautics.com, Energynautics GmbH, Longen, Germany, 2010.
- [2] S. Seme, G. Stumberg, and J. Vorsic, "Maximum efficiency trajectories of a two-axis sun tracking system determined considering tracking system consumption," *IEEE Trans. On Power Electronics*, vol. 26, no. 4, pp. 1280-1290, Apr. 2011.
- [3] W. De. Soto, S. A. Klein, and W. A. Beckman, "Improvement and validation of a model for photovoltaic array performance," *ELSEVIER Solar Energy*, vol. 80, pp. 78-88, 2006.
- [4] Y. Riffonneau, S. Bacha, S. Barruel and S. Ploix, "Optimal Power Management for grid connected PV Systems with batteries", *IEEE Transaction on Sustainable Energy*, vol. 2, no. 3, pp. 309-320, July 2011.

- [5] E. Skoplaski, A. G. Boudouvis and J. A. Polyvos, "A simple correlation for the operating temperature of photovoltaic modules of arbitrary mounting", *ELSEVIER Solar Energy Materials*, pp. 1393-1402, 2008.
- [6] K. Murat, S. Mehmet, B. Yunus, D. Sedat, "Determining optimum tilt angles and orientations of photovoltaic panels in Saliurfa", *IEEE Transaction on Renewable Energy*, vol. 29, issue 8, pp. 1265-1275, 2004.
- [7] H. Jiayi, J. Chuanwen, and X. Rong, "A review on distributed energy resources and MicroGrid", *ELSEVIER Renewable & Sustainable Energy Reviews*, vol. 12, pp. 2472-2483, 2008.
- [8] M. G. Villalva, J. R. Gazoli, E. R. Filho, "Comprehensive Approach to Modelling and Simulation of Photovoltaic Arrays", *IEEE Transaction on Power Electronics*, vol. 24, issue: 5, pp. 1198-1208, 2009.
- [9] D. Y. Goswami, *Principles of Solar Engineering*, (2 nd ed.), Philadelphia: Taylor & Francis, 2000, p. 81-98.
- [10] M. Jansen, R. Louie, M. E. Amoli and F. Sami, "Model and simulation of a 75 kW PV solar array", in *Proc. 2010 IEEE PES Transmission and Distribution Conference and Exposition*, pp. 1-5.
- [11] D. Sera, R. Teodorescu, and P. Rodriguez, "PV panel model based on datasheet values", in *Proc. 2007 IEEE International Symposium on Industrial Electronics*, pp. 2392-2396.
- [12] H. Liu, L. Jin, D. Le and A. A. Chowdhury, "Impact of high penetration of solar photovoltaic generation on power system small signal stability", in *Proc. 2010 POWERCON*, pp. 1-7.
- [13] A.D. Hansen, P. Sørensen, L.H. Hansen, H. Bindner, "Models for a Stand-Alone PV System", Risø National Laboratory, Roskilde, Risø-R-1219(EN) / SEC-R-12, Dec. 2000.
- [14] *IEEE Standard for Interconnecting Distributed Resources with Electric Power Systems*, IEEE Standard 1547-2008.
- [15] H. Bidner, C. Ekman, O. Gehrke and F. Isleifsson, "Characterization of Vanadium Flow Battery", Risø-R-1753 Report, Roskilde, Denmark, October 2010.
- [16] L. Barote, R. Weissbach, R. Teodorescu, C. Marinescu, M. Cirstea, "Stand-Alone Wind System with Vanadium Redox Battery Energy Storage", IEEE, International Conference on Optimization of Electrical and Electronic Equipments, OPTIM'08, pp. 407-412, 22-24 May 2008, Brasov, Romania.
- [17] W. Wang, B. Ge, D. Bi and D. Sun, "Grid-Connected Wind Farm Power Control using VRB-based Energy Storage System", *IEEE Transaction on Energy Conversion*, pp.3772-3777, 2010.
- [18] DlgSILENT PowerFactory, User's Manual and Tutorial-Version 14.1, Gomaringen-Germany, November 2011.

Development, Improvements and Validation of a PV System Simulation Model in a Micro-Grid

Lucian Mihet-Popa^{*,**}, C. Koch-Ciobotaru^{**}, F. Isleifsson^{*} and H. Bindner^{*}

^{*} Department of Electrical Engineering, Technical University of Denmark, 4000 Roskilde, Frederiksborgvej 399, Denmark
Phone: (45) 2365 2984, E-Mail: lmih@elektro.dtu.dk, WWW: <http://www.elektro.dtu.dk>

^{**} Department of Electrical Engineering, POLITEHNICA University of Timisoara, 300223 Timisoara, V. Parvan 2, Romania
Phone: (40) 256-403464, E-Mail: lucian.mihet@et.upt.ro, WWW: <http://www.et.upt.ro>

Abstract – *The increasing amount of Distributed Energy Resources (DER) components into distribution networks involves the development of accurate simulation models that take into account an increasing number of factors that influence the output power from the Distributed Generators (DG) systems. The modeling of DER components in power systems and the relative control architecture are an important part for the introduction of relevant quantity of renewable energy in the future smart grid. Therefore it is a strong necessity to have proper validated models to help operators to perform better studies and to be more confident with the results. This paper presents two simulation models developed and implemented in MATLAB/Simulink and DIGSILENT Power Factory of a PV system using the single-diode four-parameter model based on data sheet values. The component models were implemented first in MATLAB/Simulink and the simulation results have been compared with the data sheet values and with the characteristics of the units. To point out the strong dependency on ambient conditions and to validate the simulation models a complex data processing subsystem model has also been developed. A PV inverter model have also been developed and implemented in PowerFactory to study load flow, steady-state voltage stability and dynamic behavior of a distribution system. Validation of simulation models have been carried out using RISO experimental facility SYSLAB which include a PV System as well as a Vanadium Redox Flow Battery-VRB and various loads including an office building-FlexHouse in a LV network which can be operated in different configurations.*

Keywords: *Distributed Energy Resources, Distributed Generators, incident and tilt angle, Micro-Grid, PV panels, solar radiation.*

I. INTRODUCTION

Renewable energy systems are expanding due to not only environmental aspect but also due to social, economical

and political interest. The European Union is aiming at a specific CO₂ reduction in the electricity sector in the near future (20 % reduction by 2020). This will involve a significant growth of PV installation all over Europe resulting in a few hundred Giga watts of capacity [1-3].

The increased PV capacity will influence power system operation and design. Power supplied from a PV array depends mostly on present ambient conditions such as: irradiation and temperature [3-7].

The distributed generation is taking importance pointing out that the future utility line will be formed by distributed energy resources and micro-grids. The flexible micro-grid has to be able to import/export energy from/to the grid, control the active and reactive power flows and manage of the storage energy [3, 8].

PV output voltage changes mainly with temperature while PV output current changes mainly with irradiation. Therefore in order to develop a very precise simulation model the local wind speed and the solar radiation incidence angle, in terms of the slope and surface azimuth, should be considered [4-7, 9-11].

In order to determine the hourly incident radiation on a surface of any orientation it is necessary to evaluate the ratio of incident radiation on the tilted surface to that on a horizontal surface considering beam, sky diffuse and ground reflected radiation separately [4], [6], [9].

Increased distributed generation is becoming more important in the current power system and in the future it will rely more on distributed energy resources and micro-grids. The flexible micro-grid has to be able to import/export energy from/to the grid, control the active and reactive power flows and manage of the storage energy [12-13].

This paper focuses on the simulation models of a small-scale PV System connected to a distributed network and on improvements and validating it using experimental facility of an active and distributed power systems laboratory. In order to find out the differences between DER components in power systems and to study the impact on bus voltage and frequency the system has been implemented in MATLAB/Simulink and PowerFactory.

II. DISTRIBUTED ENERGY SYSTEM ARCHITECTURE. EXPERIMENTAL FACILITY

SYSLAB is a laboratory for research in distributed control and smart grids with a high share of renewable energy production. Its experimental facility is a Wind/PV/Diesel Hybrid Mini-Grid with local storage and a novel control infrastructure [14]. The facility is spread across three sites located several hundred meters apart, as can be seen in Fig. 1a).

It includes two wind turbines (11kW and 55kW), a PV-plant (7.8 kW), a diesel gen-set (48kW/60kVA), an intelligent office building with controllable loads (20kW), a number of loads (75kW, 3*36kW) and a Vanadium Battery of 15 kW/190 kWh. At each of the three sites there is a switchboard that allows the components installed at the site to be connected to either of two bus bars. The two bus bars at each site are connected to a crossbar switchboard allowing the flexible setup of the system(s) to be studied. The bus bars can be either connected to the national grid or can be part of an isolated system. It allows components and systems to be in grid connected operation, island operation, or operation in parallel with wind turbine or PV-plant, as it is shown in Fig. 1b).

The components are all connected in one distributed control and measurement system that enables very flexible setup with respect to experimental configuration.

A. PV Panels

The PV panels are mounted in three strings: two strings having 18 panels of 165 W each, and another one containing 12 panels of 100 W [15-18]. The strings are connected to the SYSLAB grid through a three-phase PV inverter (SMA Sunny Tripower [19]).

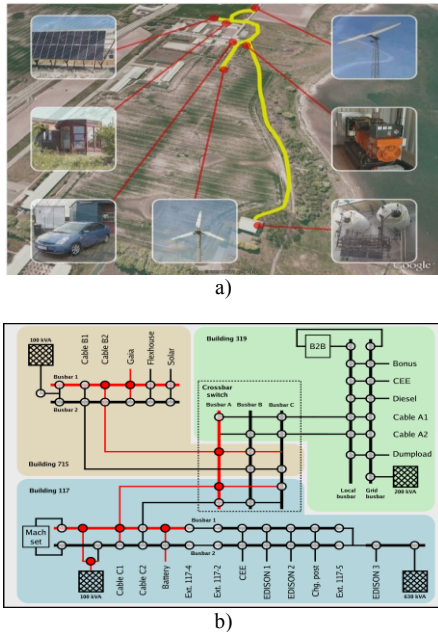


Fig. 1. a) SYSLAB Risø's new laboratory for intelligent, active and distributed power systems and b) details about SYSLAB Micro-Grid architecture.

From PV system two sets of data are provided. The first set consists of the ambient measurements from the weather station: solar irradiance on the horizontal, ambient temperature, and wind speed. The second set represents the electric measurements taken from the inverter: the AC output power to the grid, and on each PV string the DC power, voltage, and current. The two sets of data are read at different sampling frequencies: 1 Hz for the electrical and 0.1 Hz for the ambient. These large sets of data are used to develop an accurate model of the existing PV setup and to validate it.

B. Data Acquisition and Control System

The data acquisition and control system (hardware and software) is responsible for the supervision and control of the research platform for distributed intelligent energy systems with a high penetration of renewable energy. The supervisory software code was written in Java and is able to manage the data acquisition, processes the data and executes the control loop and outputs the control variables. The sensors outputs are connected to a signal conditioning board, which in turn is connected to the data acquisition (DAQ) board based on a PC (SCADA System).

III. PV PANELS and ARRAY MODELING

A. Modeling of the PV Panels

This paper uses a single diode equivalent circuit for the PV model, described by a simple exponential function [15-18]:

$$i = I_{sc} - I_0 \cdot \left(e^{(v+iR_s)/n_s V_T} - 1 \right) \quad (1)$$

In which I_{sc} and I_0 are the short-circuit and open-circuit currents, R_s is the cell series resistance, n_s is the number of cells in the panel connected in series and V_T represents the junction thermal voltage which includes the diode quality factor, the Boltzmann's constant, the temperature at standard test conditions (STC) and the charge of the electron.

Manufacturers typically provide limited operational data for photovoltaic panels. These data are available only at standard rating conditions, for which the irradiance G_a is 1000 W/m^2 and the cell temperature T_{cell} is $25 \text{ }^\circ\text{C}$, except for the nominal operation conditions (NOCT) which is determined at 800 W/m^2 and an ambient temperature T_a of $20 \text{ }^\circ\text{C}$.

Equations for the short circuit current I_{sc} and the open circuit voltage V_{oc} as a function of absolute temperature ΔT include temperature coefficients that provide the rate of change with respect to temperature of the PV performance parameters, can be express as [20-22]:

$$\begin{aligned} I_{sc} &= I_{sc25} \cdot (1 + \beta_I \cdot \Delta T) \\ V_{oc} &= V_{oc25} \cdot (1 + \chi \cdot \Delta T) \\ \Delta T &= T_{cell} - T_a \end{aligned} \quad (2)$$

To complete the model it is also necessary to take into account the variation of the parameters with respect to irradiance [20-22]:

$$I_{sc} = I_{sc25} \cdot (G_a / 1000) \quad (3)$$

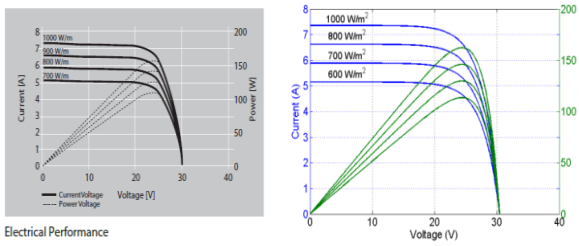
The model used to obtain the static characteristics of the PV panels has been developed in MATLAB using the equations presented above. The model was developed for one panel, as a function of irradiance and temperature. The model has as inputs G_a and T_{cell} on the panel and it sweeps the voltage range of the PV panel in order to calculate the output current and power. PV cells have nonlinear i-v and p-v characteristics. Its output voltage and power change according to temperature and irradiation [15-17].

Fig. 2 shows the typical characteristics for a PV model and also a comparison between PV technical characteristics of the Schuko S165-SP panel from datasheet (on the left) versus simulation results for the panel.

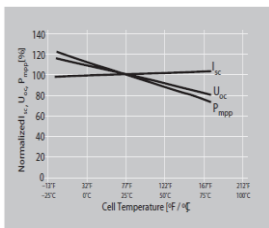
B. Modeling and Implementation of the PV Array

Using a four parameters model of a single diode equivalent circuit, the v-i characteristics for a solar panel string depending on irradiance and temperature has the following expressions:

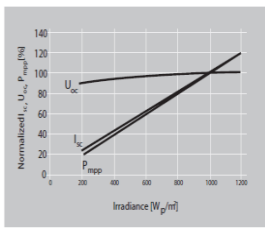
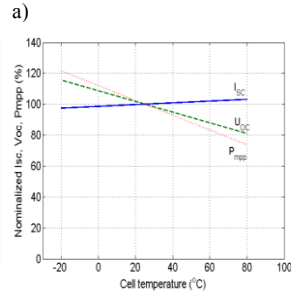
$$v = n_{ps} \cdot V_{oc} + n_{ps} \cdot n_s \cdot V_T \cdot \ln\left(1 - i / (n_{sp} \cdot I_{sc25} \cdot G_a / 1000)\right) \quad (4)$$



Electrical Performance



Temperature Dependence of I_{sc} , U_{oc} & P_{mpp}



Irradiance Dependence of I_{sc} , U_{oc} & P_{mpp}

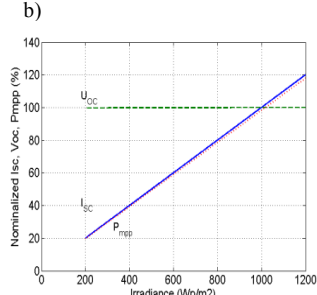


Fig. 2. Comparison between PV technical characteristics from datasheet (on the left) and simulation results for one panel.

$$i = n_{sp} \cdot I_{sc} \cdot \left(1 - e^{-(v - n_{ps} \cdot V_{oc} + R_s \cdot i) / (n_{ps} \cdot n_s \cdot v)}\right) \quad (5)$$

The equations (4) and (5) were obtained replacing (2) and (3) in (1) and also introducing the number of panels in series (n_{ps}) for each string and the number of strings in parallel (n_{sp}) and can be used to calculate the voltage and current over a string of panels [20-22].

For obtaining the maximum power of the panel strings, the condition ($dp/dv=0$) should be fulfilled.

The block diagram implemented in Simulink that was developed to implement this model is depicted in Fig. 3.

IV. IMPROVEMENTS and VALIDATION of the PV ARRAY MODEL

A. Parameters dependence on operating conditions

Two types of measurements are taken from the experimental facility: ambient measurements from the weather station and electrical measurements taken from the inverter as can be seen in Fig. 4a). All these measurements are implemented into our model using a subsystem called *Measurements*, as it is shown in Fig. 4b).

The three ambient measurements: ambient temperature, horizontal solar radiation, and wind speed are fed to a module that calculates the cell temperature of the PV panels and the solar radiation on them.

The simulation model implemented in MATLAB/Simulink for a PV array with three strings is depicted in Fig. 4b). The irradiation, ambient temperature and wind speed are reading from a real data file measured by SCADA system as a function of time and then converted by Data processing subsystem in cell temperature and irradiation, parameters used as inputs to PV panels, as can also be seen in Fig. 4b).

1) Cell Temperature dependence

The cell temperature T_{cell} can be very different from the ambient temperature T_a and it depends on the solar irradiation G_a , T_a and also on the wind speed W_s . Solar irradiation acts on increasing T_{cell} and the wind speed has a cooling effect and lowers T_{cell} [4], [15-17].

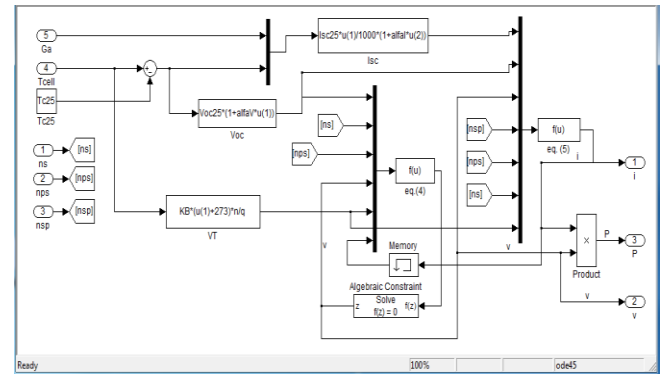
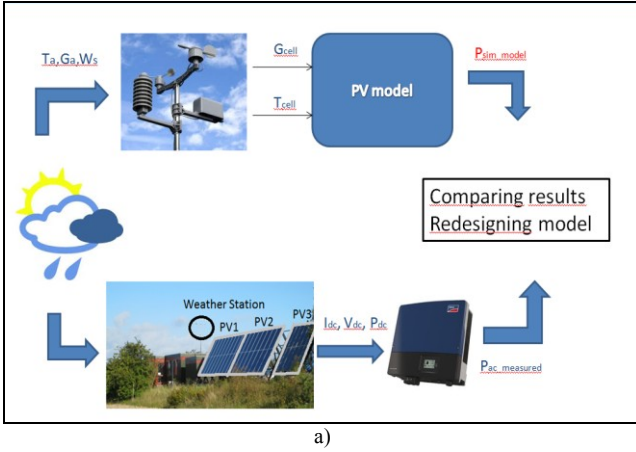
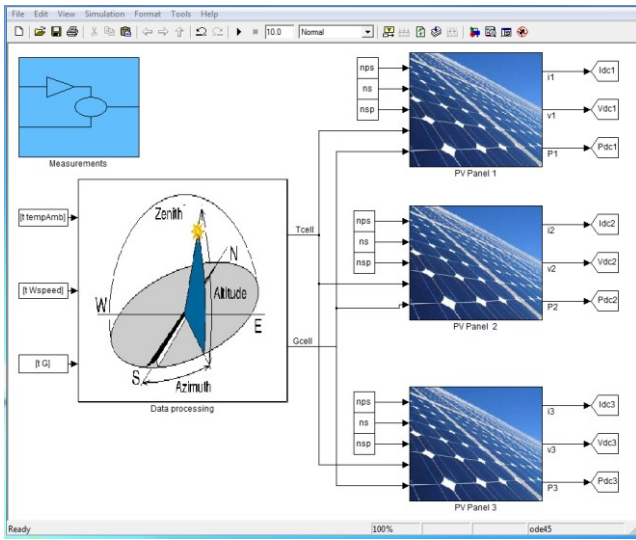


Fig. 3. PV string model implemented in Simulink



a)



b)

Fig. 4. a) Description of the PV system model input values and b) the block diagram of the simulation model for PV array.

If the PV panels are mounted in the regions with high wind potential (as in our case) the wind speed must be considered. The forced (wind) convection is large for high wind speeds and the cell temperature function takes the following form [6]:

$$T_{cell} = T_a + \omega \cdot (0.32 / (8.91 + 2 \cdot W_s / 0.67)) \cdot G_a \quad (6)$$

Where ω is the mounting coefficient, which depends on the mounting conditions of the PV panels and W_s is the wind speed measured on horizontal plane.

The wind that produces the cooling effect through forced convection is the wind parallel to the panel surface; that is why the transformation $W_{\text{parallel}} = W_s / 0.67$ is used.

For a better understanding on the influence of solar irradiance and wind speed on the cell temperature, a graphical representation of these values is depicted in Fig. 5. The differences in temperature of the PV cells according to different considerations are also pointed out.

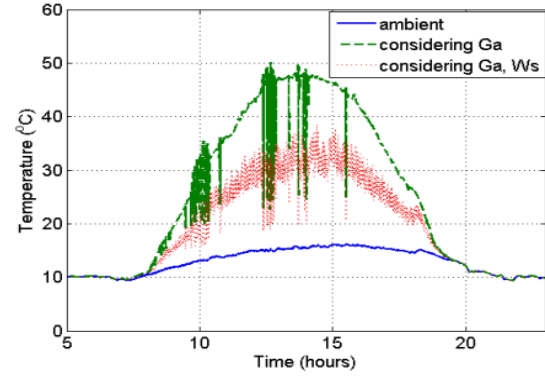


Fig. 5. Ambient measurements and their effect on the PV cell temperature.

2) Solar irradiance dependence

As can also be seen in Fig. 5 the solar irradiance has a high heating effect, at noon it can be seen around 50°C increase of cell temperature. Considering also the wind effect, the cell temperature is lowered, at noon, with 12°C. This change in temperature has an effect on the output power; as was shown in Fig. 2b). At each degree change in temperature, the efficiency modifies with approximately 0.44%: That means that if the temperature rises, the efficiency decreases and vice versa [20, 21].

The solar radiance has influence only on the current (Fig. 2c) and implicitly on the output power of the PV panel, so the plots contain the effect of the change in the input solar irradiance, according to the 'adaptation' of the horizontal solar irradiance to the real case of the PV panel, implemented in *Data processing* subsystem in Fig. 4b).

The solar irradiance input to the model (G_{cell}) is the horizontal value measured from the weather station. This translates into substantial differences as can also be seen in Fig 5 [15-17].

B. Validation of the Simulation Model

In order to validate the simulation model for the PV system, implemented in MATLAB/Simulink, and to point out the importance of considering the atmospheric conditions, such as irradiation, temperature and wind speed, and also the orientation and tilt angle of the panels, the simulations will be compared with experiments carried out using RISO experimental facility-SYSLAB.

In Fig. 6 are presented the simulation results versus measurements at different stages of the modeling. These Figures also shows the importance of several factors that have to be taken in consideration for obtaining a good accuracy of the simulation models.

In Fig. 6 a) is shown a comparison between measured and simulated output power of the panels (P_{DC}) for a time series of one day without considering wind speed effect or any improvements. As can be seen the difference between both curves is very big that means the simulation model should be improved to fit the measurement.

Fig. 6 b) shows the same waveforms for output power, with the same peak values, and the same changes in power due

to shading effect in a synchronous manner. The simulation has a delay of around 50 minutes. This is the effect of the PV panels' orientation, which have a 13° deviation from the E-W axis.

Considering the tilt angle and the orientation of the panels, the influence of solar irradiance and wind speed on the cell temperature the measurements and simulations are almost identically, as can be seen in Fig. 6 c).

In Fig. 7 are presented some simulation results versus measurements for Schuko165 PV panel installed at RISO campus. A good alignment between simulations and measurements was found, as can also be seen in Fig. 7.

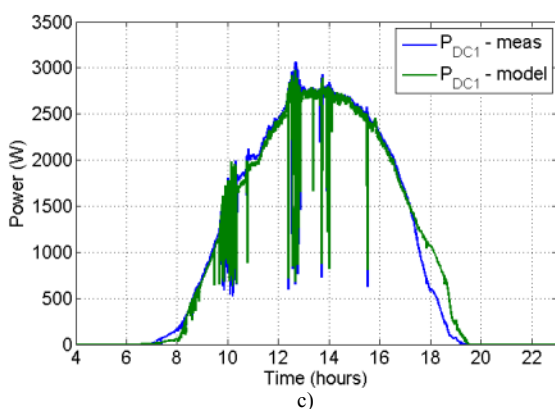
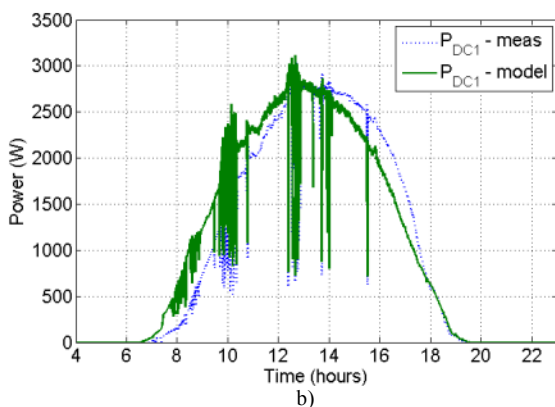
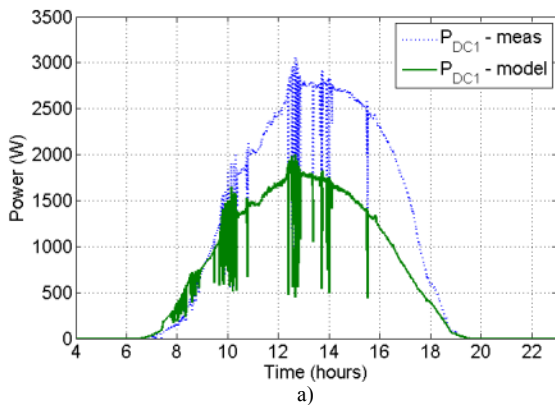


Fig. 6. Simulation results versus measurements at different stages of the modeling.

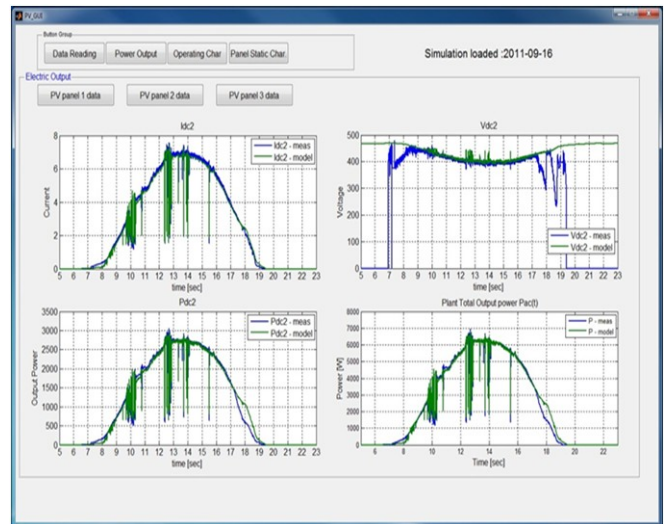


Fig. 7. DC Current, Voltage and Power for Schuko165 PV panel and the output power of the inverter (P_{ac}) as a function of time for 24 hours.

V. SIMULATION MODEL of the PV SYSTEM DEVELOPED and IMPLEMENTED in POWERFACTORY for DISTRIBUTION NETWORKS

Computer models of power systems are widely used by power system utilities to study load flow, steady-state voltage stability and dynamic and transient behavior.

DIgSILENT PowerFactory has been chosen because provides the ability to simulate load flow, RMS fluctuations in the same software environment. It provides a comprehensive library of models for electrical components in the power system [23].

The dynamic model of the PV System implemented in PowerFactory has been built with standard components library and is based on the same equations used for MATLAB/Simulink model presented before.

The blocks of the PV model, DC-Link and controller of the Static Generator are implemented in the dynamic simulation language DSL of DIgSILENT. DSL allows the user to implement specific models that are not standard in the DIgSILENT library and thus to create own developed blocks either as modifications of existing models or as completely new models. The internal simulation language DSL has also been used to define the PV characteristics and to initialize the parameters and variables of the model. Fig. 8 a) shows a single line diagram of the SYSLAB laboratory architecture implemented in PowerFactory [15-17].

Fig. 8 b) shows the schematic structure of the PV System model, developed for time-domain simulations where a DSL model is required, including Photovoltaic Model, DC-Link Model, PLL block and Static Generator with its Controller. The Static Generator is an easy to use model of any kind of static (non rotating) generators. The common characteristic of these generators is that they are all connected to the grid through a static converter. Applications are PV Generators, Storage devices, wind generators etc.

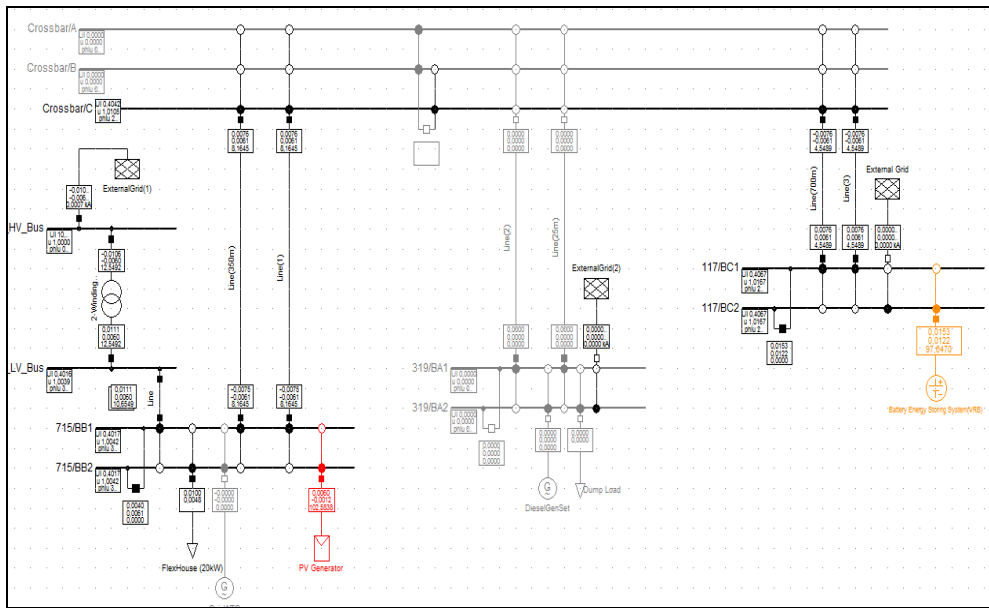
On the basic data tab of the single line diagram it is possible to set up the number of parallel generators and the power ratings of one PV panel.

For load flow analysis, also shown in Fig. 9, the local voltage controller could be set to three different modes: $\cos\phi$, V and droop [23].

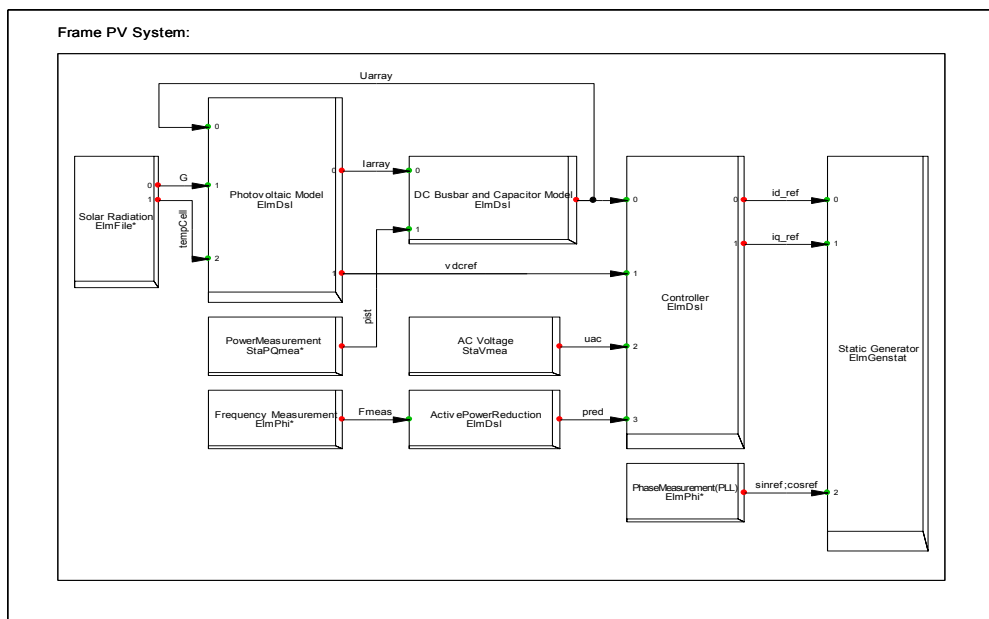
For RMS and EMT simulations the static generator supports two different models: controlled current and voltage source models. In our case we use a controlled current source model which has as inputs d-q axis reference current coming from the controller and d-q reference angles (\cosref and \sinref) from a PLL built-in model.

Photovoltaic Model has as inputs irradiation G and cell temperature $tempCell$, obtained from MATLAB-Simulink model considering the tilt angle, orientation and the influence of solar irradiation and wind speed on the cell temperature (Fig. 4), implemented as a look-up table in our model. Also the MPP of current, power and voltage as a function of time for one module are shown.

In Fig. 10 is presented a comparison between measurements and simulations of the inverter output power for both PV modules (Schuko165 and SOLEL100) installed at RISO campus in three strings, two strings of 18 Schuko165 panels each and one string of 12 SOLEL panels



a)



b)

Fig. 8. a) Single line diagram of SYSLAB configuration implemented in PowerFactory and b) schematic block diagram of the PV system model.

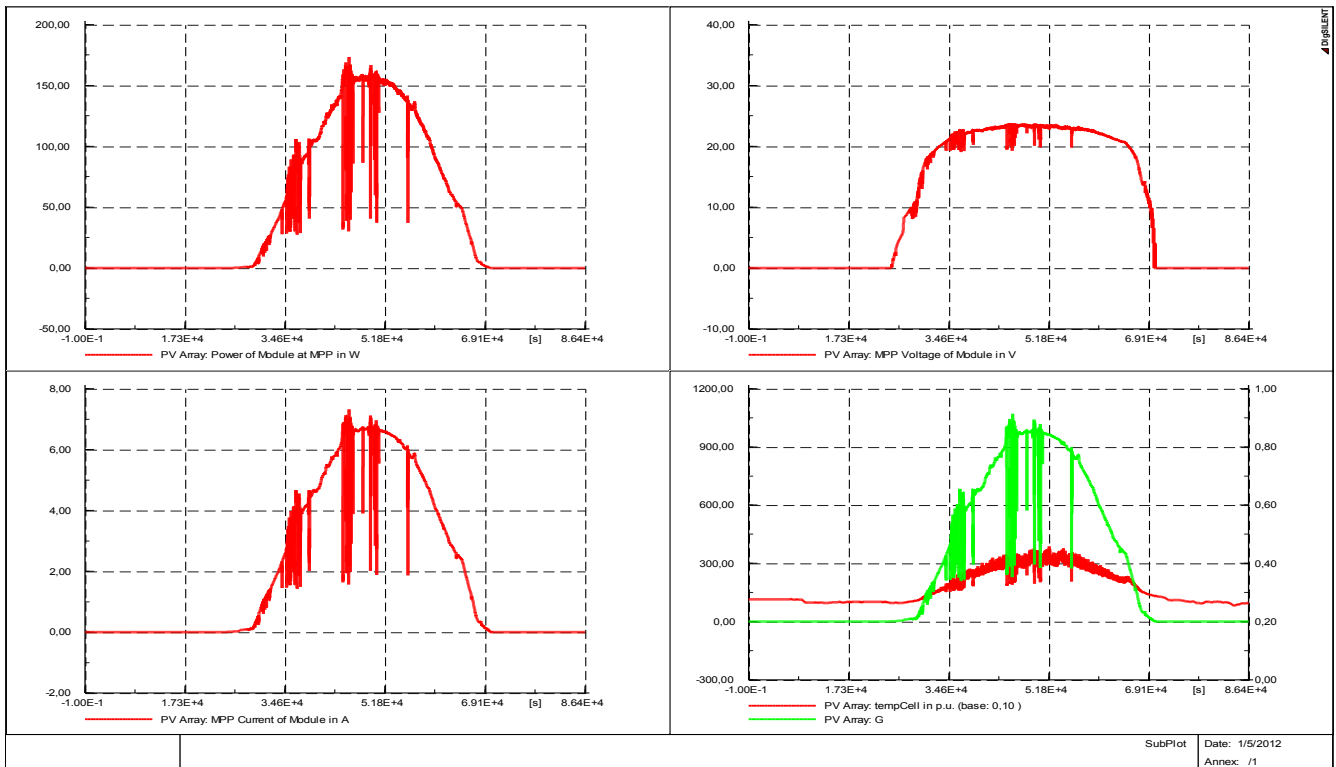


Fig. 9. Simulation results of the PV system model implemented in PowerFactory.

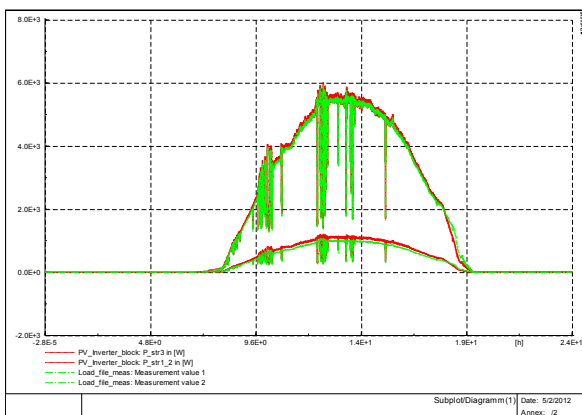


Fig. 10. Comparison between simulations and measurements of the PV inverter output power for both types of panels (Sucho and Solel).

VI. CONCLUSIONS

This paper proposes a four-parameter model of a PV panel and a PV system, implemented in MATLAB/Simulink, using data provided by the manufacturer with semi-empirical equations to predict the PV characteristics for any condition. PV characteristics are modeled according to a single diode four parameter equivalent circuit and PV parameters values taken from the manufacturer technical data.

The paper also proposes a model that relies on ambient data from a local weather station, like most common in a real situation, not from sensors mounted on the PV panels. The model calculates the cell temperature and the solar irradiance on the PV panels considering, among others, the tilt angle, the orientation of the panels, and the wind cooling effect. The paper shows that these factors significantly influence the power output from the PV panels.

Comparison with experimental data, acquired by SCADA system and processed by MATLAB, and with the characteristics of the PV panels, provided by manufacturers, has shown that the model implemented in MATLAB/Simulink can be an accurate tool for the prediction of energy production.

A PV system model, using the same equations and parameters as in MATLAB/Simulink to define the PV module and characteristics, has also been developed and implemented in PowerFactory to study load flow, steady-state voltage stability and dynamic behavior of a distributed power system.

A comparison between both simulation models, implemented in MATLAB/Simulink and PowerFactory, has shown a good similarity. The models have also been validated against measurements using SYSLAB experimental facilities. That means that this work can be used for further development of tools for DER components in a distributed network.

APPENDIX

TABLE 1. Data sheet parameters and values for PV panel [24]

| Parameter (unit) | Value | Description |
|---|--------|---|
| for STC – solar irradiance (G_a)=1000W/m ² , cell temperature(T_c)=25°C, wind speed 1m/s | | |
| P_{mpp} (W) | 165 | Rated output power |
| V_{mpp} (V) | 24.2 | Nominal voltage |
| I_{mpp} (A) | 6.83 | Nominal current |
| V_{oc25} (V) | 30.4 | Open circuit voltage |
| I_{sc25} (A) | 7.36 | Short circuit current |
| α (%/°C) | -0.478 | Temperature coefficient for change in (P_{mpp}) |
| β (%/°C) | 0.057 | Temperature coefficient for change in (I_{sc}) |
| χ (%/°C) | -0.346 | Temperature coefficient for change in (U_{oc}) |
| δ (%/°C) | -0.004 | Temperature coefficient for change in (I_{mpp}) |
| ϵ (%/°C) | 50 | Temperature coefficient for change in (U_{mpp}) |
| for NOCT – solar irradiance(G_{aNOCT})=800W/m ² , ambient air temperature(T_{aNOCT})=20°C, wind speed 1m/s | | |
| NOCT (°C) | 46.2 | Cell temperature on the above mentioned conditions |

ACKNOWLEDGMENTS

This work was supported in part by the E.U. Project-Smooth PV, No. 10580/2011-2012 and also partially supported by the strategic grant POSDRU/88/1.5/S/50783 (2009) of the Ministry of Labor, Family and Social Protection, Romania, co-financed by the European Social Fund – Investing in people.

REFERENCES

[1] K. Richardson, D. Dahl-Jensen, J. Elmeskov, C. Hagem, J. Henningsen, J. A. Korstgård, N. B. Kristensen, P. E. Morthorst, J. E. Olesen, and M. Wier, "Green energy - the road to a Danish energy system without fossil fuels," Danish Commission on Climate Change Policy, 2010. Available: <http://greengrowthleaders.org/green-energy-the-road-to-a-danish-energy-system-without-fossil-fuels/>.

[2] Energynautics GmbH, Longen, Germany, 2010. Available: www.energynautics.com/;

[3] H. Jiayi, J. Chuanwen, and X. Rong, "A review on distributed energy resources and MicroGrid", ELSEVIER Renewable & Sustainable Energy Reviews, vol. 12, pp. 2472-2483, 2008.

[4] S. Seme, G. Stumberg, and J. Vorsic, "Maximum efficiency trajectories of a two-axis sun tracking system determined considering tracking system consumption," IEEE Trans. On Power Electronics, vol. 26, no. 4, pp. 1280-1290, Apr. 2011.

[5] W. De. Soto, S. A. Klein, and W. A. Beckman, "Improvement and validation of a model for photovoltaic array performance," ELSEVIER Solar Energy, vol. 80, pp. 78-88, 2006.

[6] Y. Riffonneau, S. Bacha, S. Barruel and S. Ploix, "Optimal Power Management for grid connected PV Systems with batteries", IEEE Transaction on Sustainable Energy, vol. 2, no. 3, pp. 309-320, July 2011.

[7] J E. Skoplaki, A. G. Boudouvis and J. A. Polyvos, "A simple correlation for the operating temperature of photovoltaic modules of arbitrary mounting", ELSEVIER Solar Energy Materials, pp. 1393-1402, 2008.

[8] Global Smart Grid Federation, "Intelligent PV Integration into the Local Grid", January 23, 2012, www.globalsmartgridfederation.org/prod/news/;

[9] K. Murat, S. Mehmet, B. Yunus, D. Sedat, "Determining optimum tilt angles and orientations of photovoltaic panels in Saliurfa", IEEE Transaction on Renewable Energy, vol. 29, issue 8, pp. 1265-1275, 2004.

[10] M. G. Villalva, J. R. Gazoli, E. R. Filho, "Comprehensive Approach to Modelling and Simulation of Photovoltaic Arrays", IEEE Transaction on Power Electronics, vol. 24, issue: 5, pp. 1198-1208, 2009.

[11] D. Y. Goswami, Principles of Solar Engineering, (2nd ed.), Philadelphia: Taylor & Francis, 2000, p. 81-98.

[12] W. Wang, B. Ge, D. Bi and D. Sun, "Grid-Connected Wind Farm Power Control using VRB-based Energy Storage System", IEEE Transaction on Energy Conversion, pp.3772-3777, 2010.

[13] A. Gabash and P. Li, "Evaluation of Reactive Power Capability by Optimal Control of Wind-Vanadium Redox Battery Stations in Electricity Market", International Conference on Renewable Energies and Power Quality-ICREPQ'11, Las Palmas de Gran Canarias-Spain, 13-15th April, 2011.

[14] <http://www.powerlab.dk/English/facilities/SysLab.aspx>, Research facility for distributed power systems.

[15] L. Mihet-Popa, C. Koch-Ciobotaru, F. Isleifsson and H. Bindner, „Development of tools for simulation systems in a distribution network and validated by measurements”, the 13th IEEE International Conference on Optimisation of Electrical and Electronic Equipment, OPTIM 2012, May 24-26, Brasov-Romania, pp. 1022-1031.

[16] C. Koch-Ciobotaru, L. Mihet-Popa, F. Isleifsson and H. Bindner, „Simulation Model developed for a Small-Scale PV-System in a Distribution Network”, Proceedings of the 7th IEEE International Symposium on Applied Computational Intelligence and Informatics-SACI 2012, Timisoara-Romania, May 24-26, pp. 257-261, ISBN: 1-4244-1234-X.

[17] L. Mihet-Popa, C. Koch-Ciobotaru, F. Isleifsson and H. Bindner, „Development of tools for DER Components in a distribution network”, the 20th IEEE International Conference on Electrical Machines, ICEM 2012, September 2-5, Marseille-France, pp. 1022-1031, ISSN 1842-0133.

[18] Y. Zong, L. Mihet-Popa, D. Kullman, A. Thavlov, O. Gehrke and H. Bindner, „Model Predictive Controller for Active Demand Side Management with PV Self-Consumption in an Intelligent Building”, IEEE PES Innovative Smart Grid Technologies Europe, Berlin-Germany, October 14-17.

[19] PV Inverters: SUNNY TRIPOWER 10000TL Installation Manual, SMA Solar Technology AG.

[20] D. Sera, "Real time modeling, diagnostics & optimized MPPT for residential PV systems", Ph. D. Thesis, Aalborg University, Denmark, 2009.

[21] S. Dezso, R. Teodorescu and P. Rodriguez, "PV panel model based on datasheet values", Proceedings of IEEE International Symposium on Industrial Electronics, Vigo, Spain, 2007, pp. 2392-2396.

[22] D. Sera, R. Teodorescu and P. Rodriguez, "Photovoltaic module diagnostics by series resistance monitoring and temperature and rated power estimation", Proceedings of 34th Annual Conference of IEEE IECON- Industrial Electronics Conference, 2008.

[23] DiGSILENT PowerFactory, User's Manual and Tutorial-Version 14.1, Gomaringen-Germany, November 2011.

[24] Schuco S 165-SPU, Data sheet and technical data of the Photovoltaic Module.

Manuscript received June 25, 2012; revised September 24, 2012; accepted for publication September 27, 2012.

Model Predictive Controller for Active Demand Side Management with PV Self-consumption in an Intelligent Building

Yi Zong, *Member, IEEE*, Lucian Mihet-Popa, *Member, IEEE*, Daniel Kullmann, Anders Thavlov, Oliver Gehrke, *Member, IEEE*, and Henrik W. Bindner, *Member, IEEE*

Abstract—This paper presents a Model Predictive Controller (MPC) for electrical heaters’ predictive power consumption including maximizing the use of local generation (e.g. solar power) in an intelligent building. The MPC is based on dynamic power price and weather forecast, considering users’ comfort settings to meet an optimization objective such as minimum cost and minimum reference temperature error. It demonstrates that this MPC strategy can realize load shifting, and maximize the PV self-consumption in the residential sector. With this demand side control study, it is expected that MPC strategy for Active Demand Side Management (ADSM) can dramatically save energy and improve grid reliability, when there is a high penetration of Renewable Energy Sources (RESs) in the power system.

Index Terms— Active demand side management; load shifting; model predictive control; solar/wind power penetration

NOMENCLATURE

Abbreviation:

| | |
|------|----------------------------------|
| ADSM | Active demand side management. |
| CPS | Conventional power supply. |
| DERs | Distributed energy resources. |
| DG | Distributed generation. |
| DSM | Demand side management |
| DTU | Technical university of Denmark. |
| MPC | Model predictive control. |
| RESs | Renewable Energy Sources. |
| RMI | Remote method invocation. |
| RPS | Renewable power supply. |

Variables & Parameters:

| | |
|-------|------------------------|
| FF | Fill factor. |
| G_a | Solar irradiation. |
| H_p | Prediction horizon. |
| I_o | Open-circuit currents. |

| | |
|---------------------|---|
| I_{sc} | Short-circuit currents. |
| n_s | Number of cells in the panel connected in series. |
| n_{ps} | Number of panels in series. |
| n_{sp} | Number of strings in parallel. |
| $P_{C(k)}$ | Dynamic power price signal of CPS at control step k . |
| $P_{heat-max}$ | Maximum permitted electrical power consumption of heating units. |
| P_{max} | Maximum power point of a solar cell. |
| $P_{R(k)}$ | Dynamic power price signal of RPS at control step k . |
| R_s | Cell series resistance. |
| T_a | Ambient (outdoor) temperature. |
| T_c | Cell temperature. |
| T_i | Indoor air temperature. |
| T_i^k | Predictive indoor temperatures at each control step k over the prediction horizon H_p . |
| T_{im} | Temperature of the heat accumulating layer in the inner walls and floor. |
| T_{om} | Temperature of the heat accumulating layer in the building envelope. |
| T_{ref} | Reference indoor air temperature. |
| V_{oc} | Open circuit voltage. |
| V_T | Junction thermal voltage. |
| W_s | Wind speed. |
| Φ_h | Energy input from the electrical heaters. |
| β_I | Correction coefficients for current. |
| χ | Correction coefficients for voltage. |
| $\mathbf{u}^{(k)}$ | Optimized heat input sequence at control step k . |
| $\mathbf{u}_{s(k)}$ | Predictive solar power at control step k . |
| ΔT | Absolute temperature. |

I. INTRODUCTION

TO MEET the rapidly increasing demand of the energy consumption, and to achieve a significant reduction in CO₂ emissions, more Renewable Energy Sources (RESs), and other low-carbon energy sources will become major contributors to the future electricity system. The Danish government has adopted a long term goal that the Danish energy system (including transport) can be completely independent of fossil fuels by 2050 without using nuclear energy, based on 100% renewable energy from combinations of wind, biomass, solar power and wave [1], and wind power will cover 50% of the Danish electricity consumption in 2025 [2].

This work was supported by Interreg IV A program, project “Wind in Oresund”, and the EU project “Smooth PV” (No. 228449).

The authors are with the department of Electrical Engineering, Intelligent Energy Systems, Risø Campus, Technical University of Denmark, 4000 Roskilde, Denmark (e-mail: yizo@elektro.dtu.dk; lmih@elektro.dtu.dk; daku@elektro.dtu.dk; atha@elektro.dtu.dk; olga@elektro.dtu.dk; hwbi@elektro.dtu.dk).

Due to an increased contribution of fluctuating RESs to the energy system, there are many concerns about the flexibility, variability, non-controllability of these sources, and they have the impact on the ability to keep the balance between supply and demand. Currently, the main method to regulate the supply-demand imbalance is a set of supply-side generation reserves, known as ancillary services, which operate on various scales of time and frequency. The rising share of RESs decreases the controllability of the supply side. The rise in needed balancing power can be fulfilled by utilizing the flexibility potential in demand and Distributed Generation (DG). The introduction of Distributed Energy Resources (DERs) (e.g. household, industrial consumers and electric vehicles), together with the introduction of more information and communication technology in the electricity system provides interesting and novel automated Demand Side Management (DSM) opportunities at the end user level. The combination of DSM with an automatic control of the DERs demand can be called as Active Demand Side Management (ADSM) [3, 4]. ADSM can modify the demand profile to reduce the losses in the grid, maximize consumption while RESs are available, decrease congestions, and save energy [5, 6].

MPC is a control algorithm that optimizes a sequence of manipulated variable adjustments over a prediction horizon by utilizing a process model to optimize forecasts of process behavior based on a linear or quadratic objective, which is subjected to equality or inequality constraints. In MPC, the optimization is performed repeatedly *on-line*. This is the meaning of receding horizon, and the intrinsic difference between MPC and the traditional optimal control. The limitation of this finite-horizon optimization is that, under ideal situations only the suboptimal solution for the global solution can be obtained. However, the receding horizon optimization can effectively incorporate the uncertainties incurred by model-plant mismatch, time-varying behavior and disturbances [7]. MPC is now recognized as a very powerful approach with well established theoretical foundations and proven capability to handle a large number of industrial control problems [8]. The building sector is one of the largest energy consumptions. Based on the vision of the future electricity system, building controls design becomes challenging since it is necessary to move beyond standard controls approaches and to integrate predictions of weather, occupancy, renewable energy availability, and dynamic power price signals. MPC naturally enters the picture as a control algorithm that can systematically incorporate all the aforementioned predictions to improve building thermal comfort, decrease peak load, and reduce energy costs [9]. MPC for building climate control has been investigated in several papers before [9]-[13], mainly with the purpose of increasing the energy efficiency. The potential of MPC in power management was investigated in [14]-[18], but the weather forecast information (e.g. the ambient temperature) was assumed to be constant in their simulation scenarios.

The goal of our research is to implement an MPC-based control strategy for ADSM, using DERs' predictive optimization potential to support the introduction of a large penetration level of renewable energy. In this paper, an MPC controller was implemented for load shifting in an intelligent

office building's heating power consumption scheme, with a maximization of the PV self-consumption. The term "self-consumption" focuses on the usage of the own generated energy, while the energy provided by the grid remains an optional generator. The original contributions of this work are: 1) building an easy, fast to implement model for PV installed at an intelligent building (called PowerFlexHouse), and a stochastic discrete-time linear state-space model for this building; 2) implementing a low-complexity MPC-based scheme which is used to realize the load shifting for the heaters' power consumption, including PV maximum self-consumption in PowerFlexHouse; 3) integrating weather forecast information and dynamic power price into the MPC-based control strategy; and 4) simulating and testing an MPC controller on a real power grid with high penetration of RESs.

The remaining of this paper is organized as follows: in Section II, we present a test platform for intelligent, active and distributed power systems at the Technical University of Denmark (DTU), Risø campus. How to implement a thermal MPC controller for the power consumption prediction in an intelligent building-PowerFlexHouse is provided in Section III, including a simple PV model for solar power prediction, a heat dynamic model for PowerFlexHouse's inside temperature prediction, and formulated MPC objective functions. Some field test results will be shown in Section IV. Finally, conclusion is drawn in Section V, followed by the discussion on future research.

II. TEST PLATFORM DESCRIPTION

SYSLAB is a laboratory for intelligent distributed power systems [19] in DTU Elektro, Risø campus. It is built around a small power grid with renewable (wind (11+10kW), solar (7kWp)) and conventional (diesel) power generation, battery storage, and various types of consumers (See Fig. 1). The whole system can be run centrally from any point on the network, or serve as a platform for fully decentralized control. All SYSLAB controller nodes run the SYSLAB software stack, which is a modular framework for developing distributed control systems for power systems. It is written in the Java (TM) programming language. Distributed controllers can control these components by using one of the supported types of communication, for example, the Java Remote Method Invocation (RMI).



Fig. 1. Components on SYSLAB.

One of the components on the SYSLAB grid is a small, intelligent office building, PowerFlexHouse. It contains seven offices, a meeting room and a kitchen. Each room is equipped with a motion detector, temperature sensors, light switches, window and door contacts and actuators. A weather station outside of the building supplies local environmental measurements of ambient temperature, wind speed, wind direction, and solar irradiation. The electrical load of the building consists of heating, lighting, air-conditioning, a hot-water supply and various household appliances, such as a refrigerator and a coffee machine. The combined peak load of the building is close to 20kW. All individual loads in the building are remote-controllable from a central building controller. The controller software runs on a Linux-based PC. It is also written in Java (TM) and is based on the SYSLAB software stack. The controller can communicate with the SYSLAB grid through its own node computer (See Fig. 2). Information can also flow in the other direction, for example providing the power system supervisor controller with the expected near-future behavior of the building loads.

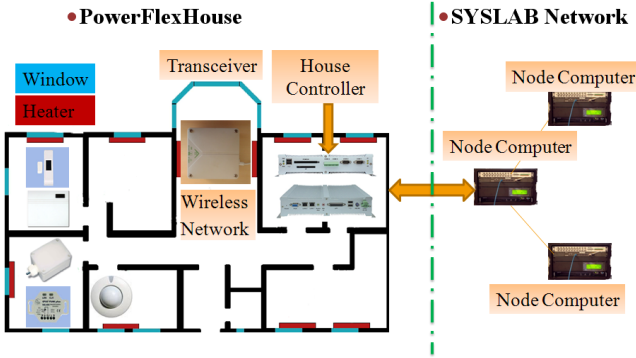


Fig. 2. Communication between PowerFlexHouse and SYSLAB.

III. MPC FOR ADSM IN AN INTELLIGENT BUILDING'S HEATING POWER CONSUMPTION

As described in Section II, the hybrid power supply system (SYSLAB) presented in this paper consists of two parts: a Conventional Power Supply (CPS), and a Renewable Power Supply (RPS). To use the power system efficiently, one of the good ways is to take the advantage of renewable power supply in a maximum degree. Therefore, home appliances primarily use RPS, and CPS is used when RPS is not enough to support the power required by the home appliances. We suppose that RPS has a low cost of power than CPS, considering its generation and CO₂ impact, etc. We denote the dynamic power prices of CPS and RPS by P_C and P_R , respectively. In this paper, to realize the load shifting, we use an MPC control strategy to minimize the daily operational cost of heating in PowerFlexHouse, at the same time to ensure the maximum self-consumption of solar power produced at PowerFlexHouse, and to guarantee users' comfort. There are three important components in MPC, such as the prediction model, the objective function, and the control law, which are present as following.

A. PV Model

We use a single diode equivalent circuit for the PV model described by a simple exponential equation:

$$i = I_{sc} - I_o \cdot \left(e^{(v+iR_s)/n_s \cdot V_T} - 1 \right) \quad (1)$$

where I_{sc} and I_o are the short-circuit and open-circuit currents, R_s is the cell series resistance, n_s is the number of cells in the panel connected in series, and V_T represents the junction thermal voltage, which includes the diode quality factor, the Boltzmann's constant, the temperature at standard condition and the charge of the electron.

A solar cell can be characterized by the following fundamental parameters: the short circuit current I_{sc} , the open circuit voltage V_{oc} , the maximum power point P_{max} and the fill factor FF , which is the ratio of the maximum power that can be delivered to the load and the product of I_{sc} and V_{oc}

($FF = \frac{P_{max}}{V_{oc} I_{sc}} = \frac{V_{max} I_{max}}{V_{oc} I_{sc}}$). The fill factor can be taken from

the manufacturers' data. Then it can be used to obtain P_{max} ($P_{max} = FF \times V_{oc} I_{sc}$) under non-standard conditions.

Equations for I_{sc} and V_{oc} as a function of absolute temperature ΔT including temperature coefficients (β_I , χ : correction coefficients for current and voltage) that provide the rate of change with respect to temperature of the PV performance parameters, can be expressed as:

$$\begin{aligned} I_{sc} &= I_{sc25} \cdot (1 + \beta_I \cdot \Delta T) \\ V_{oc} &= V_{oc25} \cdot (1 + \chi \cdot \Delta T) \\ \Delta T &= T_c - T_a \end{aligned} \quad (2)$$

To complete the model it is also necessary to take into account the variation of the parameters with respect to irradiance:

$$I_{sc} = I_{sc25} \cdot (G_a / 1000) \quad (3)$$

Using a four-parameters model of a single diode equivalent circuit, the v - i characteristics for a solar panel string depending on irradiance and temperature has the following expressions:

$$v = n_{ps} \cdot V_{oc} + n_{ps} \cdot n_s \cdot V_T \cdot \ln(1 - i / (n_{sp} \cdot I_{sc25} \cdot G_a / 1000)) \quad (4)$$

$$i = n_{sp} \cdot I_{sc} \cdot \left(1 - e^{(v - n_{ps} \cdot V_{oc} + R_s \cdot i) / (n_{ps} \cdot n_s \cdot V_T)} \right) \quad (5)$$

where n_{ps} and n_{sp} represent the number of panels in series and the number of strings in parallel, respectively. The equations (4) and (5) can be used to calculate the voltage and current over a string of panels [20][21].

The temperature and irradiance play a central role in PV conversion process since it affects basic electrical parameters, such as the voltage and the current of the PV generator. If the PV panels are mounted in a region with high wind potential (as in our case), the wind speed must also be considered because it has a large influence [22].

The model was developed in MATLAB, using the equations presented above, and has the solar irradiation G_a and the cell temperature T_c as inputs on the panel, and it sweeps the voltage range of the PV panel in order to calculate the output current and power.

For the model input values, the measurements from the weather station had to be translated via additional function that were implemented, in order to reproduce the values on the

actual PV panel conditions. The three ambient measurements: ambient temperature, horizontal solar irradiation and wind speed are fed to an additional simulation module that calculates the cell temperature of the PV panel and the solar radiation on it, as can be seen in Fig. 3.

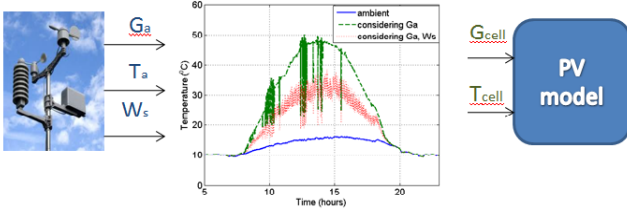


Fig. 3. Description of the PV model input values.

In Fig. 4 is shown a comparison between measured and simulated output power of the PV panel considering the influence of solar irradiance and wind speed on the cell temperature. Comparison with experimental data, acquired by SCADA system and processed by MATLAB, and with the characteristics of the PV panels [22], provided by manufacturers, has shown that this PV model implemented in MATLAB can be an accurate simulation tool to study and analyze the characteristics of individual units and for the prediction of energy production within MPC controller and active loads.

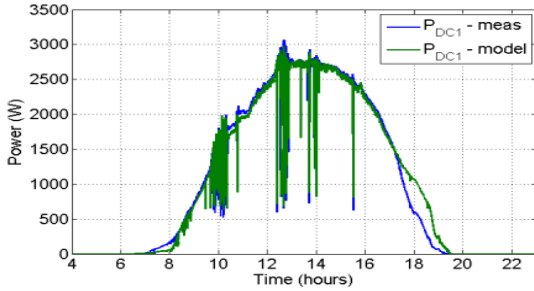


Fig. 4. Comparison between simulations (green) and measurements (blue) of the PV panel output power.

B. Simple Thermal Model for PowerFlexHouse

The indoor temperature model of PowerFlexHouse is given as a stochastic discrete-time linear state-space model, which was directly obtained from the reference [23]. To reduce the complexity, the model of heat dynamics of the PowerFlexHouse is formulated as one large room exchanging heat with an ambient environment. The heat flow in PowerFlexHouse is modelled by a grey-box approach, using physical knowledge about heat transfer together with statistical methods to estimate model parameters. The heat transfer due to conduction, convection and ventilation is assumed linear with the temperature difference on each side of the medium. The estimator was Continuous Time Stochastic Modelling (CTSM), which is an estimation tool developed at the department of Informatics and Mathematical Modeling DTU [24]. The model's states space equations are described by (6) and (7):

$$\mathbf{T}(t+1) = \Phi \mathbf{T}(t) + \Gamma \mathbf{U}(t) \quad (6)$$

$$\text{Output: } \mathbf{y}(t) = \mathbf{C} \mathbf{T}(t) = [1 \ 0 \ 0] \begin{bmatrix} T_i(t) \\ T_{im}(t) \\ T_{om}(t) \end{bmatrix} \quad (7)$$

where

$$\Phi = \begin{bmatrix} 9.93 \times 10^{-1} & 1.87 \times 10^{-4} & 5.64 \times 10^{-3} \\ 2.74 \times 10^{-1} & 7.25 \times 10^{-1} & 8.19 \times 10^{-4} \\ 1.56 \times 10^{-4} & 1.55 \times 10^{-8} & 9.96 \times 10^{-1} \end{bmatrix}$$

$$\Gamma = \begin{bmatrix} 1.28 \times 10^{-3} & 3.00 \times 10^{-2} & 1.02 \times 10^{-2} \\ 1.86 \times 10^{-4} & 2.61 \times 10^2 & 1.48 \times 10^{-3} \\ 3.36 \times 10^{-3} & 1.61 \times 10^{-6} & 8.04 \times 10^{-7} \end{bmatrix}$$

$\mathbf{T} = [T_i, T_{im}, T_{om}]$ is the state vector and $\mathbf{U} = [T_a, G_a, \Phi_h]$ is the input vector to the system. Here, $T_i(t)$ is the indoor air temperature; $T_{im}(t)$ and $T_{om}(t)$, which are the temperature of heat accumulating layer in the building envelope and the temperature in the heat accumulating layer in the inner walls and floor, can not be measured. State estimator-Kalman filter can be used to estimate these two states; T_a is the ambient (outdoor) temperature; G_a is the solar radiation; and Φ_h is the energy input from the electrical heaters. Using this model, the predicted indoor air temperature was compared with the measured values (See Fig. 5). It was shown that this simple discrete-time linear thermal model for PowerFlexHouse is good enough to be plicated in MPC.

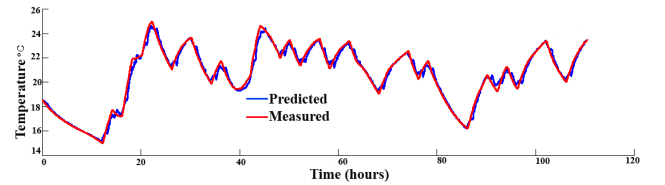


Fig. 5. Predictive (blue) & actual measured (red) indoor air temperature.

C. MPC Objective Function

In MPC the control objectives are translated into an optimization problem, which is formulated over a finite prediction horizon. The result of the optimization is a sequence of optimal control moves which drives the system states (or outputs) towards a given reference while respecting system constraints (such as upper and lower limits on the temperature) and minimizing a selected performance criterion (e.g. the reference temperature error, and minimum cost). The goal of the MPC control strategy for the electrical space heaters in PowerFlexHouse is to minimize the total cost of the energy used in heating over a prediction horizon (H_p). At the same time, it should keep the indoor air temperature close to the given reference temperature T_{ref} . In general, the objective function can be formulated as:

$$J = \alpha \sum_{k=0}^{H_p-1} P_{C(k)} \times u_{(k)} + (1 - \alpha) \left[\sum_{k=0}^{H_p-1} P_{R(k)} \times u_{s(k)} + \sum_{k=0}^{H_p-1} P_{C(k)} \times (u_{(k)} - u_{s(k)}) \right] + w \sum_{k=0}^{H_p-1} |T_i^k - T_{ref}| \quad (8)$$

and

$$\alpha = \begin{cases} 0; & \text{when } u_{s(k)} \geq \min_{(rps)} \\ 1; & \text{when } u_{s(k)} < \min_{(rps)} \end{cases}$$

Subject to: $u_{(k)} \in \text{integer} [0, 1, 2, 3, 4, 5, 6, 7, 8, 9, 10]$ in kW, which means the heat input that the MPC controller determines by using a mixed integer optimization approach. There are totally 10 heaters in the PowerFlexHouse. Each of them has a power of 1kW. Therefore the maximum permitted electrical power consumption of heating units is $P_{heat-max}=10 \times 1\text{kW}=10\text{kW}$. The available solar power at control step k is expressed as $u_{s(k)}$. The minimum solar power supply $\text{Min}_{(rps)}=1\text{kW}$. To simplify the problem, $P_{R(k)}$ are assumed to $[0]$. The above formulation provides a means of incorporating both the economic and user's comfort concerns. By assigning different weight coefficient w in (8) to user's comfort term, behaviour on trade-off between economic performance and user's comfort can be studied. In (8), $P_{C(k)}$ is the dynamic power price signal of CPS obtained from the Nord Pool spot market [25]. Its trading horizon is 12-36 hours ahead and it is done for the next day's 24 hours period. That is to say, the minimum prediction horizon is at least 12 hours and the actual maximal prediction horizon can reach 36 hours. In case $u_{s(k)} \geq \min_{(rps)}$, the objective function can be:

$$J = \sum_{k=0}^{H_p-1} P_{C(k)} \times (u_{(k)} - u_{s(k)}) + w \sum_{k=0}^{H_p-1} |T_i^k - T_{ref}| \quad (9);$$

in case $u_{s(k)} < \min_{(rps)}$, the objective function can be expressed as :

$$J = \sum_{k=0}^{H_p-1} P_{C(k)} \times u_{(k)} + w \sum_{k=0}^{H_p-1} |T_i^k - T_{ref}| \quad (10)$$

To find the best predicted performance over the prediction horizon, the mixed-integer linear programming problem is solved by GLPK's (GNU Linear Programming Kit) solver with Java native interface [26].

D. MPC control law

The main principle of MPC is to transform the control problem into an optimization one and solve this optimization problem over a prediction horizon (e.g.12-36 hours) at each control step (e.g. 10 minutes). The MPC controller obtains a measurement of the current state of the house, including the disturbances like the state of doors and windows, and the grid information, such as dynamic power price signal, available power and frequency signal from the test platform SYSLAB. It also integrates the weather forecast data (ambient temperature and solar irradiation, etc.) with the PV model for the predictive solar power, and with the prediction model for the house indoor temperature. All of them subjected to system dynamics, the objective function (linear or quadratic), constraints on states (e.g. user comfort could be transformed to a set of linear constraints.), and inputs. At each control step the optimization obtains a sequence of actions optimizing

expected system behavior over the prediction horizon. But only the first step of the sequence of control actions is executed by the controller on the system until the next control step, after which the procedure is repeated with new process measurements. (See Fig. 6).

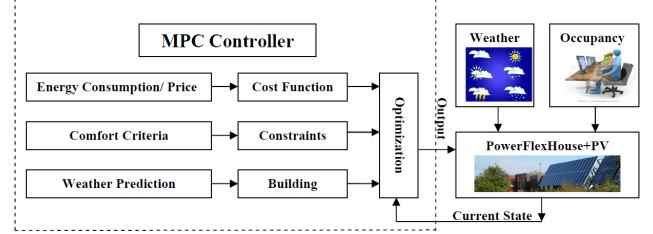


Fig. 6. Basic principle of MPC for building.

IV. RESULTS

We obtained some results from the field test on 18-20, February 2012. The local forecast data of the ambient temperature T_a and the solar irradiation G_a are provided by the meteorology group in DTU Wind Energy at Risø campus. Fig. 7 shows the predictive and the actual measured outside temperature; and in Fig. 8 the predictive and the actual solar irradiation is shown during the test period. The maximum relative error between the actual weather measurement and the weather forecast data is $\pm 5\%$ on test. Therefore, we concluded that the local weather forecast data are accurate in some degree to be integrated into the MPC-based control strategy. Using the PV model described in Section III A together with the local weather forecast data (Fig. 7(red) & Fig. 8(red)), we can obtain the predictive solar power for PowerFlexHouse PV from 8:00 18th to 0:00 20th, February 2012 (See Fig. 9). It was observed that the weather on 18th, February 2012 was bad and there was not solar power to be consumed by heaters. Only during the period of 9:00 to 16:00 on 19th, Feb 2012, there was available solar power supply. In this paper, PV electricity has been used as a local generator, and the concept of self-consumption is meaningful, only when the local generation is available.

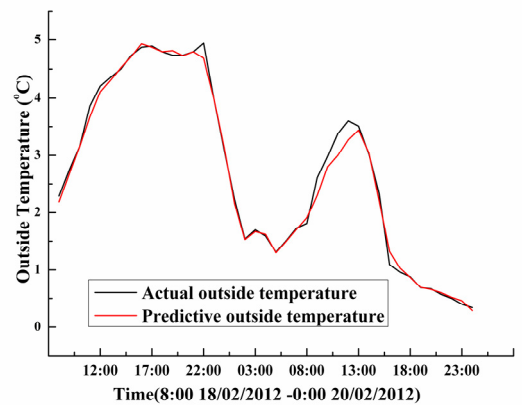


Fig. 7. Predictive (red) and actual measured outside temperature.

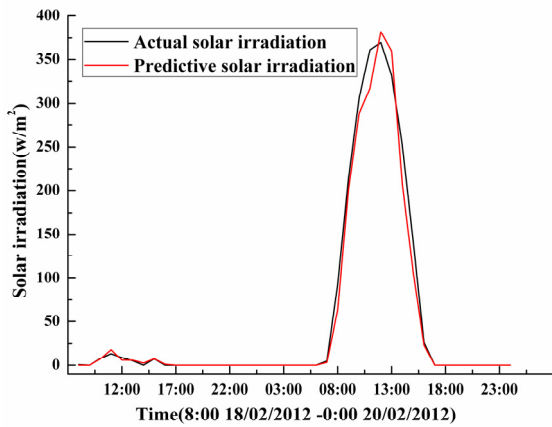


Fig. 8. Predictive (red) and actual measured solar irradiation.

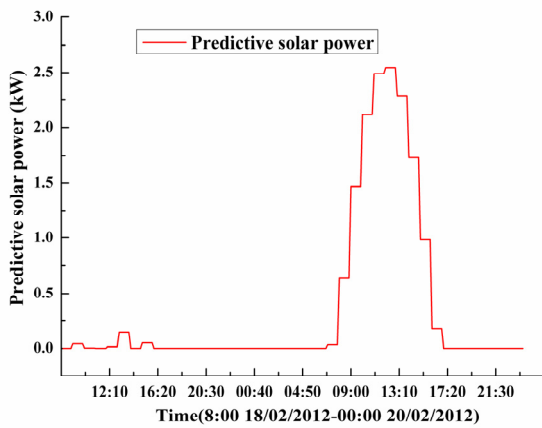


Fig. 9. Predictive solar power.

At 8:00 (18th, February 2012) the MPC control algorithm was running on the SYSLAB platform and it provided the optimized profile of the predictive power consumption in the next approximately 16 hours for the PowerFlexHouse's heaters, as shown in Fig. 10. Fig. 11 demonstrates the predictive indoor air temperature in the next 16 hours according to the optimized switch schedule (the same as in Fig. 10). At 13:00 (18th, February 2012), the MPC produced the results shown in Fig. 12. It presents the optimized profile of the predictive total power consumption in the next almost 35 hours for the PowerFlexHouse's heaters. At this moment, the prediction horizon could reach 35 hours, because the Nord Pool spot market at 13:00 (on the same day) provided next day's 24 hours' price information for the users. Since the solar power has a high priority to be used, the green area in Fig. 12 is the solar power consumption, which would be consumed by heaters from 9:00 to 16:00 on 19th, Feb 2012. The predictive indoor air temperature in the next 35 hours is shown in Fig. 13, according to the optimized switch schedule for heaters supplied with RPS and CPS, shown in Fig. 12. It was observed that the MPC-based controller almost worked within the low price period, including when there is solar power, and it was able to shift the load and reduce the total cost of operating electrical heaters to meet certain indoor temperature

requirements. It is also shown that preheating during the night is a possible way to achieve energy savings.

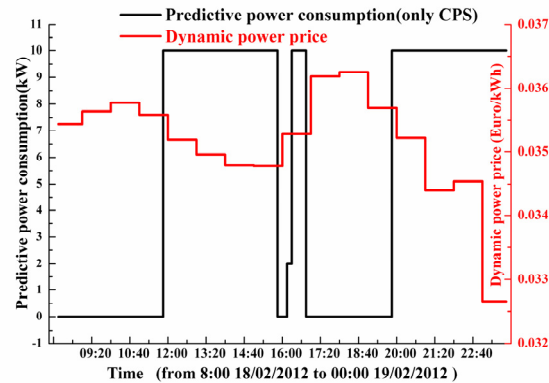


Fig. 10. Optimized heaters' power consumption (black) & dynamic power price (red) in the next 16 hours.

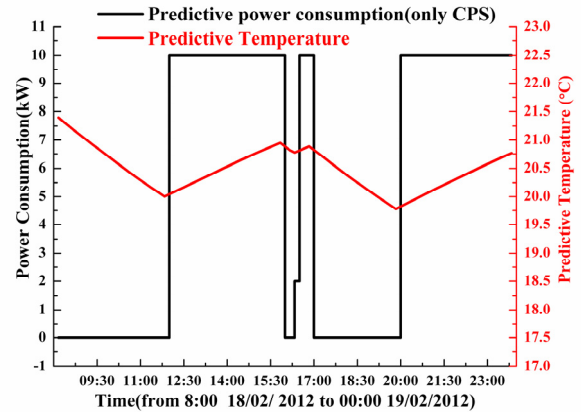


Fig. 11. Predictive indoor air temperature (red) according to the optimized heaters' power consumption (black) in the next 16 hours.

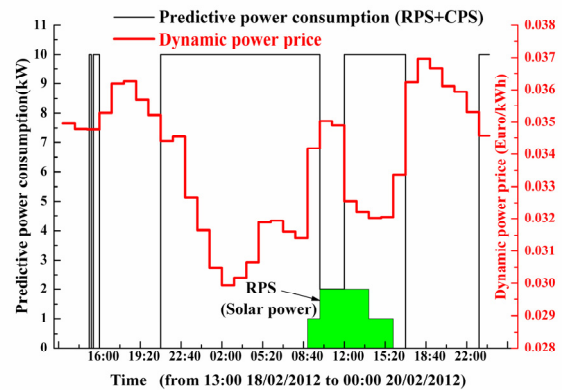


Fig. 12. Optimized heaters' power consumption (black) & dynamic power price (red) in the next 35 hours.

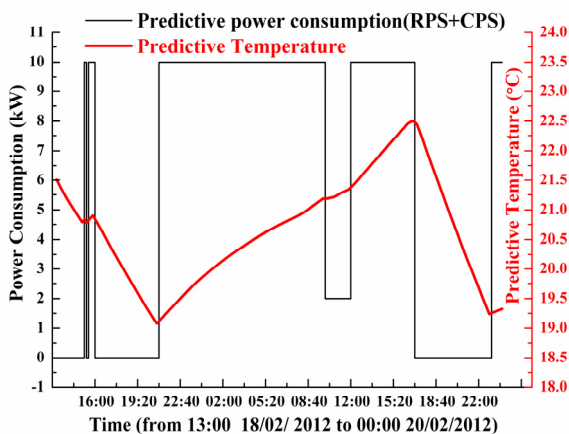


Fig. 13. Predictive indoor air temperature (red) according to the optimized heaters' power consumption (black) in the next 35 hours.

After analyzing the data of Nord Pool in 2010, it is concluded that there is certain predictability in the occurrence of peak load periods during the day in Denmark, and this predictability is reflected in the hourly spot price. The peak load periods and high spot prices occur mainly in the same hours of the day (morning 8:00-11:00 and afternoon 17:00-20:00) and the low spot prices take place in the deep of night [27]. In the Nordic system at night-hours, there is a large production by wind turbine. This is correlated with the dynamic power price, which is much lower during the period from 21:00 to 7:00. According to [28], it is concluded that the spot price, generally decreases when the wind power penetration in the power system increases, that is to say, the Nordic Electricity spot prices reflect the amount of wind power in the system. Fig. 10 and Fig. 12 illustrate that heaters are always switched on late at night and MPC control strategy can achieve energy savings by shifting load from on-peak to off-peak period. At the same time, it shows that MPC control strategy can be investigated on ADSM in this intelligent house, which is used to stabilize fluctuations in the power grid with a high penetration of wind power or other renewable energy, and it can maximize the use of local PV generation.

V. CONCLUSION AND FUTURE RESEARCH

In order to enable more use of renewable energy in the future power system, ADSM should be established to encourage consumers to improve energy efficiency, reduce energy cost, change the time of usage, or promote the use of different energy sources. From the control systems view, smart grids are essentially predictive optimal control problems, which can be formulated as optimizing the cost, the use of the storage, the use of the wind/PV source, and to match the production with the consumption in a predictive horizon.

Simulations and experimental results have shown the effectiveness of the MPC-based control scheme. The predictive optimal problem, which is set up a residential sector, can be naturally modeled with discrete time steps, because balance settlement and markets work within discrete periods. Complex models cannot be readily used for control purposes, since the computation time for the optimal load

scheduling should be low. Meanwhile in real conditions, efficiency of the predictive schedule depends on accuracy of the forecasts.

To improve the operation of various energy resources, operation efficiency of building energy, and loads should be coordinated and optimized. The predictive behavior of power consumption for residential sectors shows that MPC-based strategies are feasible for active DSM in a distributed power system with high renewable energy penetration. Integrating dynamic power prices and the weather forecast data, it demonstrates that MPC control strategies are able to shift the electrical load to periods with low prices. The end users can avoid high electricity price charge at peak time, and the power grid can benefit from load control.

The future work will focus on the other different optimization methods for predictive controllers and the computation time for their optimal scheduling. Moreover, we need to analyze the effect of the predictive horizon length on the performance in the MPC strategies, and the robustness of these controllers against uncertainty in measurements and forecasts. At the same time, the different home appliances, such as a water heater, can be used for maximum PV self-consumption.

VI. ACKNOWLEDGMENT

The authors would like to express their appreciation to Andrea N. Hahmann, Senior Scientist, from DTU Wind Energy, Risø campus, Technical University of Denmark, for providing us with the local weather forecast data.

VII. REFERENCES

- [1] K. Richardson, D. Dahl-Jensen, J. Elmeskov, C. Hagem, J. Henningsen, J. A. Korstgård, N. B. Kristensen, P. E. Morthorst, J. E. Olesen, and M. Wier, "Green energy - the road to a Danish energy system without fossil fuels," Danish Commission on Climate Change Policy, 2010. [Online]. Available: <http://greengrowthleaders.org/green-energy-the-road-to-a-danish-energy-system-without-fossil-fuels/>
- [2] Ministry of Transport and Energy, "Energistrategi 2025", 2007.
- [3] M. Castillo-Cagigal, E. Caamaño-Martín, D. Masa-Bote, A. Gutiérrez, F. Monasterio-Huelin, and J. Jiménez-Leube, "PV selfconsumption optimization with storage and Active DSM for the residential sector", *Solar Energy*, vol. 85, issue 9, pp. 2338-2248, 2011.
- [4] Y. Zong, D. Kullmann, A. Thavlov, O. Gehrke, and H.W. Bindner, "Active load management in an intelligent building using model predictive control strategy," in *Proc. 2011 PowerTech Conf.* pp. 1700589.
- [5] G. Papagiannis, A. Dagoumas, N. Lettas, and P. Dokopoulos, "Economic and environmental impacts from the implementation of an intelligent demand side management system at the European level," *Energy Policy*, vol. 36, issue 1, pp. 163-180, 2008.
- [6] G. Strbac, "Demand side management: benefits and challenges", *Energy Policy*, vol.36, issue 12, pp.4419-4426, 2008.
- [7] D. Q. Mayne, J. B. Rawlings, C. V. Rao, and P. O. M. Scokaert, "Constrained model predictive control: stability and optimality," *Automatica* 36, pp.789-814, 2000.
- [8] B. C. Ding, *Modern predictive control*, chapter 1. CRC Press ,2010, United States.
- [9] Y. Ma, A. Kelman, and A. Daly, "Predictive control for energy efficient buildings with thermal storage," *IEEE control systems magazine*, pp. 44-64, Feb. 2012.
- [10] J. Šíroký, F. Oldewurtel, J. Cigler, and S. Průvara, "Experimental analysis of model predictive control for an energy efficient building heating system," *Applied Energy*, vol. 88, issue9, pp. 3079-3087, Sep. 2011.

- [11] Y. Ma, G. Anderson, and F. Borrelli, "A distributed predictive control approach to building temperature regulation," in *Proc. 2011 American Control Conf.* pp.2089-2094.
- [12] F. Oldewurtel, A. Parisio, C. N. Jones, M. Morari, D. Gyalistras, M. Gwerder, V. Stauch, B. Lehmann, and K. Wirth, "Energy Efficient Building Climate Control using Stochastic Model Predictive Control and Weather Predictions", in *Proc. 2010 American Control Conf.*, pp.5100-5105
- [13] Y. Ma, F. Borrelli, B. Hancey, B. Hancey, B. Coffey and P. Haves, "Model predictive control for the operation of building cooling systems", *IEEE Trans. Control Systems Technology*, pp. 1-8, Mar. 2011.
- [14] F. Oldewurtel, A. Ulbig, A. Parisio, G. Andersson, and M. Morari "Reducing peak electricity demand in building climate control using real-time pricing and model predictive control," in *Proc. 2010 IEEE Conference on Decision & Control (CDC)*, pp. 1927-1932
- [15] H. Hindi, D. Greene, and C. Laventall, "Coordinating regulation and demand response in electrical power grids using multirate model predictive control," in *Proc. 2011 IEEE PES Innovative Smart Grid Technologies Conf.* pp.1-8.
- [16] T. G. Hovgaard, K. Edlund, and J. B. Jørgensen, "The potential of economic MPC for power management", in *Proc. 2010 IEEE Conference on Decision & Control (CDC)*, pp. 7533-7538
- [17] L. Xie and M. D. Ilić, "Model predictive economic/environmental dispatch of power systems with intermittent resources," in *Proc. 2009 IEEE PES General Meeting*, pp.1-6.
- [18] D. Zhu, and G. Hug-Glanzmann, "Real-time control of energy storage devices in future electric power systems," in *Proc. 2011 PowerTech Conf.* pp.1-7.
- [19] <http://www.powerlab.dk/English/facilities/SysLab.aspx>
- [20] D. Sera; R. Teodorescu and P. Rodriguez, "PV panel model based on datasheet values", in *Proc. 2007 IEEE International Symposium on Industrial Electronics*, pp. 2392-2396.
- [21] D. Y. Goswami, *Principles of Solar Engineering*, (2nd ed.), Philadelphia: Taylor & Francis, 2000, p. 81-98.
- [22] L. Mihet-Popa, C. Koch-Ciobotaru, F. Isleifsson and H. Bindner, "Development of Tools for Simulation Systems in a Distribution Network and Validated by Measurements", *The 13th IEEE OPTIM International Conference*, May 24-26, Brasov 2012, pp. 1022-1031.
- [23] A. Thavlov, "Dynamic Optimization of Power Consumption", Chapter 7. Master thesis. Kongens Lynby 2008.
- [24] Continuous Time Stochastic Modelling [Online] available: <http://www2.imm.dtu.dk/~ctsm/>
- [25] The Nord Pool spot market [Online] available: <http://www.nordpoolspot.com/reports/systemprice>
- [26] GNU Linear Programming Kit, [Online] available: <http://glpk-java.sourceforge.net/>
- [27] Y. Zong, D. Kullmann, A. Thavlov, O. Gehrke and H. W. Bindner, "Application of Model Predictive Control for Active Load Management in a Distributed Power System with High Wind Penetration", *IEEE Transactions on Smart Grid*, vol. 3, issue 2, pp. 1055-1062, Jun. 2012.
- [28] W. Hu, Z. Chen, B. Bak-Jensen, "The relationship between electricity price and wind power generation in Danish electricity markets", in *Proc. 2010 Asia-Pacific Power and Energy Engineering Conf.* pp. 5448739.

VIII. BIOGRAPHIES



Yi Zong (M'12) was born in Wuhan, Hubei province, China, on August 21, 1971. She graduated in Control Engineering and Control Theory from Wuhan University of Science and Technology. She got PhD degree on System Engineering and Automation in 2006, at the University Complutense of Madrid, Spain.

Her employment experience included the Wuhan Institute of Technology, China. Since 2006 she had been employed as Post.doc at the Wind Energy Division of Risø DTU. She is currently a Scientist at the department of Electrical Engineering, Intelligent Energy Systems, Risø Campus, Technical University of Denmark. Her special fields of interest include the integration of renewable energy sources in building energy management, optimization control for demand side units in households and industry supporting flexible power consumption.



Lucian Mihet-Popa (M'12) was born in Romania, in 1969. He received the B.S. degree, M.S. degree and Ph.D. degree from the POLITEHNICA University of Timisoara, Romania, in 1999, 2000 and 2003, respectively, all in electrical engineering.

He is currently working as a Scientist with the department of Electrical Engineering, Technical University of Denmark, since 1st March 2011. He is also an Associate Professor in the Department of Electrical Engineering at the POLITEHNICA University of Timisoara. His research interest includes control and modeling of DER components in micro grids, electrical machines and drives, detection and diagnosis of faults, especially for wind turbine applications.

Dr. Mihet-Popa received in 2005 the second prize paper award of the IEEE Industry Applications Society.



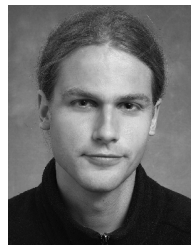
Daniel Kullmann was born in Frankfurt/Main, Germany, on August 15, 1973. He graduated in Computer Science from Darmstadt University of Technology in 2002. He is currently working toward the Ph.D. degree at department of Electrical Engineering, Technical University of Denmark.

He worked for several years in the IT industry. His fields of interest are distributed control and communication in power systems.



Anders Thavlov was born in Copenhagen, Denmark, on June 3, 1979. He graduated from Department of Informatics and Mathematical Modeling at Technical University of Denmark in 2008. He is currently conducting his Ph.D. study in the Intelligent Energy Systems group at department of Electrical Engineering, Technical University of Denmark.

His main research interests are power systems, modeling of demand, flexible power consumption and control.



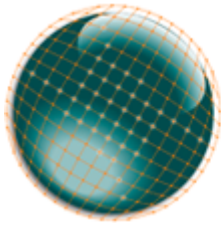
Oliver Gehrke (M'12) was born in Frankfurt am Main, Germany, on March 15, 1975. He graduated in Electrical Power Engineering from Darmstadt University of Technology and got his PhD degree at Risø National Laboratory in Denmark.

He is currently a Scientist at the department of Electrical Engineering, Intelligent Energy Systems, Risø Campus, Technical University of Denmark. His special fields of interest include the embedded and distributed control of power systems with a high penetration of renewable energy sources.



Henrik Bindner (M'12) was born on 30 June 1964 in Copenhagen, Denmark. He received his master in electrical engineering from the Technical University of Denmark in 1988.

Since 1990 he has been with Risø DTU National Laboratory for Sustainable Energy in the Wind Energy Division, currently as a Senior Scientist at the department of Electrical Engineering, Intelligent Energy Systems, Risø Campus, Technical University of Denmark. He has mainly been working on integration of wind energy into power system. The work has included analysis, design and control of small island systems as well as technologies and techniques for integration of wind in large systems. Currently, he is researching how distributed energy resources can be applied to increase penetration of wind energy.



Characterisation of the rapid fluctuation of the aggregated power output from distributed PV panels

Per Nørgaard and Oscar Camacho

Electrical Engineering, DTU – Technical University of Denmark
 Roskilde, Denmark

pern@elektro.dtu.dk and osmfc@elektro.dtu.dk



Figure 2: The SYSLAB experimental power system at DTU, Risø Campus. The large and rapid power fluctuations caused by these passing clouds is a challenge for the power system – for the control, the power quality and the stability. However, the fluctuations of the aggregated power from the distributed PV panels are clearly reduced.

Even at a good day in Denmark, clouds will typically partly shadow for the sun, resulting in fluctuating power generation from PV panels. At the DTU Risø Campus, PV power panels connected to our experimental power system facility SYSLAB are distributed over 1 km at three sites. The large and rapid power fluctuations caused by these passing clouds is a challenge for the power system – for the control, the power quality and the stability. However, the fluctuations of the aggregated power from the



Figure 1: Typical clouds at a sunny day in Denmark.

I. EXPERIMENTAL SET-UP

SYSLAB is a very flexible, experimental power system at DTU Risø Campus (Figure 2). PV power is connected to the SYSLAB power system at three sites (117, 319 and 725) distributed over 1 km (Figure 4). The very flexible SYSLAB power connection set-up makes it possible to connect the PV panels at the three sites to a dedicated power line and connect the power line to the national grid (Figure 3). The SYSLAB monitoring system measures the power for each PV installation and the aggregated power at the grid connection with a time resolution of 1 sec.

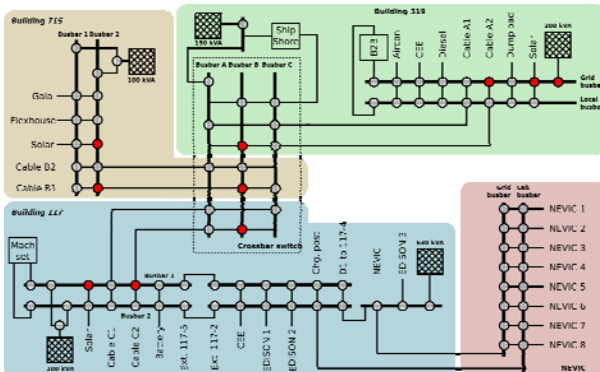


Figure 3: The flexible power connection of SYSLAB.

The large and rapid power fluctuations (on 2012-06-01) from one of the PV installations are presented in Figure 5. The variation over the day of the maximum power from the three PV

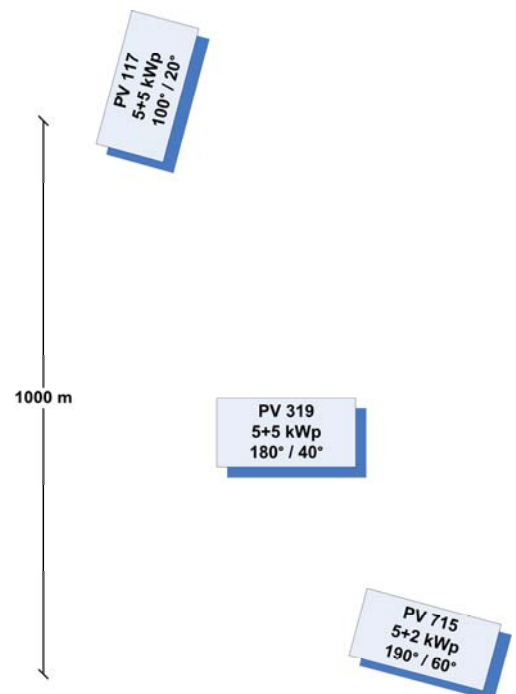
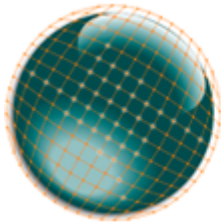


Figure 4: The PV panels connected to SYSLAB.



panels is presented in Figure 6. For comparison, the power outputs from each of the PV panels and for the aggregated value are presented as normalized power relative to the maximum power during the day. The three panels have different profiles during the day due to their different orientations and tilt-angles (Table 1).

| Site | Orientation | Tilt | Technology | Nominal power |
|------|-------------|------|----------------------------|---------------|
| 715 | 190° | 60° | poly-crystalline | 2 kWp |
| | | | mono-crystalline | 5 kWp |
| 319 | 180° | 40° | poly-crystalline thin film | 5 kWp |
| 117 | 100° | 20° | poly-crystalline thin film | 5 kWp |

Table 1: PV installations in SYSLAB (2012).

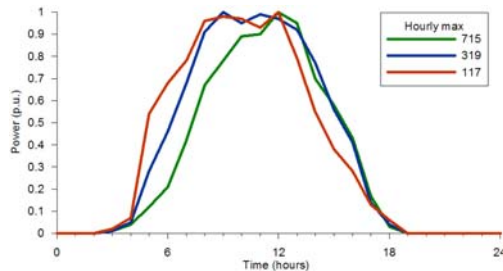


Figure 6: The hourly maximum power for the three PV installations over the day.

II. RESULTS

Detailed examples of the power fluctuations are presented in Figure 7 around 10 o'clock with passing clouds causing dips in the power generations, and in Figure 8 around 12 o'clock with passing holes in the clouds causing spikes in the power

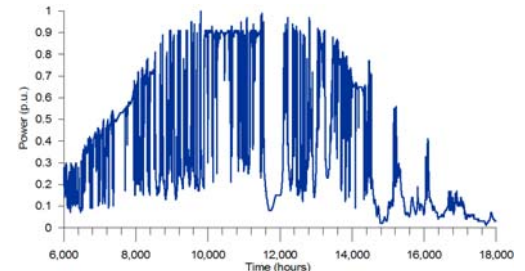


Figure 5: The fluctuations of the power from one of the PV installations.

generations.

Even with the relative short distances between the PV panels, it is very clear that the power fluctuations to some degree are uncorrelated, reducing the relative fluctuations of the aggregated power.

In Figure 7 around 9:55 a cloud passed the PV-117 panel without affecting the PV-319 and PV-715 panels. Around 10:00 other clouds passed PV-715 and to some degree the PV-319 panel, but with almost no impact on the PV-117 panel.

In Figure 8 around 12:05 holes in the clouds are passing the PV panels, resulting in large, but to some degree uncorrelated fluctuations. The relative fluctuations of the aggregated power (the power to the grid) are a lot less.

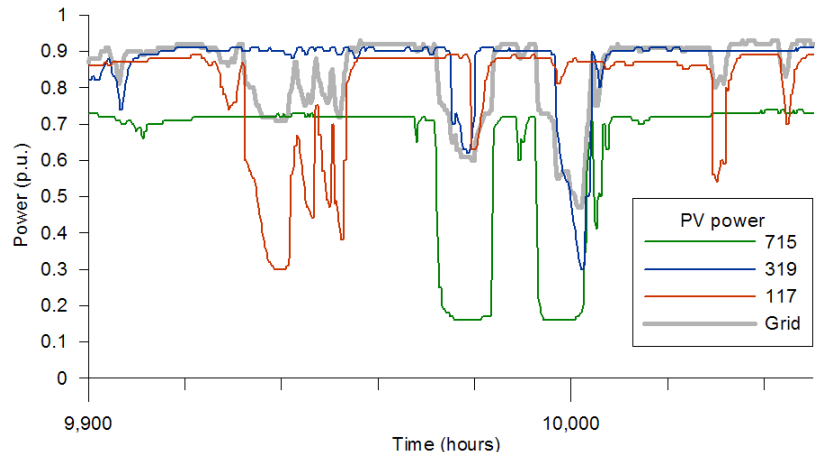


Figure 7: Details of power dips. (Approx 1 minute between the time marks)

III. CONCLUSION

In Denmark, a distribution of PV panels over only 1 km will have a significant impact on the rapid power fluctuations of the aggregated power generation from the panels caused by passing clouds.

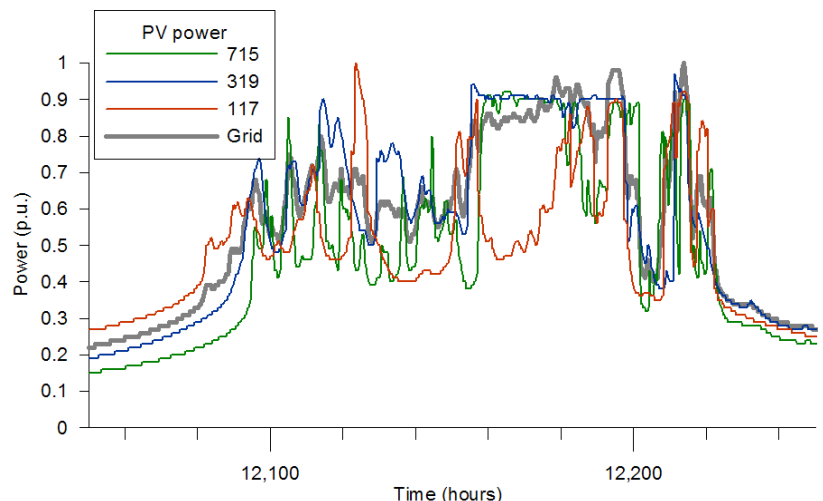


Figure 8: Details of power spikes. (Approx 1 minute between the time marks)

Comparison of a Three-Phase Single-Stage PV System in PSCAD and PowerFactory

Afshin Samadi, Robert Eriksson, Della Jose, Farhan Mahmood, Mehrdad Ghandhari and Lennart Söder
Department of Electric Power Systems
KTH Royal Institute of Technology
Stockholm, Sweden 10044

Email: afshin.samadi@ee.kth.se, robert.eriksson@ee.kth.se, mehrdad.gandhari@ee.kth.se, lennart.soder@ee.kth.se

Abstract—Accommodating more and more distributed PhotoVoltaic (PV) systems within load pockets has changed the shape of distribution grids. It is not, therefore, accurate anymore to address distribution grids just only as a lumped load. So it will be crucial in the near future to have an aggregate model of PV systems in distribution grids. By doing so, it is important to develop models for PV systems in different simulation platforms to study their behavior in order to derive an aggregate model of them. Although, there have been several detailed-switching model of a PV system in EMTDC/PSCAD simulation platform in literature, these non-proprietary switching models are slow in simulation, particularly when the number of the PV systems increases on the grounds that in PSCAD the simulation is based on time domain instantaneous values and requires more mathematical details of components. Therefore, in this paper a model of the PV system in DIgSILENT/PowerFactory is developed, which is a proper environment to run rms simulation and works based on the phasors and, moreover, from mathematical perspective is more simplified. The performance of the stemming model is compared with the switching model in PSCAD. Comparing the simulation results of the proposed model in PowerFactory with the model in PSCAD shows the credibility and accuracy of the proposed model.

Keywords: Photovoltaic, PSCAD, PowerFactory, Reactive power support

I. INTRODUCTION

High penetration of solar PhotoVoltaic (PV) systems has shaped a new structure for distribution grid. Growing trends in generating power from distributed PV systems have accommodated more and more PV systems in distribution grids. In Germany, for instance, there are currently 20 GW installed PV systems, of which 80% have been connected in low voltage grids [1]. This high penetration of PV systems has also raised new challenges in distribution grids such as voltage profile. Violation of voltage profile in some regions in Germany has led to stopping PV installation by utilities. To contrive a way to solve the unwanted problems associated with high penetration, several approaches have been proposed in recent standards and literature, for instance the reactive power support and the active power curtailment [2]–[5].

In power system studies, distribution grids have mainly been modeled as a lumped load. However it is not anymore wise to just address distribution grids as a passive load [6], [7]. The aforementioned changes that gradually happen in distribution grids require deeming new models of distribution grids for static and dynamic studies of power systems. Therefore, it is crucial to find a proper aggregate model of distribution grids consisting of PV systems in order to

properly study the behavior of distribution grids on power system stability and dynamics.

In order to find out a suitable aggregate model of distributed PV systems, it is required to study the behavior of an individual PV system to discover how it functions in the grid. A power test system including PV systems is simulated either as a transient simulation, which uses instantaneous values, or an rms simulation which is based on the phasor model. In the transient simulation, components are needed to be modeled in more mathematical details; however, it, in turn, takes more simulation time. Although rms simulation of the PV system using phasor model is run faster, it excludes some mathematical details. Nevertheless, it is important to find out differences and similarities between these two simulation platforms and models, and then if the dynamic behavior of both models are similar, using phasor model is more time efficient and convenient in order to investigate and attain an aggregated model of distributed PV systems.

Models of a PV system in PSCAD have been addressed in literature such as [8]–[11]. Due to the old standards in the past, those models did not consider different reactive power strategies; however contemporary standards, e.g. German Grid Codes [12], allow reactive power support by PV systems. For instance, [8] only considers unity power factor operation and does not address the reactive power support; Ref. [9] does not consider Maximum Power Point Tracking (MPPT) and reactive power support; proposed model in [10] has been mainly developed for utility application and does not address different reactive power support strategies in distribution grids. Ref. [11] developed a model of a PV system which comprises four different reactive power supports and this model was incorporated in a test distribution grid with two PV systems. In this research a model of the PV system based on the proposed model in [11] is developed in PowerFactory for the rms simulation. There is already one developed generic PV model in PowerFactory Library, however this model has a few differences with the developed PSCAD model, for instance the standard MPPT function is not included and dc-link capacitor has been modeled through power equation. Therefore, since the main aim is comparing two identical models in a similar way, a new model is needed to be developed in PowerFactory.

The objective of this paper is to validate two identical models of a three-phase single-stage PV system in two different simulation platforms, namely PSCAD and PowerFactory, which perform simulations based on time domain instan-

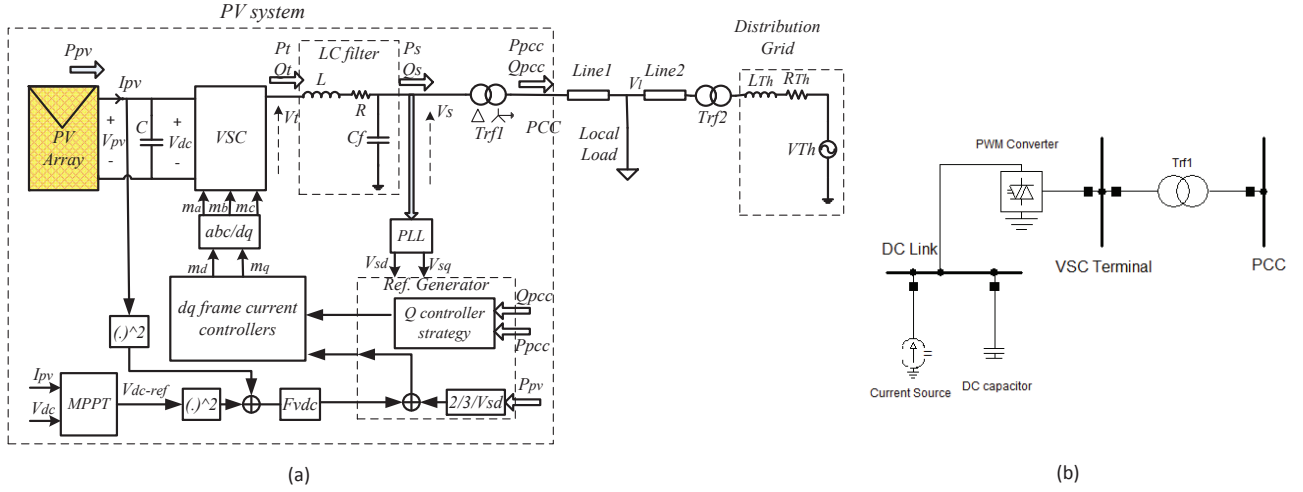


Figure 1. a) Schematic of a PV system structure connected to a distribution grid. b) Schematic of a PV system in PowerFactory.

taneous values and rms values, respectively. Four different reactive power support strategies have been incorporated into the models, i.e. fixed power factor, power factor as a function of feed-in power (hereinafter called dynamic power factor), reactive power depending the voltage $Q(V)$, and AC-Bus voltage regulator. In conclusion, the both designed models are compared and simulation results demonstrate the credibility of those models; differences between them are shown and evaluated.

In the following, a general overview of PV systems structure will be given in section 2, differences and similarities between two models are presented in section 3, section 4 presents results of comparison of a single PV system connected to grid in the both simulation platforms and finally the conclusion comes at section 5.

II. PV SYSTEMS STRUCTURE

Fig. 1 illustrates the one-line diagram schematic of a three phase single-stage PV system connected through a transformer to a distribution grid. The PV system consists of PV array, dc-link capacitor, Voltage Source Converter (VSC) and peripheral control systems.

Solar cells are connected in series to form PV modules and PV modules are, in turn, connected in series or in parallel to form PV panels. PV panels are connected in series and in parallel to form solar array in order to provide adequate power and voltage for being connected to a grid. The output power of PV array feeds in dc-capacitor link which is connected in parallel and is transformed through parallel connected VSC to AC power. The VSC terminals are connected to the Point of Common Coupling (PCC) via the interface reactor, shown by L and R , and a transformer. The transformer makes an isolated ground for PV system as well as boosting the level of output voltage of PV system to the grid voltage level. C_f is the shunt capacitor filter that absorbs undesirable low-frequency current harmonics generated by PV system. Distribution grid is assumed by Thevenin model where R_{Th} and L_{Th} are equivalent grid resistance and inductance, respectively.

Control system is performed in a dq-frame reference. Phase Locked Loop (PLL) is used to synchronize control

system with the grid frequency by moving from the abc-frame reference to a proper dq-frame reference.

A. PV array model

Analogous with a diode, PV panel current-voltage characteristic is exponential and is depicted as follows:

$$I = I_{ph} - I_0 \left(\exp \left(\frac{V - R_s I}{V_T} \right) - 1 \right) \quad (1)$$

In (1), I and V are output current and voltage of a PV panel respectively, I_0 is the dark saturation current, R_s is the cell series resistance, I_{ph} is the photo-generated current and V_T is the junction thermal voltage. Ref. [13] shows how to calculate solar panel parameters R_s , I_0 and I_{ph} by means of datasheet values in Standard Test Condition (STC). I_{ph} , short circuit current and open circuit voltage of the panel are linearly dependent on the irradiance and the temperature, while I_0 is only the temperature-dependent [13].

As mentioned earlier solar panels are connected in series and parallel, so the (1) can be extended as follows:

$$I_{pv} = n_p I_{ph} - n_p I_0 \left(\exp \left(\frac{V_{pv} - R_s I_{pv}}{n_s V_T} \right) - 1 \right) \quad (2)$$

where V_{pv} and I_{pv} are PV array output voltage and current, and n_s and n_p are number of series and parallel panels, respectively.

B. Controller model of PV system converter

Due to the different abc/dqo transformation, active power and reactive power are controlled on q and d axes in PSCAD, respectively, while it is the other way around in PowerFactory. Nevertheless, for integrity it is here assumed that active power is controlled on the d axis and reactive power on the q axis. Control system in a PV system on the each axis comprises two control loops where the inner loop is the current control (Fig. 2) and the outer loop is the dc-link voltage controller, which regulates active power, on the d axis and reactive power regulator on the q axis.

Active power control in PV systems is performed through regulating the dc-link voltage. The dc-link voltage regulator in the Laplace domain, $F_{vdc}(s)$, which in this study is an

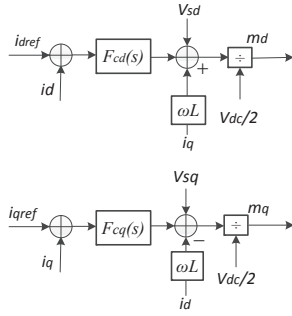


Figure 2. Schematic of current control block diagram.

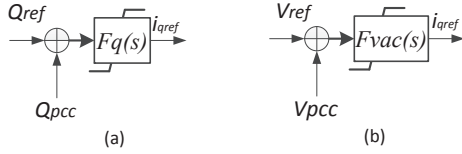


Figure 3. a) Block diagram of reactive power control loop. b) Block diagram of voltage control.

integrator and a lead compensator, adjusts i_{dref} through the dc-link voltage deviation signal (ΔV_{dc}). In order to augment the performance of the dc-link voltage regulator, output power of PV can also be deployed as a feed-forward to eliminate the nonlinearity and the destabilizing impact of the PV array output power [9], [14].

Reactive power control can be done by different strategies. Nevertheless, from regulator design perspective it can be done either by regulating reactive power at a reference value (Fig. 3(a)) or controlling the voltage at the connection point to a set-point value (Fig. 3(b)). It must, however, be considered that the reactive power contribution of the PV system is limited according to the current standards [12]. Reactive power regulators, $F_q(s)$ or $F_{vac}(s)$, which in general can be a PI controller, adjust i_{qref} using the reactive power deviation signal (ΔQ) or the AC-bus voltage deviation signal (ΔV_{AC}) depending on the reactive power control strategy. $\Delta i_d = i_{dref} - i_d$ and $\Delta i_q = i_{qref} - i_q$ are passed through current controllers to produce Sinusoidal Pulse Width Modulation (SPWM) signals for VSC in PSCAD.

Regarding reactive power contribution, a PV system could carry out this task through one of the following approaches:

- I *Constant power factor operation*: PV system feeds reactive power into the grid irrespective of the voltage profile.
- II *Dynamic power factor operation, PF(P)*: This method was proposed by German Grid Codes [12] (Fig. 4).
- III *Droop-based control strategy, Q(V)*: This approach is a droop-based control strategy and Fig. 5 depicts a linear droop curve where the value of the dead-band (D) depends on the network impedance [15].
- IV *Voltage control*: this approach is sensitive to the set-point adjustment to the extent that reactive power pumping interactions among PV systems in a distribution grid can occur [11].

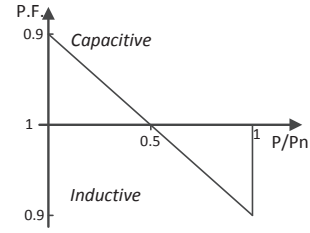


Figure 4. Dynamic power factor characteristic, PF(P).

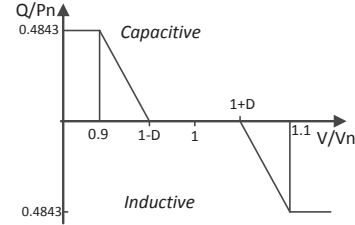


Figure 5. Droop control strategy, Q(V).

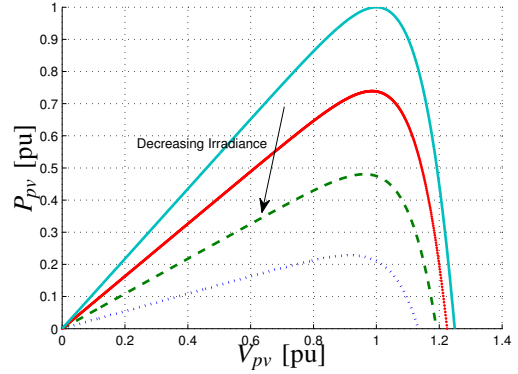


Figure 6. Voltage-Power characteristic of a PV array for different irradiance levels.

C. MPPT of PV system

The energy captured from PV array is not only proportional to irradiance, but also depends upon the location of the operating point, in Fig. 6 it can be noticed. Therefore, the output of PV array is not necessarily equal to its maximum and by doing so, PV system always needs additional function to exploit maximum power of PV array which is named Maximum Power Point Tracking in literature. As can be seen in Fig. 1, MPPT determines the dc-link voltage reference. MPPT is actually the most outer control loop of the PV system that has a memory to provide the dc-link voltage reference by measuring the output voltage and current of PV arrays and comparing them with previous states through a processing algorithm. Here in this paper, Incremental Conductance (INC) [16] algorithm is employed.

III. DIFFERENCES AND SIMILARITIES

In PSCAD, active power is controlled on the q axis and reactive power on the d axis due to abc/dq transformation characteristic. However, in PowerFactory the d axis represents the active power control and the q axis represents

Table I
SYSTEM PARAMETERS.

| PV system parameter | Value |
|--|---|
| Vmp panel voltage at mpp | 33.7 V |
| Imp panel current at mpp | 3.56 A |
| Isc panel short circuit current | 3.87 A |
| Voc panel open circuit voltage | 42.1 V |
| Panel temperature coef. of Isc | 0.065 %/°C |
| Panel temperature coef. of Voc | -160 mV/°C |
| n_s num. of series panels | 14 |
| n_p num. of parallel panels | 6 |
| DC link capacitor C | 10 mF |
| Interface reactor L | 4 mH |
| Interface reactor R | 3 mΩ |
| Trf1 rated power | 15 kVA |
| Trf1 voltage ratio | 0.38/0.18 kV |
| MPPT frequency | 20 Hz |
| MPPT perturbation size | 0.337 V |
| Line Parameter | Value |
| Line1 impedance | 6 + 7.5j mΩ |
| Line2 impedance | 15.5 + 3.4j mΩ |
| Grid Parameter | Value |
| Grid voltage | 20 kV |
| Grid short circuit capacity | 1.15 MVA |
| Grid R/X ratio | 0.6 |
| Trf2 rated power | 250 kVA |
| Trf2 voltage ratio | 0.38/0.18 kV |
| Load Parameter | Value |
| Rated active power | 0.6 kW |
| Rated reactive power | 0.3 kVar |
| Rated voltage | 20 kV |
| Controller Parameter | Value |
| $F_{Vdc} = \frac{k}{s} \times \frac{1+sT_1}{1+sT_2}$ | $k=8.65e3$ A/V/s $T_1=0.0232$ s ⁻¹ $T_2=0.0011$ s ⁻¹ |
| $F_{cc} = k_{pcc} + \frac{k_{icc}}{s}$ | $k_{pcc}=8\Omega$ $k_{icc}=2\Omega/s$ |
| $F_q = k_{pq} + \frac{k_{iq}}{s}$ | $k_{pq}=-0.227$ A/Var $k_{iq}=-453.5$ A/Var/s |

reactive power. In PowerFactory, PWM converter block contains the current control block internally and it is possible to enable or disable it. The current control in PSCAD as can be seen in Fig. 2 comprises of decoupled terms while in PowerFactory the model of the current control is different. Therefore, the built-in current control is disabled by setting all the controller parameters to zero. Moreover, series reactor has been also located inside the PWM converter block in PowerFactory while in PSCAD the reactor is outside the converter. MPPT function uses same INC algorithm in both models.

IV. COMPARISON OF A SINGLE PV SYSTEM CONNECTED TO GRID IN THE BOTH SIMULATIONS PLATFORMS

Two models according to Fig. 1 are built in two simulation platforms, PSCAD and PowerFactory. The parameters of the system are presented in Table I.

An identical simulation scenario is carried out in order to make a fair and comprehensive comparison between two models. Fig. 7 depicts irradiance variations during simulation which varies stepwise for simplicity. Since PowerFactory starts simulation around one operating point while PSCAD simulates from scratch, the simulation are shown from the point that PSCAD has been settled down at the initial operating point for the both models, where irradiance is around 1000 W/m².

- *Case 1: Comparison without MPPT*

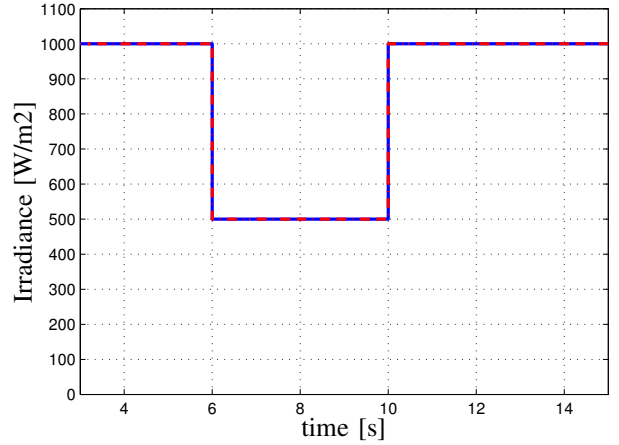


Figure 7. Irradiance variation

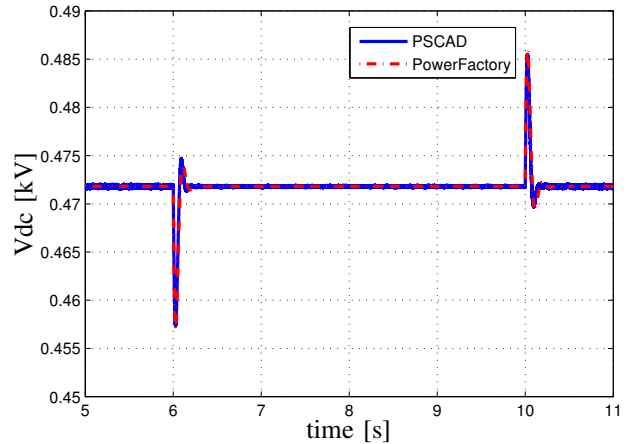


Figure 8. The dc-link voltage response to irradiance variations, without MPPT.

In this case study MPPT is disabled and dc-link voltage set-point v_{dc-ref} is imposed by a constant value equal to 471.8 V which is the voltage at the maximum power point for irradiance equal to 1000 W/m². The objective of this section is only to compare the performance of both models from numerical solving perspective not showing the necessity of MPPT, therefore the dc-link voltage is regulated at the STC value. Fig. 8 demonstrates the dc-link voltage for both models followed by irradiance variation according to Fig. 7, and as it shows the dynamic performance of the both models are quiet similar. Fig. 9 depicts the output power of PV system, as can be seen the general dynamic response structures of the both models are same, with the same numbers of overshoot and undershoot, although the only difference is that the size of overshoot in PowerFactory model is a bit higher than PSCAD that might be due to the converter model in PowerFactory.

- *Case 2: Comparison with MPPT*

This case study is similar to the prior case study, except that the MPPT is enabled in this case study. Fig. 10 shows the dc-link voltage in PowerFactory model has more oscillatory transients than PSCAD. Although the

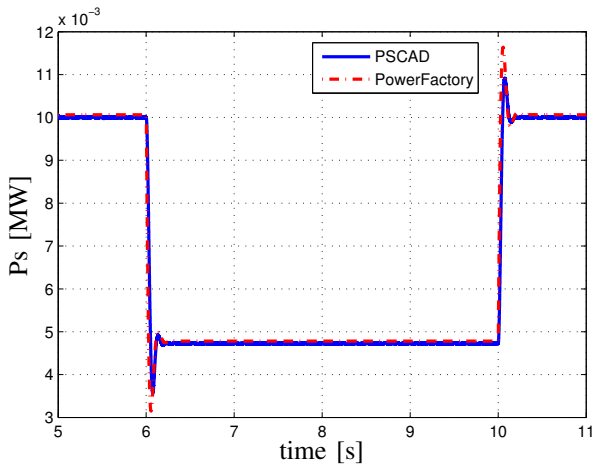


Figure 9. Active power response to irradiance variations, without MPPT.

same algorithm for implementing MPPT has been taken into consideration for the both models, the difference in the transient response might be owing to different solvers of software. At the steady-state stage, PowerFactory model shows no distortion around the operating point which can be due to the switching in PSCAD that makes confusion for the perturbation orientation in MPPT algorithm and so it leads to oscillations around MPP for the PV system in PSCAD. Fig. 11 depicts the output active power of the PV system and as can be seen the PowerFactory model response has more oscillatory transient with higher overshoot that could be expected from the result of the previous case study.

Increasing the MPPT frequency decreases oscillations, as Fig. 12 shows increasing the MPPT frequency to 30 decreases considerably oscillations. Although the final values of V_{dc} in different frequencies are not the same, the difference is too small and it is due to the perturbation step and the design criterion in INC algorithm [16]. It boils down to this fact that once the PV system operating point goes close to MPP, the MPPT algorithm stops generating new perturbation as long as the absolute summation of the incremental conductance and the instantaneous conductance is smaller than a selective small value that is 0.001 in this study [16]. Furthermore, it is obvious that increasing the MPPT frequency increases noticeably the speed of the dc-link voltage response.

- *Case 3: Different specification for dc-link voltage controller*

This case study is analogous with the previous case study, the only exception is the dc-link controller that has been designed for another specifications. In case 2 the specifications are 60 degree phase margin and 200 Hz bandwidth, but in this case study the phase margin is increased to 70 degree and bandwidth is also reduced to 130 HZ that is expected to get a slower system response. Figs. 13 and 14 show the dc-link voltage and active power, respectively. Although both models have more or less similar responses, the output power response of the PV system has higher overshoots and

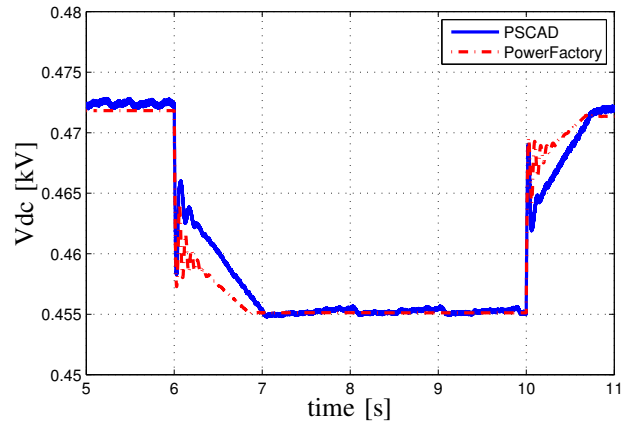


Figure 10. The dc-link voltage response to irradiance variations, with MPPT.

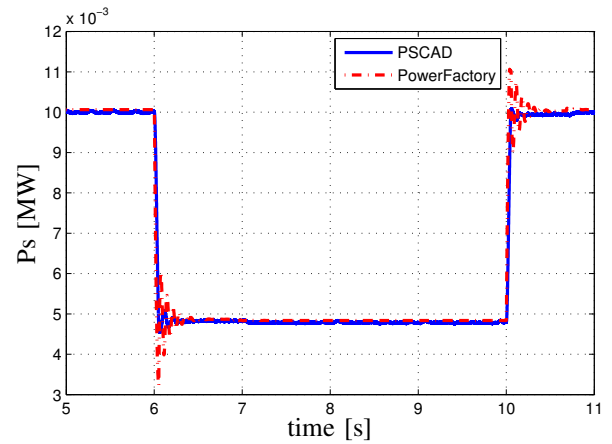


Figure 11. Active power response to irradiance variations, with MPPT.

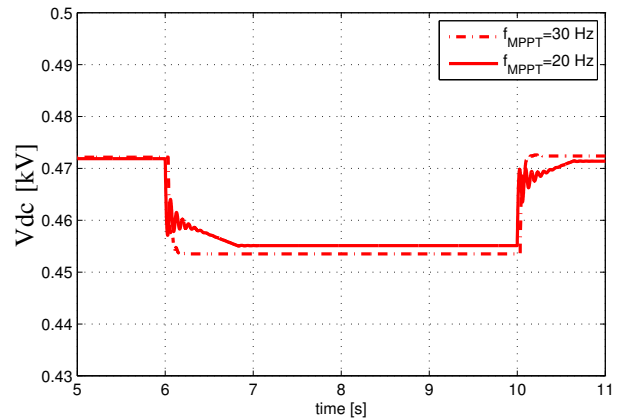


Figure 12. The dc-link voltage response to irradiance variations in PowerFactory for different MPPT frequencies.

undershoots. Apart from the models comparison, comparison of different design specifications shows that the performance of the PV system is considerably affected by changing dc-link specifications to the extent that in the second design, the PV system response becomes slower. Therefore, regarding making equivalent of PV systems in grid, one should deem this issue.

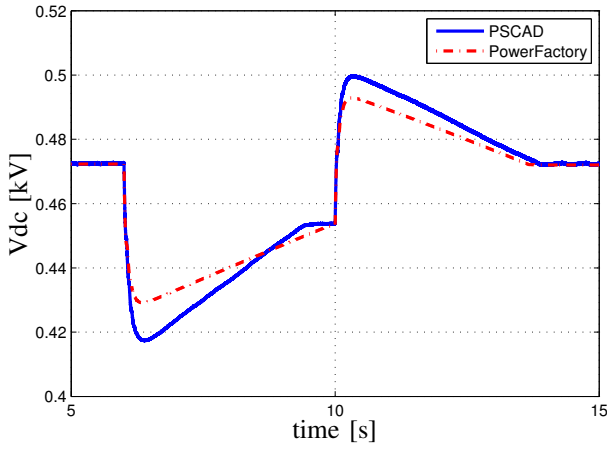


Figure 13. dc-link voltage response to irradiance variation, with MPPT.

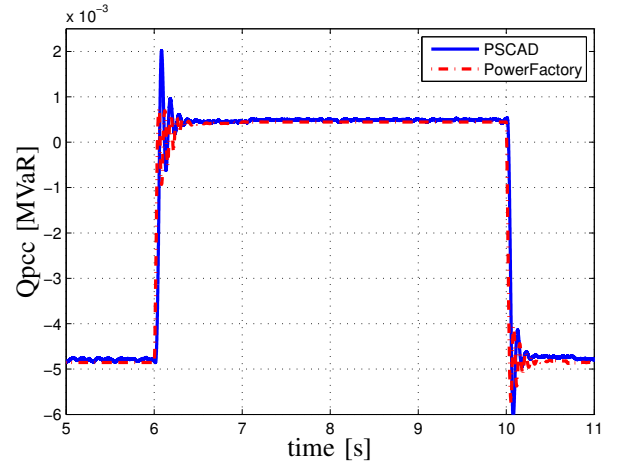


Figure 15. Reactive power at PCC, dynamic power factor strategy (II), with MPPT.

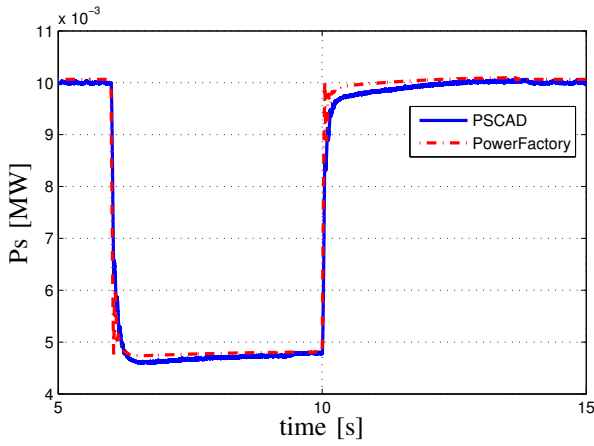


Figure 14. Active power response to irradiance variation, with MPPT.

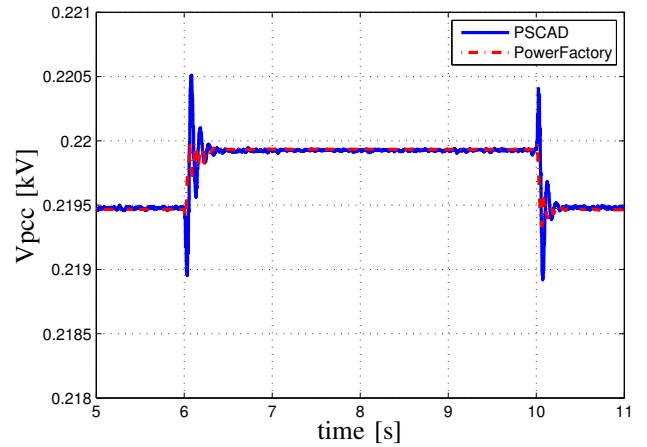


Figure 16. The PCC voltage, dynamic power factor strategy (II), with MPPT.

- *Case 4: Comparison reactive power strategies with MPPT*

In this case study, the behavior of the PV system in both models, with the last three aforementioned reactive power strategies, is taken into account. Figs. 15 and 16 show reactive power at PCC and the PCC voltage for the dynamic power factor control (strategy II). The reactive power is less oscillatory in the PowerFactory model.

For studying the droop-based reactive power control strategy (strategy III), a grid voltage incident is created by increasing 5 % the grid voltage at t=6 sec and return to its initial value after 1 sec while the irradiance remains constant at 1000 W/m^2 . The droop parameter, D, in Fig. 5 is set to 0.03. Figs. 17 and 18 show the reactive power at PCC and the PCC voltage for droop-based reactive power control strategy, respectively.

In the voltage control method (strategy IV), the voltage of the PCC is regulated to a desired set-point. The voltage set-point for the voltage control strategy is chosen according to the voltage at PCC once the PV system is connected to the grid and works with half of the nominal power. Figs. 19 and 20 show reactive power at PCC and the PCC voltage for voltage control strategy, respectively.

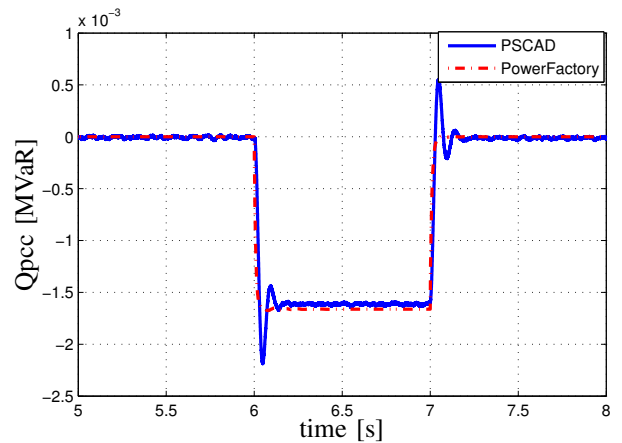


Figure 17. Reactive power at PCC, droop control strategy (III), with MPPT.

- *Case 5: Three-phase to ground fault with MPPT*

This case study demonstrates the effect of the three-phase to ground fault on the PV system for the strategy IV. Irradiance is kept constant at 1000 W/m^2 and a fault incident is occurred at the load connection point

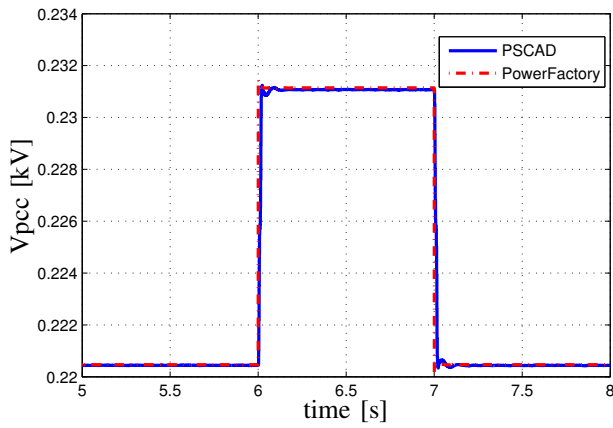


Figure 18. The PCC voltage, droop control strategy (III), with MPPT.

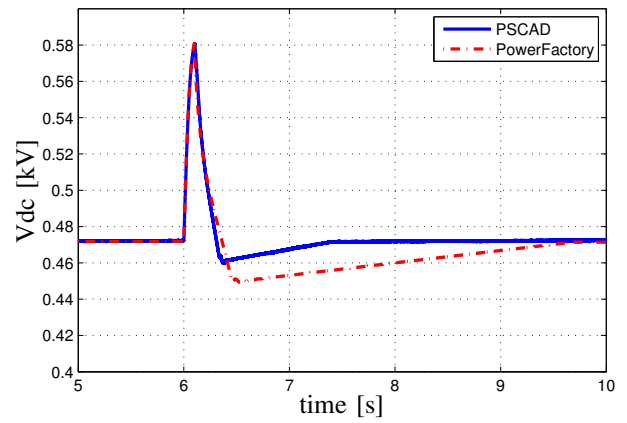


Figure 21. dc-link voltage response to three-phase to ground fault, with MPPT.

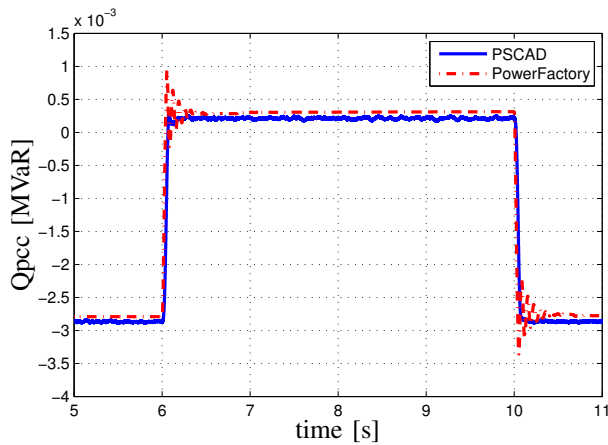


Figure 19. Reactive power at PCC, voltage control strategy (IV), with MPPT.

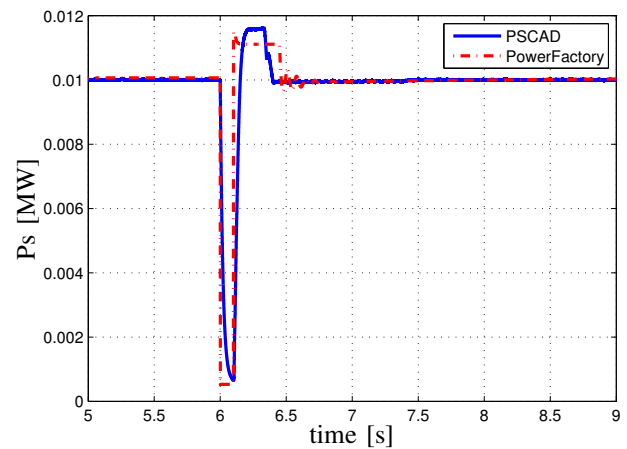


Figure 22. PV active power response to three-phase to ground fault, with MPPT.

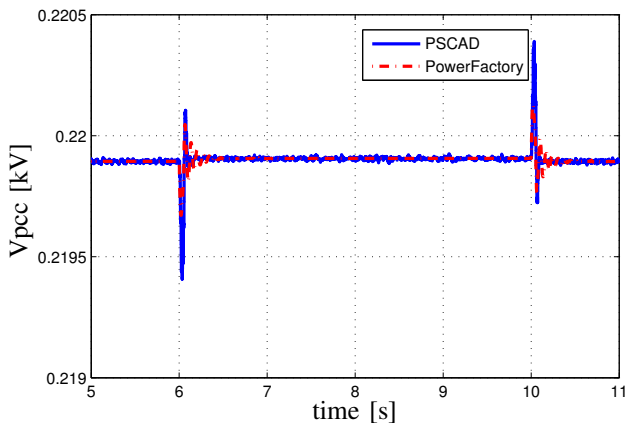


Figure 20. The PCC voltage, voltage control strategy (IV), with MPPT.

at $t=6$ s and cleared 100 ms later. The fault impedance is resistive and equal to 0.008Ω . The dc-link bus voltage is shown in Fig. 21, as expected from power equation across the dc-link capacitor, the dc-link voltage is boosted. During fault interval, the transient behavior of both model are quiet similar. However, after fault clearance the transient response of both models have slight differences. Figs. 22 and 23 show active power

and reactive power of the PV system, respectively. As can be seen, the general trajectory of responses is the same in both models, however there are slight differences specially after fault clearance. The reactive power contribution during fault is too small. This is because of small active power that is provided by PV array to feed dc-link capacitor and it is, in turn, due to the PV output voltage that is shifted towards the open circuit voltage where the PV output power becomes zero.

V. CONCLUSION

In this paper a model of a three-phase single-stage PV system was developed in PowerFactory platform. The performance of the developed was compared and confirmed with the PSCAD model, which was stemming from the previous research. The results show that both models are responding similarly to irradiance variation, although there are slight differences in the transient period subsequent to changes that might be due to MPPT function and numerical solving issues in the control system that are related to different solvers that are used in both software. Nevertheless, the results show that using rms values based simulations in PowerFactory

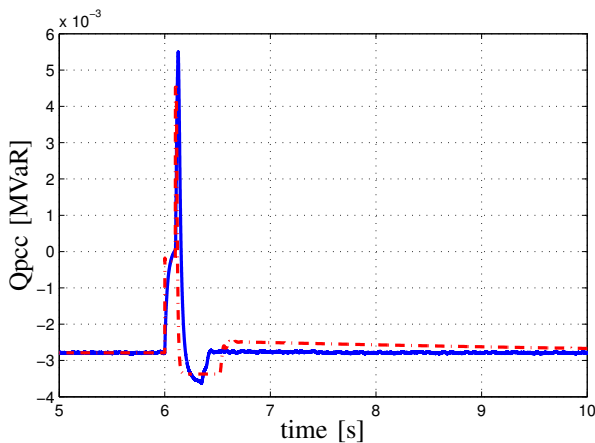


Figure 23. Reactive power at PCC, three-phase to ground fault, with MPPT.

can provide us with quite similar results using time domain instantaneous values. Therefore, the performance of large number of PV systems can be easily studied using rms simulations.

ACKNOWLEDGMENT

This project has been funded by SETS Erasmus Mundus Joint Doctorate and Smooth PV. The authors would like to express their gratitude towards all partner institutions within the programme as well as the European Commission for their support.

REFERENCES

- [1] J. C. Boeme and et al, "Overview of german grid issues and retrofit of photovoltaic power plants in germany for the prevention of frequency stability problems in abnormal system conditions of the ENTSO-E region continental europe," in *1st International Workshop on Integration of Solar Power into Power Systems*, (Aarhus, Denmark), pp. 3–8, Oct. 2011.
- [2] M. Braun, "Reactive power supply by distributed generators," in *2008 IEEE Power and Energy Society General Meeting - Conversion and Delivery of Electrical Energy in the 21st Century*, pp. 1–8, July 2008.
- [3] P. Sulc, K. Turitsyn, S. Backhaus, and M. Chertkov, "Options for control of reactive power by distributed photovoltaic generators," *arXiv:1008.0878*, Aug. 2010. Proceedings of the IEEE, vol.99, no.6, pp.1063-1073, June 2011.
- [4] R. Tonkoski, L. Lopes, and T. EL-Fouly, "Droop-based active power curtailment for overvoltage prevention in grid connected PV inverters," in *2010 IEEE International Symposium on Industrial Electronics (ISIE)*, pp. 2388–2393, July 2010.
- [5] E. Demirok, D. Sera, R. Teodorescu, P. Rodriguez, and U. Borup, "Evaluation of the voltage support strategies for the low voltage grid connected PV generators," in *2010 IEEE Energy Conversion Congress and Exposition (ECCE)*, pp. 710–717, Sept. 2010.
- [6] A. Ellis, M. Behnke, and J. Keller, "Model makers," *IEEE Power and Energy Magazine*, vol. 9, pp. 55–61, June 2011.
- [7] A. Ellis, M. Behnke, and C. Barker, "PV system modeling for grid planning studies," in *2011 37th IEEE Photovoltaic Specialists Conference (PVSC)*, pp. 002589–002593, June 2011.
- [8] S.-K. Kim, J.-H. Jeon, C.-H. Cho, E.-S. Kim, and J.-B. Ahn, "Modeling and simulation of a grid-connected PV generation system for electromagnetic transient analysis," *Solar Energy*, vol. 83, pp. 664–678, May 2009.
- [9] A. Yazdani and P. Dash, "A control methodology and characterization of dynamics for a photovoltaic (PV) system interfaced with a distribution network," *IEEE Transactions on Power Delivery*, vol. 24, pp. 1538–1551, July 2009.
- [10] A. Yazdani, A. Di Fazio, H. Ghoddami, M. Russo, M. Kazerani, J. Jatskevich, K. Strunz, S. Leva, and J. Martinez, "Modeling guidelines and a benchmark for power system simulation studies of three-phase single-stage photovoltaic systems," *IEEE Transactions on Power Delivery*, vol. 26, pp. 1247–1264, Apr. 2011.
- [11] A. Samadi, M. Ghandhari, and L. Söder, "Reactive power dynamic assessment of a PV system in a distribution grid," *Energy Procedia*, vol. 20, pp. 98–107, 2012.
- [12] "Verband der elektrotechnik elektronik Informationstechnike.V. (VDN) (2010). erzeugungsanlagen am niederspannungsnetz technische mindestanforderungen für anschluss und parallelbetrieb von erzeugungsanlagen am niederspannungsnetz. draft of 07-08-2010. berlin."
- [13] D. Sera, R. Teodorescu, and P. Rodriguez, "PV panel model based on datasheet values," in *IEEE International Symposium on Industrial Electronics, 2007. ISIE 2007*, pp. 2392–2396, June 2007.
- [14] A. Yazdani and R. Iravani, *Voltage-Sourced Converters in Power Systems*. Wiley, 1 ed., Feb. 2010.
- [15] G. Kerber, R. Witzmann, and H. Sappl, "Voltage limitation by autonomous reactive power control of grid connected photovoltaic inverters," in *Compatibility and Power Electronics, 2009. CPE '09.*, pp. 129–133, May 2009.
- [16] K. Hussein, I. Muta, T. Hoshino, and M. Osakada, "Maximum photovoltaic power tracking: an algorithm for rapidly changing atmospheric conditions," *Generation, Transmission and Distribution, IEE Proceedings-*, vol. 142, pp. 59–64, Jan. 1995.

Coordinated droop based reactive power control for distribution grid voltage regulation with PV systems

A. Samadi, R. Eriksson and L. Söder

The German Grid Codes (GGC) proposes a standard active power dependent (APD) characteristic, $Q(P)$, to support the voltage profile via a PV system's reactive power as shown in Fig. 1, where P and P_{\max} show the feed-in and the maximum active power of the generator unit, respectively [1]. The GGC standard $Q(P)$ characteristic requires the PV system to operate in an under-excited mode when the feed-in active power goes beyond a threshold of 50% of P_{\max} in order to alleviate the possible voltage rise. In the GGC standard characteristic, the required reactive power of each PV system is determined based on its feed-in power and independent of its location in the grid. According to the GGC, the distribution system operators (DSO) can use a different characteristic from the standard characteristic depending upon the grid configuration, however, it is not clarified how to define such a characteristic and it is devolved to the DSO. Moreover, since the standard characteristic does not consider the voltage profile, its employment can cause unnecessary reactive power consumption. Considering large number of PV systems in grids, unnecessary reactive power consumption boosts the total line losses. Moreover, large amount consumption of reactive power by PV systems may also jeopardize the stability of the network in the case of contingencies in conventional power plants, which supply reactive power [2].

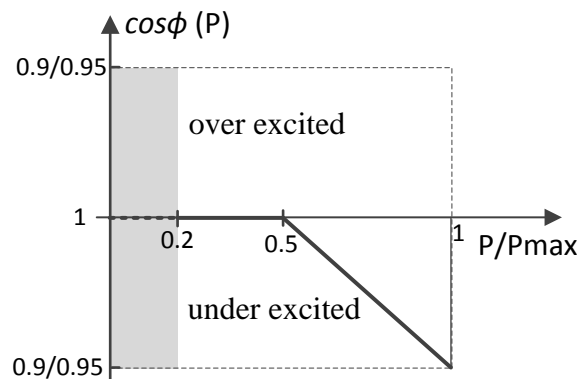


Fig. 1: Standard characteristic curve for $\cos\phi (P)$

Therefore, it is a matter of need to develop an APD method that can provide a coordinated, systematic characteristic for each PV system along a feeder. The voltage sensitivity matrix is utilized to propose a coordinated individual characteristic curves between reactive power and active power for each PV system along a radial feeder by using only local measurements. Since the grid configuration is addressed in the voltage sensitivity matrix, the proposed method basically introduces a characteristic based on the grid configuration for each PV system. The voltage sensitivity matrix has been used in [3] to compare impacts of active power curtailing and reactive power support through

PV systems on the voltage profile in low voltage grids. The voltage sensitivity matrix in [4] is used to define coordinated droop factors in the active power curtailment of PV systems. The sensitivity matrix contents and control theories are employed in [5] to demonstrate the voltage control interaction among PV systems. The voltage sensitivity matrix is used in [6] to eliminate the voltage variation at a target node due to the operation of a wind turbine in a microgrid via reactive power support. In the proposed APD method, the voltage sensitivity matrix is employed to systematically design two main parameters of the GGC Q(P) characteristic for each individual PV system in a radial grid, namely the active power threshold and the slope factor. The proposed APD method considers all the variants for designing the slope factor and the power threshold. The results demonstrate that the proposed method can regulate the voltage to the steady-state voltage limit, while the voltage regulation in the GGC method is not addressed. Because the proposed method explicitly includes the steady-state voltage limits. By doing so, the proposed APD method can decrease the total consumed reactive power by PV systems as well as active power loss caused by reactive power in comparison with the GGC.

In active power dependent methods do not directly measure the voltage as an input. This can, therefore, be noted as a shortcoming of these methods on the grounds that demand variations might simultaneously be in a harmony with the generation for the long range of time periods. PV systems may consequently consume reactive power while there is no voltage violation. Concerning high penetration of PV systems, as mentioned earlier unnecessary reactive power consumption by PV systems is undesirable. Therefore, using the droop-based voltage (DBV) regulation can prevent unnecessary reactive power usage.

Coordination of droop parameters among several PV systems is a challenge on the grounds that PV systems at the beginning of the feeder participate less in the voltage regulation compared to those at the end. The voltage sensitivity matrix is used to propose a coordinated voltage droop parameters for individual PV systems along a radial grid.

The graphical DBV regulation is shown in Fig. 2 . In the DBV regulation, reactive power supports the voltage profile once the voltage is outside a dead-band, which is defined either by standards or distribution system operators. Since voltage rise is more of a concern in this approach, only the right hand side of the graph shown in Fig. 2 is taken into consideration. Once the voltage profile hits the dead-band limit, PV systems must contribute reactive power to support the voltage in accordance with occurred voltage deviations.

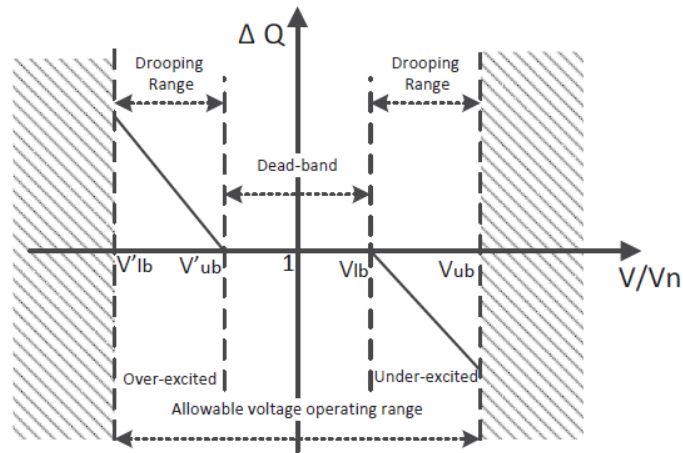


Fig.2 : Graphical schematic of droop-based voltage control.

Reference :

- [1] "Power generation systems connected to the low/voltage distribution network," in *VDE application rule VDE-AR-N 4105:2011-08*, 2011.
- [2] "Studie zur Ermittlung der technischen Mindesterzeugung des konventionellen Kraftwerksparks zur Gewährleistung der Systemstabilität in den deutschen Übertragungsnetzen bei hoher Einspeisung aus erneuerbaren Energien," tech. rep., Studie im Auftrag der deutschen Übertragungsnetzbetreiber, Jan. 2012.
- [3] R. Tonkoski and L. Lopes, "Voltage regulation in radial distribution feeders with high penetration of photovoltaic," in *IEEE Energy 2030 Conference, 2008. ENERGY 2008*, pp. 1–7, Nov. 2008.
- [4] R. Tonkoski, L. Lopes, and T. El-Fouly, "Coordinated active power curtailment of grid connected PV inverters for overvoltage prevention," *IEEE Transactions on Sustainable Energy*, vol. 2, pp. 139–147, Apr. 2011.
- [5] A. Samadi, R. Eriksson, and L. Söder, "Evaluation of reactive power support interactions among PV systems using sensitivity analysis," in *2nd International Workshop on Integration of Solar Power into Power Systems*, (Lisbon, Portugal), pp. 245–252.
- [6] R. Aghatehrani and R. Kavasseri, "Reactive power management of a DFIG wind system in microgrids based on voltage sensitivity analysis," *IEEE Transactions on Sustainable Energy*, vol. 2, pp. 451–458, Oct. 2011.

Equivalent modelling of several PV power plants

A. Samadi and R. Eriksson

I. Introduction:

The main objective of this study and report is making an equivalent model of several PV power plants connected to a grid and, along with it, investigating the probability of reactive power counteractions among PV plants that might not be seen and addressed in the equivalent model. Therefore the work that has been done so far is bulleted as follows:

- Studying and inspecting the final model that was developed by [1]
- Making the template of the aforementioned model in PowerFactory to make integration of duplicated models easily
- Making equivalent of the PV plant model by scaling up the current model
- Running different scenarios

II. PV System Model in PowerFactory

The employed PV model in PowerFactory in this research consists of PV array model, Maximum Power Point Tracking (MPPT), dc-bus capacitor, static generator and peripheral control systems. The PV model is also associated with a voltage control regulator as Fig. 1, where $F_{vac}(s)$ can, in general, be a PI controller. $F_{vac}(s)$ adjusts reactive power in such a way to regulate the voltage.

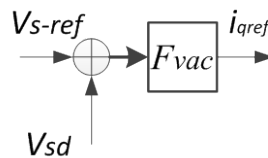


Fig.1 Block diagram of the voltage control in the PV model.

III. Equivalent Model

Since the equivalent (aggregated) model is supposed to be connected to the same voltage level as individual PV systems in the non-aggregated model, only the power level of the current PV model should be manipulated to make the equivalent model. In other words, the dc-link voltage remains

similar in the both equivalent PV model and individual PV systems in non-aggregated model. In order to change the power level, the number of the parallel solar panels must be changed. Furthermore, considering identical voltage level and the following power equation across the dc-link capacitor, it is clear that the capacitor size must be also multiplied by the number of individual PV systems in the equivalent.

$$\frac{1}{2} C \frac{dv_{dc}^2}{dt} \approx P_{dc} - P_{ac}$$

The power rating of the equivalent transformer for the equivalent model is calculated based on the number of individual PV systems in the equivalent model and the transformer rating of one individual PV system. In PowerFactory the transformer impedance is indicated in per-unit. Therefore via increasing the rating power of the transformer by the factor of the number of individual PV systems, the impedance of the equivalent transformer decreases by the same factor, which is in conjunction with the Thevenin impedance of the parallel transformers in case of individual PV systems.

IV. Case Study

It is assumed that three individual PV systems are connected through three transformers to the medium voltage bus-bar (MV-A) and, in turn, through a line to the Thevenin model of the grid, it is shown on the right hand side of Fig. 2. As can be also seen on the left hand side of Fig. 2, the equivalent of these three PV systems has been built and incorporated into the same simulation framework, and it is connected through the equivalent transformer to a medium voltage bus (MV-B) and, in turn, through the same identical line to the Thevenin model of the grid. Nominal power of non-aggregated PV model is 450 kW. The grid and PV data has been given in Table I.

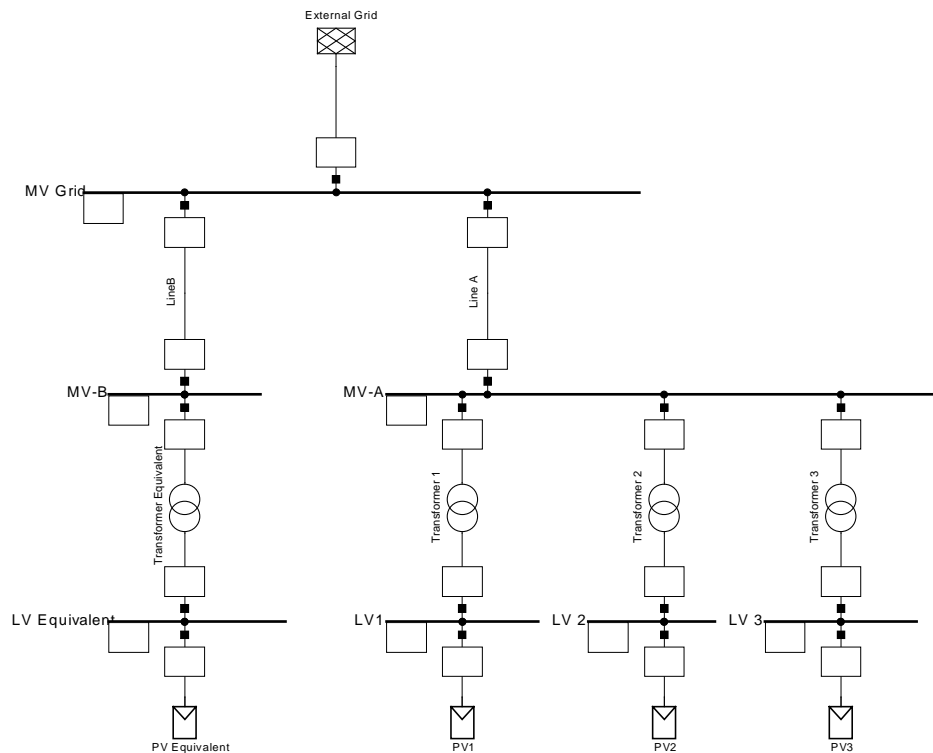


Fig. 2: Schematic of the case study grid

Table I: The grid and PV system data are

| | | | | |
|---|-----------------------------|-----------------------------|-----------------------------------|--|
| PV Panel Parameters | Maximum Current I_{mp} | Maximum Voltage V_{mp} | Short Circuit Current I_{sc} | Short Circuit Voltage V_{sc} |
| | 3.56A | 33.7 V | 3.87 | 42.1 A |
| Non-Aggregated Transformer Parameter | Nominal Power | Voltage ratio and type | Short Circuit voltage, u_k | Resistive Short Circuit voltage, u_{kr} |
| | 560 kVA | 10/0.4 kV, Dyn11 | 4% | 2% |
| Equivalent Transformer Parameters | Nominal Power | Voltage ratio | Short Circuit voltage, u_k | Resistive Short Circuit voltage, u_{kr} |
| | 1.89 MVA | 10/0.4 kV, Dyn11 | 4% | 2% |
| Line parameters | Rated Voltage | Rated Current | Resistance | Reactance |
| | 15 kV | 355A | 2.5 Ω | 5 Ω |

V. Simulation Results

For simplicity, irradiance is varied step-wise. In order to consider and address all the aspects, possible scenarios are studied. The following assumptions are similar in all scenarios:

- All PV systems are associated with MPPT.
- All PV systems are associated with the voltage controller.
- The voltage controller is a pure integrator (I).

A. Scenario 1

In this scenario following assumptions are considered:

- Irradiance level is varied identically for all PV systems in the non-aggregated model.
- In the non-aggregated model, all individual transformers are identical.
- Voltage controller parameters are identical.
- PV systems are supposed to regulate the voltage at the LV bus.
- The voltage set-point is adjusted to 1.01 p.u.

Fig. 3 shows that the irradiance initially is 1000 W/m^2 for both PV models and then at $t=1.5 \text{ s}$ the irradiance is changed identically to 500 W/m^2 for both PV models.

As can be seen in the Fig. 4, the total injected active powers are same in the both non-aggregated and aggregated model. The dc-link voltages for PV systems in both models have been shown in Fig. 5, and as expected, they are identical which boils down to identical irradiance variations. As Fig. 6 depicts, the total contributed reactive powers to regulate the voltage to the set-point are also same. In other words, there is no counteraction among individual PV systems in non-aggregated model, and aggregated model is, therefore, a correct representative of the aggregation. Fig. 7 (a) illustrates that LV-bus voltages, in non-aggregated and aggregated model, have been kept constant and are identical in both models. Fig. 7 (b) also shows MV-bus voltages for both models, and as can be seen MV-bus voltages are also similar in both models.

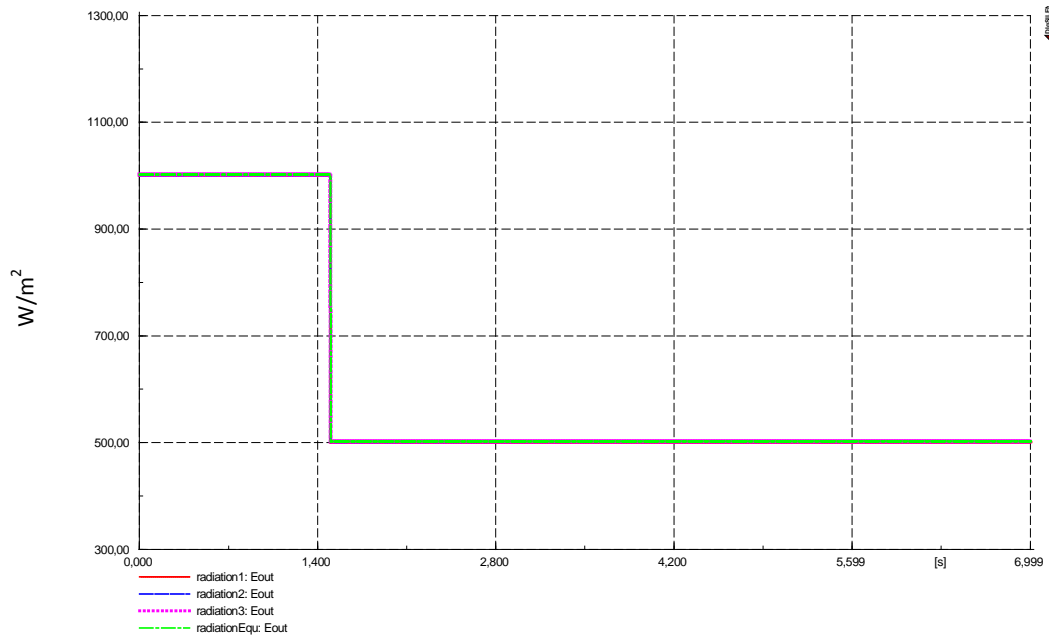


Fig.3: Irradiance variation in Scenario 1

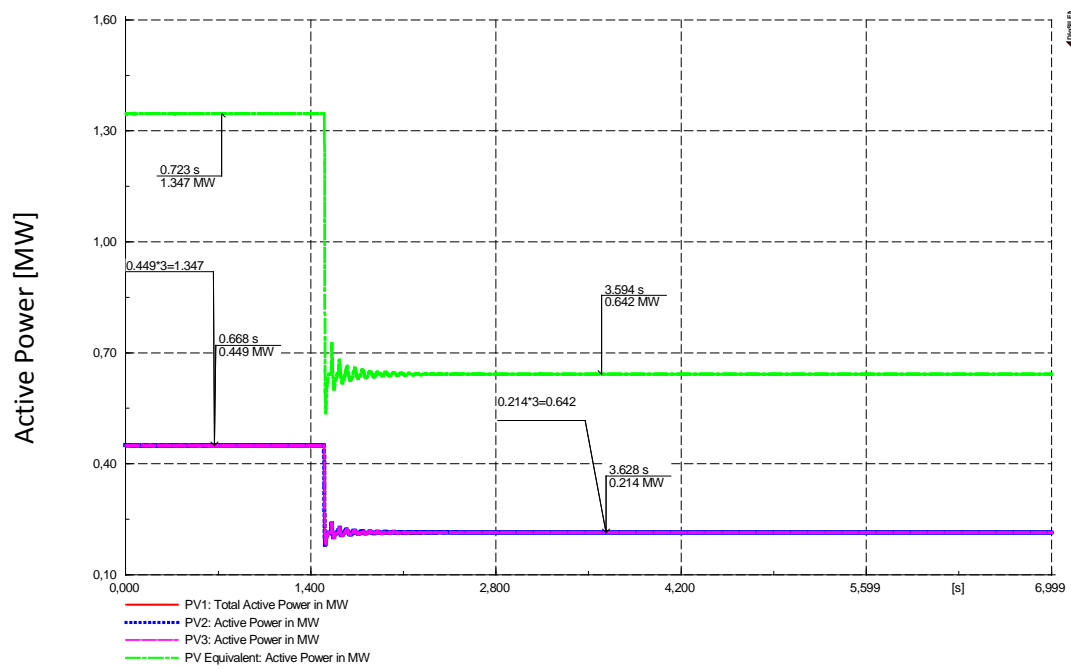


Fig.4: Total active power in scenario 1

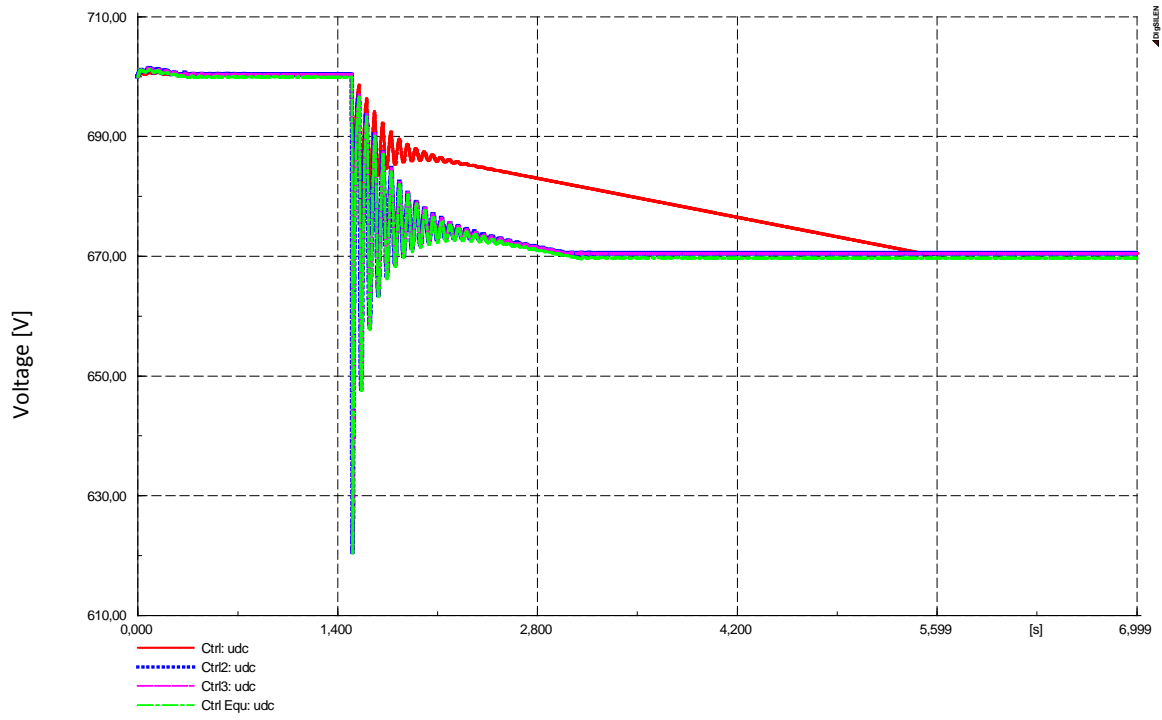


Fig.5: dc-link voltages in scenario 1

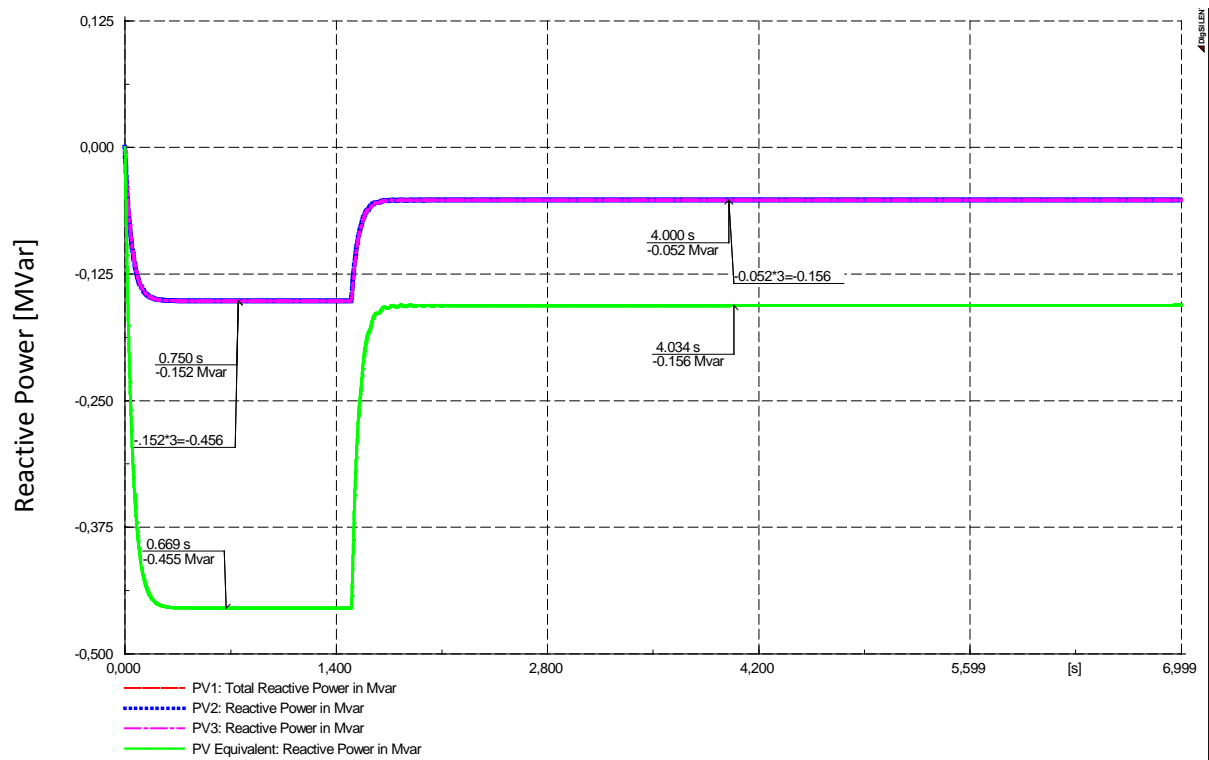


Fig.6: Total reactive powers in scenario 1

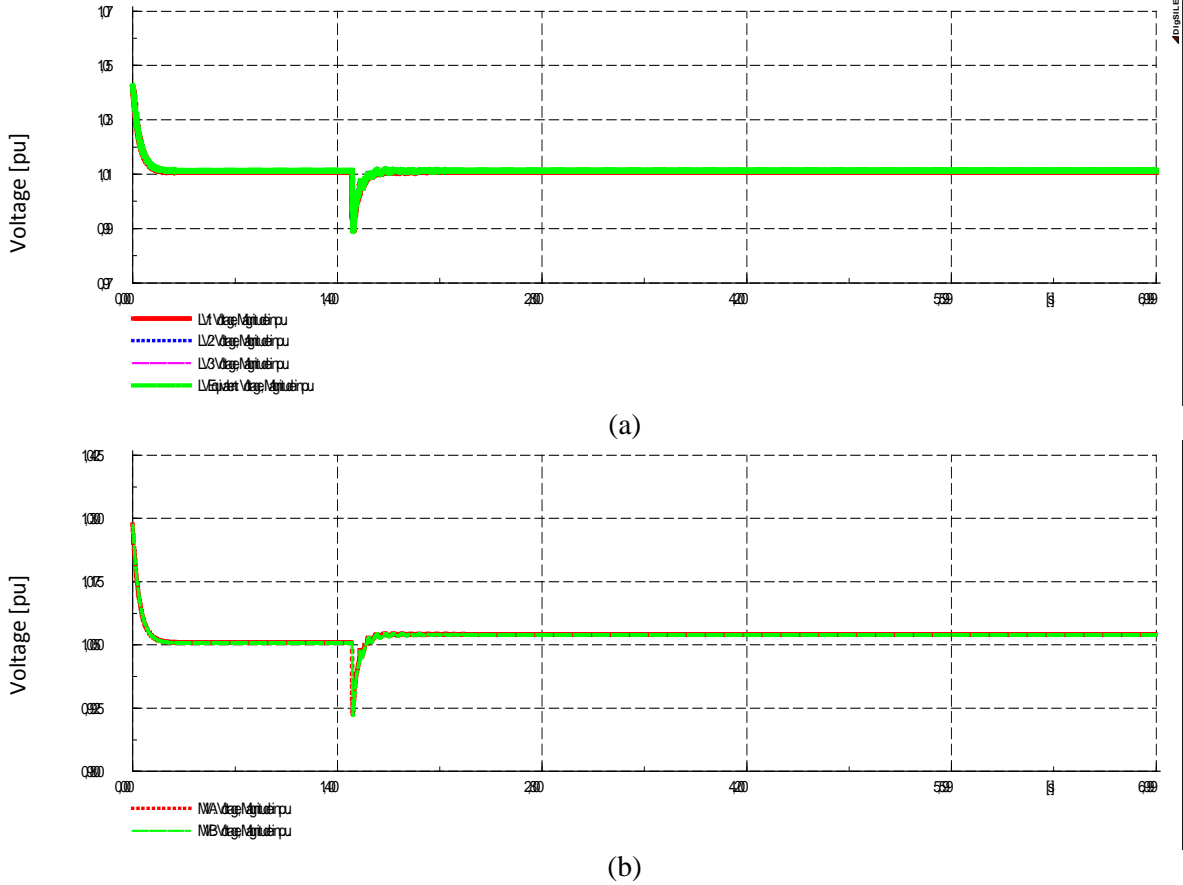


Fig. 7: AC voltages in scenario 1: (a) LV buses. (b) MV buses.

B. Scenario 2

In this scenario following assumptions are considered:

- Irradiance level is varied differently for PV systems in the non-aggregated model.
- In the non-aggregated model, all individual transformers are identical.
- Voltage controller parameters are identical.
- PV systems are supposed to regulate the voltage at the LV bus.
- The voltage set-point is adjusted to 1.01 p.u.

In contrast to scenario 1, in this scenario the variability of the irradiance among individual PV systems is also taken into account. In other words, it is assumed that individual PV systems in non-aggregated model are exposed to the different irradiance. Furthermore, the irradiance of the aggregated model is assumed to be the mean value of irradiance levels of individual PV systems in non-aggregated model. As Fig. 8 shows, the irradiance initially is 1000 W/m^2 and it is varied at $t=1.5 \text{ s}$ to $500, 400$ and 300 W/m^2 for PV1, PV2 and PV3 in non-aggregated model, respectively, and, in turn, the irradiance of aggregated model (PV Equ) is varied to 400 W/m^2 .

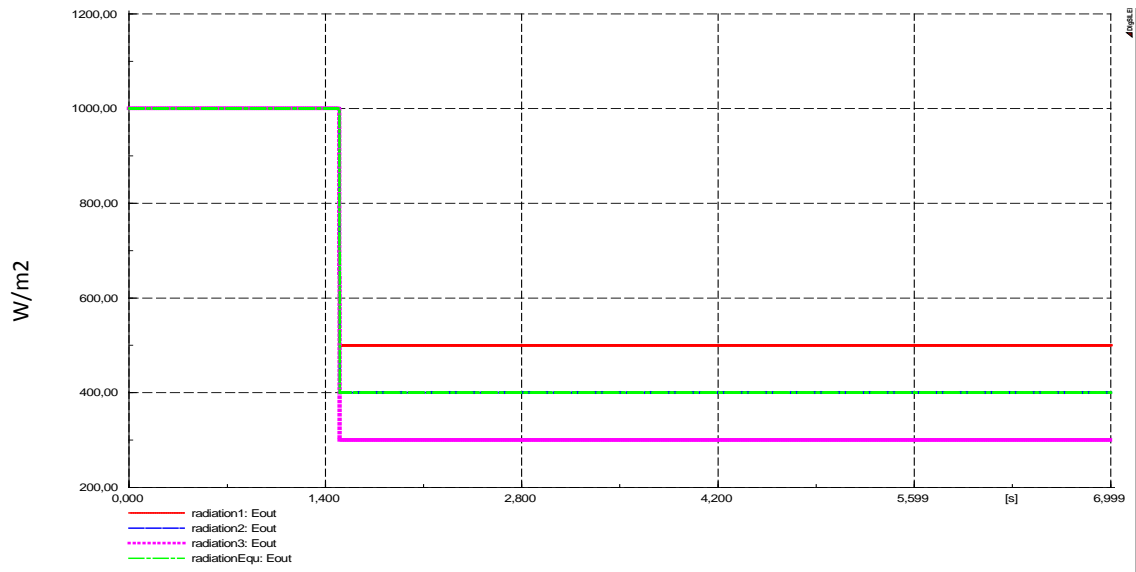


Fig. 8: Irradiance variation in Scenario 2

As can be seen in the Fig. 9, similar to scenario 1, the total injected active powers are same in the both non-aggregated and aggregated model. The dc-link voltages for PV systems in both models have been shown in Fig. 10, they are identical before $t=1.5$ s and afterwards they settle down in conjunction with the related irradiance and since the PV2 in the non-aggregated model and the aggregated PV model are exposed to the same irradiance, their steady-state voltages are same.

As Fig. 11 depicts, the total contributed reactive powers to regulate voltage to the set-point are also same in both models ($= -0.026$ Mvar). Nevertheless, it is obvious that the reactive power of PV3 is on the edge towards capacitive; therefore, in scenario 3 another irradiance variation will be addressed to investigate more. Fig. 12 (a) illustrates that LV-bus voltages in non-aggregated and aggregated model have been kept constant and are identical in both models. Fig. 12 (b) also shows MV-bus voltages for both models, and as can be seen MV-bus voltages are also similar in both models.

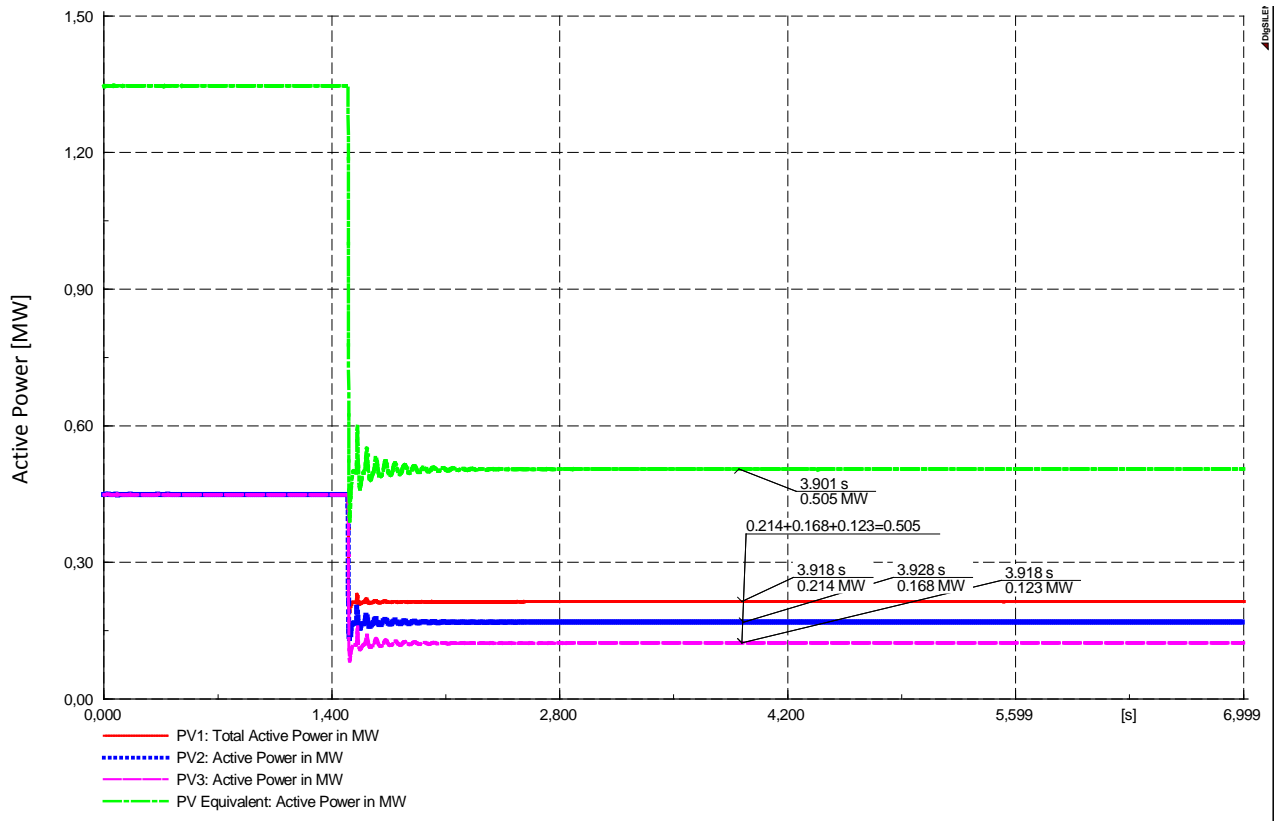


Fig. 9: Total active power in scenario 2

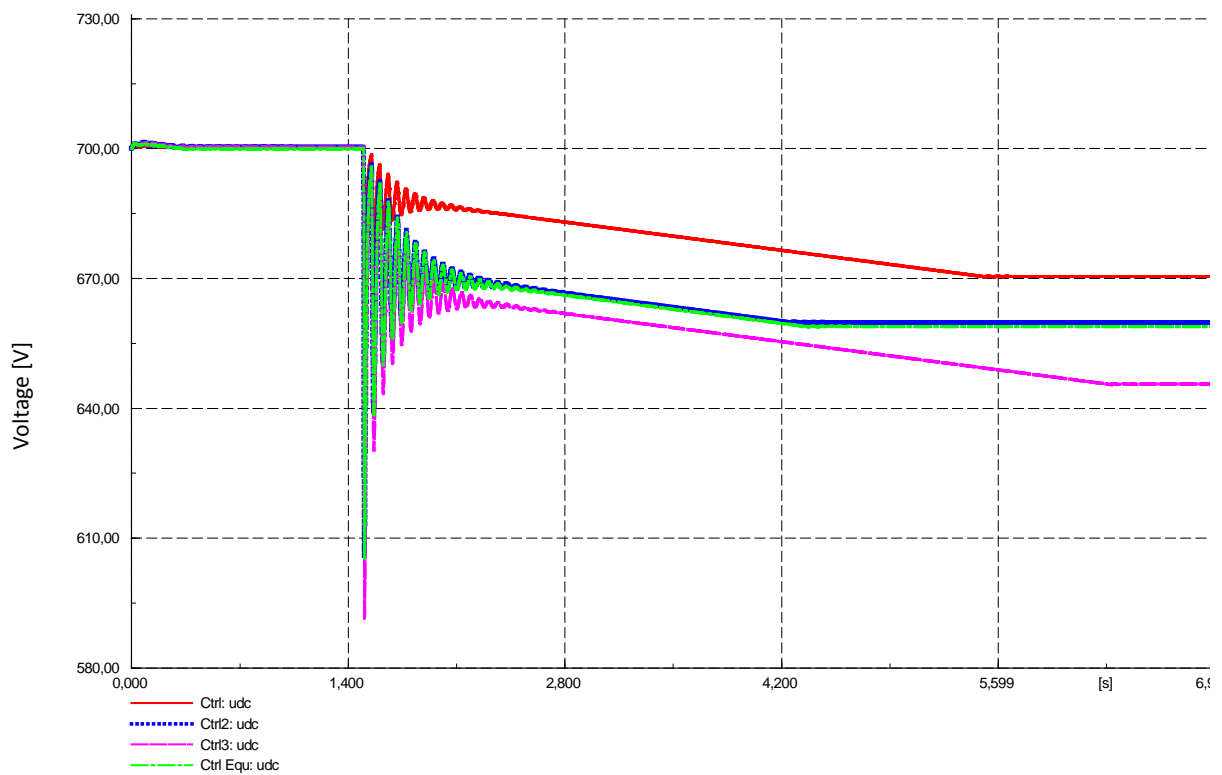


Fig. 10: dc-link voltages in scenario 2

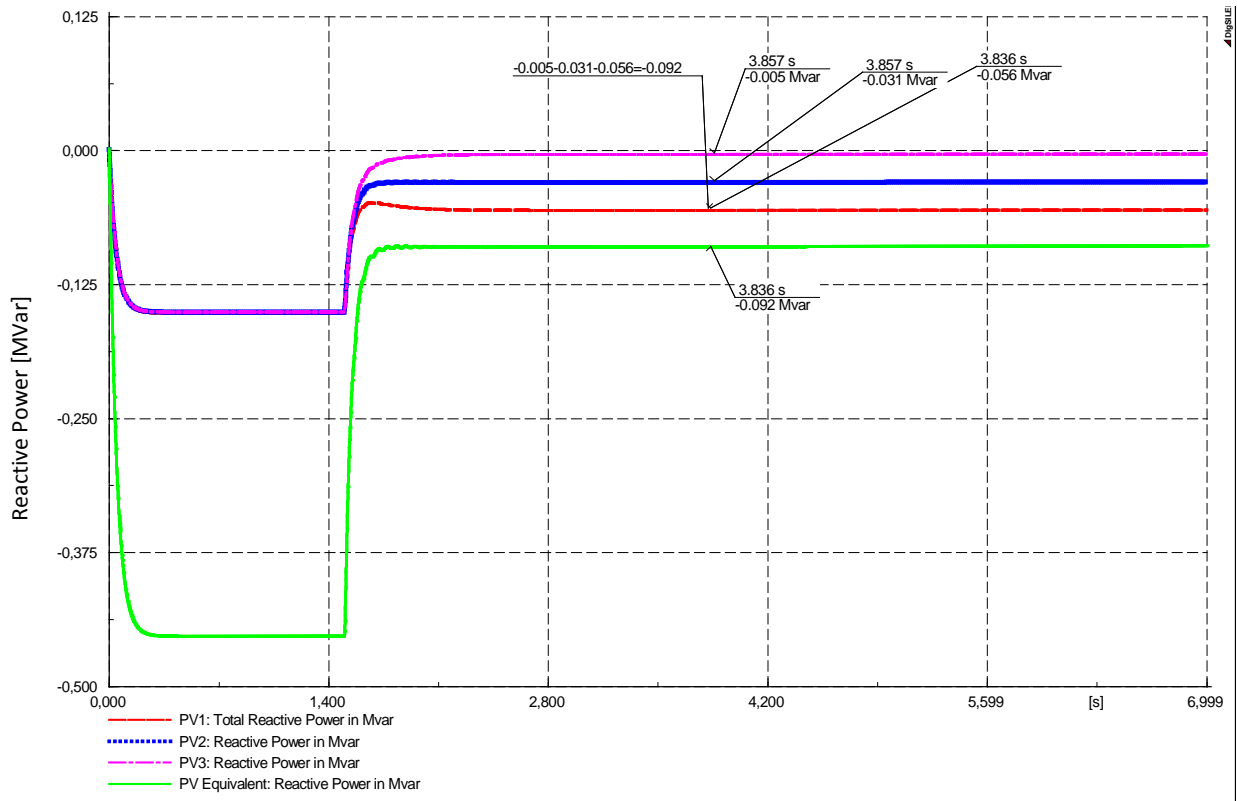
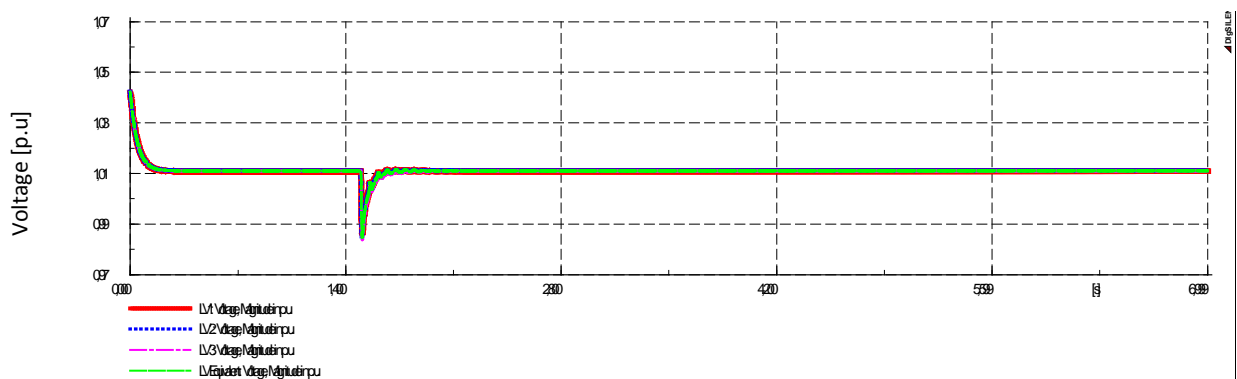
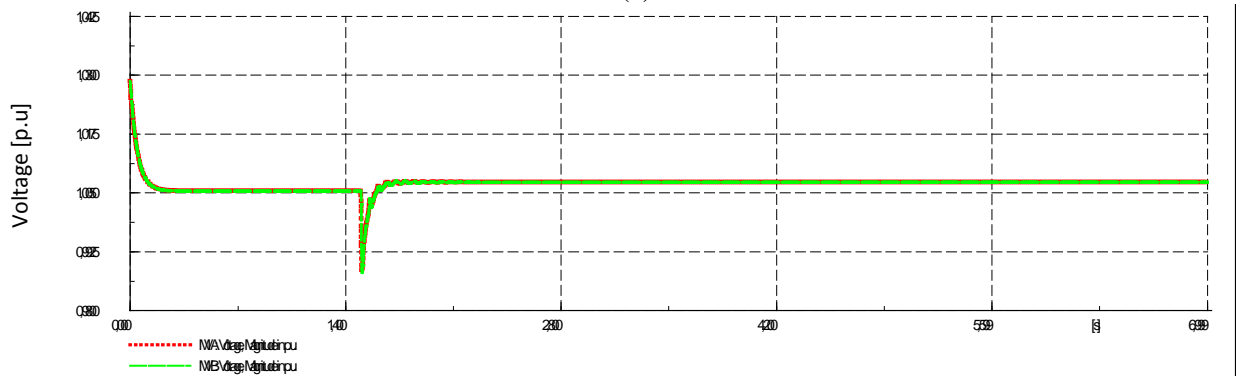


Fig. 11: Total reactive powers in scenario 2



(a)



(b)

Fig. 12: AC voltages in scenario 2: (a) LV buses. (b) lower figure) MV buses

C. Scenario 3

In this scenario following assumptions are considered:

- Irradiance level is varied differently for PV systems in the non-aggregated model.
- In the non-aggregated model, all individual transformers are identical.
- Voltage controller parameters are identical.
- PV systems are supposed to regulate the voltage at the LV bus.
- The voltage set-point is adjusted to 1.01 p.u.

This scenario except the irradiance variation scheme is similar to scenario 2. In scenario 3 the irradiance is changed as Fig. 12.

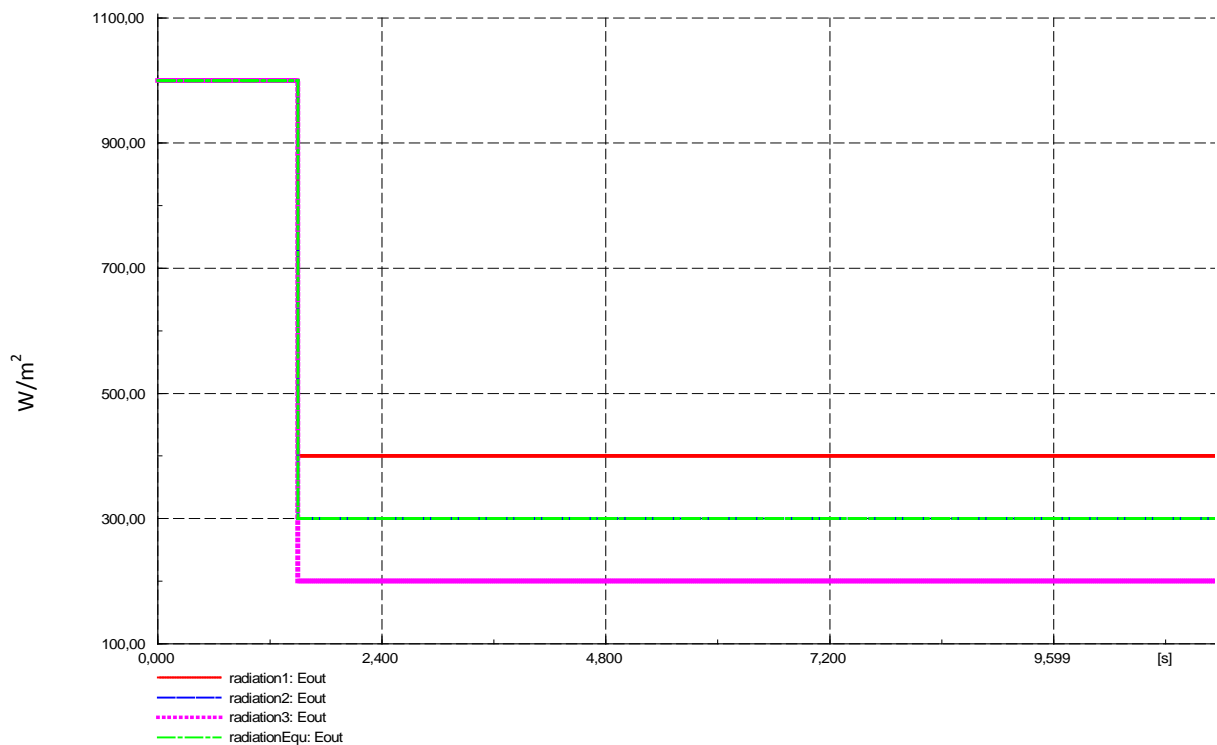


Fig. 13: Irradiance variation in Scenario 3

Concerning the active power, the summation of individual active power of each non-aggregated PV models is equal to 0.370 MW that is analogous to aggregated model (Fig. 14). Fig. 15 shows that dc-link voltages.

Regarding the reactive power, Fig. 16, it is obvious that in non-aggregated model, PV3 works in capacitive mode while PV1 and PV 2 work in inductive mode. Nevertheless, the total reactive power in non-aggregated model is equal to the aggregated model ($= -0.026 \text{ Mvar}$). Furthermore, as can be seen in Fig. 17 (a), LV-bus voltages are also regulated to the set-point properly. Therefore, even though the PV systems in non-aggregated model are working in different modes (inductive and capacitive), it has no negative effect on the voltage regulator performance.

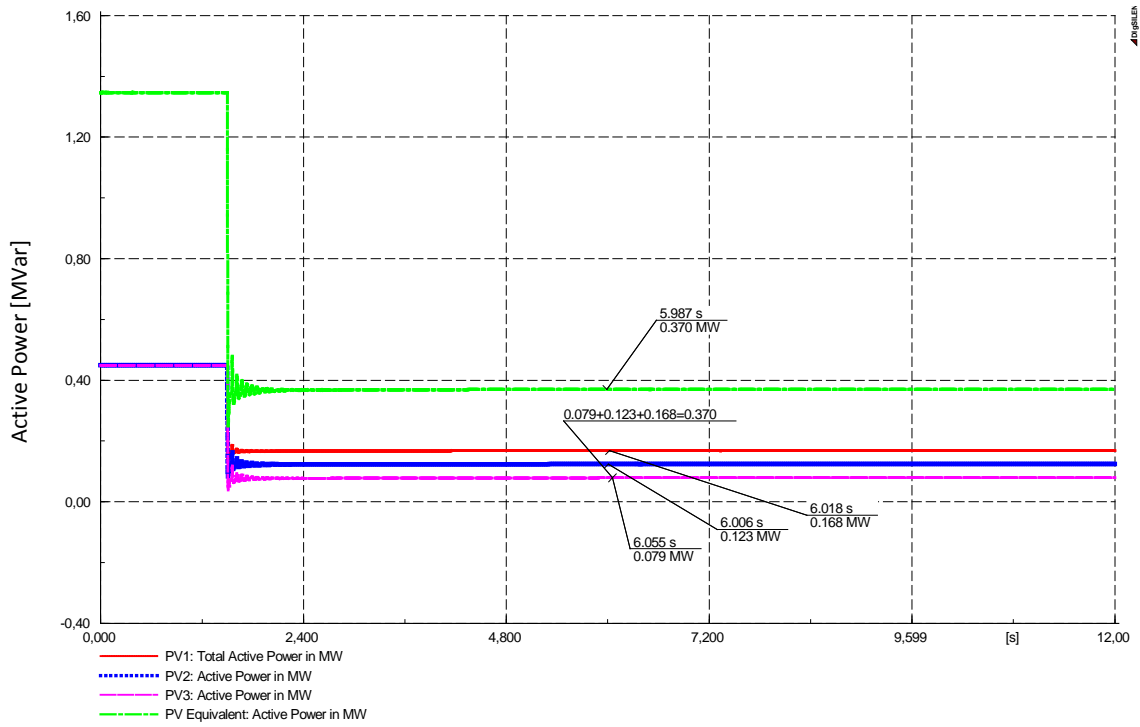


Fig. 14: Total active power in scenario 3

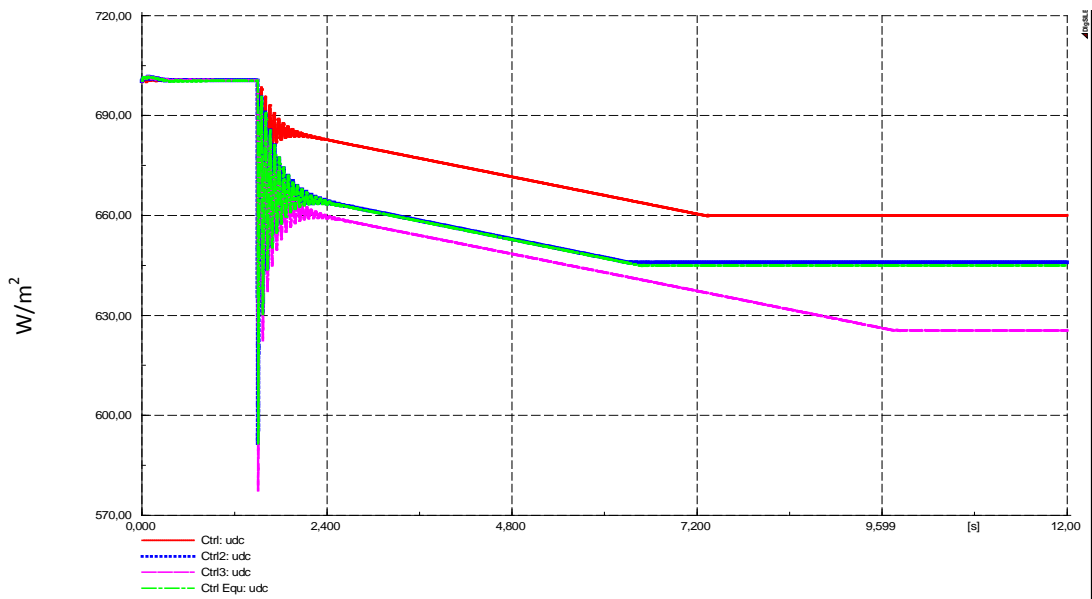


Fig. 15: dc-link voltages in scenario 3

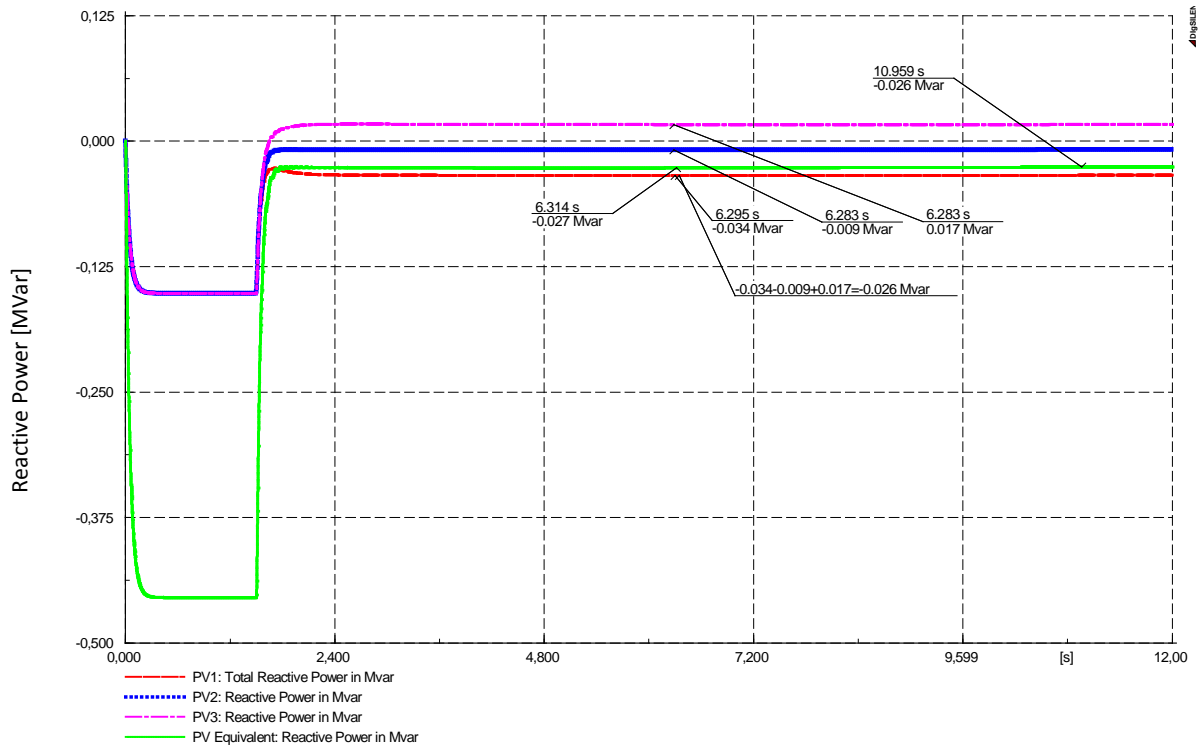
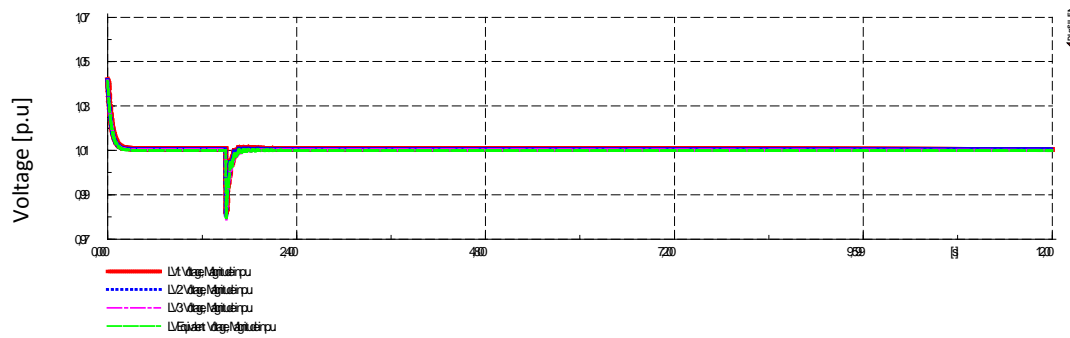
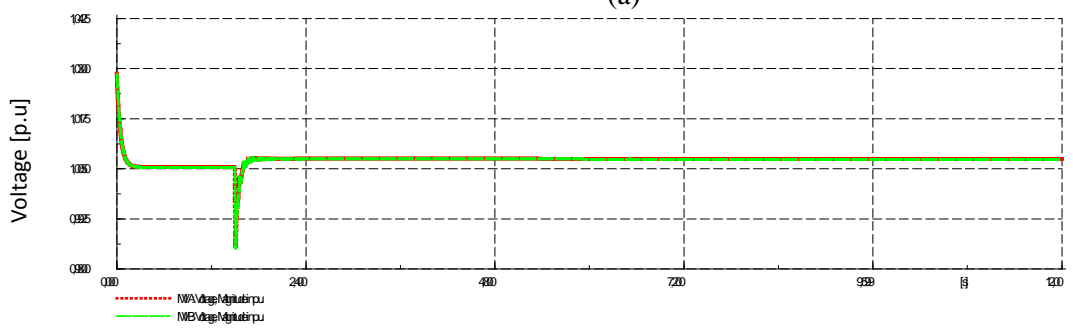


Fig. 16: Total reactive powers in scenario 3



(a)



(b)

Fig. 17: AC voltages in scenario 3. (a) LV buses. (b) MV buses.

D. Scenario 4

In this scenario following assumptions are considered:

- Irradiance level is varied differently for PV systems in the non-aggregated model.

- In the non-aggregated model, individual transformers are different.
- Voltage controller parameters are identical.
- PV systems are supposed to regulate the voltage at the LV bus.
- The voltage set-point is adjusted to 1.01 p.u.

In contrast to scenario 3, in this scenario is assumed that individual transformers in non-aggregated model are not identical anymore. Therefore, the rating power of transformer 2 and 3 is decreased by 10%. The results show that the main difference is in the reactive power. Fig. 18 shows total reactive powers in both models. Before $t=1.5$ s all PV systems are working in inductive mode and the total reactive power of the non-aggregated model is equal to $(-0.143 \times 2 - 0.159) = -0.445$ Mvar while the total reactive power of the aggregated model is -0.455 Mvar. Therefore, there is 0.01 Mvar difference between non-aggregated and aggregated model. It can be seen from Fig. 18 that by changing irradiance at $t=1.5$ s, PV2 and PV3 start working in capacitive mode while PV1 functions in inductive mode. Therefore, compared to scenario 3 the operation mode of the PV2 has changed. Moreover, the total reactive power of the non-aggregated model and aggregated model settle down at $(-0.045 + 0.001 + 0.026) = -0.018$ Mvar and -0.026 Mvar, respectively. Therefore, the difference between reactive power of non-aggregated model and aggregated model is 0.008 Mvar. Fig. 19 shows LV-bus and MV-bus voltages, it can be seen that LV-bus voltages are regulated to the set-point. Therefore, one can draw this conclusion that there is no counteraction between controllers on the grounds that irrespective of different operation modes (capacitive or inductive) among individual PV systems and different total reactive powers between aggregated and non-aggregated model, the voltage regulation is fulfilled satisfactory. Moreover, compared to scenario 3, one can also conclude that the total reactive power deviation is due to non-uniformity of individual transformers in non-aggregated model.

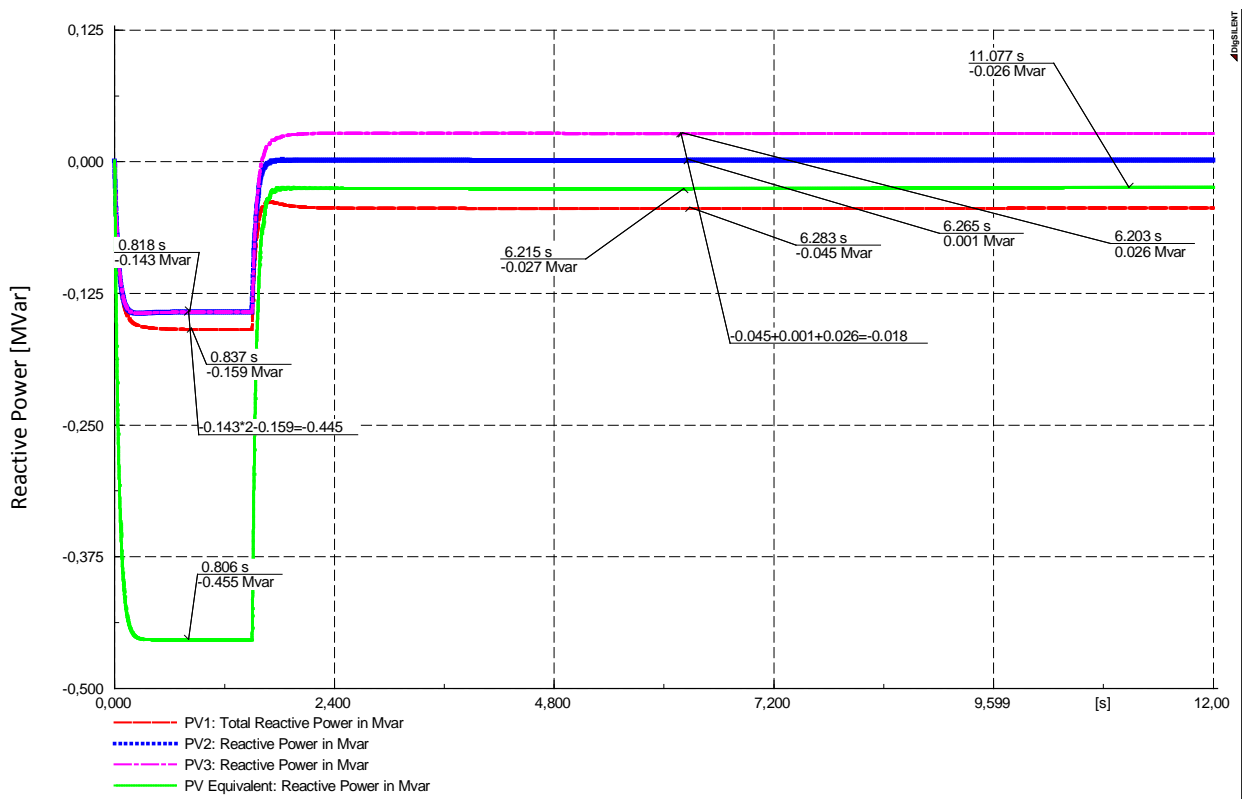


Fig. 18: Total reactive powers in scenario 4

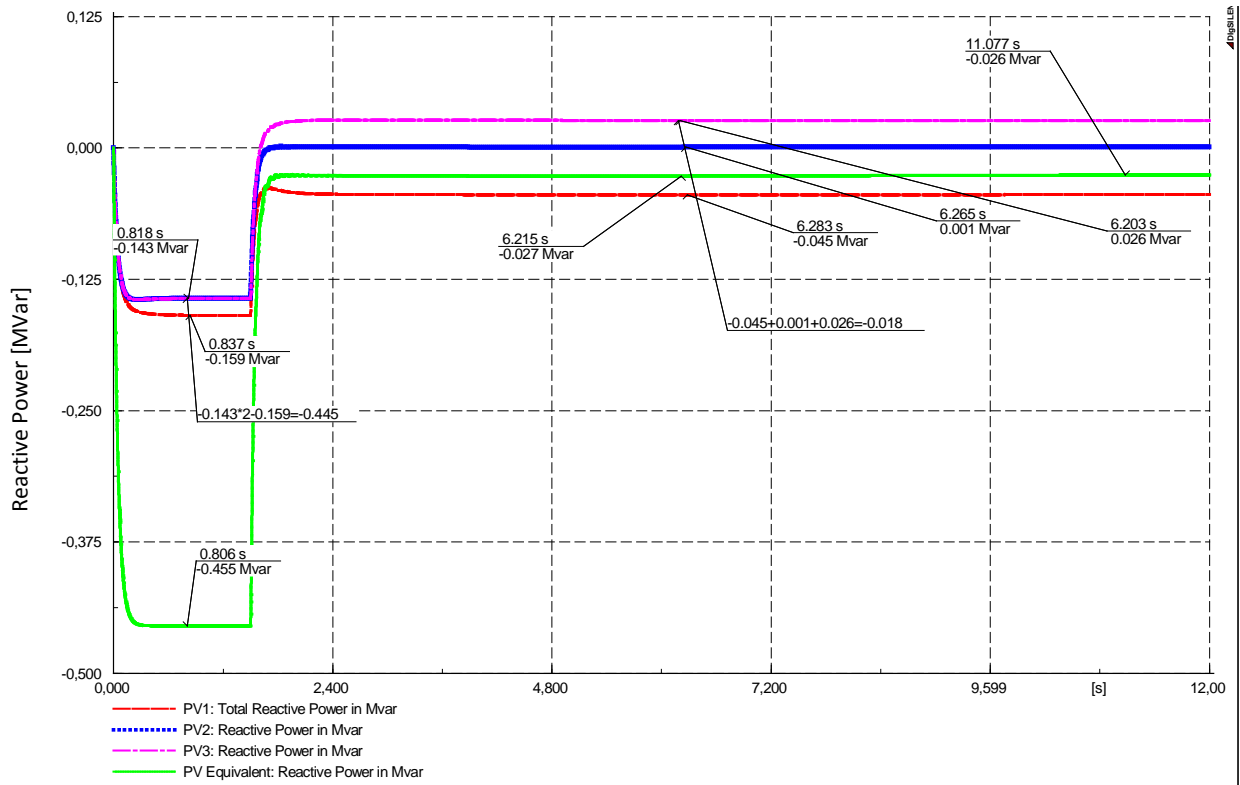


Fig. 18: Total reactive powers in scenario 4.

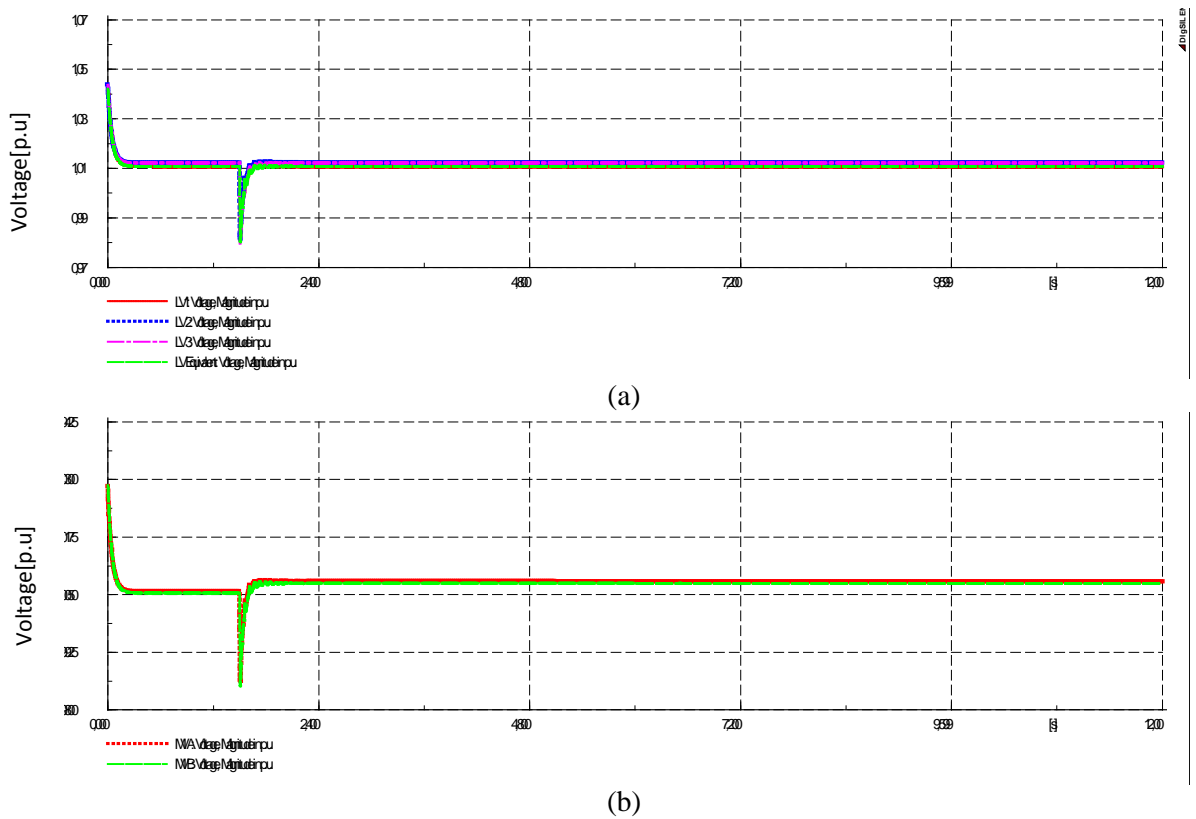


Fig. 19: AC voltages in scenario 4. (a) LV buses. (b) MV buses.

E. Scenario 5

In this scenario following assumptions are considered:

- Irradiance level is varied differently for PV systems in the non-aggregated model.
- In the non-aggregated model, individual transformers are not identical.
- Voltage controller parameters are different.
- PV systems are supposed to regulate the voltage at the LV bus.
- The voltage set-point is adjusted to 1.01 p.u.

In contrast to scenario 4, in this scenario voltage controller parameters of PV systems in non-aggregated model are also varied to make voltage controllers dissimilar. As mentioned earlier, the voltage controller is a pure integrator (I). In this scenario the integral gain of PV1 and PV2 voltage controllers are varied from -0.005 to -0.002 and -0.009, respectively, and the integral gain of PV1 voltage controller is kept as previous (-0.005). The results show that there is no difference in steady-state values compared to scenario 4. However, as can be seen in Fig. 20, the dynamic behavior of reactive powers is slightly different in scenario 5 compared to scenario 4.

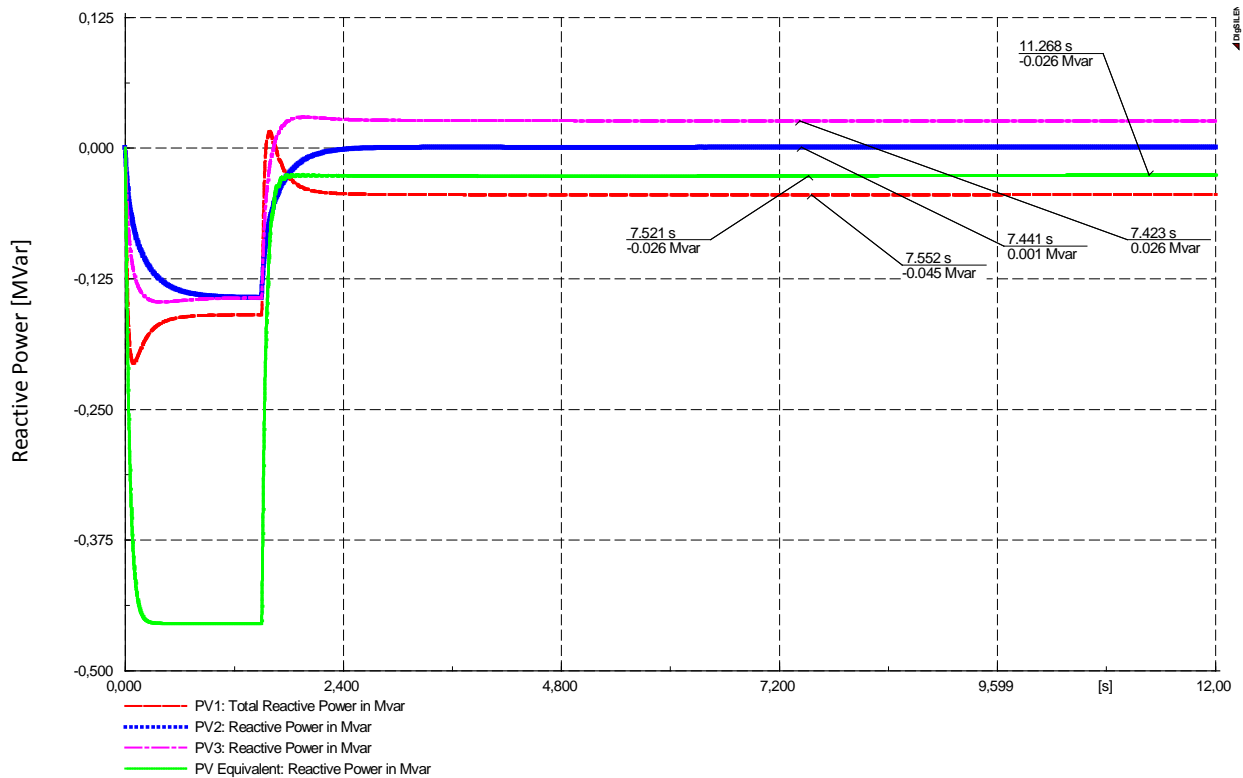


Fig. 20: Total reactive powers in scenario 5

F. Scenario 6

In this scenario following assumptions are considered:

- Irradiance level is varied differently for PV systems in the non-aggregated model.
- In the non-aggregated model, individual transformers are different.
- Voltage controller parameters are considered both identical and different.
- PV systems are supposed to regulate the voltage at the MV bus.

- The voltage set-point is adjusted to 1 p.u.

In contrast to scenario 4, in this simulation assumed that PV systems are supposed to regulate the voltage at the MV-bus. Moreover, the voltage controller is firstly assumed to be identical and then it will be changed.

In the case of similar voltage controllers, the results demonstrate that there is no difference in the total injected active power and dc-link voltage. However, there is significant change in the reactive power behavior. As shown in Fig. 21, reactive powers of individual PV systems in non-aggregated model are equally participating in the voltage regulation. In other words there is no reactive power circulation among individual PV systems. However, there is small deviation between total reactive power of aggregated and non-aggregated model that might be due to dissimilar individual transformers. Fig. 22 (b) shows that MV-bus voltages have been identically regulated.

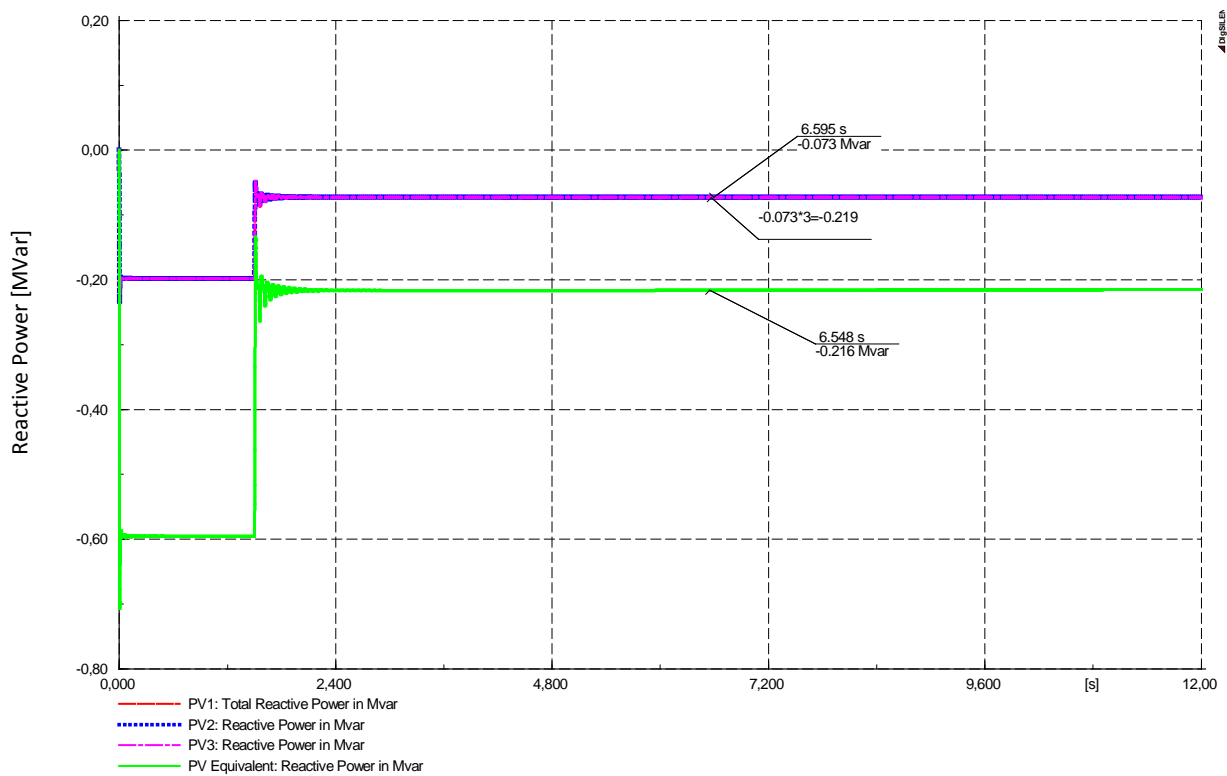
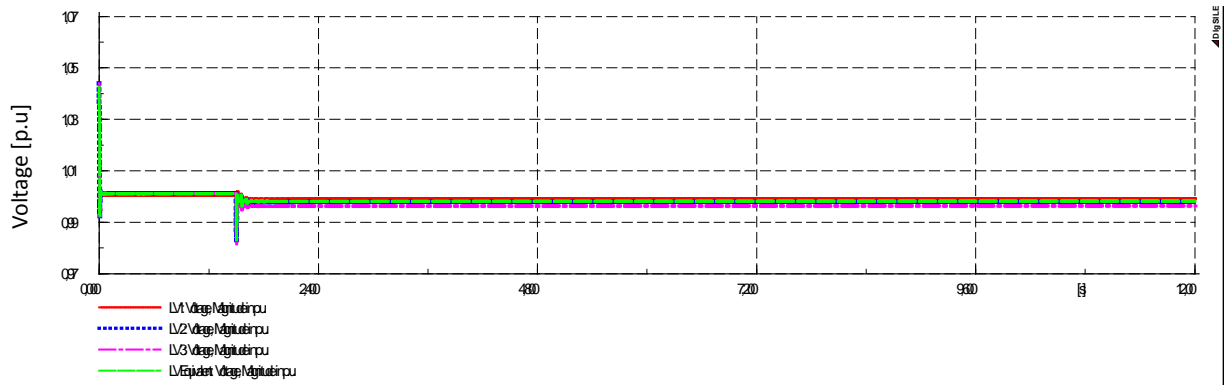
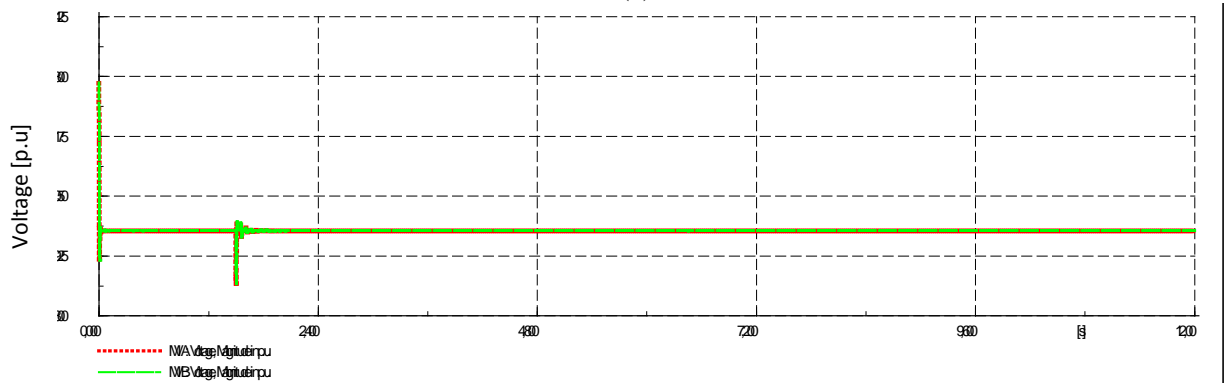


Fig. 21: Total reactive powers in scenario 6, similar regulators



(a)



(b)

Fig. 22: AC voltages in scenario 6 with similar regulators: (a) LV buses. (b) MV buses.

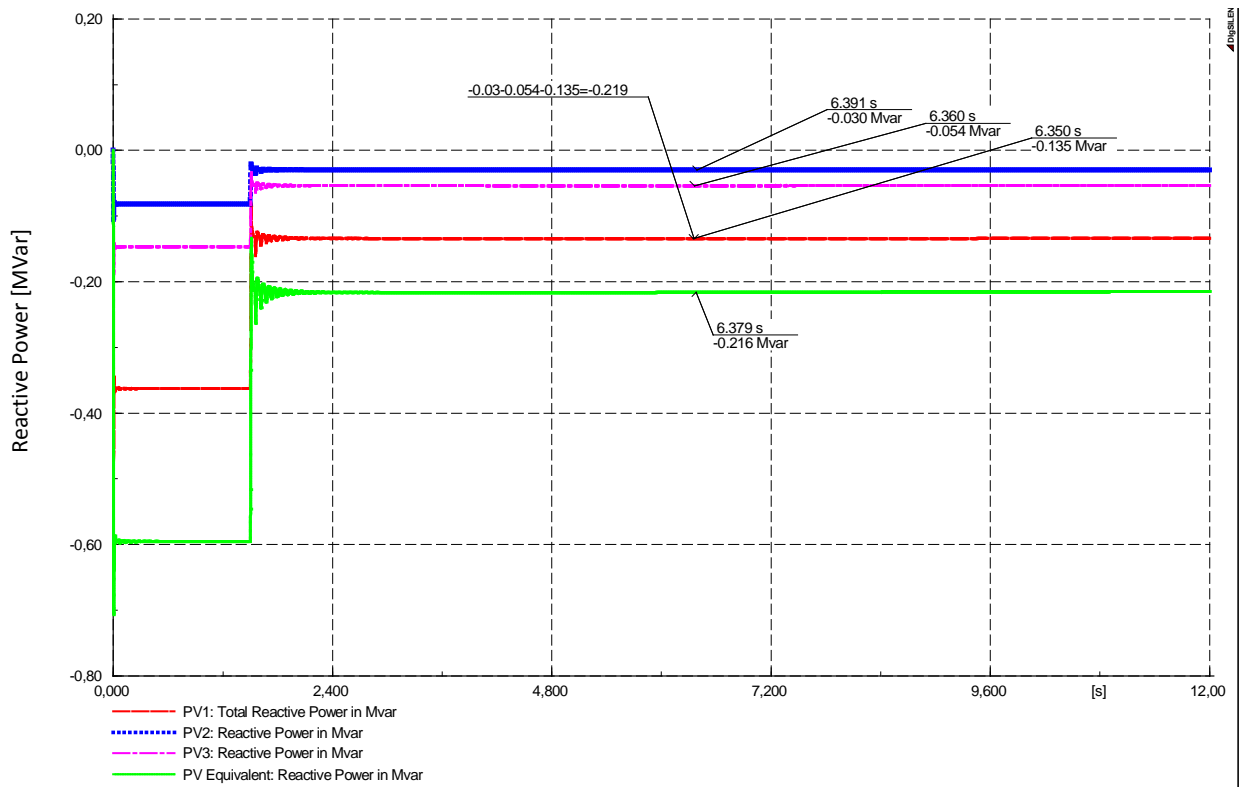


Fig. 23: Total reactive powers in scenario 6, dissimilar regulators

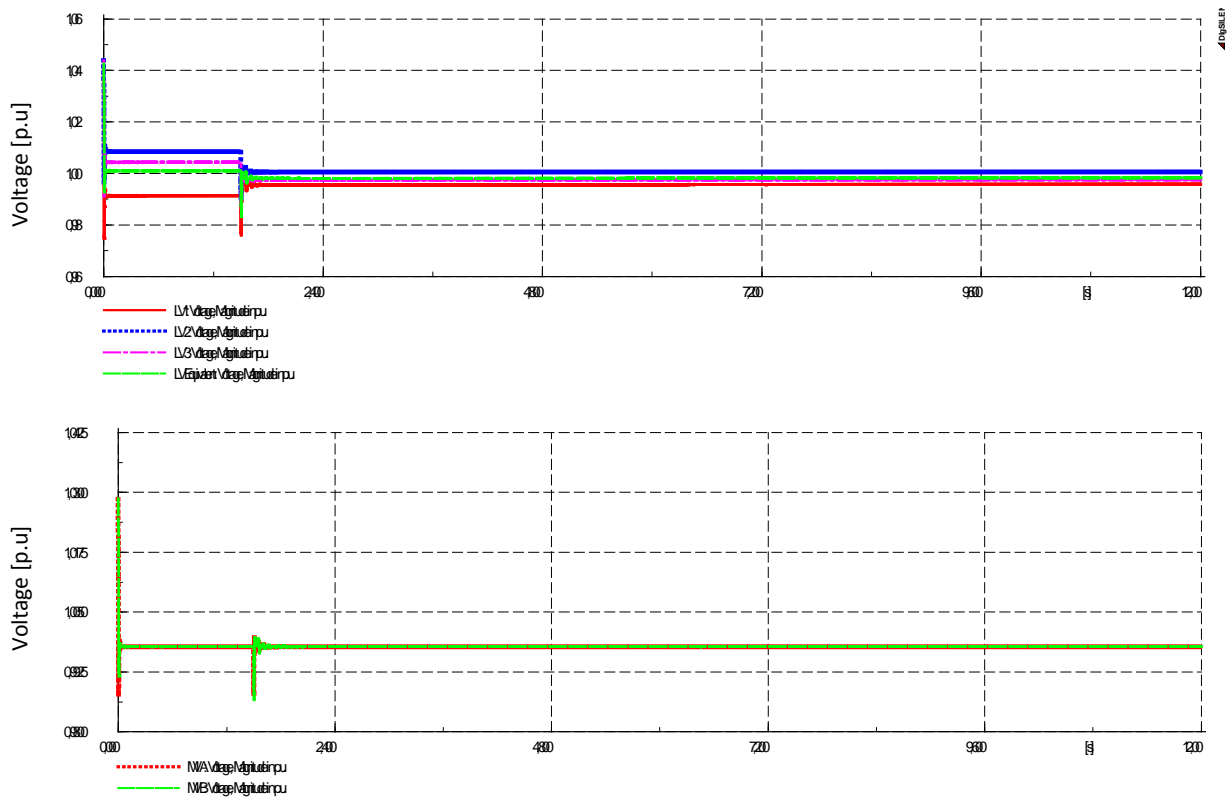


Fig. 24: AC voltages in scenario 6 with dissimilar regulators: (a) LV buses. (b) MV buses.

In order to consider the effect of different voltage regulator parameters, voltage regulator parameters are changed similar to the scenario 5. Fig. 23 depicts that reactive power contribution are not anymore equally distributed between individual PV systems in non-aggregated model. Nevertheless, the total reactive power of non-aggregated model (-0.219 Mvar) remains as previous. Fig. 24 (b) shows MV-bus voltages have been identically regulated.

VI. Conclusion

The bottom line of this study is that, although, reactive power operation mode of individual PV systems in non-aggregated model might be different (capacitive or inductive), the performance of the voltage regulator in both aggregated and non-aggregated model would be similar.

VII. References

- [1] Mahmood F. Improving the Photovoltaic Model in PowerFactory. 2012. EES Examensarbete / Master Thesis, XR-EE-ES 2012:017 <http://www.diva-portal.org/smash/record.jsf?searchId=2&pid=diva2:571921>

Evaluation of Reactive Power Support Interactions Among PV Systems Using Sensitivity Analysis

Afshin Samadi, Robert Eriksson and Lennart Söder

KTH Royal Institute of Technology

School of Electrical Engineering

Department of Electric Power Systems

Stockholm, Sweden 10044

Email: afshin.samadi@ee.kth.se, robert.eriksson@ee.kth.se, lennart.soder@ee.kth.se

Abstract—Growing trends in generating power from distributed PhotoVoltaic (PV) systems has accommodated more and more PV systems within load pockets in distribution grid. This high penetration has brought about new challenges such as voltage profile violation, reverse load flow and etc. A few remedies have been imposed by grid codes such as reactive power contribution of PV systems and active power curtailment. This study applies two analytical methods from control science to find the possibility of controllability among the PV systems in a distribution grid for voltage profile control at specific set-points through reactive power regulation and active power curtailment. For this purpose, the voltage sensitivity matrix is used as the steady-state gain of the multi-variable system. The first method is Relative Gain Array (RGA), in which RGA of the voltage sensitivity matrix is utilized as a quantitative measure to address controllability and the level of voltage control interaction among PV systems. The second method is Condition Number (CN), in which Singular Value Decomposition (SVD) of the voltage sensitivity matrix is used as a mathematical measure to indicate the voltage control directionality among PV systems. Two radial test distribution grids with different feeder R/X ratio, overhead line and underground cable, which consist of five PV systems, are used to calculate load flow and, in turn, voltage sensitivity matrix. The results demonstrate that decentralized voltage control to specific set-points is basically impossible in the both systems. It is also shown that voltage control directionality of the both systems is increased by reactive power regulation compared to active power curtailment.

Keyword: Photovoltaic, Voltage sensitivity matrix, RGA, SVD.

I. INTRODUCTION

Growing trends in PhotoVoltaic (PV) system installations due to encouraging feed-in-tariffs and long-term incentives have led to high penetration of PV systems in distribution grids. In Germany, for instance, there are currently 20 GW installed PV systems, of which 80% have been connected in low voltage grids [1]. Due to recent drop in costs of PV systems, especially PV panel technologies, grid-parity is not anymore unimaginable and will in near future come close to reality [2]–[4]. High penetration of PV systems without incentives is more likely to be interesting in different countries and markets rather than limited countries. For example, Italy and Spain are following Germany. This high penetration of PV systems has also raised new challenges in the distribution grid such as voltage rise. Violation of voltage profile in some regions in Germany has led to stopping PV installation by utilities. To contrive a way to solve the unwanted problems associated with high participation of PV systems, reactive power contribution of

PV systems has been proposed in recently under-codified standards, e.g. German Grid Codes [5]. Several approaches have been proposed for reactive power support [6]–[9]. One of these approaches is voltage control at the connection point of PV to grid. In the previous research [10], it was shown that this method is sensitive to adjusting set-points to the extent that improper set-points may lead to interaction among PV systems in the same vicinity. In [11], determinant of voltage sensitivity matrix from load flow calculation has been employed to study the impact of the R/X ratio on the effectiveness of using active and reactive power for regulating voltage profile. In [9], sensitivity matrix has also been used to show the difference between a system with overhead line and underground cable. However, the level of interaction and directionality among the PV systems regarding voltage control to specific set-points has not been addressed in the previous literature.

The aim of this paper is to address the possibility of controllability among PV systems for voltage profile regulation to specific set-points via two analytical control methods. For this investigation, the voltage sensitivity matrix, which can be derived via the load flow calculation, is used as the steady-state gain of the understudy system. The first method is Relative Gain Array (RGA) [12], [13] that is employed to analyze and evaluate the controllability and level of voltage control interaction among the PV systems. The second method is Condition Number (CN), in which mathematical measure of directionality is provided by Singular Value Decomposition (SVD). This method is a useful way to quantify how the range of possible gains of a multi-variable process varies for an input direction [13], [14]. Wide (or narrow) range of possible gains for a process implies large (or small) directionality.

Sub-matrices of the voltage sensitivity matrix indicate the sensitivity of the bus voltages and angles to the variation of active and reactive power at buses. The RGA and CN of the voltage sensitivity sub-matrices, in turn, indicate the degree of the interaction and directionality, respectively. The relation of feeder R/X ratio and the distance between buses in a distribution grid for voltage control is of concern. Applying the aforementioned methods provides an analytical view that how the voltage control interaction and directionality among PV systems in a distribution grid would be affected by the distance and R/X variation.

Two radial test distribution grids with different feeder R/X ratio, overhead line and underground cable, are employed as

the test platform. MATLAB environment is used to calculate the voltage sensitivity matrix and investigate it further via RGA and CN. Derived results, in conclusion, demonstrate decentralized voltage control to specific set-points through the PV systems in the distribution grid is fundamentally impossible due to the high level voltage control interaction and directionality among the PV systems.

In the following, a general overview of the voltage sensitivity will be given in section 2, basic of RGA and condition number are presented in section 3 and section 4 respectively, section 5 presents the simulation platform and section 6 deals with the results and finally the conclusion comes at section 7.

II. VOLTAGE SENSITIVITY MATRIX

Voltage Sensitivity matrix is a measure to quantify the sensitivity of bus voltages ($|V|$) and bus angles (θ) with respect to injected active and reactive power for each bus except slack bus. Sensitivity matrix is obtained through partial derivative of load flow equations, $g(|V|, \theta)$, as follows [15]:

$$\begin{aligned} \begin{bmatrix} \Delta\theta \\ \Delta|V| \end{bmatrix} &= \begin{bmatrix} \frac{\partial g_P(\theta, |V|)}{\partial \theta} & \frac{\partial g_P(\theta, |V|)}{\partial |V|} \\ \frac{\partial g_Q(\theta, |V|)}{\partial \theta} & \frac{\partial g_Q(\theta, |V|)}{\partial |V|} \end{bmatrix}^{-1} \begin{bmatrix} \Delta P \\ \Delta Q \end{bmatrix} = \\ &= \begin{bmatrix} S_{\theta, P}^V & S_{\theta, Q}^V \\ S_{|V|, P}^V & S_{|V|, Q}^V \end{bmatrix} \begin{bmatrix} \Delta P \\ \Delta Q \end{bmatrix} \end{aligned} \quad (1)$$

Voltage sensitivity matrix consists of four sub-matrices that denote the partial derivatives of bus voltage magnitude and angle with respect to active and reactive power. Due to importance of the voltage magnitude regulation by variation of active and reactive power, sub matrices that are related to variation of voltage magnitude, $S_{|V|, P}^V$ and $S_{|V|, Q}^V$, are of more interest and concern in this study. Each element of these sub matrices, e.g. S_{ij}^V , is interpreted as the variation that would happen in a voltage at bus i if the active power (or reactive power) at bus j changed 1 p.u. Voltage sensitivity matrix represents the open loop gain of the system which is later used as the steady state transfer function of the system to conduct some investigation.

Equation (1) represents a linearized form of the system equations. Keeping this in perspective, it follows from (1) that voltage magnitude variation corresponds to active and reactive power variation and consequently in order to keep the voltage magnitude theoretically constant, following is deduced which can be also employed as a measure to determine the degree of active-reactive power dependency.

$$\Delta Q = -S_{|V|, Q}^V{}^{-1} S_{|V|, P}^V \Delta P = J \Delta P. \quad (2)$$

Equation (2) is used later to compare the relation between the reactive power and active power while the voltage profile is perfectly controlled.

III. RGA METHOD

Although the RGA was basically introduced by Britsol [12] for pairing the input and output variables in a decentralized control system, it has also been exploited as a general measure of controllability [13], [14]. The relative gain array has been addressed in many literatures and is frequently

employed as a quantitative measure of controllability and control loop interaction in decentralized control design. The RGA is originally formulated for steady state analysis and later it was extended to include the dynamics [13]. In this study, the RGA concept is used to analyze the voltage sensitivity matrix, which is calculated from system algebraic equations and therefore does not comprise dynamic.

The proposed interaction measure through RGA indicates how the apparent transfer function between manipulated or input variable (u_i) and controlled or output variable (y_j) is affected by control of other controlled variables. This measure is shown by λ_{ij} and is described by the ratio of the transfer function between a given manipulated variable and controlled variable while all other loops are open, and the transfer function between the same variables while all other outputs are closed as follows:

$$\lambda_{ij} = \frac{\left(\frac{\partial y_i}{\partial u_j} \right) | u_{k \neq j} \text{ constant}}{\left(\frac{\partial y_i}{\partial u_j} \right) | y_{k \neq j} \text{ constant}} \quad (3)$$

In other words, the RGA is the ratio of the open loop gain between two variables to the closed loop gain of the same variables while other outputs are perfectly controlled. For a MIMO system with $G(0)$ as the steady state transfer function, the RGA is attained as follows:

$$\Lambda(G(0)) = G(0) \times (G(0)^{-1})^T \quad (4)$$

Where \times denotes element-by-element multiplication.

Equation (3) demonstrates that the open loop gain between y_j and u_i changes by the factor λ_{ij}^{-1} while the rest of loops are closed by integral feedback control. This implies that the pairing should be preferred for RGAs that are as close to unity as possible. $\lambda_{ij}=1$ implies that there is no interaction with other control loops. Intuitively, decentralized control requires an RGA matrix close to identity [13]. In a decentralized control, the MIMO process works as several independent SISO sub-plants. If RGA elements are greater than one, the decoupling or inverse-based controller can be used to decouple interactions. However, systems with large RGA elements are basically hard to control owing to big interactions and input uncertainties; by doing so, inverse based controller should be prevented since it is not robust. Pairing with negative RGA elements must be avoided because those lead to integral instability.

Sub-matrices of the voltage sensitivity matrix in (1) are steady-state gain of the system and by doing so the RGA of $S_{|V|, P}^V$ and $S_{|V|, Q}^V$ are given as follows:

$$\Lambda(S_{|V|, Q}^V) = S_{|V|, P}^V \times \left((S_{|V|, P}^V)^{-1} \right)^T \quad (5)$$

$$\Lambda(S_{|V|, Q}^V) = S_{|V|, Q}^V \times \left((S_{|V|, Q}^V)^{-1} \right)^T \quad (6)$$

The RGA of $S_{|V|, P}^V$ in (5) can be used to study the possibility of controllability and interaction among voltage controllers of PV systems via power curtailing in order to regulate the voltage of buses to specific set-points. The RGA of $S_{|V|, Q}^V$ in (6) is used to investigate the possibility of controllability and interaction among voltage controllers of PV systems to

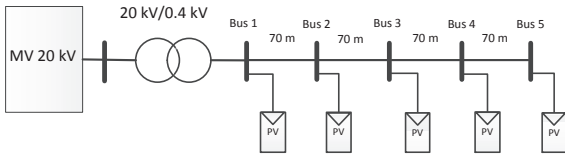


Figure 1. Test distribution grid.

regulate voltage of buses to specific set-points via regulating reactive power.

To sum up, in RGA method, the voltage sensitivity matrix must first be derived. Then, RGA of sub-matrices $S_{|V|,P}^V$ and $S_{|V|,Q}^V$ are calculated. In the next step RGA values are evaluated. RGA values close to one demonstrate a decentralized system. If the RGA values are big but less than 5, the decoupling compensators can be used to make the system decentralized. However, large RGA values, more than 5, correspond to controllability problems because of big interactions and input uncertainties [13].

IV. CN METHOD

Another measure to quantify the level of interaction in multi-variable systems is condition number. CN of a system is defined as the ratio between maximum and minimum singular values of the system, which are computed using SVD [13], [14]:

$$\gamma(G(0)) = \frac{\bar{\sigma}(G(0))}{\underline{\sigma}(G(0))} \quad (7)$$

A process with large CN implies high directionality and is called to be ill-conditioned [13]. The steady state gain of MIMO process varies between $\underline{\sigma}(G(0))$ and $\bar{\sigma}(G(0))$. Wide range of possible gains for a MIMO system indicates large directionality. Such a plant is often considered sensitive to uncertainty that, in turn, will lead to a poor robust performance [13]. Moreover, a large CN results in control problem. A large CN may be brought about by a small singular value that is generally undesirable.

In a nutshell, in CN method, the voltage sensitivity matrix must first be derived. Then, SVD of sub-matrices $S_{|V|,P}^V$ and $S_{|V|,Q}^V$ are computed and consequently CN is calculated. CN larger than 50 demonstrates controllability problems [13].

V. PLATFORM OF THE SIMULATION

Radial grid in Fig. 1, which consists of five houses connected through a step down transformer to a medium voltage grid, is employed as a test grid in this paper. In this study, it is assumed that all the houses have been equipped with PV systems. In this grid both overhead lines and underground cables are taken into consideration in order to study the effect of the R/X ratio. The parameters of the test radial grid have been given in Table I [9].

In the load flow calculation, the slack bus is naturally excluded from sensitivity matrix. Moreover, in the sensitivity matrix, rows and columns corresponding to buses that have no PV systems are also neglected.

Table I
RADIAL TEST GRID PARAMETERS.

| | |
|------------------------------------|-----------------------|
| Grid impedance | 1.4e-4 + 1.4e-4i p.u. |
| Transformer impedance | 0.0043 + 0.0067i p.u. |
| Over head line impedance per km | 0.0516 + 0.0375i p.u. |
| Underground cable impedance per km | 0.0400 + 0.0102i p.u. |
| Rated total net load | 20 kW |
| Base Voltage | 400 V |
| Base Power | 20 kW |

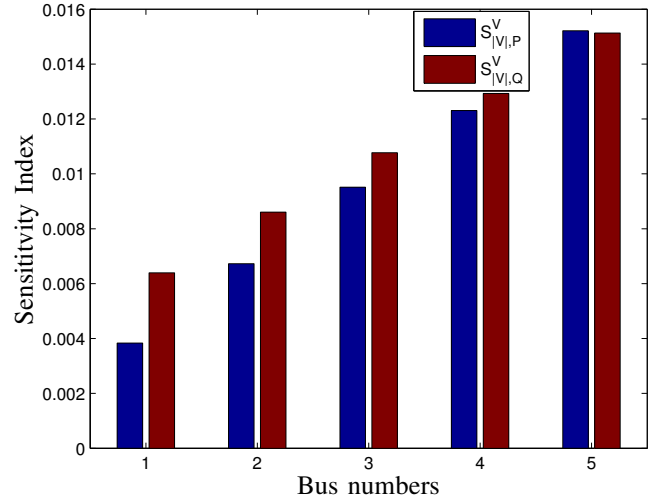


Figure 2. The sensitivity spectrum of the diagonal elements of $S_{|V|,P}^V$ and $S_{|V|,Q}^V$ for overhead lines.

VI. RESULTS

A. Sensitivity matrix characteristic

Figs. 2 and 3 show the spectrum of the diagonal elements of $S_{|V|,P}^V$ and $S_{|V|,Q}^V$ for overhead lines and cables, respectively. As it was expected the sensitivity to reactive power in overhead line is noticeably bigger than underground cable. Nevertheless, in case of underground cable, it can be seen that at the beginning of the feeder, sensitivity to reactive power is higher compared to active power, but as approaching to the end of feeder it gets the other way around. Therefore, even though resistive part of the underground cable is dominant, controlling voltage profile by regulating reactive power at the beginning of the feeder, seems to be more effective.

B. Voltage regulation active-reactive power dependency

Irrespective of the operating point and R/X ratio, (2) yields an upper triangular matrix. Nevertheless, the diagonal elements and first row of the matrix, which are dominant elements, vary significantly between the overhead line and underground cable. Figs. 4 and 5 depict the spectrum of those elements.

The characteristics of the matrix is summarized as follows:

- The first entry in the diagonal and the first row are common and corresponds to the first bus, which can only see the impedance of the grid, and by doing so it gets same value in both systems with overhead line and underground cable.

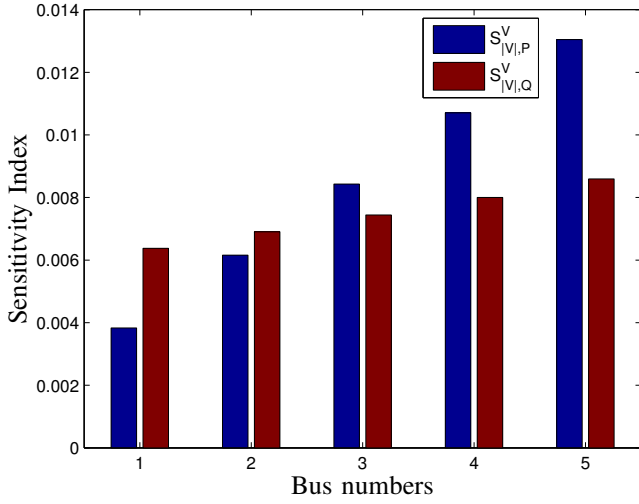


Figure 3. The sensitivity spectrum of the diagonal elements of $S_{|V|,P}^V$ and $S_{|V|,Q}^V$ for underground cable.

- Diagonal entries, except the first entry, are almost similar; first row entries, except the first entry, are also almost similar.
- The diagonal entries are almost equal to the feeder R/X ratio in both systems, overhead line and underground cable.
- The absolute difference between corresponding diagonal and first row entries, except the common entry, is almost equal to the absolute value of the common entry.
- Large elements in case of underground cables, which is in conjunction with large R/X ratio, implies that for an identical change in active power of buses, required reactive power to keep voltage profile constant varies largely. In other words, the required reactive power to keep voltage differences equal to zero ($\Delta V = 0$), is proportional to the feeder R/X ratio. By doing so, for feeders with R/X ratio more than one the required reactive power change (ΔQ) at each bus would be greater than the active power difference (ΔP) in the same bus.
- Depending upon the R/X ratio value, the sign of the first row entries except the first entry changes. In order to study the effect of the $k=R/X$ ratio, the total amount of the overhead line impedance is taken into account, and its R/X ratio is varied. It is observed that for k smaller than 0.58 the sign of the first row entries is negative. Therefore, for small R/X ratio, if the active power difference (ΔP) in all buses are in one direction, the reactive power difference (ΔQ) at all buses will be in one direction as well. However, for large k values the sign of the first row entries are positive and opposite of the diagonal entries which means the reactive power variation at bus one is always in contrary with other buses.

Eq. (2) is used to calculate the required reactive power adjustment to compensate the voltage profile fluctuation owing to the variation of active power. Considering the initial

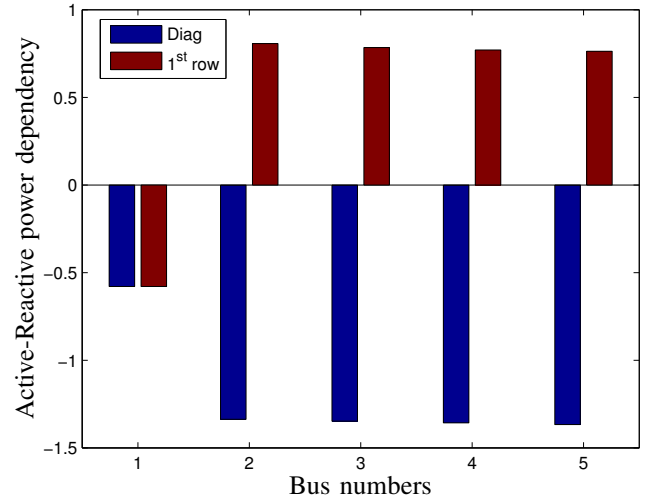


Figure 4. Spectrum of diagonal and first row elements of active-reactive power dependency for overhead line.

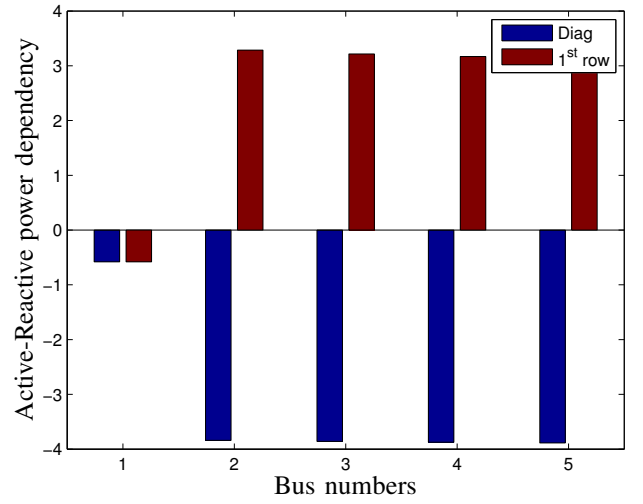


Figure 5. Spectrum of diagonal elements and first row of active-reactive power dependency for underground cable.

operating point at $P_0 = 0$ and $Q_0 = 0$ gives

$$\begin{aligned}\Delta P &= P - P_0 = P \\ \Delta Q &= Q - Q_0 = Q \\ P &= JQ\end{aligned}\quad (8)$$

Consequently, the needed power factors for the PV connected buses are calculated as follows:

$$PF = \frac{P}{\sqrt{P^2 + ((\sum J')P)^2}}\quad (9)$$

Where PF is a vector consisting of power factors at each PV installed bus. Fig. 6 depicts the power factor of each bus for different R/X ratio while it is assumed that the total net power at each bus has been changed 1 p.u. ($P=1$ p.u.), as can be seen the required power factor varies drastically by increasing R/X ratio. It boils down to this fact that required reactive power to compensate voltage fluctuation depends upon R/X ratio.

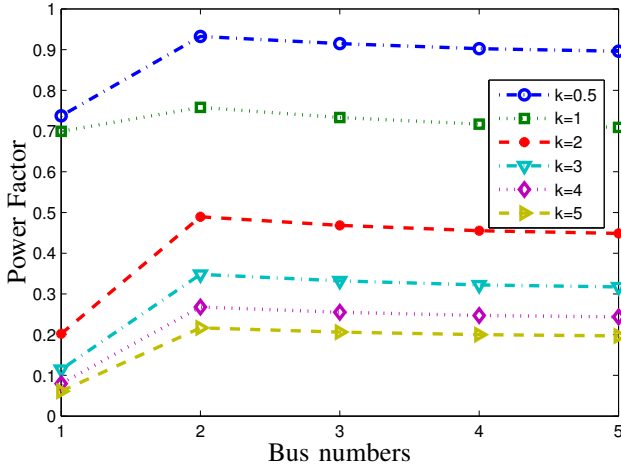


Figure 6. Required power factor for each PV system for different $k=R/X$ ratio and $\Delta P = 1 p.u.$

C. RGA

Subsequent to the previous section upshot, if adequate reactive power can be provided by PV systems, this question is raised whether it is possible to regulate the voltage of each bus with installed PV system to a fixed set-point through reactive power regulation or not. In this section and following, the interaction among PV systems in a radial distribution grid is quantified by RGA concept to address the possibility of controllability concerning voltage profile regulation to specific set-points.

The RGA of the $S_{|V|,P}^V$ and $S_{|V|,Q}^V$ look like a block tridiagonal matrix which positive elements are only located on the diagonal and elements on the upper diagonal and on the lower diagonal are negative. According to the RGA pairing rule, therefore, the elements on the diagonal must be paired. This block tridiagonal shape of the RGA of voltage sensitivity sub-matrices indicate that open loop gain of the system, which is the sensitivity matrix, is changed with positive sign on the diagonal and with negative sign on the upper diagonal and lower diagonal. Moreover, since the other elements of the RGA are almost zero, open loop gain of the system on these positions are changed with infinite factor which means these loops are considerably affected by other loops. Figs. 7 and 8 depict the diagonal entries spectrum of RGA of $S_{|V|,P}^V$ and $S_{|V|,Q}^V$ for overhead lines and cables while all buses are on full production, respectively. It can be seen by moving towards end of the feeder, except the last bus, the level of interaction is increasing. Since the last bus at the end of feeder is affected only by one previous neighbor bus, the level of interaction drops at this bus.

Concerning overhead line, Figs. 9 and 10 demonstrate maximum RGA of $S_{|V|,P}^V$ and $S_{|V|,Q}^V$ for different net load levels and different line distances between buses. One sees that the interaction level decreases by increasing the distance between the buses, or in turn by increasing the impedance. Moreover, it can be seen that the maximum RGA of $S_{|V|,P}^V$ declines by shifting total net load from consumption to production. Similar results, not shown here, are derived for under ground cable.

Figs. 11 and 12 show the impact of the lagging and leading

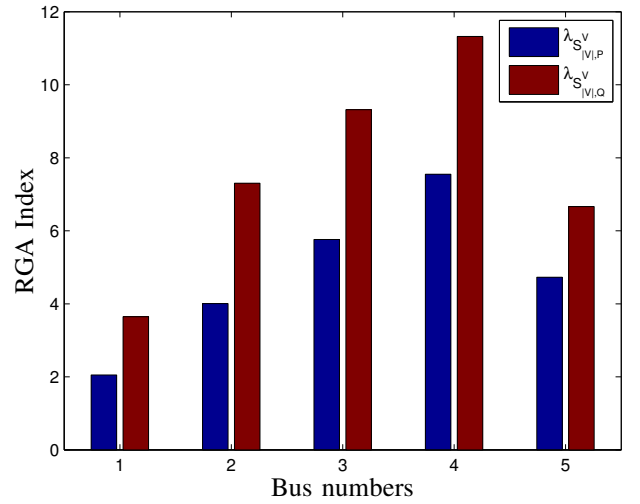


Figure 7. The RGA spectrum of the diagonal elements of $S_{|V|,P}^V$ and $S_{|V|,Q}^V$ for overhead line.

power factor on the maximum RGA of $S_{|V|,P}^V$ and $S_{|V|,Q}^V$ for different loading conditions, while it is assumed that overhead line segments are 70 m. As can be seen the power factor has relatively very small effect on the maximum RGA of $S_{|V|,P}^V$ while the maximum RGA of $S_{|V|,Q}^V$ slightly increases by lagging power factor and decreases by leading power factor. The performance of the system with underground cable, not shown here, is analogues with overhead line.

The results of the maximum RGA for different $k=R/X$ ratio are shown in Figs. 13 and 14. It is assumed that the distance between buses are 70 m and power factor is unity. It is obvious that maximum RGA of $S_{|V|,Q}^V$ increases for larger k values. It is, therefore, deduced that increasing R/X ratio would boost the interaction level among voltage controllers of PV systems regarding reactive power regulation. However, it can be seen in Fig. 13 that the maximum RGA of $S_{|V|,P}^V$ declines by large k values.

Based on the depicted results, the positive elements of the RGA of $S_{|V|,Q}^V$ are always much bigger than one irrespective of the R/X ratio, total net load and power factor. It can be, therefore, concluded that it is not possible to have decentralized voltage control in order to regulate voltage to a specific set-point at each bus even for small R/X ratio that technically adequate reactive power can be produced by PV systems [13]. Since the RGA of $S_{|V|,P}^V$ are much bigger than one, decentralized control based on the power curtailing is not also possible.

Furthermore, the results demonstrate that maximum positive elements of RGA of the voltage sensitivity matrix are large, more than 5, by doing so using decoupling controllers, in order to make a decentralized system, can fundamentally lead to control problems due to sensitivity to inputs [13]. Thus, inverse-based controllers must be avoided.

D. Condition number

At production net load level with unity power factor, CN of $S_{|V|,P}^V$ and $S_{|V|,Q}^V$ for overhead line are $\gamma_P^{OHL}=44.2$ and $\gamma_Q^{OHL}=72.1$, and for underground cable are $\gamma_P^{UGC}=50.8$ and $\gamma_Q^{UGC}=197.2$. These CNs denote that sensitivity matrix is

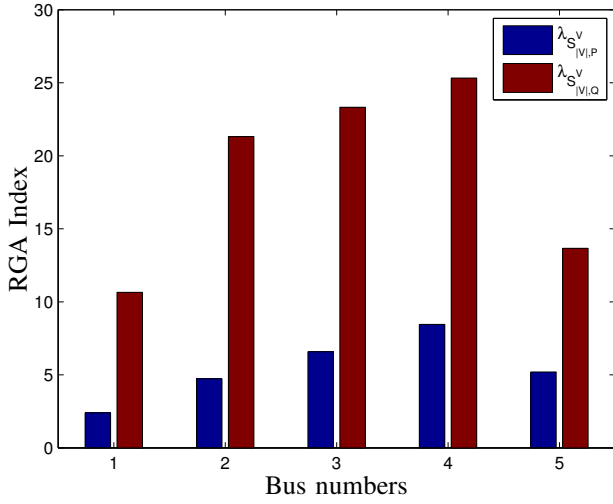


Figure 8. The RGA spectrum of the diagonal elements of $S^V_{|V|,P}$ and $S^V_{|V|,Q}$ underground cable line.

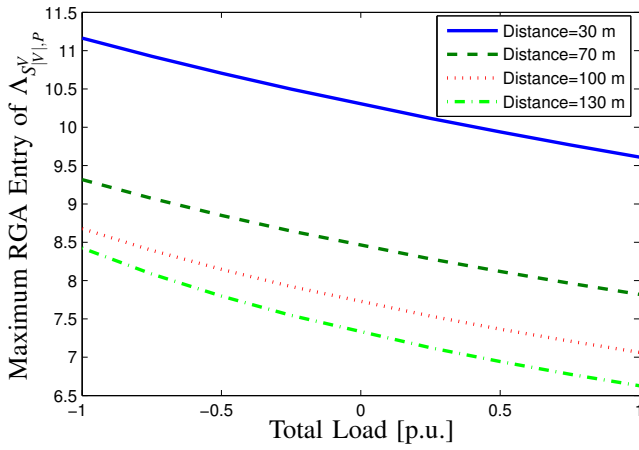


Figure 9. Maximum RGA entry of $S^V_{|V|,P}$ for different net load levels and different distances between buses, overhead line.

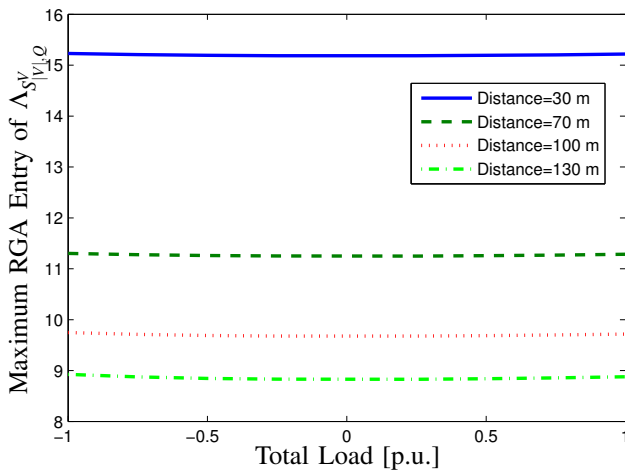


Figure 10. Maximum RGA entry of $S^V_{|V|,Q}$ for different net load levels and different distances between buses, overhead line.

ill-conditioned and the severe case is for $S^V_{|V|,Q}$. Figs. 15

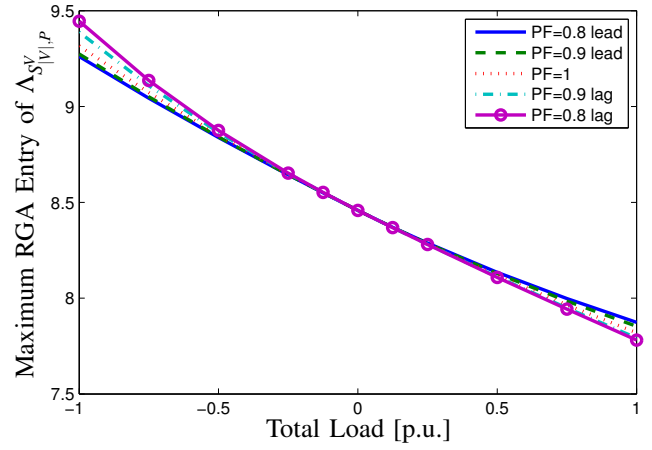


Figure 11. Maximum RGA entry of $S^V_{|V|,P}$ for different net load levels and different power factors, overhead line.

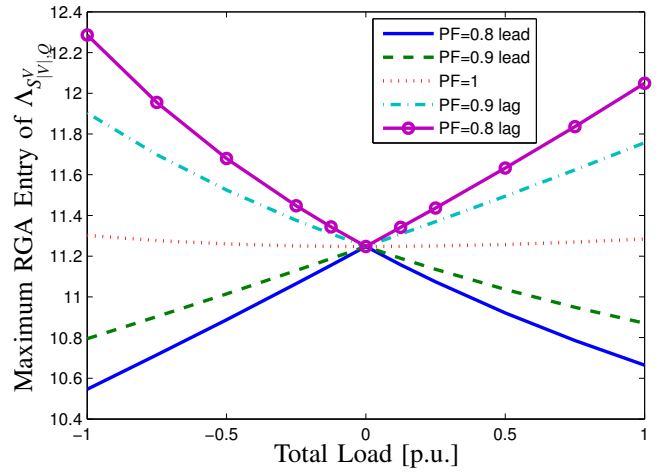


Figure 12. Maximum RGA entry of $S^V_{|V|,Q}$ for different net load levels and different power factors, overhead line.

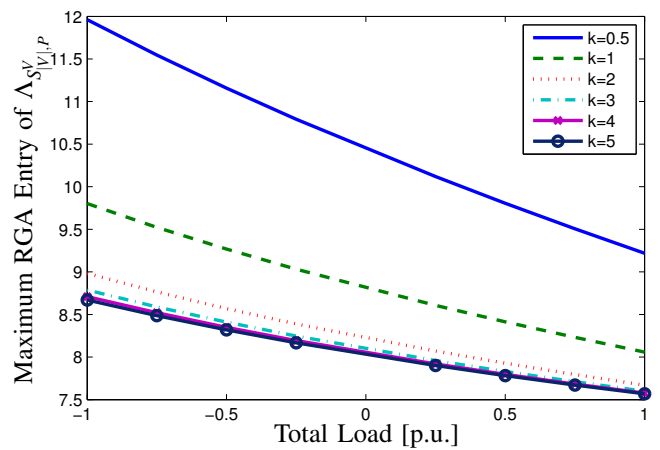


Figure 13. Maximum RGA entry of $S^V_{|V|,P}$ for different net load levels and different $k=R/X$ ratios.

and 16 illustrate the spectrum of the singular values of $S^V_{|V|,P}$ and $S^V_{|V|,Q}$, respectively. As can be seen the sensitivity matrix in both systems suffers from high directionality.

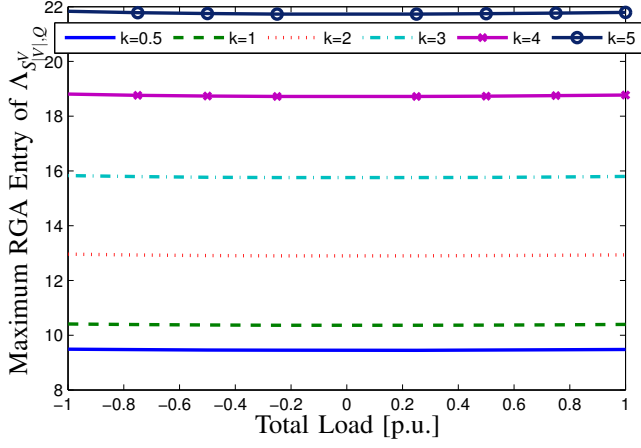


Figure 14. Maximum RGA entry of $S_{|V|,Q}^V$ for different net load levels and different $k=R/X$ ratios.

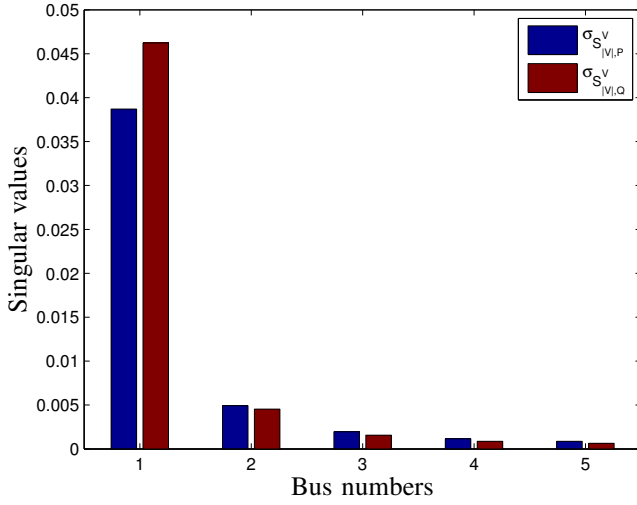


Figure 15. The singular values of $S_{|V|,P}^V$ and $S_{|V|,Q}^V$ for overhead line.

Furthermore, smallest singular value for $S_{|V|,Q}^V$ in the system with the underground cable is smaller than the system with overhead line that implies more directionality and more control problems. These results are in conjunction with RGA results.

Figs. 17 and 18 demonstrate the condition numbers of $S_{|V|,P}^V$ and $S_{|V|,Q}^V$ for different R/X ratio and different total net load levels. Regarding $S_{|V|,Q}^V$ the more increasing k the further CN goes that is along with the RGA results. Analogous with the RGA results, large R/X ratio results in relatively smaller CN for $S_{|V|,P}^V$. Changing power factor and the distance between buses yield similar results, not shown here, for CN as the RGA results in the previous section.

VII. CONCLUSION

This paper applies two analytical control methods, namely Relative Gain Array and Condition Number, to voltage sensitivity matrix in order to find the possibility of the controllability. RGA and CN are used to quantify the level of interaction and directionality among PV systems in distribution grids regarding voltage control, respectively. The

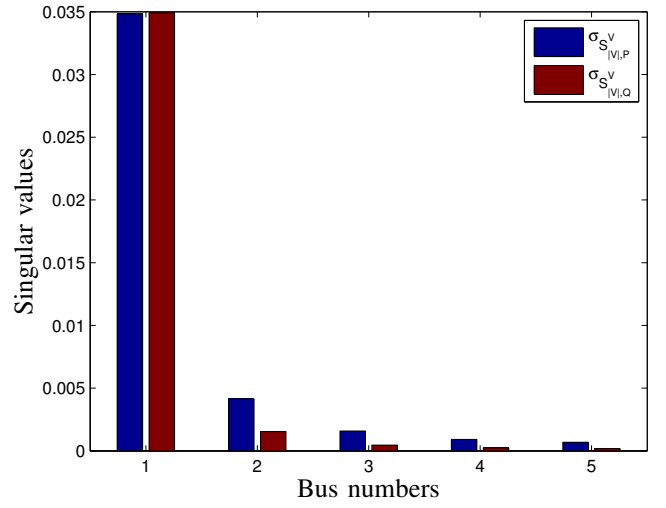


Figure 16. The singular values of $S_{|V|,P}^V$ and $S_{|V|,Q}^V$ underground cable.

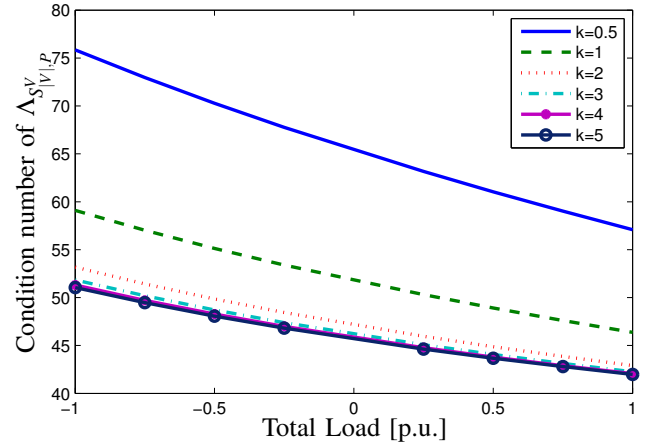


Figure 17. Condition number of $S_{|V|,P}^V$ for different net load levels and different $k=R/X$ ratios.

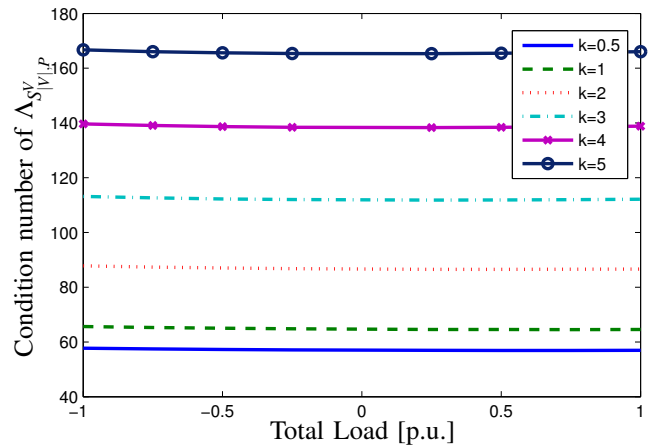


Figure 18. Condition number of $S_{|V|,Q}^V$ for different net load levels and different $k=R/X$ ratios.

sensitivity matrix is used as the steady-state gain of the system in this study. Moreover, the characteristic of the sensitivity matrix is employed to show the level of dependency

of reactive power to active power for voltage control. The results show that decentralized voltage control to specific set-points through reactive power regulation or active power curtailment is not possible due to large RGA elements and large CN of voltage sensitivity matrix. It is, furthermore, shown that using decoupling controllers to make system decentralized must also be avoided on the grounds that the RGA elements of the voltage sensitivity matrix are too big, larger than 5, that would result in poor control performance.

ACKNOWLEDGMENT

This project has been funded by SETS Erasmus Mundus Joint Doctorate and Smooth PV. The authors would like to express their gratitude towards all partner institutions within the programme as well as the European Commission for their support.

REFERENCES

- [1] J. C. Boeme and et al, "Overview of german grid issues and retrofit of photovoltaic power plants in germany for the prevention of frequency stability problems in abnormal system conditions of the ENTSO-E region continental europe," in *1st International Workshop on Integration of Solar Power into Power Systems*, (Aarhus, Denmark), pp. 3–8, Oct. 2011.
- [2] D. Verma, O. Midtgard, and T. Satre, "Review of photovoltaic status in a european (EU) perspective," in *2011 37th IEEE Photovoltaic Specialists Conference (PVSC)*, pp. 003292 –003297, June 2011.
- [3] U. Schwabe and P. Jansson, "Utility-interconnected photovoltaic systems reaching grid parity in new jersey," in *2010 IEEE Power and Energy Society General Meeting*, pp. 1 –5, July 2010.
- [4] J. H. Wohlgemuth, D. W. Cunningham, R. F. Clark, J. P. Posbic, J. M. Zahler, P. Garvison, D. E. Carlson, and M. Gleaton, "Reaching grid parity using BP solar crystalline silicon technology," in *33rd IEEE Photovoltaic Specialists Conference, 2008. PVSC '08*, pp. 1 –4, May 2008.
- [5] "Verband der elektrotechnik elektronik Informationstechnike.V. (VDN) (2010). erzeugungsanlagen am niederspannungsnetz technische mindestanforderungen für anschluss und parallelbetrieb von erzeugungsanlagen am niederspannungsnetz. draft of 07-08-2010. berlin."
- [6] M. Braun, "Reactive power supply by distributed generators," in *2008 IEEE Power and Energy Society General Meeting - Conversion and Delivery of Electrical Energy in the 21st Century*, pp. 1 –8, July 2008.
- [7] P. Sulc, K. Turitsyn, S. Backhaus, and M. Chertkov, "Options for control of reactive power by distributed photovoltaic generators," *arXiv:1008.0878*, Aug. 2010. Proceedings of the IEEE , vol.99, no.6, pp.1063-1073, June 2011.
- [8] R. Tonkoski, L. Lopes, and T. EL-Fouly, "Droop-based active power curtailment for overvoltage prevention in grid connected PV inverters," in *2010 IEEE International Symposium on Industrial Electronics (ISIE)*, pp. 2388 –2393, July 2010.
- [9] E. Demirok, D. Sera, R. Teodorescu, P. Rodriguez, and U. Borup, "Evaluation of the voltage support strategies for the low voltage grid connected PV generators," in *2010 IEEE Energy Conversion Congress and Exposition (ECCE)*, pp. 710 –717, Sept. 2010.
- [10] A. Samadi, M. Ghandhari, and L. Söder, "Reactive power dynamic assessment of a PV system in a distribution grid," *Energy Procedia*, vol. 20, pp. 98–107, 2012.
- [11] R. Tonkoski and L. Lopes, "Voltage regulation in radial distribution feeders with high penetration of photovoltaic," in *IEEE Energy 2030 Conference, 2008. ENERGY 2008*, pp. 1 –7, Nov. 2008.
- [12] E. Bristol, "On a new measure of interaction for multivariable process control," *IEEE Transactions on Automatic Control*, vol. 11, pp. 133 –134, Jan. 1966.
- [13] S. Skogestad and I. Postlethwaite, *Multivariable Feedback Control: Analysis and Design*. Wiley-Interscience, 2 ed., Nov. 2005.
- [14] S. Skogestad and K. Havre, "The use of RGA and condition number as robustness measures," *Computers & Chemical Engineering*, vol. 20, Supplement 2, no. 0, pp. S1005–S1010, 1996.
- [15] H. Saadat, *Power System Analysis Third Edition*. PSA Publishing, THIRD EDITION ed., June 2010.

Modeling the Frequency Response of Photovoltaic Inverters

E. C. Aprilia, V. Čuk, *Student Member, IEEE*, J. F. G. Cobben, P. F. Ribeiro, *Fellow, IEEE*, and W.L. Kling, *Member, IEEE*

Abstract—The increased presence of photovoltaic (PV) systems inevitably affects the power quality in the grid. This new reality demands grid power quality studies involving PV inverters. This paper proposes several frequency response models in the form of equivalent circuits. Models are based on laboratory measurements performed on five types of commercially available PV inverters, and fitted to obtain circuit parameters. The proposed models show a good agreement with the measured data.

Index Terms— distributed power generation, frequency response, grid-connected inverters, harmonic analysis.

I. INTRODUCTION

WITH the growing interest in energy generation from renewable sources, the number of installed photovoltaic (PV) systems will continue to grow. These systems can be either stand-alone or grid-connected. In both cases, the DC output generated by PV cells is converted to AC power using inverters. Conversion using power electronics results in non-sinusoidal current waveforms.

To smooth the output waveform, grid-interfaced inverters are equipped with filters to attenuate the lower and higher frequency components of the harmonics. The filter, however, might interact with grid impedance and add an additional resonance in the system. This situation can increase the local voltage distortion. This is especially true with ever-increasing interest and development in smart grid which is meant to accommodate more renewable energy sources in distribution networks. It leads to more PV modules and inverters in the networks, and this brings the need to analyze different aspects of PV interaction, including harmonic studies. A common

approach to study the behavior of PV inverters in the network is by simulating and analyzing the network using models of PV inverters and other network elements. The model used to represent PV inverters depends on the purpose of the study.

Examples of distribution network simulations with a large number of residential PV systems can be found in [1] and [2]. An adequate model of PV inverters found in harmonic studies is the Norton equivalent model (consisting of a harmonic current source with a parallel impedance), sometimes in series with an additional impedance [1]–[7], as depicted in Fig. 1. The series and parallel impedances usually simulate the output filter of the inverter, either represented by a resultant impedance ([1],[2],[4],[7]), or as physical components ([3],[5],[6]). The values of these impedances are also obtained from different approaches. Some are taken from typical values of commercial inverters ([1],[3]) while others are calculated from the nominal power of the inverters ([4],[5]). In [2], the current source is paralleled with a single capacitance.

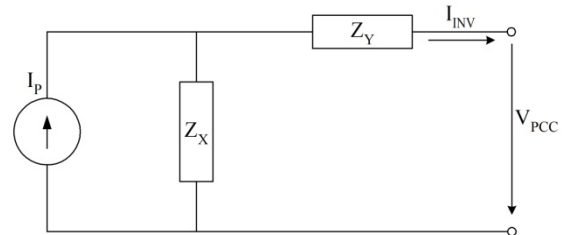


Fig. 1. An impedance and current source circuit as PV inverter model.

A different approach has been taken to calculate the parameter values of the impedance model in [8]. This approach measures the harmonic voltage across and the harmonic current at the terminal output of the inverter (see Fig. 1) for several particular frequencies. The parameter values for each frequency ($I_p(h)$, $Z_x(h)$, and $Z_y(h)$) are then calculated iteratively using the Newton-Raphson algorithm:

$$[I_p(h)Z_x(h)] - [I_{INV}(h)Z_x(h)] - [I_{INV}(h)Z_y(h)] = V_{PCC}(h) \quad (1)$$

where I_p is the harmonic current emitted by the inverter, I_{INV} is the harmonic current at the output of the inverter, V_{PCC} is the voltage at the connection point between the inverter and the grid, Z_x and Z_y are the series and parallel impedance, respectively.

This approach is using a look-up table (there will be a different model for every frequency) which is not favorable

E. C. Aprilia is a Master student in the Electrical Energy System (EES) group of the Eindhoven University of Technology, The Netherlands (e-mail: e.c.aprilia@student.tue.nl).

V. Čuk is a PhD candidate in the Electrical Energy System (EES) group of the Eindhoven University of Technology, The Netherlands (e-mail: v.cuk@tue.nl).

J. F. G. Cobben is currently working at Alliander and as a part-time assistant professor at the EES group of the Eindhoven University of Technology, The Netherlands, (e-mail: j.f.g.cobben@tue.nl).

P. F. Ribeiro is an associate professor at the EES group of the Eindhoven University of Technology, The Netherlands, (e-mail: p.f.ribeiro@tue.nl).

W.L.Kling is a full-time professor and the head of the Electrical Energy Systems group at the Eindhoven University of Technology, the Netherlands, (e-mail: w.l.kling@tue.nl).

because a large number of iterations are required to solve 3 unknown variables from only one equation. Moreover, since there are different models for different frequencies and the impedance value does not represent a particular element (capacitance/inductance), it is not possible to estimate the resonant frequency from this approach.

This paper presents an alternative impedance circuit as a PV inverter model, in order to investigate the relationship between the inverter and the network in the frequency domain. An experiment is set-up to measure the frequency response of inverters and an analytical approach is used to create the impedance model.

II. MEASUREMENT SETUP

The PV inverter impedance is estimated from harmonic voltages generated by a voltage source and the current responses of the inverter, as shown in Fig. 2. The impedance is calculated as:

$$\overline{Z}_h = \frac{\overline{V}_h - \overline{V}_{h0}}{\overline{I}_h - \overline{I}_{h0}}, 2 \leq h \leq 50 \quad (2)$$

where Z_h is the impedance, V_h is harmonic voltage source, I_h is the harmonic current at the output of the inverter, V_{h0} and I_{h0} are measured harmonic voltage and current when the fundamental voltage is applied without distortion.

The analog harmonic current and voltage are measured and sampled by a PC-based scope and analytically transformed into frequency domain with DFT using Matlab.

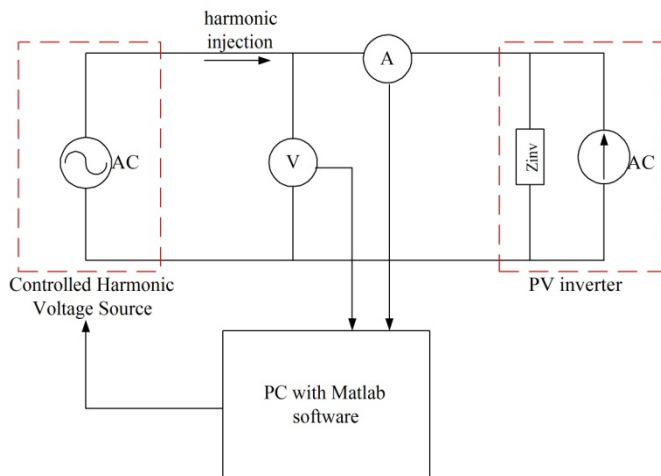


Fig. 2. Measurement schematic.

The harmonic source is varied in amplitude and phase angle so that for every frequency several values of impedance are obtained. It is expected that these values are convergent and therefore can be averaged. The average impedance of every frequency is then plotted against the frequency to get impedance-frequency profile, from which the impedance model will be build. To obtain better profile, measurement is also done for interharmonic frequencies (from 75 until 2475 Hz, with a step of 50 Hz). The amplitudes of the voltage stimuli are chosen not to exceed the standards for harmonic

voltage level in LV network (EN50610 and IEC61000-3-6).

III. MEASUREMENT RESULTS

The experiment is done on 5 commercial PV inverters: three single-phase inverters, one power router, and one three-phase inverter. Single-phase inverters (Inverter1, Inverter2, and Inverter3) have nominal output powers of 1200 W, 1500 W, and 1500 W, respectively. The single-phase power router has a nominal power of 5000 W, and the three-phase inverter 2600 W. Although the latter needs a 3-phase connection, it only feeds-in to the grid via 1 phase (hence it can be treated as a single-phase inverter).

A. Single-phase (SP) Inverters

All three SP inverters have impedance profile similar to that of a capacitor (i.e. the impedance is inversely proportional to the frequency). Thus, a single capacitor is adequate to model the impedance. For Inverter2, however, a better fitting is obtained when the model includes a resistor in series with the capacitance. The impedance profile of each of the inverters is shown in Fig. 3, Fig. 4, and Fig. 5, while the impedance models of all three inverters are shown in Fig. 6. The impedance profile consists of harmonic and interharmonic measurement results. All three inverters are measured at the same input power, 900Wdc.

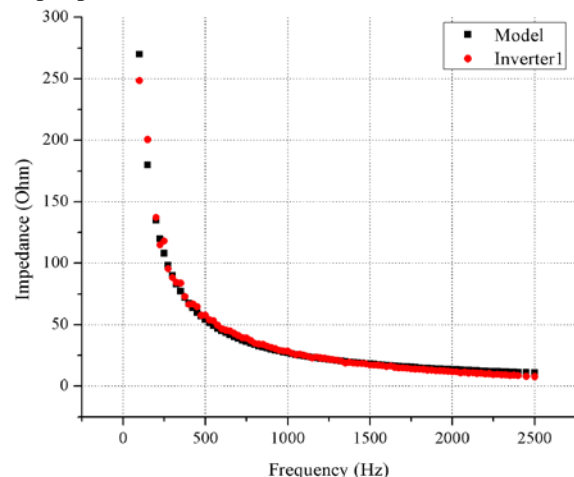


Fig. 3. The impedance profile of Inverter1 and the model.

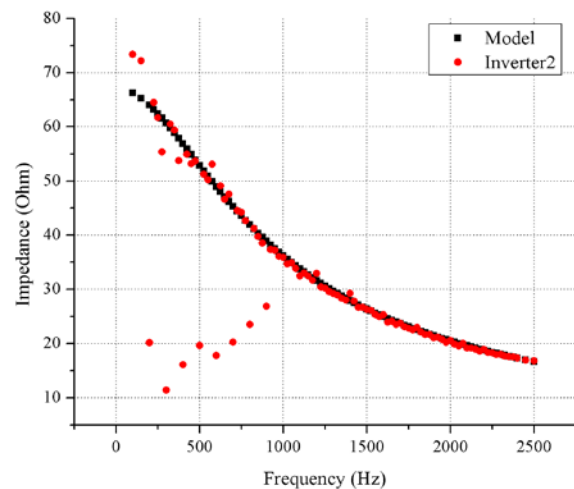


Fig. 4. The impedance profile of Inverter2 and the model.

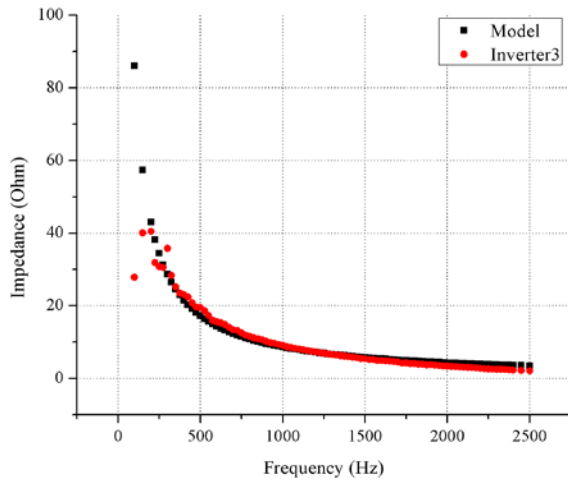


Fig. 5. The impedance profile of Inverter3 and the model.

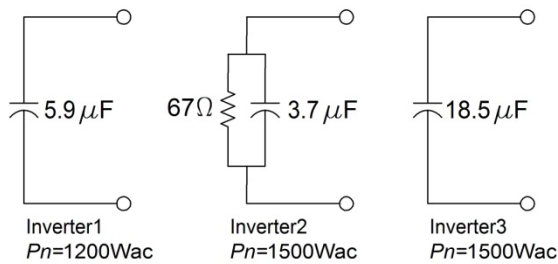


Fig. 6. The impedance models of SP inverters.

B. Single-phase (SP) Power Router

A power router operates in a slightly different way from most commercial PV inverters complying with “anti-islanding” regulation. A power router can be connected to a DC storage that delivers the power during grid faults. Although in principal it works as a SP inverter, the impedance profile differs from the other SP inverters; there is a parallel resonance at $h=33$. This happens due to the different topology of the filter inside the inverter. Only harmonic measurement results are presented here because it is not possible to do interharmonic measurements on this inverter. Interharmonic components of the voltage trigger the protection system of the power router.

Due to its unique profile, it is difficult to create the impedance model that fits very well. A good estimation, however, was obtained based on below considerations:

- the resonance is parallel, at $f=1650\text{Hz}$,
- a series resistor determines the values at lower harmonics,
- a damping resistor determines the peak values, and
- since lower harmonics are more common in the grid, more attention is given to fit the measurement curve at lower harmonics, as shown in Fig. 7.

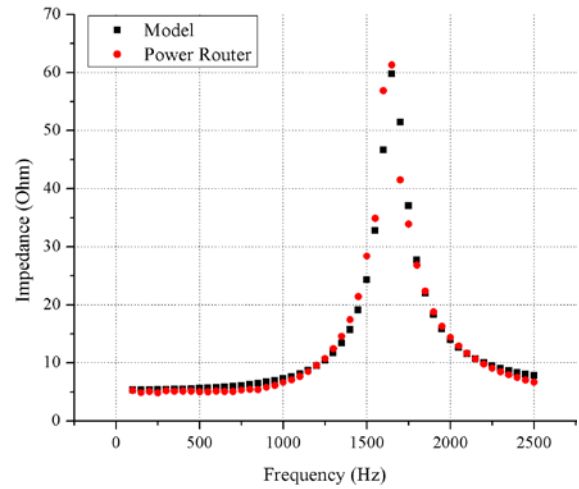


Fig. 7. The impedance profile of SP power router and the model.

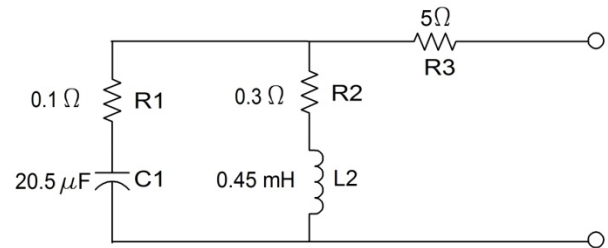


Fig. 8. The impedance model of SP power router.

C. Three-phase (TP) Inverter

Although in principal this TP inverter works like a SP inverter (because it feeds-in to one phase), the impedance profile looks different from other SP inverters. It still has the negative characteristic (the impedance decreases when the frequency increases) but it is unlike a capacitor behavior. Therefore, a complex impedance model like that of the power router is applied with different parameter values. Fig. 9 shows the impedance model and Fig. 10 shows the impedance profile.

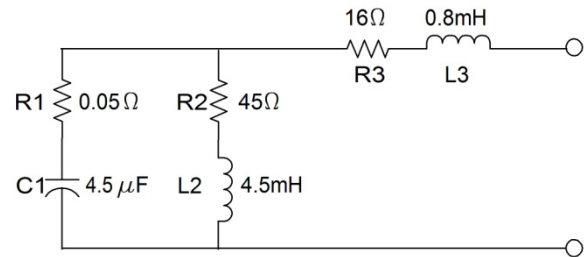


Fig. 9. The impedance model of TP inverter.

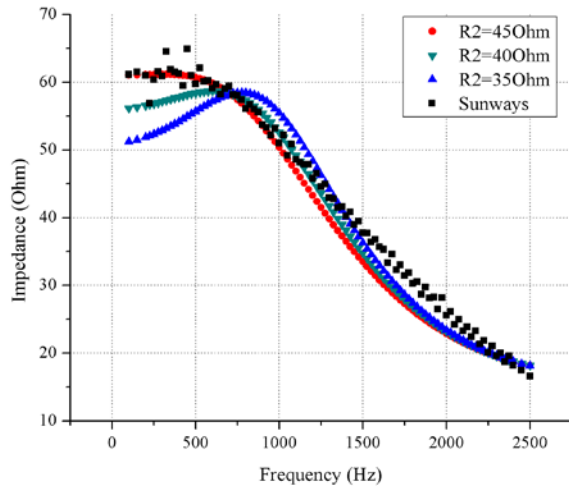


Fig. 10. The impedance profile of TP inverter and the model.

IV. GENERAL MODEL AND AGGREGATED MODEL

To keep all controlled variables similar among different SP inverters, all measurements are carried-out at 900Wdc input power. Looking at the similarity between the three SP inverter output impedances, a simple general model to represent the output impedance of commercial SP inverters for 1-2kW can be deduced. It is a single capacitor with values ranging between 3.7-18.5 μ F. Typical values of output capacitor of commercial 1-3kW PV inverters are between 0.5-10 μ F, as reported in [2]. A single capacitance value cannot represent every inverter but using several values from the range is adequate. Note that the TP inverter in this experiment cannot be taken as a general case of SP inverter in 2-3kW power class because although it feeds in via 1 phase, it still needs 3-phase connection.

As for higher power class SP inverters, the model shown for the TP inverter and power router can serve as a general representation of the output impedance. The parameter values will surely be different from one inverter to the others and the exact parameter values can only be obtained from measurement. However, a look-up table of parameters for different power class (e.g. 4kW, 5kW) can be build which speaks for all inverters in that particular power class. If one wants to make a network simulation using this model, one can use the impedance circuit depicted in Fig. 11 with parameters from the look-up table.

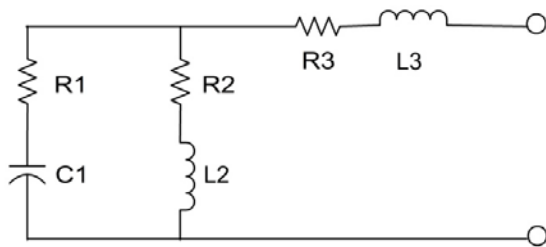


Fig. 11. General model to represent a single phase PV inverter

When multiple inverters are connected to the grid, the parallel capacitance value will be higher and it might result in a lower resonant frequency. It is important, therefore, to

include a model for an aggregation of inverters in the network simulation. It is adequate to use the same topology of simple and complex impedance circuit already presented; the only difference will be the parameters which result from parallel summation of individual parameters.

To validate this, an experiment was carried-out to measure the output impedance of all three SP inverters connected in parallel. Fig. 11 shows the result of harmonic and interharmonic measurement.

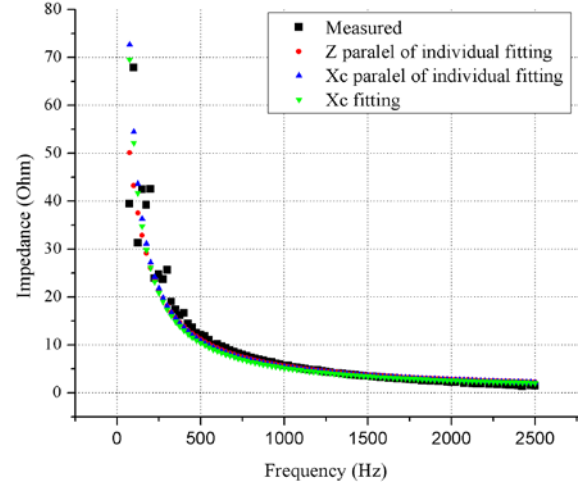


Fig. 12. The impedance profile of an aggregation of three SP inverters.

Also shown in Fig.11 is the resultant impedance from the inverter's individual impedances connected in parallel, calculated by Eq. 3, where Z_p is the resultant impedance, $X_{C,1}$ is Inverter1's capacitive reactance, $Z_{S,2}$ is the series of resistor and capacitor of Inverter2, and $X_{C,3}$ is Inverter3's capacitive reactance. As with individual measurement of SP inverters, a curve fitting was also applied to the impedance and the curve of a single capacitor fits the measurement curve the best. The capacitance found from curve fitting is 30.5 μ F, which is close to the resultant capacitance of paralleled inverters 28.1 μ F (summation of 5.9 μ F, 3.7 μ F, and 18.5 μ F). The impedance profile from both capacitance values are shown in blue and green marker, respectively.

$$\frac{1}{Z_p} = \frac{1}{X_{C,1}} + \frac{1}{Z_{S,2}} + \frac{1}{X_{C,3}} \quad (3)$$

The influence of each individual inverter is also seen in the aggregated model. Fig. 4 shows significant discrepancies between measured and model impedance of Inverter2, particularly at lower frequencies. It translates to discrepancies between measured and calculated impedance of the aggregated model at lower frequencies, only much less because the other two inverters damp this phenomenon.

V. CONCLUSIONS

To understand the influence of PV inverters on harmonic voltages in low-voltage networks, it is useful to simulate the network including a proper inverter model. This paper has proposed several equivalent circuit models that can be used to represent the dominant resonant frequency of the inverter. The

model is developed from voltage and current measurements at the output of the inverter. Measurements are done on harmonic and interharmonic frequencies to estimate the influence of inverters harmonic suppression. The results of measurements on harmonic and interharmonic frequencies are in good agreement.

From the impedance-frequency plot, the models represent the inverters' characteristic adequately on most of the frequency range observed. The discrepancies come from several assumptions made before the measurement:

- the line impedance is zero: this is not true although it is really small,
- there are two harmonic sources (voltage source and inverter current): theoretically it can be solved using the superposition theorem by eliminating one harmonic source each time but it is not applicable because it is not possible to operate the inverter without its harmonic current source.

A general model can be deduced using parameters that represent every power class. An aggregated model is also presented using the same topologies presented for individual inverter with parameters calculated from the parallel connection between the inverters. This model has been validated during the experiment. Another interesting thing found from the experiment is that the measured impedance is not influenced by the power rating of the inverter during measurement.

To have a complete Norton model of a PV inverter, further measurements and modeling of the harmonic currents emitted by the inverter needs to be done. With this complete model, one can simulate harmonic flow stemming from PV inverters in the network.

VI. REFERENCES

- [1] E. Vasanasong and E. D. Spooner, "The effect of net harmonic currents produced by numbers of the Sydney Olympic Village's PV systems on the power quality of local electrical network," in *Proc. 2000 International Conference on Power System Technology*, pp. 1001-1006.
- [2] J. H. R. Enslin and P. J. M. Heskes, "Harmonic interaction between a large number of distributed power inverters and the distribution network," in *Proc. 2003 IEEE Power Electronics Specialist Conf.*, pp. 1742-1747.
- [3] J. L. Agorreta, M. Borrega, J. López, and L. Marroyo, "Modeling and Control of N-Paralleled Grid-Connected Inverters With LCL Filter Coupled Due to Grid Impedance in PV Plants," *IEEE Trans. Power Electronics*, vol. 26, pp. 770-785, Mar. 2011.
- [4] P. J. M. Heskes, P. M. Rooij, J. F. G. Cobben, and H. E. Oldenkamp, "Estimation of the potential to pollute the electricity network with harmonics due to the use of small micro generators with inverters," ECN, Tech. Rep. ECN-C--04-087, Aug. 2004. [Online]. Available: <http://www.ecn.nl/docs/library/report/2004/c04087.pdf>
- [5] J. N. Paquin and D. Turqotte, "PV Inverter Modelling for Power Quality Studies," CANMET Energy Technology Centre, Varennes, QC, Tech. Rep. CETC 2007-202 (TR), Nov. 2007.
- [6] Y. Li, P. Jing, Y. Luo, B. Zhang, C. Mao, and X. Ruan, "A study on dynamic power flow caused by the grid-connected PV systems," in *Proc. 2010 IEEE International Symposium on Power Electronics for Distributed Generation Systems (PEDG)*, pp. 76-80.
- [7] F. Wang, J. L. Duarte, and M. A. M. Hendrix, "Analysis of harmonic interactions between DG inverters and polluted grids," in *Proc. 2010 IEEE International Energy Conference and Exhibition*, pp. 194-199.
- [8] C. Limsakul, A. Sangswang, D. Chenvidhya, M. Seapan, B. Meunpinij, N. Chayavanich, and C. Jivacate, "An impedance model of a PV grid-connected system," in *Proc. 2008 IEEE Photovoltaic Specialists Conf.*, pp. 1-4.

- [9] J. P. Rhode, A. W. Kelley, and M. E. Baran, "Complete characterization of utilization-voltage power system impedance using wideband measurement," *IEEE Trans. Industry Applications*, vol. 33, pp. 1472-1479.

VII. BIOGRAPHIES



Ernauli Aprilia received her Bachelor degree in Electrical Engineering from Institut Teknologi Bandung, Indonesia, in 2007. Since 2010 she is pursuing a Master degree in Sustainable Energy Technology in Eindhoven University of Technology. Her graduation project is carried out at Electrical Energy Systems group.



Vladimir Ćuk received his dip. ing. (M.Sc.) degree in electrical engineering from the School of Electrical Engineering, University of Belgrade, Serbia, in 2005. During 2006-2009 he was with the Electrical Engineering Institute "Nikola Tesla" in Belgrade. Since 2009 he is a PhD candidate at the Electrical Energy Systems group of the Eindhoven University of Technology. His main research topic is electrical power quality.



Sjef Cobben was born in Nuth, Netherlands, in 1956. He received the Bachelors degree in Electrical Engineering from the Technical University of Heerlen in 1979. In 2002 he received the Masters degree in Electrical Engineering from Eindhoven, University of Technology (TU/e).

In 1979 he joined NUON, one of the largest energy organizations in the Netherlands. Since 2000 he is working for the Dutch grid operator Liander, where he is engaged in Power Quality problems and safety requirements. From 2003 to 2007 he worked part time on a Ph.D. project about "intelligent grids" with as special topic Power Quality problems. Sjef Cobben is member of several national and international standardization commissions about requirements for low and high voltage installations and characteristics of the supply voltage. He is author of several books about power quality and low voltage installations. Since 2007 he is working as assistant professor at the University of Technology in Eindhoven, Netherlands.



Paulo Ribeiro received a BS in Electrical Engineering from the Universidade Federal de Pernambuco, Recife, Brazil in 1975; completed the Electric Power Systems Engineering Course with Power Technologies, Inc. (PTI), in 1979; and received Ph.D. from the University of Manchester, Manchester, UK in 1985. He is an Associate Professor of Electrical Engineering at the Technical University of Eindhoven, Eindhoven, the Netherlands. His research interests include power electronics, power quality, system modeling and simulation.



Wil Kling received his M.Sc. degree in Electrical Engineering from the Eindhoven University of Technology, Eindhoven, the Netherlands, in 1978. Since 1993, he has been a part-time Professor with the Delft University of Technology, the Netherlands in the field of Electrical Power Systems. Up till the end of 2008 he was also with TenneT, the Dutch Transmission System Operator, as senior engineer for network planning and strategy. Since Dec. 2008, he has been appointed Chair of the Electrical Energy Systems group, Eindhoven University of Technology. He is leading research programs on distributed generation, integration of wind power, network concepts and reliability issues.

Prof. Kling is involved in scientific organizations such as CIGRE and the IEEE. As Netherlands' representative, he is a member of CIGRE Study Committee C6 on Distribution Systems and Dispersed Generation, and the Administrative Council of CIGRE.

Considerations on Harmonic Impedance Estimation in Low Voltage Networks

V. Čuk, *Student Member, IEEE*, J. F. G. Cobben, W.L. Kling, *Member, IEEE*, and P. F. Ribeiro, *Fellow, IEEE*

Abstract—One difficulty in calculating harmonic voltages and currents throughout a transmission or distribution system is the need for a precise model of the linear load, both in magnitude and composition, fed from each bus. It has become evident that the use of equivalents without a comprehensive check on the effects of all impedances actually present can lead to inaccurate estimation of the harmonic voltages and currents. Considerations on harmonic impedance estimation in low voltage networks are presented in the paper. Influences of model abstractions and uncertainties in parameter estimations are analyzed analytically and tested on a model of a real low voltage network. The parameters analyzed include different load compositions, cable lengths, lumping loads and feeders, and medium voltage network representations. It is observed that some of these parameter changes have only a minor effect on the frequency of the first parallel resonance, while other effects have to be included in the calculation to avoid misleading results. This analysis can be used as a guideline when harmonic voltages are estimated in low voltage networks.

Index Terms—Impedance, power system harmonics, uncertainty, resonance.

I. INTRODUCTION

HARMONIC analysis is performed for power systems to determine the effect of harmonic sources on the harmonic voltage levels in the system. As the number of non-linear devices (both loads and generators) in low voltage (LV) networks is increasing, these studies are often performed for low voltage distribution systems.

Simulating the impact of one or more harmonic sources faces two difficulties, modeling the source of harmonics and modeling the equivalent system impedance. This paper

This research has been performed within the framework of the IOP-EMVT research project 'Power Quality and EMC' that is supported financially by Agentschap NL. Agentschap NL is an agency of the Dutch Ministry of Economic Affairs, Agriculture and Innovation.

V. Čuk is a PhD candidate at the Eindhoven University of Technology, the Netherlands (e-mail: v.cuk@tue.nl).

J.F.G. Cobben is working at Alliander, the Netherlands. He is also a part-time professor at the Eindhoven University of Technology, the Netherlands (e-mail: j.f.g.cobben@tue.nl).

W.L. Kling is a full professor and the head of the Electrical Energy Systems group at the Eindhoven University of Technology, the Netherlands (e-mail: w.l.kling@tue.nl).

P.F. Ribeiro is an associate professor at the Eindhoven University of Technology, the Netherlands (e-mail: p.f.ribeiro@tue.nl).

focuses on the harmonic impedance modeling.

The system impedance is influenced by many elements. Knowing the exact composition of loads, both in the low voltage network and upstream networks, is usually difficult and also changing in time. Network reconfigurations also add to the time varying nature of the impedance, so each calculation can serve only for a particular moment in time. For this reason it is usual to calculate the polar diagram of the impedance for all predicted topology and load changes.

Calculations and analysis of harmonic impedances in transmission systems can be found in [1]-[5]. Different models of system elements are described in [1], [3]-[4], and [6]-[10]. Examples of distribution system impedance modeling are given in [6], [11]-[14]. Sensitivity of impedance estimations are discussed in [2], [4], and [15]-[17].

Uncertainties of impedance modeling in low voltage networks and errors caused by simplifications and parameter errors were not analyzed in previous works. The aim of this paper is to analyze these effects, and to estimate possible errors in harmonic impedance calculations due to different model and parameter changes.

Model changes were analyzed analytically, and on an example of a real low voltage cable network, in which a parallel resonance was observed. This analysis can be used as a guideline in the low voltage modeling process. It emphasizes which parameters of the network have a significant impact on the resulting harmonic impedance, in contrast with parameters which can be simplified with minor errors.

II. ELEMENT MODELS AND EXAMPLE NETWORK

The adopted test network is a household low voltage network with a large amount of PV inverters connected. This network was chosen because the capacitance of PV inverters shifts the first parallel resonance in the low frequency range [18].

Cables were modeled with their PI equivalents. Skin effect was not taken into account. Both the LV and the medium voltage (MV) networks are cable networks.

Transformers were modeled as series *RL* circuits. Their capacitances were not taken into account as the maximal frequency of interest was 3 kHz.

Power factor correction (PFC) units were modeled only as a capacitance without losses.

Household loads were modeled as parallel *RC* circuits and

parallel RLC circuits (several scenarios). The capacitance should represent the input capacitance of all power electronic devices, mainly their input filters. In [13], a range of $(0.6 - 6)$ μF per house is proposed. In this paper $0.6 \mu\text{F}$ per house is adopted. Induction motors were modeled as their locked rotor inductance, as proposed in [10], [12]. The total adopted power of linear loads in houses was 500 W , and induction motors were accounted as $(0 - 30)$ % of this load, in several steps. Resistance should represent the linear loads without motors. Depending on the amount of induction motors, resistance was changed to get the same total power of linear loads.

Photovoltaic inverters were modeled as their input capacitance. Reference [13] proposes using values of $(0.5 - 10)$ μF for a $(1 - 3)$ kW inverter, based on measurements. In this paper, several values are used, to show the effect if this value is not known. The total installed power of PV inverters in the low voltage network is 300 kW , mostly composed of 2 kW units, while the peak load of all loads together is approximately 150 kVA .

The effect of lumping loads was examined in three steps. In the first step, all loads were connected directly at the low voltage busbar. In the second step, feeders were separated in the low voltage network, with lumped loads on feeders and feeder branches. In the last step, all houses and inverters were modeled separately.

The medium voltage network was modeled in two ways. The simple version of the model is a series RL circuit, representing the short-circuit power of the network and the R to X ratio. A more detailed model was also used, representing all MV feeders until the HV/MV substation, and one 1.4 MW CHP (combined heat and power) generator in the MV network and several configurations of PFC in the MV network. The HV network was represented with its short-circuit level.

A schematic diagram of the low voltage part of the example network is shown in Fig. 1. The medium voltage part of the network is presented in Fig. 2. The low voltage network is connected to busbar 13 of the MV network.

All four feeders are numbered on Fig. 1, while on Fig. 2 only four busbars are numbered (2, 9, 12, and 13), since changes of elements were applied only on these busbars.

III. ANALYSIS OF THE HARMONIC IMPEDANCE

The analysis of the network harmonic impedance is divided into several parts. The effect of lumping loads, load models, cable lengths, and MV network models are investigated separately. Mechanisms of parameter changes are examined analytically (for a simplified example), and on a DIGSILENT Power Factory model of the example network, using the frequency scan. In all cases the impedance was observed on the low voltage side of the MV/LV transformer.

A. The effect of lumping loads

The number of loads in a LV network is usually too large to allow for modeling each load separately. For this reason, loads are commonly lumped into equivalent loads with some feeders and load parameters neglected. This leads to uncertainty of the outcome.

To illustrate the effect of lumping analytically, we can look at a simplified network model with two parallel feeders as in Fig. 3 and derive its equivalent impedance. In this figure, L represents the upstream system inductance, L_1 and L_2 represent feeder inductances, and C_1 and C_2 represent capacitances of loads connected to these two feeders.

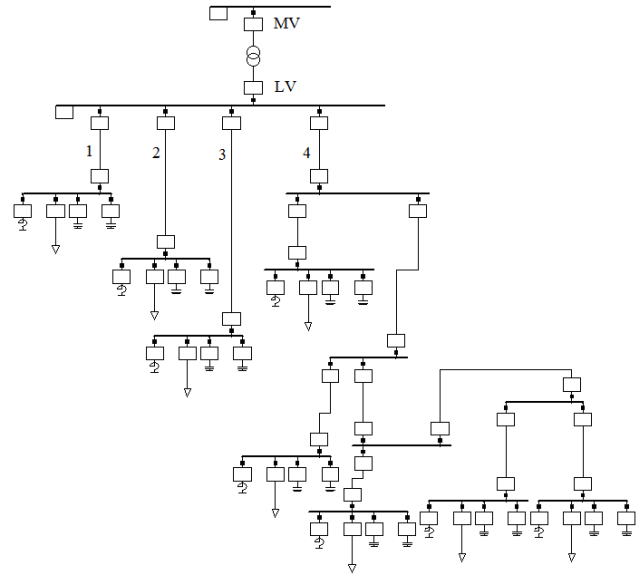


Fig. 1. Low voltage part of the example network

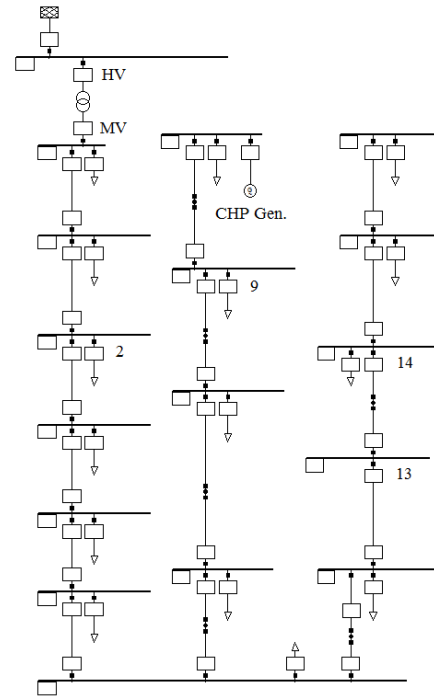


Fig. 2. Medium voltage part of the example network

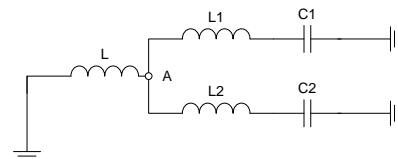


Fig. 3. Simplified example for lumping feeders

If we lump the two capacitances together (as $C_1 + C_2$), and neglect the inductances L_1 and L_2 , the impedance Z_A at point A is given by:

$$Z_A = j\omega L / (1 - \omega^2 L(C_1 + C_2)) \quad (1)$$

If we do not lump the two feeders and take inductances L_1 and L_2 into consideration, the impedance is given by:

$$Z_A = \frac{j\omega L(1 - \omega^2 L_1 C_1)(1 - \omega^2 L_2 C_2)}{1 + \omega^4 L_1 L_2 C_1 C_2 - \omega^2(L(C_1 + C_2) + L_1 C_1 + L_2 C_2)} \quad (2)$$

If the inductance L is much greater than L_1 and L_2 , and the lowest parallel resonance frequency f_{r1} is in the low frequency range, equation (2) will give a solution for f_{r1} which is close to the solution of (1). Besides the difference in calculated f_{r1} , L_1 and L_2 also introduce two series resonances and an additional parallel resonance with a higher resonant frequency. The second parallel resonant frequency increases as L_1 and L_2 decrease. If cable lengths are not very long, the resonant frequency of the second parallel resonance and both series resonances are usually too high to be of interest for distribution systems.

To illustrate the difference between (1) and (2), we assume $C_1 = C_2$ and $L_1 = L_2$ and vary the ratio between L and L_1 from 50 to 5. The difference in the lower parallel resonant frequency calculated by (2) and (1) is shown in Fig. 4.

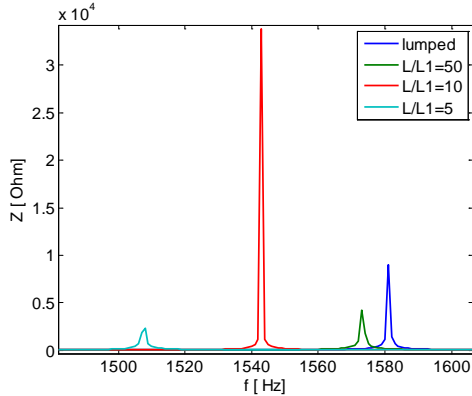


Fig. 4. The first parallel resonance for different element values

The shown uncertainty is dependent on the ratio of impedances. If we know that the feeder inductance is much lower than the upstream system inductance, lumping will not lead to large errors when we calculate the resonant frequency (amplitude will be affected more). However, as feeder length become longer, and this is mostly the case, this error increases.

In a realistic scenario the topology is much more complex than in Fig. 3. To illustrate the effect of lumping on a realistic low voltage network, we compare the harmonic impedance versus frequency at the low voltage busbar of the example network from Fig. 1, for three cases. In the first case we look at the whole low voltage network as a single parallel RLC load connected directly at the transformer (case: all lumped). In the second step, we lump the separate feeders as shown in Fig. 1, with feeders and feeder branches lumped as parallel RLC loads after cables (case: lumped feeders). In the third step, we uncouple the loads to more branches, with short feeders

divided in five sections, and longer feeders in 10 sections (case: no lumping). Results are presented in Fig. 5.

The solution of the “most realistic” case (no lumping) falls between the two other cases. In comparison with the case with everything lumped at the busbar, lumping complete feeders will add extra inductance in the circuit, resulting with a lower resonant frequency (in this case almost 30 Hz). In the case where nothing is lumped, most capacitances are connected via a lower inductance, resulting in a smaller frequency change from the first case (less than 20 Hz).

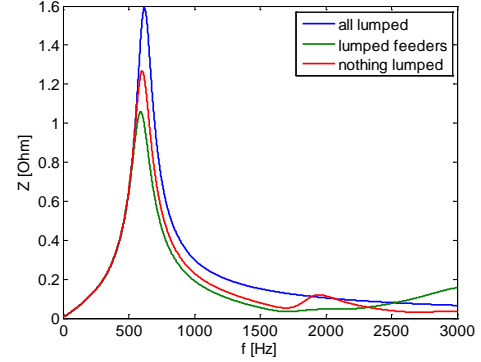


Fig. 5. Effects of lumping loads on the example network impedance

In conclusion, lumping all loads leads to an increase of the resonant frequency, but with acceptable errors if feeder lengths are short. It does not reveal all resonances in the system. Lumping separate feeders leads to a decrease in the resonant frequency, with smaller errors. It also reveals additional resonances but the uncertainty is larger at higher frequencies.

To avoid high model complexity, in the following subsections the model with lumped feeders is used for analyzing other effects.

B. The effect of different load models

Determining appropriate load models is very important and difficult at the same time. Loads are the main damping element in the network, but can also change the resonant conditions, especially at higher frequencies [12].

Load demand and composition change in time, making it necessary to assess several scenarios. Basic assumptions for modeling loads were proposed in [12]:

- Distribution lines and cables should be represented by an equivalent π . The capacitance of lines should be included.
- Transformers should be represented by an equivalent element. Series RL circuits are proposed for low frequencies.
- For rotating machines the active power does not represent the damping value, so the active and reactive power demand at the fundamental frequency may not be used straightforwardly. A locked-rotor reactance or a parallel RL circuit are proposed.
- Power factor correction capacitance should be estimated as accurately as possible.
- Other elements, such as line inductors, filters and generators should be represented according to their actual configuration and composition.

- The active power of electronic loads should not be taken into account as a resistance. Power electronics should be taken into account as input impedance, e.g. their filter capacitance, or as an open circuit if their input impedance is too high.

Measured active and reactive powers should not be used directly to determine values of linear elements. Active power of power electronic and motor loads should not be included in the value of the resistance. Measured reactive power does not reveal the mixture of inductive and capacitive loads, and short-circuit inductance of motors is lower than the one calculated from reactive power. Finally, the measured reactive power usually contains the distortion power, which does not correspond to physical inductances or capacitances.

To analyze the impact of motor loads, we start with a simplified model from Fig. 6. In this figure, L is the inductance of the upstream system, C is the capacitance of loads, and L_m is the locked-rotor inductance of motor loads.

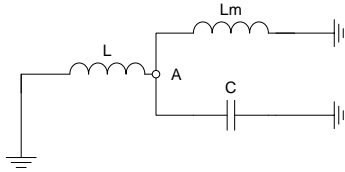


Fig. 6. Simplified example for motor load impact

In this case, the impedance at point A is given by:

$$Z_A = j\omega L_{par} / (1 - \omega^2 L_{par} C) \quad (3)$$

where L_{par} is an inductance equal to the value of L in parallel with L_m . Its value is lower than the lower of the two inductances, and if L_m is much higher than L (motor of low power), it will be almost identical to L . As we decrease L_m (increase the power of the motor) the resonant frequency will become higher. If the power of the motor is very large, the resonant frequency would be affected more by the motor inductance.

In a realistic network this dependency becomes more complicated. To illustrate it on the example network, we look at the impedance at the low voltage busbar for different motor load shares in the network – see Fig. 7.

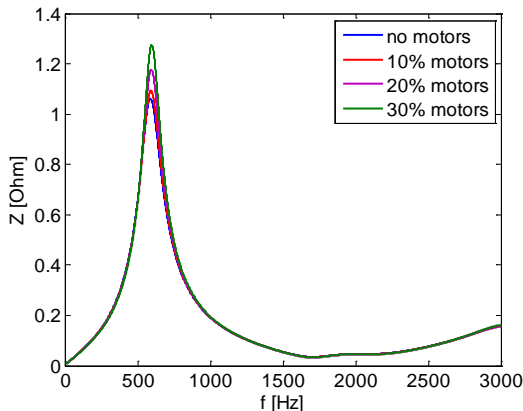


Fig. 7. The effect of motor load share on the impedance characteristic

In the first iteration, no motors were added in the network, and then in several steps the motor share was increased up to 30 % of the active power consumption. These changes result in the changes of the resonant peak (mostly due to the change of resistance), but the resonant frequency is shifted up for only 5 Hz. If the short-circuit power would be lower, the upstream network would have a larger inductance leading to larger differences. This leads to the conclusion that if the amount of small motors is not known in the network, it should not lead to significant errors when determining the lowest resonant frequency. However, neglecting a large motor would lead to larger differences.

To analyze the impact of capacitive loads, we can look at expression (3) again. Capacitances change the resonant frequency directly, a ΔC change of capacitance changes the resonant frequency by $1/\sqrt{\Delta C}$.

In the example network there are no PFC units in the low voltage network, the capacitances are mostly located in input filters of PV inverters. If the value of this capacitances is not known, this leads to a large range of possible solutions. Fig. 8 shows the impedance characteristic for four capacitance assumptions. Initially, 8 μF is assumed for each 2 kW inverter; then a $\pm 20\%$ capacitance uncertainty is taken into account; in the end, it was assumed that 2 μF is the input capacitance of each 2 kW inverter.

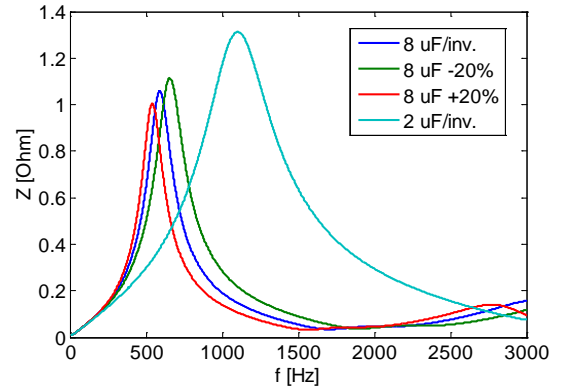


Fig. 8. The effect of capacitance on the impedance characteristic

If the capacitance is not known initially, the difference between assuming 2 and 8 μF per inverter in this case leads to a 500 Hz difference in the resonant frequency. If the capacitance is known, and the uncertainty is taken into account as $\pm 20\%$, differences of 60 Hz can be noticed.

The frequency of the lowest parallel resonance is usually not influenced by the value of resistive loads used. However, resistive loads provide damping in the system, so they are also responsible for peak values of impedance. If we neglect resistive loads, it may happen that we overestimate harmonic voltages due to unrealistic values of impedance. In contrast, if we overestimate the power of resistive loads, we may underestimate the impedance and harmonic voltages.

Fig. 9 shows the effect of variable load resistance in the example network. The initial resistive load was changed for $\pm 20\%$, without changes in other parameters.

The value of the resonant peak changed by about 20 % for both changes, while the resonant frequency changed for only 1

Hz. This is a convenient property of resistance modeling: changing its value will not affect the resonant frequency significantly, and the critical case is always the lowest resistive load (highest resistance). While other parameters need to be analyzed in several conditions, for the resistance it is usually sufficient to observe the case with the lowest resistive loading. As mentioned earlier, this loading should exclude power electronic devices and electrical motors. Also, if higher frequencies are of interest, resistances have a more complicated impact.

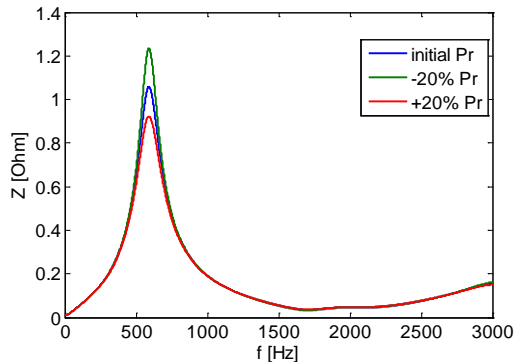


Fig. 9. The effect of resistive loads on the impedance characteristic

C. The effect of cable lengths

The effect of cable lengths was already mentioned in the analysis of lumping loads. It was noticed that complete load lumping with neglected low voltage feeders introduces errors in the resonance analysis, both for the frequency and peak amplitude. In this subsection we analyze the effect of cable length uncertainty on a model with loads lumped on feeders.

Equation (2) can be used to explain this effect. Inductances L_1 and L_2 carry the uncertainty of cable lengths. If these inductances are comparable with L , the final result will be influenced significantly. If they are much lower than L , the effect will not be significant. Fig. 10 shows the effect of $\pm 20\%$ cable length changes in the example network. In this example, 20% changes lead to 5 Hz changes in the resonant frequency. Peaks of the impedance change approximately by 10%.

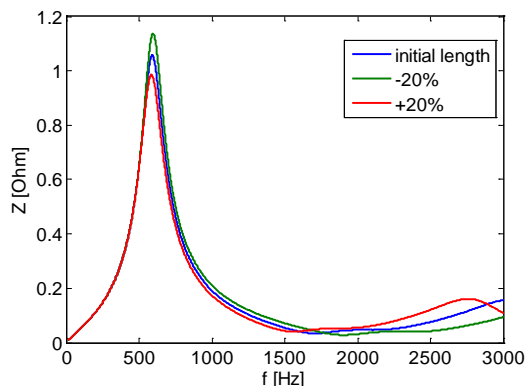


Fig. 10. The effect of low voltage cable lengths on the impedance

D. The effect of MV network representations

In the first approximation, the MV network is usually considered just as its short-circuit impedance. However, some elements of the MV network may be very important for

impedance estimation, especially PFC units and generators. Since the impedance of MV network elements is transposed to the low voltage level, approximations in the MV network are similar as approximations on one of the low voltage feeders.

To illustrate the effect of different MV network representations, several topology variations were introduced to the network from Fig. 2: the CHP generator was switched on and off, PFC of 0.5 MVar was connected to busbars 2, 9, and 14, and PFC of 1 MVar was connected to busbar 14 directly and through a MV/LV transformer.

In Fig. 11 the model with a single impedance MV network is compared with the model from Fig. 2, with and without the CHP generator connected.

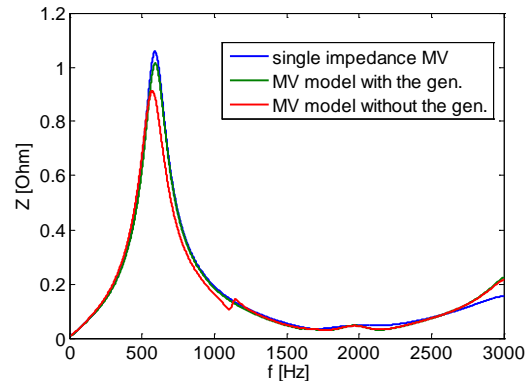


Fig. 11. MV network as a single impedance, and with MV feeders and busbars

In these three cases the first parallel resonance is being shifted by 20 Hz. Also, the peak amplitude is changing by 15%, and additional resonances with small peaks are visible with the more complex model.

In Fig. 12 the effect of PFC in the MV network is considered, with and without the CHP generator connected.

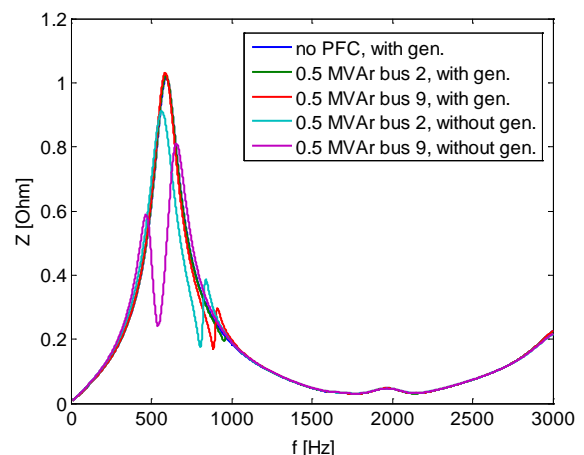


Fig. 12. The effect of PFC in the MV network, busbars 2 and 9

On busbars 2 and 9, 0.5 MVar PFC causes only minor effects if the generator is connected (resonant frequency reduced for 5 Hz, additional smaller resonance). However, if the generator is disconnected, the effect is much larger.

In Fig. 13 the effect of PFC on busbar 14, which is nearer to the observed LV network than busbars 2 and 9, is considered. It is visible that the effect is more significant if the PFC is nearer the busbar of interest. Also, similarly as with

long MV feeders, PFC on other LV busbars has only a minor effect due to the extra MV/LV transformer in between. Generators in the MV network make this interaction more complex, since additional series resonances can create additional impedance peaks near the parallel resonance.

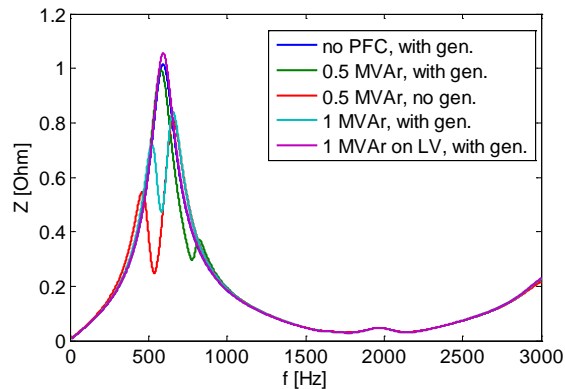


Fig. 13. The effect of PFC on busbar 14 of the MV network

IV. CONCLUSIONS

Considerations on harmonic impedance estimation in low voltage networks are presented in the paper. Effects of different model abstractions, linear load compositions, and parameter changes were analyzed analytically and illustrated on an example low voltage network.

The results of the analysis can be summarized as follows:

- Lumping of low voltage loads in some cases introduces large differences in the network impedance. For short feeders in weak grids this effect is not significant.
- The uncertainty of capacitance of loads in the low voltage network has the most significant impact. If this value has to be assumed, large errors should be expected.
- Resistive loads have a minor impact on the frequency of the first parallel resonance. Due to the damping, resistances are important to determine the resonant peak, but the frequency can be determined even with the first approximation.
- The share of motor loads has a significant impact only if the motor locked-rotor inductance is comparable to the upstream system inductance.
- Values of load resistances, inductances, and capacitances should not be derived directly from power measurements. Resistances should be derived from the active power without power electronic and motor loads. Motors should be represented by their locked-rotor equivalents. Capacitances should account only for physical capacitances in the network.
- Cable length assumptions have a significant impact only for long feeders. In other cases, small deviations of cable lengths do not lead to large result changes.
- MV network representations and reconfigurations are very important if power factor correction units are connected directly on the MV level, and/or if generators are present. PFC units in nearby low voltage networks have only a minor impact.

This analysis can be used as a guideline for low voltage harmonic analysis. Choosing appropriate load models and network representations is a vital step for determining harmonic voltages in the network.

V. REFERENCES

- [1] N.G. Hingorani and M.F. Burberry, "Simulation of AC system impedance in HVDC system studies", *IEEE Trans. Power Apparatus and Systems*, vol. PAS-89, no. 5/6, May/June 1970.
- [2] G.D. Breuer, G. Addis, R.H. Lasseter, and J.J. Vithayathil, "HVDC-AC harmonic interaction, Part II: AC system harmonic model with comparison of calculated and measured data", *IEEE Trans. Power Apparatus and Systems*, vol. PAS-101, no. 3, March 1982.
- [3] T.J. Densem, P.S. Bodger, and J. Arrillaga, "Three phase transmission system modelling for harmonic penetration studies", *IEEE Trans. Power Apparatus and Systems*, vol. PAS-103, no. 2, February 1984.
- [4] P.F. Ribeiro, "Investigations of Harmonic Penetration in Transmission Systems," Ph.D. Dissertation, Victoria University of Manchester, England, July, 1985.
- [5] A.A. Girgis, W.H. Quaintance III, J. Qiu, and E.B. Makram, "A time-domain three-phase power system impedance modeling approach for harmonic filter analysis", *IEEE Trans. Power Delivery*, vol. 8, no. 2, April 1993.
- [6] M.F. McGranaghan, R.C. Dugan, and W.L. Sponsler, "Digital simulation of distribution system frequency-response characteristics", *IEEE Trans. Power Apparatus and Systems*, vol. PAS-100, no. 3, March 1981.
- [7] A.S. Morched, P. Kundur, "Identification and modelling of load characteristics at high frequencies", *IEEE Trans. Power Systems*, vol. PWRS-2, no. 1, February 1987.
- [8] Task Force on Harmonic Modeling and Simulation, "Modeling and simulation of the propagation of harmonics in electric power networks, Part I: Concepts, models, and simulation techniques", *IEEE Trans. Power Delivery*, vol. 11, no. 1, January 1996.
- [9] Task Force on Harmonic Modeling and Simulation, "Modeling and simulation of the propagation of harmonics in electric power networks, Part II: Sample systems and examples", *IEEE Trans. Power Delivery*, vol. 11, no. 1, January 1996.
- [10] W. Xu and S.J. Ranade, "Overview of harmonics modeling and simulation", Harmonic Modeling Tutorial, Chapter 1, IEEE.
- [11] T. Hiyama, M.S.A.A. Hammam, and T.H. Ortmeier, "Distribution system modeling with distributed harmonic sources", *IEEE Trans. Power Delivery*, vol. 4, no. 2, April 1989.
- [12] P.F. Ribeiro, "Guidelines on distribution system and load representation for harmonic studies", in *Proc. 1992 International Conference on Harmonics in Power Systems*, pp. 272-280.
- [13] J.H.R. Enslin and P.J.M. Heskes, "Harmonic interaction between a large number of distributed power inverters and the distribution network", *IEEE Trans. Power Electronics*, vol. 19, no. 6, November 2004.
- [14] F. Wang, J.L. Duarte, M.A.M. Hendrix, and P.F. Ribeiro, "Modeling and analysis of grid harmonic distortion impact of aggregated DG inverters", *IEEE Trans. Power Electronics*, vol. 26, no. 3, March 2011.
- [15] A. De Lorenzi, P. Bettini, and L. Zanotto, "Harmonic impedance measurement and calculations in the EHV transmission network", in *Proc. 2002 International Conference on Harmonics and Quality of Power*, pp. 1698-1706.
- [16] V. Sharma, R.J. Fleming, and L. Niekamp, "An iterative approach for analysis of harmonic penetration in the power transmission networks", *IEEE Trans. Power Delivery*, vol. 6, no. 4, January 1991.
- [17] A. Testa, D. Castaldo, and R. Langella, "Probabilistic aspects of harmonic impedances", in *Proc. 2002 IEEE Power Engineering Society Winter Meeting*, pp. 1076-1081.
- [18] J. Lava, J.F.G. Cobben, W.L. Kling, and F. van Overbeeke, "Addressing LV network power quality issues through the implementation of a microgrid", presented at *ICREPQ 2010*, available online: <http://www.icrepq.com/papers-icrepq10.html>

Aspects of a generic photovoltaic model examined under the German Grid Code for Medium Voltage

Ioannis-Thomas Theologitis¹, Eckehard Troester², Thomas Ackermann³

Abstract--The increasing penetration of photovoltaic power systems into the power grid has attracted attention to the issue of ensuring the smooth absorbance of the solar energy, while securing the normal and steady operation of the grid as well. Nowadays, the PV systems must meet a number of technical requirements to address this issue.

This paper investigates a generic grid-connected photovoltaic model that was developed by DIgSILENT and is part of the library in the new version of PowerFactory v.14.1 software that is used in this study. The model has a nominal rated peak power of 0.5 MVA and a designed power factor $\cos\phi=0.95$. The study focuses on the description of the model, its control system and its ability to reflect important requirements that a grid-connected PV system should have by January 2011 according to the German grid code for medium voltage. The model undergoes various simulations. Static voltage support, active power control and dynamic voltage support – Fault Ride Through (FRT) is examined.

The results show that the generic model is capable for active power reduction under over-frequency occasions and FRT behavior in cases of voltage dips. The reactive power control that is added in the model improves the control system and makes the model capable for static voltage support in sudden active power injection changes at the point of common coupling.

Beside the simplifications and shortcomings of this generic model, basic requirements of the modern PV systems can be addressed. Further improvements could make it more complete and applicable for more detailed studies.

Index Terms--Grid-connected Photovoltaic, PV inverter, German Grid Code for MV, PV model, PowerFactory of DIgSILENT, Reactive power control

I. NOMENCLATURE

AC – Alternative Current
 DC – Direct Current
 DIgSILENT – Digital SIMuLator for Electrical NeTwork
 FRT – Fault Ride Through (Low Voltage Ride Through)
 LV – Low Voltage
 MPP – Maximum Power Point
 MV – Medium Voltage

PCC – Point of Common Coupling
 PF – Power Factor
 PLL – Phase Locked Loop
 PV – Photovoltaic
 PVPS – Photovoltaic Power Systems
 Q – Reactive power
 RET – Renewable Energy Technology
 STC – Standard Test Condition

II. INTRODUCTION

The great potential in Renewable Energy Technologies (RET) has been seen since a long time ago. However, mostly technical and economical restrictions combined with the lack of a defined policy context around these technologies, has prevented the large scale deployment. Nevertheless, the increasing demand of energy due to population growth, the target of energy-independence from fossil fuels (mostly coal) set by many countries, the general need for more carbon-free energy sources due to environmental reasons and the legislation scheme that has been started to take form, have brought RET to the fore, especially the last decade.

Germany is a strong example of a country that has invested time and money towards renewable energy evolvement. Its leading position in the field among the EU countries and its key role worldwide, especially in wind and solar power, are reflected by facts. As far as the PV technology is concerned, by September 2010 the total number of installed capacity was 15 GWp, which was almost 30% of the total RET installed and 37.5% of the minimum electricity load of 2009 [1].

Germany has set a goal of 38.6% renewable electricity share [2] and in order to achieve that, PV technology should contribute significantly. Fig.1 presents a future scenario showing the increment of the installed PV capacity and the relevant PV price share of the total additional cost per kWh.

However, this PV penetration must not jeopardize the normal operation of the power grid. Thus, technical specifications should ensure and facilitate the proper interconnection and reinforcement of the grid. According to the German grid code any distributed generation plants should support the steady state operation (e.g. provide reactive power) and contribute to the stability of the power grid in cases of fault (e.g. voltage dips) at the connection point.

¹ Intern at Energynautics GmbH, Mühlstrasse 51, 63225 Langen, Germany (e-mail: i.t.theologitis@energynautics.com)

² Senior engineer at Energynautics GmbH, Mühlstrasse 51, 63225 Langen, Germany (e-mail: e.troester@energynautics.com)

³ CEO at Energynautics GmbH, Mühlstrasse 51, 63225 Langen, Germany (e-mail: t.ackermann@energynautics.com)

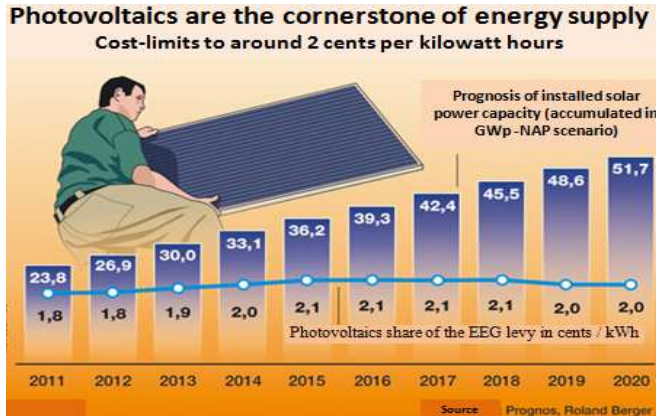


Fig. 1. Future scenario of PV installed capacity and renewable electricity levy for the next decade in Germany [3]

Photovoltaic Power Systems (PVPS) are connected mostly to the low and medium-voltage network and only approximately 1% of the total PV installations is connected to the high voltage network [1], meaning that the demand for grid stability refers to the low and medium voltage networks. Table 1 aggregates the basic requirements that grid-tied generators should meet in order to be integrated to the network. In this study the focus is:

- Active power control
- Dynamic voltage support – FRT
- Static voltage support

Certainly there are other requirements and issues to be considered when designing a grid-connected inverter that include power quality problems (e.g. harmonics), safety issues

(e.g. anti-islanding protection, under /over voltage protection, under/over frequency protection), electromagnetic interference etc. Those issues usually follow local rules that have been adopted by general European or International standards. Some examples can be found in [5].

III. MODEL

The PV model that is analyzed in this paper is developed using a static generator and can be seen in Fig.2.

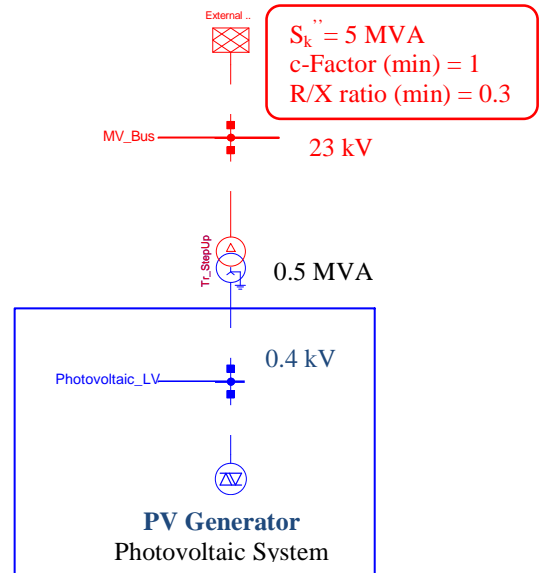


Fig. 2. The PV system model

TABLE 1. NEW REQUIREMENTS FOR GRID TIED GENERATORS [4] [7]

| Grid Codes | Voltage Band range | Fault Ride Through capability | Reactive Power Supply | | | Frequency Band range | Active Power Derating capability | | |
|---|--|----------------------------------|-----------------------|---|---------------------|-------------------------|-------------------------------------|------------------|----------|
| | | | capability | range | function | | | | |
| High Voltage (>110 kV) | 0,8 U _N ↔ 1,16 U _N | ✓ | ✓ | Based on 3 different possible variants*: 0,228 _{leading} < Q/P _n < 0,48 _{lagging} 0,33 _{leading} < Q/P _n < 0,41 _{lagging} 0,41 _{leading} < Q/P _n < 0,33 _{lagging} | | 47,5 Hz ↔ 51,5 Hz | ✓ | | |
| | | | | Q(U) | cosφ _{fix} | | Q _{fix} | function | |
| | | | | Δ($\frac{P}{P_M}$) = 40 $\frac{\%}{Hz}$ (50,2Hz - f) 50,2Hz < f < 51,5Hz | | | | | |
| Medium Voltage (<110 kV & >10 kV) | 0,9 U _N ↔ 1,15 U _N | ✓ | ✓ | 0,95 _{lagging} to 0,95 _{leading} | | 47,5 Hz ↔ 51,5 Hz | ✓ | | |
| | | | | cosφ(P) | Q(U) | | cosφ _{fix} | Q _{fix} | function |
| | | | | Δ($\frac{P}{P_M}$) = 40 $\frac{\%}{Hz}$ (50,2Hz - f) 50,2Hz < f < 51,5Hz | | | | | |
| Low Voltage (<10 kV) | 0,9 U _N ↔ 1,15 U _N | ✓** | ✓ | 0,90 _{lagging} to 0,90 _{leading} *** | | 47,5 Hz ↔ 50,2 Hz | ✓ | | |
| | | | | cosφ(P) | cosφ _{fix} | | function | | |
| | | | | Δ($\frac{P}{P_M}$) = 40 $\frac{\%}{Hz}$ (50,2Hz - f) 50,2Hz < f < 51,5Hz | | | | | |

* Also dependent on the voltage level at the PCC [6]. Below P/P_n=0,2 reduced reactive power can be provided.

** However, no reactive current injection is defined [7]

*** Depending on the total apparent power of the plant [7]

It is a generic model that was built by DIGSILENT as part of a past study and is available in the newest version of the PowerFactory tool. The template consists of the PV generator with a number of control systems and design features, which are integrated in it and also a Low Voltage (LV) terminal of nominal voltage 0.4 kV that the generator is connected with. The capacity of the system is 0.5 MVA. The rest of the configuration, which includes an external grid component, a MV bus bar of 23 kV nominal voltage and a step up transformer of 0.5 MVA rated power, were used in order to serve the needs of the examination.

The short circuit power of the external grid component is chosen 5 MVA (ten times the PV capacity) in order to represent a weak grid according to [8] and facilitate the study of the reactive power impact on the voltage support. Normally, to determine the PV capacity that can be installed in a certain grid, load flow studies are necessary to check the voltage rise at the point of common coupling (PCC). The R/X ratio 0.3 is based on the findings of [9].

The PV generator under normal steady-state operation injects 448.84 kW and 0 kVar, implying power factor (PF) =1 at the point of connection with the LV terminal. The active power is defined by the parameters and the configuration of the PV array (way of interconnection of PV modules), as seen in eq. 1.

$$\begin{aligned} & (V_{MPP_{module}} \cdot 20 \text{ modules}_{series}) \cdot (I_{MPP_{module}} \cdot 140 \text{ modules}_{parallel}) = \\ & = 700 \cdot 641.2 = 448.84 \text{ kW} \end{aligned} \quad (1)$$

The V_{MPP} and I_{MPP} are given for the standard test

The features and the control frame that are integrated inside the PV generator component can be seen in Fig. 3, where a rough demarcation of the basic parts has been made.

The DC side of the model consists basically of the PV array, the DC bus and the capacitor. The most important external factors that affect the power output of the PV array, which are the incoming solar irradiation and the operating temperature, can be controlled by the relevant slots in Fig. 3 by setting parameter events and changing the output values E and θ respectively. Those values enter the *Photovoltaic Model*, where the array current and the array voltage at MPP are calculated. The algorithm that is used for the calculation of the output values of the array model is written according to the electrical equivalent of the ideal solar cell using temperature correction factors for voltage and current. More details can be found in [10]. As regards the *DC Busbar and Capacitor model*, it represents the DC bus the PV array is connected to and the necessary shunt capacitor. It calculates the voltage across the capacitor, which is the input of the inverter (DC side).

The AC side of the control frame consists of all the basic control requirements for a grid-connected PV system to be compatible with the German grid code for MV. The *Active Power Reduction* slot together with the *Slow Frequency Measurement* device is responsible for the active power curtailment in case of frequency deviations. The *Static Voltage Support*, that seen as shaded slot, is a new addition to the control scheme and is responsible for steady state support by providing reactive power using all the four methods mentioned in Table 1 for the MV grid code. The main

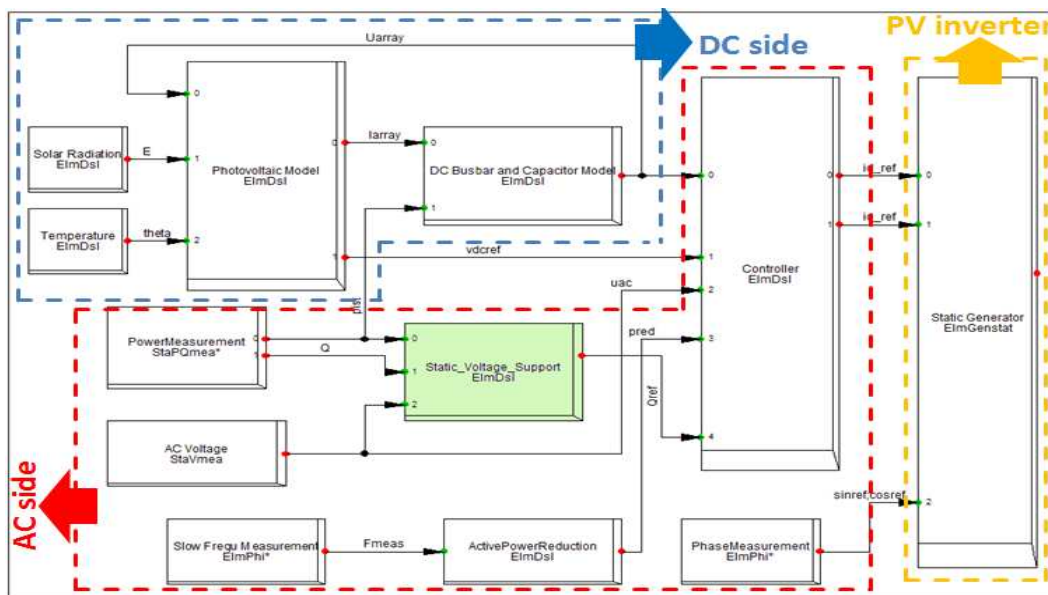


Fig. 3. The control frame of the PV system

conditions (STC) and all power values are assumed to be at the MPP. The maximum active power operational limit is 475 kW, while the reactive power limits are defined by the capability curve for three different voltage levels (0.95 p.u., 1 p.u. and 1.05 p.u.).

Controller includes *Reactive Power Support* control in case of voltage dips, written according to the Transmission Code 2007 and the System Service Ordinance SDLWindV. The Controller produces as results the components i_{d_ref} and i_{q_ref} , which are the reference values of active and reactive

power injection respectively. The *Phase Measurment* device is a Phase Locked Loop (PLL) device built by DIGSILENT that contains an oscillator that is synchronized by being phased-locked to some particular grid power signal (i.e. voltage) and generating an output signal. Normally, as well as in this case, this element is able to measure the phase of a voltage in the system and the frequency (see above Slow Frequency Measurement). The outputs of the main Controller and the PLL enter the *Static Generator*, which is basically the PV grid-tied inverter.

The above control features are explained in depth in [10] through dynamic simulations. Below the basic requirements as mentioned in the introduction part are analyzed.

IV. CONTROL ASPECTS

A. Active power control

Active power control refers to active power curtailment, meaning the ability of the generating plant to reduce its power output, as required by the network operator, or even disconnect the PV plant in order to avoid potential dangers regarding the stability of the system and human personnel. The control can be done automatically or manually [11]. As far as the automatic control is concerned, the German grid code for MV requires that the PV generator should reduce its power output when an over-frequency occurs. The over-frequency is defined above 50.2 Hz and the reduction slope is 40% of the last instantaneous value of power (just before 50.2 Hz) per Hz.

The PV model, as it can be seen in Fig. 3 at the AC side, has already a relevant slot for this requirement. In order to investigate the function an over-frequency is created, by changing the *speed* parameter of the external grid component after the 7th second. The result is seen in Fig. 4.

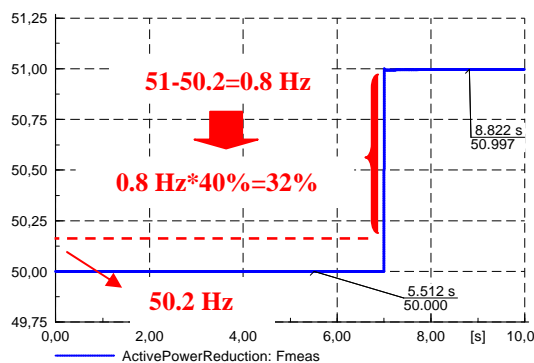


Fig. 4. Over-frequency event

In order for the control function to be in compliance with the grid code, a 32% active power output reduction should be expected since an over-frequency of 0.8 Hz is created. Indeed in Fig. 5 is proved that the generator injects around 32% (31.7%) less active power during the over-frequency. The reduction response is less than 50 ms.

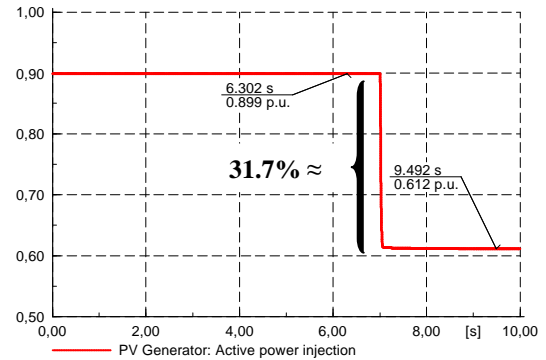


Fig. 5. Active power reduction due to 0.8 Hz over-frequency

B. Dynamic Voltage Support

When referring to dynamic voltage support, it simply implies the requirements that a PV system should fulfill under fault conditions and grid disturbances (voltage dips). Furthermore, it defines the system's behavior after the restoration of the fault. These requirements include Fault-Ride-Through (FRT) requirements and reactive current injection.

FRT describes possible scenarios of different voltage dips and how the grid-tied PV system, more specifically the PV inverter, should behave depending on the voltage dip and its duration. The PV inverter should remain connected to the grid for a certain period and if necessary support it by providing reactive current. The possible scenarios are described thoroughly in [11].

As cited before, the model contains a *Reactive Power Support* slot responsible for providing reactive current during voltage dips. To investigate this requirement, four different tests take place. In each test a different voltage dip is simulated for a different duration of PV of time. The tests performed are seen in Table 2.

TABLE 2: TESTS PERFORMED FOR FRT BEHAVIOR

| Test | Maximum line-to-line voltage U/U_n | Duration of fault [ms] |
|------|--------------------------------------|------------------------|
| 1 | 0 | 150 |
| 2 | 0.2 | 550 |
| 3 | 0.5 | 1000 |
| 4 | 0.8 | 1500 |

The tests are designed according to the specific standards for FRT examination in type-2 generating units. Type-2 units are those where no synchronous generator is involved that is directly coupled to the grid. Those standards are found in [12] for generating units and the German grid code. The different voltage dips are achieved by adjusting the fault impedance. All the obtained results are summarized in Table 3, while in Fig. 6 the results of Test 1 are seen, which corresponds to a pure short-circuit fault (100% voltage dip).

TABLE 3: AGGREGATION OF THE RESULTS OF ALL TESTS

| Voltage dip [%] | Voltage level in the LV bus [p.u.] | Injected active power by the PV [kW] | Injected reactive power by the PV [kVar] | Injected reactive current by the PV [kA] |
|-----------------|------------------------------------|--------------------------------------|--|--|
| 100 | 0.057 | 0 | 26.72 | 0.681 |
| 80 | 0.248 | 30.54 | 93.35 | 0.542 |
| 50 | 0.525 | 138.15 | 124.55 | 0.342 |
| 20 | 0.834 | 348.35 | 68.75 | 0.119 |

Seeing the results of the above table, the following conclusions can be drawn. Starting with the most expected outcome, when the voltage drop becomes bigger the active power injection of the PV generator is less and in a pure three-phase fault the injected active power is 0. The reason for this reduction of active power is to enhance the ability of the PV generator to provide reactive power for the voltage support. As seen in this case, the method is to reduce slowly the active power injection and increase at the same time the reactive power supply. Another method could have been to reduce at once the active power to zero, below a certain voltage dip (i.e. 70%), and increase the reactive power supply to facilitate the voltage stability.

As far as the reactive current injection and the voltage level at the connection point of the PV generator is concerned, which is the actual purpose of this investigation, it is seen that the reactive current injection is bigger when the voltage dip is bigger, trying to support the voltage until the fault clearance. The voltage at the connection point is never 0 not even for the 100% voltage dip, where the generator remains connected for a maximum of 150 ms (typical operating time for protection relays) providing reactive current. Furthermore, the response time of the controller for injective reactive current is found to be almost instant (less than 30ms), therefore, the results are in accordance with the grid code. The reactive current injection follows eq. 2, where K is the droop parameter, which is 1 for this case. However, normally a factor of 2 is used as default, which is equivalent for the behavior of a synchronous generator. The value du_{ac} is the result of $u_{ac}/before\ the\ fault - u_{ac}/during\ the\ fault$.

$$i_q = K |du_{ac}| \quad (2)$$

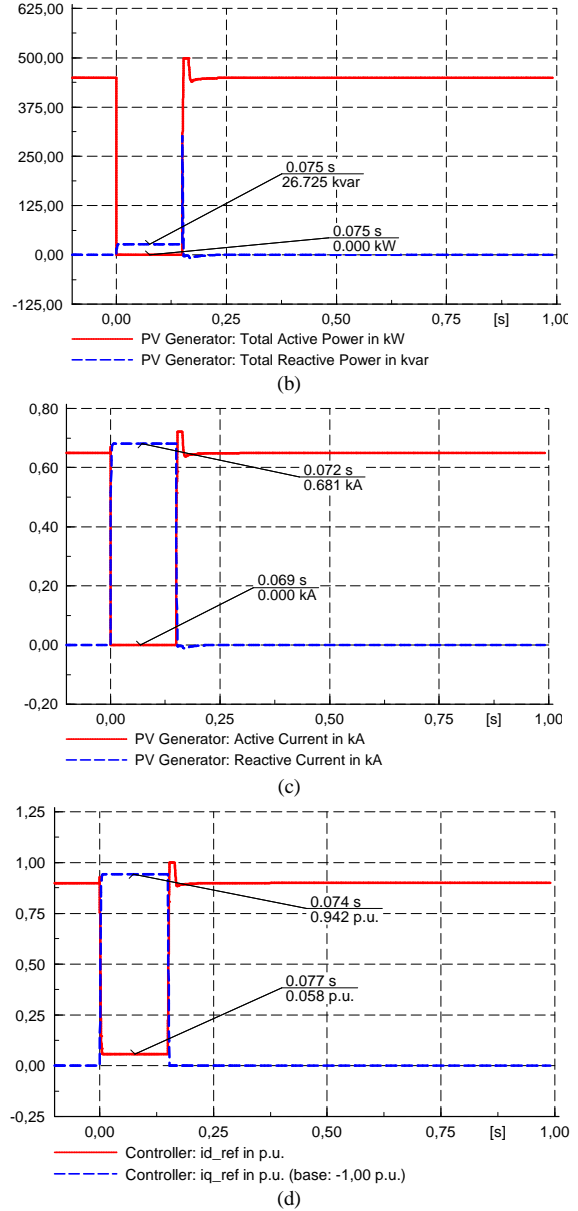
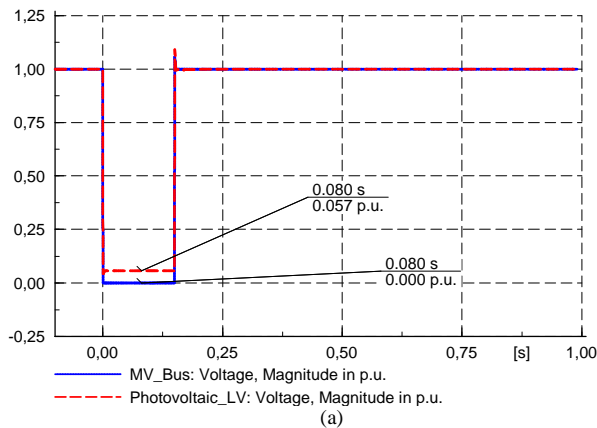


Fig. 6. FRT results during a pure short-circuit fault: (a) voltage level in LV and MV bus, (b) active and reactive power injection by the PV generator, (c) active and reactive current injection by the PV generator, (d) reference values of the i_d and i_q components of the controller

Finally, the injected reactive power by the generator is dependent on two inversely proportional factors, the voltage level and the reactive current. Thus, the maximum value should be at voltage dip of 50%, which is the case as seen in the Table 3.

The reactive current injection and LVRT requirements are fulfilled in each of the 4 tests that the PV model is examined. The voltage stabilizes almost instantly after the fault clearance ensuring that the PV is capable of dynamic voltage support.

C. Static voltage support

One important weakness of the model is the lack of ability to provide static voltage support under normal operation of the grid. The PV system must be able to address small voltage deviations at the point of connection and according to the

German grid code for MV the generator should be able to supply reactive power to maintain the voltage band within steady state operation limits (see Table 1). In order to correct this shortcoming and improve the model, a Q control is proposed, which is seen in Fig. 7.

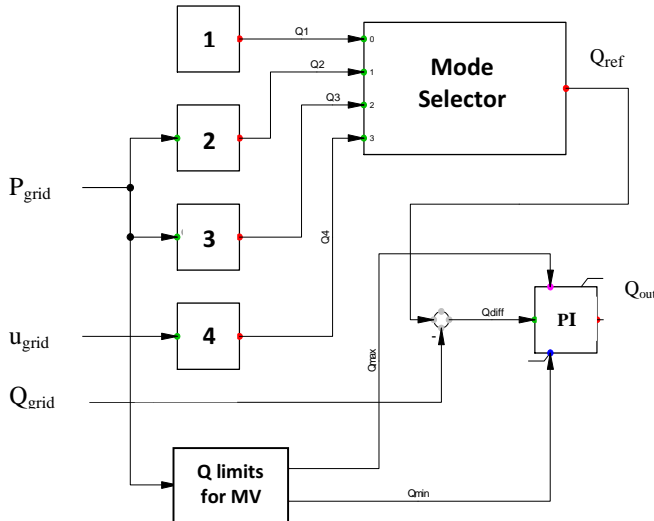


Fig. 7. Proposed Q control

The Q control is designed to operate in four different modes, which are presented in Table 4, depending on the system operator. The necessary input signals are the active power (P), the reactive power (Q) and the voltage (u) at the connection point of the PV generator (inverter).

TABLE 4: DIFFERENT OPERATING MODES FOR Q CONTROL

| Mode selector | Method of Q supply |
|---------------|---|
| 1 | Constant Q (based on a set-point value) |
| 2 | Constant cos ϕ (Q based on a set-point value of PF) |
| 3 | Function cos ϕ (P) (Q based on PF, which is dependent on P) |
| 4 | Function Q(U) (Q based on voltage) |

The controller “reads” the input values and according to the selective mode produces a Q_{ref} value. The mode selection is done by changing the parameter *Mode* from 1 to 4 in the parameter table. The Q_{ref} is then compared with the measured value of reactive power at the connection point, denoted as Q_{grid} in Fig. 7 and the difference (Q_{diff}) passes through a PI controller. The PI block is used to limit the Q_{diff} , in order the controller to provide a reactive power, which is as close as possible to the required Q_{ref} value. The PI controller uses as upper and lower limitation the values produced by the *Q limits for MV* block, which calculates the total maximum and minimum reactive power capability based on the active power at the connection point and Fig. 8.

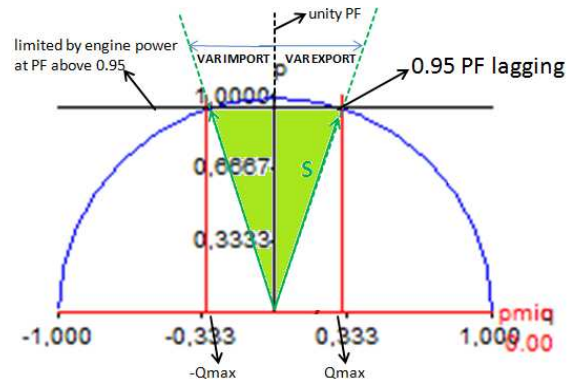


Fig. 8. Q Capability requirements according to MV grid code

The shaded area in the above figure reflects the reactive power capability requirements according to the grid code for MV. The PV inverter should be able to provide reactive power within the area defined by 0.95_{lagging} and 0.95_{leading} PF.

The final signal from the PI controller (Q_{out}), which is in fact a reactive current component, passes through the main controller and then leads to the PV generator (PV inverter). Inside the main controller the signal is not subjected to further modifications. However, for normal operation and voltage dip bigger than 10% the reactive current injection and subsequently the reactive power is provided by this Q_{out} value. Thus, inside the main controller there is a “switch” that changes between normal and fault operation according to the voltage deviation (voltage drop).

In order to test the effectiveness of the implemented control a parameter event is set, where the active power injection by the static generator is being changed and specifically is being reduced from 450 kW to 250 kW as seen in Fig. 9. That can be the result of solar radiation change by setting a parameter event and changing the E value from Fig. 3. With this test the first three methods of Table 4 are examined.

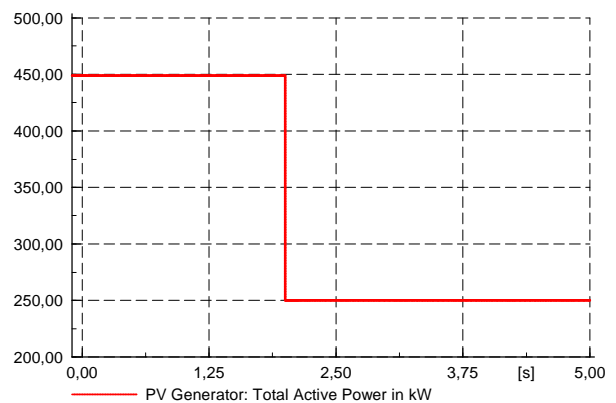


Fig. 9. Active power injection change

The Q controller is set at first to operate in Mode 1, then in Mode 2 etc. The constant Q in Mode 1 is chosen 56 kVar (which gives PF around 0.99, taking into consideration the nominal active power), while the PF in Mode 2 is chosen 0.98. In Fig. 10 the measured values of the reactive power at the connection point and for each method are presented in response to the parameter event.

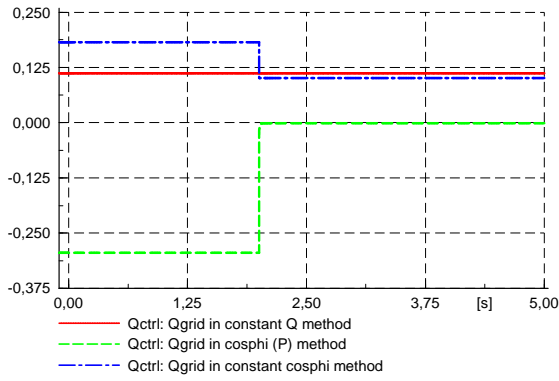


Fig. 10. The measured values of the reactive power at the connection point in each method

The results of the above graph show that when the controller operates in Mode 1, produces a constant value of reactive power based on the given set-point (reference value).

On the other hand, when the controller operates in Mode 2 (constant cosphi) and the active power is reduced at the connection point, the reactive power is reduced as well in order to maintain the PF constant at 0.98. That behavior can be clearly seen in Fig. 11

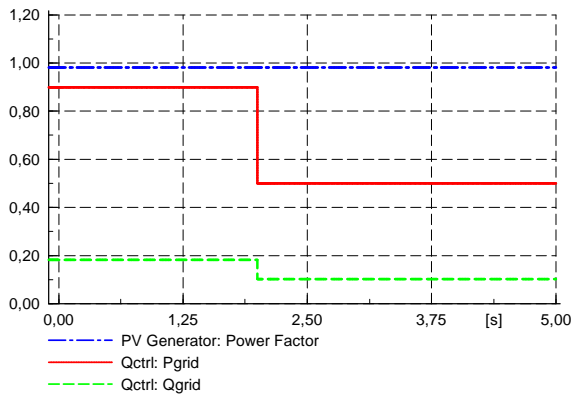


Fig. 11. The behavior of the controller under Mode 2 operation

At last when the controller operates in Mode 3, cosphi (P), the reactive power is supplied by adopting the PF according to the active power change and based on a characteristic that in reality is provided from the network operator. In this case the characteristic is seen in Fig. 12. The PF of course is kept within limits (0.95_{lagging} and 0.95_{leading}).

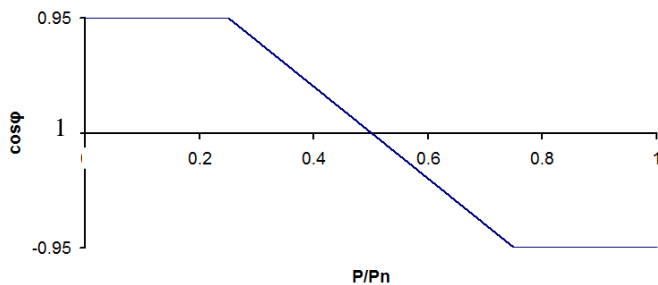


Fig. 12. The characteristic of $\cos\phi$ (P) of the controller under Mode 2 operation

As far as the last method/mode Q(U) is concerned, a different type of simulation event is set, in which, the voltage level at the connection terminal is being changed as shown in Fig. 13 with the straight line. The response of the controller in this increment of the voltage is to consume reactive power based on a specific droop.

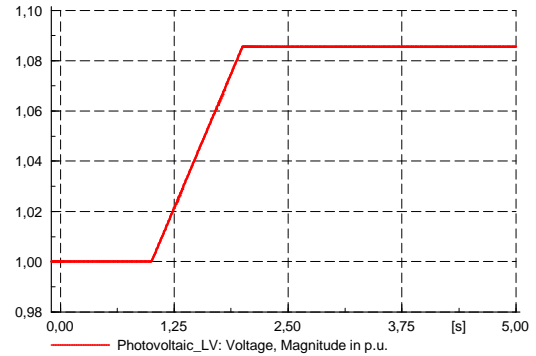


Fig. 13. Voltage change profile in Q(U) method

The marked area in the below Fig. 14 shows that the controller reached its limitations.

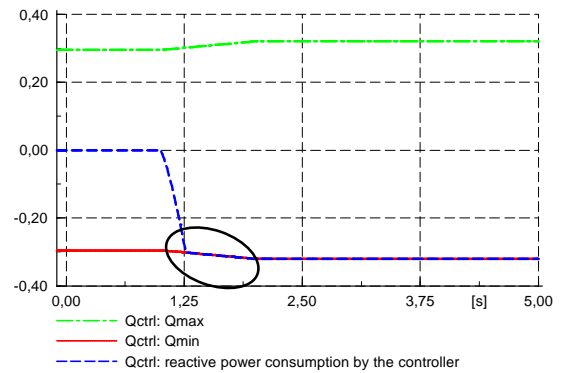


Fig. 14. Reactive power support in Q(U) method

V. CONCLUSIONS AND RECOMMENDATIONS

In this paper important aspects of a generic PV model built by DiGSILENT are examined. The model consists of a static generator with an integrated control scheme. Its static and dynamic behavior is investigated according to the requirements of the German grid code for the MV distribution network.

Active power reduction requirement is effectively adjusted and operates in case of over-frequency events. The FRT requirement is tested under four different voltage dips of different duration each according to [12] for type-2 generating units. The results support the capability of the PV model in question to remain connected when a voltage dip occurs and provide reactive current when is needed according to the grid code. Thus, the grid stability is enhanced at the point of connection since remaining the generator connected is able to provide active power the moment the grid is stabilized without jeopardizing further the grid reliability (e.g. creating frequency problems under excess load conditions, leading to supply

failure and even blackouts).

As far as the static voltage support is concerned, initially the model had no relevant control. For this reason, a Q control is implemented capable to operate in four different modes as it is described by the grid code. The controller shows sufficient behavior when changes of active power and voltage take place at the terminal that the generator is connected. The switch between static voltage support and dynamic voltage support in case of a fault is inside the main controller and ensures reactive power support in any occasion.

However, there are still many issues to be tested and improvements to be done in order the model to be able to address a wider range of requirements. Power quality studies and protection requirements are some of those issues. Furthermore and since the model includes an array model, the need of a more adequate PV array model is also necessary since no resistance losses are taken into account for the output values. However, for performing studies to examine the behavior of the network, this improvement is not considered necessary.

Rounding up the conclusions of this paper, in response to the fact that policies and incentives have brought PV market to the fore, attention should be turned to address design and control issues that will encourage a high PV penetration without compromising the stability and normal operation of the power system.

VI. ACKNOWLEDGMENTS

The authors would like to acknowledge the valuable contribution of Stefan Langanke on improving the control scheme of the generic model. His work as regards the Q control has been used in this paper. Stefan Langanke is a member of the Energynautics team working on various topics concerning electrical power supply and integration of renewable energies to the grid.

VII. REFERENCES

- [1] Brown M., "Integrating PV in Local Distribution Systems -Germany-", IEA PVPS Task 14 Meeting, Golden, CO, USA, 01.12.2010, available at www.nrel.gov/eis/pdfs/iea_task_14_workshop_braun.pdf, as accessed 25.02.2011
- [2] European Commission, "National Renewable Energy Action Plan in accordance with Directive 2009/28/EC on the promotion of the use of energy from renewable sources", Status report of Federal Republic of Germany, European Commission, 30.6.2010
- [3] Prognos, Roland, Berger, "Photovoltaik wird zur tragenden Säule der Energieversorgung", Bundesverband Solarwirtschaft (BSW), picture available at <http://www.solarwirtschaft.de/>, as accessed 25.06.2011
- [4] Borup Uffe, "Features of modern grid interconnection devices", Danfoss, PV ERA NET The Photovoltaic European Research Area Network, available at http://www.pv-era.net/doc_upload/documents/179_5Featuresofmoderngridinterconnectondevices.pdf, as accessed 27.02.2011
- [5] Teodorescu R., Liserre M., Rodriguez P., *Grid Converters for Photovoltaic and Wind Power Systems*, Wiley, United Kingdom, 2011

- [6] TransmissionCode2007 – Network and System Rules of the German Transmission System Operators, Verband der Netzbetreiber VDN e.V. beim VDEW, Berlin, 2007
- [7] Generators connected to the low-voltage distribution network – Technical requirements for the connection to and parallel operation with low-voltage distribution networks, Verband der Elektrotechnik Elektronik Informationstechnik e.V., VDE, Berlin, August 2011
- [8] Alvaro R., "System aspects of large scale implementation of a photovoltaic power plant", Master Thesis, KTH, Stockholm, Sweden, March 2011
- [9] Blazic B., Papis I., "Voltage profile support in distribution networks – influence of the network R/X ratio", *Power Electronics and Motion Control Conference 13th (EPE-PEMC)*, available at *IEEE Xplore*, 30.09.2008
- [10] Theologitis I.T., "Comparison of existing PV models and possible integration under EU specifications", Master Thesis, KTH, Stockholm, Sweden, June 2011
- [11] Troester E., "New German Grid Codes for Connecting PV Systems to the Medium Voltage Power Grid", *2nd International Workshop on Concentrating Photovoltaic Power Plants: Optical Design, Production, Grid connection*, Darmstadt, Germany, 09-10.03.2009
- [12] Fördergesellschaft Windenergie und andere Erneuerbare Energien (FGW e.V.), "Determining the electrical properties of generating units at medium, high and very high voltage grid", Technical Guidelines for generating units, Germany, 15.10.2010

VIII. BIOGRAPHY



Ioannis-Thomas Theologitis was born in Kavala in Greece, on May 26, 1984.

Since 2011, he holds a Master in Sustainable Energy Engineering from the Royal Institute of Technology (KTH) in Stockholm, Sweden. He obtained his Diploma in Electrical Engineering and Computer Engineering from the Democritus University of Xanthi, Greece in 2008. His main focus is on solar energy with experience in photovoltaic technology, modeling, market and policy issues. Since 2011 he works for Energynautics.



Eckehard Tröster was born in Marburg in Germany, on December 7, 1975.

He holds a PhD and a Master of Electrical Engineering from Darmstadt University of Technology, Germany. His research focuses on electrical power systems, renewable energies and electrical machines, especially wind power generators. He has worked as a scientific assistant at the Institute of Renewable Energies, Darmstadt. Since 2007 he works for Energynautics.



Thomas Ackermann is the founder and CEO of Energynautics GmbH a research and consulting company in the area of renewable energy and power systems. He also lectures at Royal Institute of Technology (KTH), School of Electrical Engineering in Stockholm/ Sweden. He holds a degree of a Diplom Wirtschaftsingenieur (M.Sc. in Mechanical Engineering combined with an MBA) from the Technical University Berlin/ Germany, an M.Sc. in Physics from Dunedin University/ New Zealand and a Ph.D. from the Royal Institute of

Technology in Stockholm/ Sweden. He is the editor of the book "Wind Power in Power Systems" and Co-editor of the Wind Energy Journal, both published by Wiley.

Evaluating the Impact of PV Module Orientation on Grid Operation

Eckehard Tröster, Jan-David Schmidt

Energynautics GmbH
Darmstadt, Germany
e.troester@energynautics.com

Abstract— A large number of photovoltaic (PV) systems in the power system can cause a variety of different problems in grid operation. As PV modules can have different orientation, the influence on the grid operation, such as power gradients, voltage issues or overloading of assets, is also different. In order to evaluate the impact of PV module orientation on these issues various characteristics of seven differently orientated PV systems have been investigated: seasonal capacity factor, power gradients, peak power, area utilization, and correlation between generation and consumption. The capacity factor decreases for systems with a suboptimal orientation, but on the other hand the generated peak power is also lower. This is beneficial in case of voltage problems and asset overloading. Power gradients are lower and the energy production therefore smoother which leads to a reduced need for conventional power plants or other flexibility options to follow the gradients. East/West oriented PV systems achieve higher area utilization and yield per surface area and may negate the effect of peak power reduction. The correlation of production and consumption of PV systems not facing south is worse while a south orientated façade system has the best correlation.

Keywords-PV; capacity factor; power gradient; peak power; area utilization; correlation

I. INTRODUCTION

The current strategic objective of Europe's energy policy is to reduce greenhouse gas emissions by 60-80 % by 2050 compared to 1990 [1]. This involves a commitment to achieve 20 % reduction by 2020 through the improvement of energy efficiency by 20 % and increasing the share of renewable energies to 20 % [2]. This commitment has stimulated the growth of distributed energy resources and especially PV systems.

The integration of renewable energy sources into the already existing infrastructure is a challenging task. Wind and solar power do not necessarily follow energy demand, but rather produce energy when their respective resource is available. A high penetration of renewable energy may lead to less correlation of a large proportion of energy production to demand. Since energy production and consumption within an electricity network always need to be balanced, a higher correlation is desired in order to lessen the needed controlling power range. A lower correlation of production and consumption at the lower voltage level also leads to

over voltage problems and a power flow into the higher voltage level.

The problem of over voltage stems from the peak power generation of PV systems during midday. A lower peak power would be beneficial in counteracting the issue, but decreases the yield of the PV system. A different orientation, instead of the much preferred south orientation, may be beneficial in this case. Ideally the energy production in the morning and evening could be higher, while the peak at midday is reduced. This potential behavior shall be investigated by exploring the change in key characteristics of PV energy production. The identified key characteristics are the capacity factor, power gradients, peak power, yield per surface area and correlation of production and consumption. Since the capacity factor corresponds to the yield per year and is a key indicator of profitability and likelihood of occurrence, it is considered first. Power gradients and peak power are relevant for grid operation and influence the system as a whole as well as at their respective connection point. The yield per surface area has an impact on system sizes and therefore influences potential peak power and yield. Since the balance of electrical generation and consumption always needs to be maintained in the grid, the correlation of these two is relevant for stability and difficulty of operation.

II. PV SYSTEM SETUPS

Seven PV system setups with different orientations were investigated. Their output was modeled for the city of Aachen in Germany (50°46'23" North 6°6'7" East). An overview of the setups can be found in Table I.

TABLE I. SETUP OF PV-SYSTEMS

| PV System No. | 1 | 2 | 3 | 4 | 5 | 6 | 7 |
|---------------|-------|-----|-----------|-----|-----|-----|----------|
| Orientation | South | | East/West | | | | Tracking |
| Inclination | 35° | 90° | 0° | 15° | 35° | 90° | Tracking |

The first PV-system is the reference system since it is usually the first choice when installing new PV modules. The second PV-system is a façade installation orientated to the south. The third PV-system is a horizontal system, which has been included for comparison reasons. These systems are normally not installed, as they tend to lose their

performance very fast due to dirt, which cannot be washed away by rain. The fourth and fifth systems are east/west configuration with different inclination angles. The orientation east/west means half of the installed system faces east while the other half faces west. This is also true for PV-system No. 6, which is also a façade system. Finally the tracking system is supposed to indicate the maximum possible energy yield at the chosen position. These seven PV-systems cover the whole range of reasonable PV orientations and should therefore be sufficient to get a good picture of the impact of PV module orientation on grid operation.

III. IRRADIATION DATA

In order to obtain irradiation data for the different orientations and inclinations the “Photovoltaic Geographical Information System” (PVGIS) [3] was used. With the given position, orientation and inclination, the system compiled a data set for a day of a specified month. These data sets contained typical daily irradiation values on a fixed plane or on a tracking plane. The obtained values were subdivided into average irradiation and clear-sky irradiation on a 15 minute scale. Clear-sky irradiation was used to determine maximum ramp rates and peak power values over the course of one year. The energy output of the PV-modules was derived through evaluation of the average irradiation. Figure 1 displays the average power generation of a day in April for all considered PV-setups.

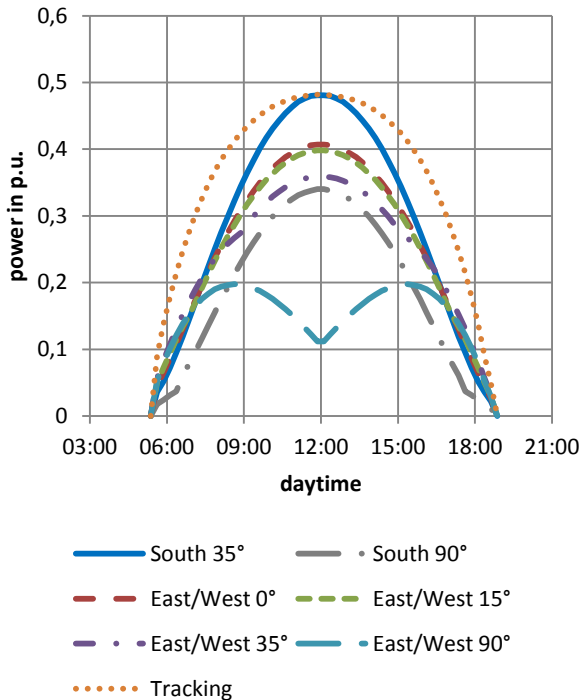


Figure 1. Average power generation of a day in April for all considered PV-setups

IV. RESULTS

A. Capacity Factor

A PV system is intended to produce energy that can be sold or consumed by the owner. Therefore it is important to evaluate the impact of different orientations and inclinations on the energy yield. The orientation and inclination of PV modules determines the average daily irradiation on the system. The irradiation is directly linked with the power generation through size and efficiency of the PV-system.

The capacity factor of the production is the ratio of yearly energy yield to theoretical generation capability per year (nominal power times 8760 h/a). When multiplying the capacity factor with 8760 h the number of full load hours can be determined. Figure 2 gives an overview of the capacity factor of all investigated setups.

The highest energy yield can be achieved with a tracking system; it is roughly 20 % higher than the south orientated system. East/West orientated systems are only slightly worse than south orientated; 10 to 20% less yield has to be taken into account as long as the inclination of the roof is not too high. A PV system on an easterly and westerly façade (PV system No. 5: East/West 90°) would produce 35% less energy than a south orientated façade system and 50% less than a south orientated system with optimal inclination. Such a system would be from an economic point of view not recommendable.

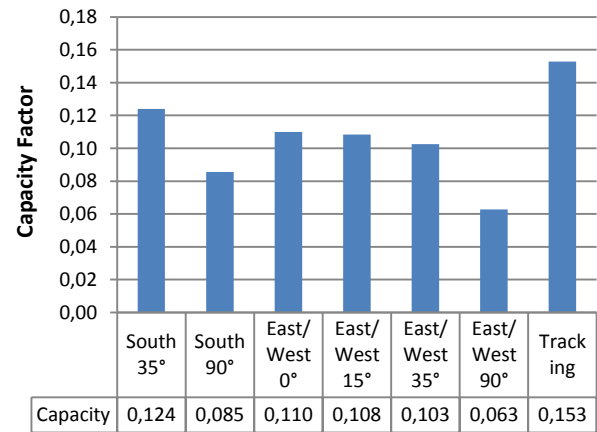


Figure 2. Capacity Factor

The load profile of residential customers in Germany is called the “H0-Profile”. It predicts the energy consumption of an average household and is normalized to a yearly consumption of 1000 kWh/a. When considering the standardized H0-Profile, there is a higher demand for electric power in winter (see Figure 4). Therefore it is reasonable to consider power generation per month. Figure 3 depicts the capacity factor of each PV setup per month.

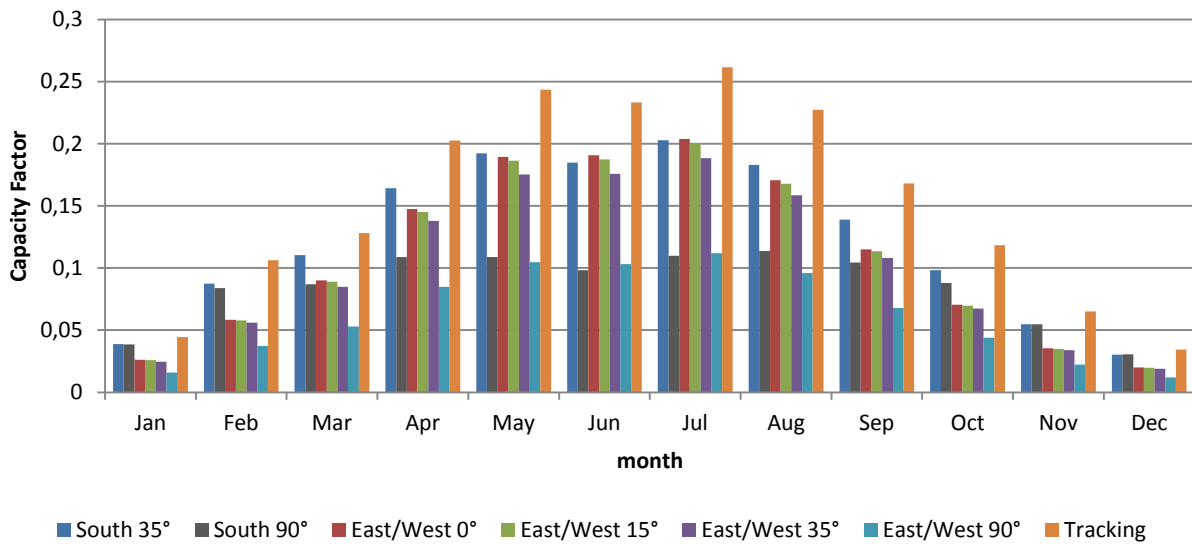


Figure 3. Monthly Capacity Factor

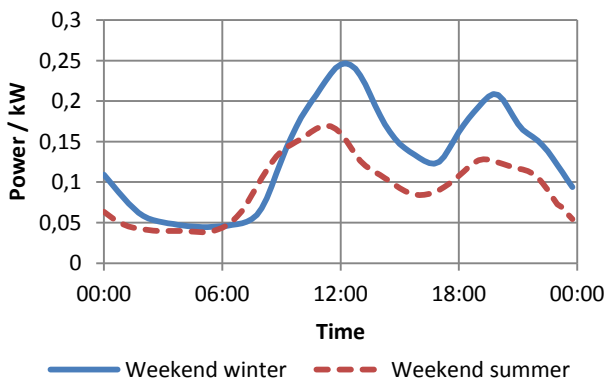


Figure 4. Typical residential customer load profile (H0-Profile)

Due to the course of the sun in summer (i.e. sunrise in the north-east and sunset in the north-west and the sun being higher in the sky) the capacity factor in June and July of an east/west orientated PV system is higher than the one of a south facing system. However when the power is really needed in the wintertime, the capacity factor of an east and west orientated PV-system is lower. A south orientated façade system provides a good capacity factor in the wintertime, while yielding slightly less in the summertime. With respect to the capacity factor, the east/west orientated system is therefore inferior to the south oriented systems.

B. Power Gradients

The energy production of solar power plants in Germany has priority dispatch and must be distributed by the grid [4]. Other power plants need to be able to follow the combined gradients of solar power generation and consumption. This is especially critical in the evening, when the sun sets and consumption grows. Hence a lower gradient for PV-systems is more desirable. Otherwise, more conventional power plants would need to be in reserve in order to match generation and consumption [5].

The values for maximum gradients within 15 minutes are shown in Figure 5.

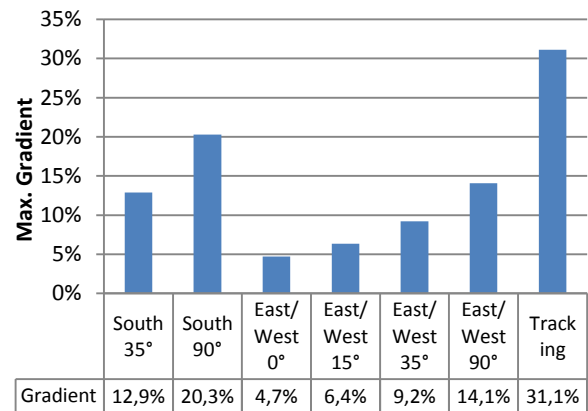


Figure 5. Maximal absolute gradient rated to nominal power within 15 minutes

These gradients are based on the clear-sky irradiation due to the course of the sun, especially at sunrise and sunset. Of course the ramp rates of individual PV systems can be much higher e.g. when a cloud is passing through, however this would be of stochastic nature and the correlation between various PV systems is in this case very low, whereas on a clear-sky the correlation between PV installations is very high, thus the gradients due to the course of the sun are the overall highest gradients to be expected.

When comparing the PV systems in Figure 5 the highest gradients can be found for tracking systems closely followed by a south façade. The lowest gradients exist for low inclination combined with an east/west orientation. Here the energy production is smoothed compared to a south oriented system. From grid operation point of view, east/west systems are therefore advantageous in terms of gradients versus south orientated or tracking systems. However this is only true for unrestricted operation. In case gradients do really produce a grid operational problem, the gradients of the PV system can be limited using the (maximum) power point tracker of the inverter as depicted in Figure 6. This is particular true for positive gradients, but also negative

gradients can be limited to a certain extent, as the clear sky power production curve can be very well predicted. The reduction in yield depends on the chosen maximum power gradient.

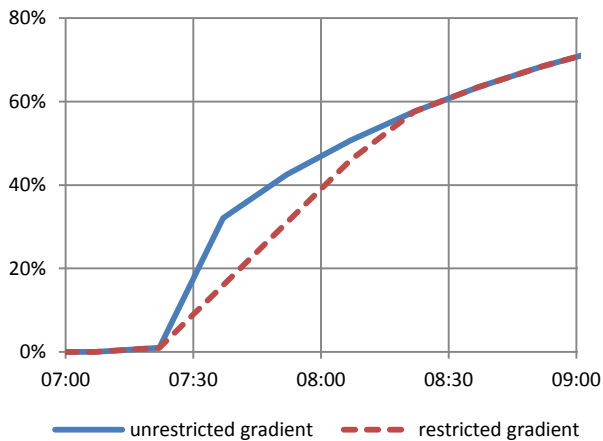


Figure 6. Example of limitation of the maximum power gradient of PV System No. 7 (Tracking)

C. Peak Power

Depending on the size of the solar power plant it will either be connected to the low-voltage grid or the medium-voltage grid. Especially in the low-voltage grid the maximum peak power generation of a PV-system determines the voltage level at the connection point and loading of transformer and cables. A high peak power and high penetration of PV may cause a breach of the allowed voltage or overloading of utilities. This could lead to costly extensions of the low-voltage grid.

As shown in Figure 7 an east/west orientation reduces the maximum peak power in relation to a south oriented PV-module. A higher inclination is beneficial in further reducing the maximal peak of east/west oriented systems.

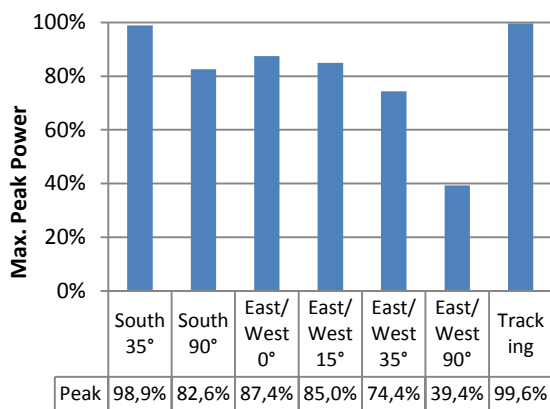


Figure 7. Maximal peak power rated to nominal power

The peak power reduction and the reduced yield compared to PV system No.1 is shown in Figure 8. Peak shaving refers to using PV system No.1 and cutting its power output at 70% of its nominal power. This results in a reduction in the yield of about 5% [6].

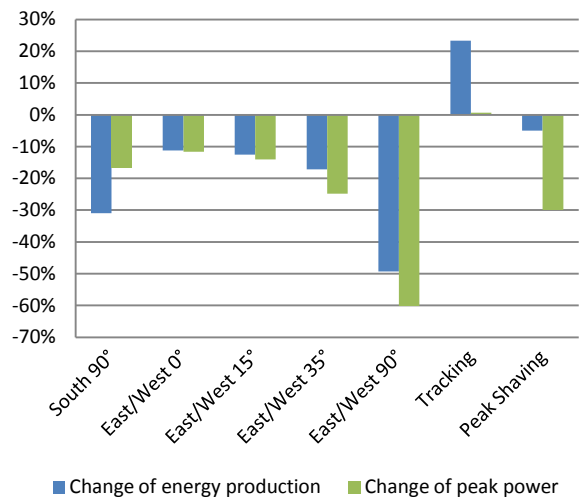


Figure 8. All PV Setups compared to PV System No. 1: South 35°

The result for a south façade system is very unfavorable, as the reduced yield is twice as high as the favorable peak reduction. For east/west orientated PV systems at a low inclination the reduction of peak power and of the yield is almost equal at a low inclination. A higher inclination (East/west 35° and 90°) pulls the individual peaks of the east and west orientated modules in relation to daytime further apart. Therefore the reduction in peak power is higher than that of the yield compared to a south oriented system. A tracking system provides higher yield without an increase of peak power. Peak shaving on the other hand provides a significant reduction of peak power while the reduction in yield is less severe.

Figure 9 displays an example of the lower peak power and lower gradients of an east and west oriented PV system in comparison to a south oriented system. The conditions are clear-sky on a day in May.

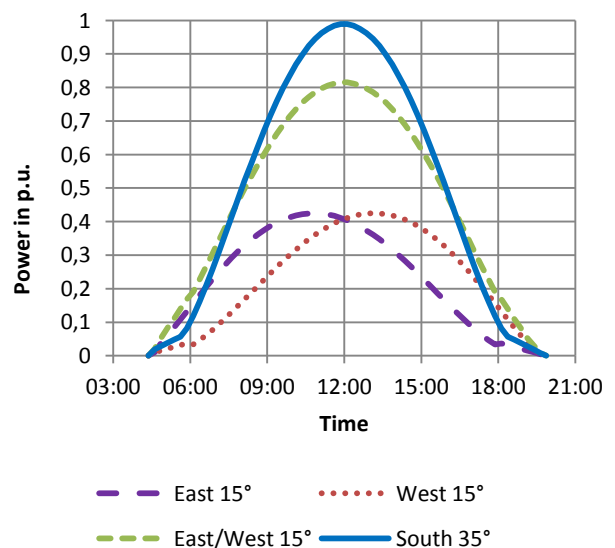


Figure 9. Comparison of the PV production on a clear day in May

D. Yield per surface area

An advantage of east/west oriented PV modules on rooftops or on an open field is the different arrangement of the system. On rooftops it may be possible to use double the amount of space compared to a south facing system, if both sides of the roof can be filled with PV modules. In an open field an area utilization of 35-40% for south oriented modules can be achieved, while an east and west oriented system has an area utilization of 70% [7]. The low area utilization of south oriented modules is given by the need to avoid shadowing.

While better area utilization is beneficial for the owner, it also compensates the lower peak power at midday due to bigger possible system sizes. This counteracts the potential of lower load and over voltage within the low voltage level. Considering an open field and filling it with PV modules would result in a 75% higher installed capacity for an east/west oriented system compared to a south oriented system. Figure 10 displays the increase of peak power and the gain of energy production compared to PV System No.1. Since façade systems would not be feasible on an open field and horizontal systems would be difficult to keep clean they have not been considered. The previously observed benefit of reduced peak power has changed to a significant increase, however the energy yield has increased even more.

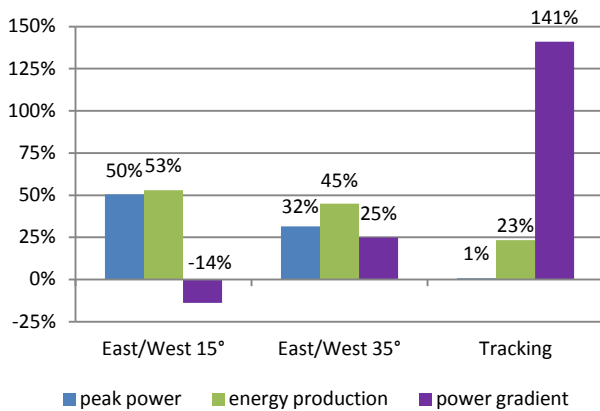


Figure 10. Effects of open field area utilization compared to PV System No.1: South 35°

E. Correlation between Production and Consumption

Assessing the matching of generation and consumption can be done through evaluation of the correlation coefficient. A correlation coefficient with respect to consumption can be within the range of minus one and plus one. A value near minus one implies a high correlation between generation and consumption whereas a value near zero means no correlation and a value near plus one indicates an anti correlation [8]. The standardized H0-Profile was used to represent the consumption, because most of the decentralized PV production should be consumed within the low voltage grid by households in order to minimize grid load. Since the average production of a PV system is in principle axially symmetric either side of midday, it has positive and negative gradients which can be more closely evaluated. Therefore the correlation coefficient over the course of one year has been calculated for the whole day, in the morning from 0 am to 12 am and in the afternoon from 0 pm to 12 pm.

The results depicted in Figure 11 indicate a worse correlation between production and consumption when PV-modules are not facing south. A higher inclination of PV-modules oriented to the east and west even worsens the relationship. The higher positive values for the latter half of the day are implying that the production decreases at the same time as the load increases. The best correlation can be observed when using south oriented façade systems.

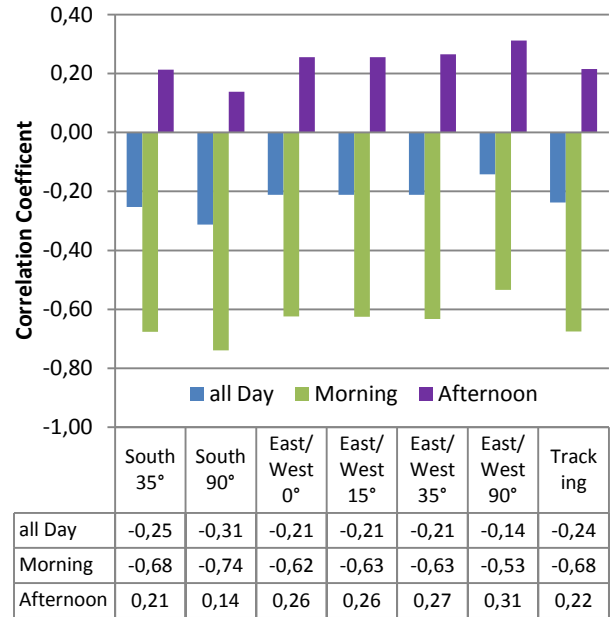


Figure 11. Correlation coefficient between PV production and load

V. CONCLUSION

This paper investigates the difference between south oriented and east/west oriented PV modules with respect to grid related characteristics. Table II gives a rated overview of all key characteristics related to PV energy production. As a benchmark of the rating, the seven PV systems are compared among each other and not against other technologies like conventional power plants.

When analyzing this table, there is no obvious optimal orientation for grid operation. Every PV setup has its pros and cons.

System No. 1 facing south with an optimal inclination performs well when looking at the energy yield, especially also in winter time. The power gradients and the peak power are pretty high, inducing some problems for grid operation. However, by limiting the peak to 70% and also restricting the gradients, this system can achieve the same good characteristic as the east/west orientated systems. The results for energy yield on an equivalent area do show an inferior characteristic compared to east/west. The correlation between production and consumption is remarkably good.

System No. 2, the south façade, performs especially well in energy yield during winter time and the correlation with consumption. Otherwise the overall yield is fairly bad.

System No. 3, the horizontal modules, is naturally good in terms of power gradients, however it has only an average correlation characteristic and a small energy yield during winter time.

TABLE II. CONCLUSION OVERVIEW

| PV System No. | | | 1 | 2 | 3 | 4 | 5 | 6 | 7 |
|--|-----------------|---------|-------|-----------|-----------|-----------|------|-----------|-----------|
| Orientation | | | South | | East/West | | | | Tracking |
| Inclination | | | 35° | 90° | 0° | 15° | 35° | 90° | Tracking |
| Equivalent rated power | Yield | overall | good | bad | o.k. | o.k. | o.k. | very bad | very good |
| | | winter | good | good | bad | bad | bad | very bad | very good |
| | | summer | good | very bad | good | good | good | very bad | very good |
| | Power Gradients | | o.k. | bad | very good | very good | good | o.k. | very bad |
| | Peak Power | | bad | o.k. | o.k. | o.k. | o.k. | very good | bad |
| Equivalent area | Yield | overall | bad | n/a | n/a | very good | good | n/a | o.k. |
| | | winter | o.k. | n/a | n/a | good | good | n/a | good |
| | | summer | bad | n/a | n/a | very good | good | n/a | o.k. |
| | Power Gradients | | good | n/a | n/a | very good | o.k. | n/a | very bad |
| | Peak Power | | good | n/a | n/a | bad | o.k. | n/a | good |
| Correlation between production and consumption | | | good | very good | o.k. | o.k. | o.k. | bad | good |

System No. 4, east/west orientation with a small inclination, has a very good natural power gradient for an equivalent rated power. However the main advantage of such a system is the usage of space. This system is particular good in overall energy yield when looking at an equivalent area. However in this case the peak power might induce some grid operational issues.

System No. 5, east/west with a higher inclination, is very similar but in many cases not as good as system No.4.

System No. 6, east/west façade, is probably the worst system. The only advantage is a fairly low power gradient and very low peak power.

System No. 7, tracking, could probably emulate all other systems. Due to its ability to capture as much energy as possible it has the highest yield but also produces, if not restricted, the highest power gradients and peaks.

All results have been determined based on calculations of a location in Germany and are therefore quite specific for Germany's latitude. For other latitudes the results will be slightly different, i.e. further to the north (e.g. Sweden) the south facing system will be more advantage and further to the south (e.g. Portugal) the advantages of East/West might be more pronounced.

REFERENCES

- [1] European Commission . Communication from the Commission to the European Council and the European Parliament - an energy policy for Europe. Brussels. January 2007.
- [2] European Commission. Limiting Global Climate Change to 2 degrees Celsius - The way ahead for 2020 and beyond. Brussels. January 2007.
- [3] European Commission, Joint Research Centre, Institute for Energy, Renewable Energy Unit. Photovoltaic Geographical Information System (PVGIS). <http://re.jrc.ec.europa.eu/pvgis/>.
- [4] Bundesministerium für Umwelt, Naturschutz und Reaktorsicherheit. Gesetz für den Vorrang Erneuerbarer Energien. 2012.
- [5] Consentec / IAEW. Bewertung der Flexibilität von Stromerzeugungs- und KWK-Anlagen. Berlin. October 2011.
- [6] Podewils, Christoph. Warum nur 30 Gigawatt? Photon. 2012, 12/2012.
- [7] Heuser, Ralf. Ost-West ist Trumpf. Photon. 2012, 6/2012.
- [8] Etherden, Nicholas. Increasing the Hosting Capacity of Distributed Energy Resources Using Storage and Communication. Luleå. 2012.

Considerations on the Modeling of Photovoltaic Systems for Grid Impact Studies

Vladimir Čuk, Paulo F. Ribeiro, Joseph F.G. Cobben, Wil L. Kling, Fridrik R. Isleifsson, Henrik W. Bindner, Nis Martensen, Afshin Samadi, and Lennart Söder

Abstract-- Photovoltaic systems continue to be deployed at increasing levels and their impact on the electric grid needs to be evaluated more accurately. This includes the impact both in the local grid where they are connected and the impact on the operation of the whole system. As a consequence, adequate models of panels, inverters, and the rest of the grid are required. Models of photovoltaic systems need to characterize their dominant characteristics and effects on the electric grid for the different types of studies, i.e. load flow, harmonic distortion, voltage stability and electromagnetic transient studies. This paper gives an overview of models that are currently in use for different types of grid impact studies, and points to their applications and limitations.

Index Terms—Photovoltaic, Grid impact, Model.

I. INTRODUCTION

Grid connected photovoltaic (PV) systems have been used for several decades already. The number of systems installed and their rated power are growing, and they are connected from low to high voltage networks. Their influence on the overall electric grid is becoming more significant, and significant attention should be given to future scenarios and preventing possible problems, as well as to increasing efficiency and reliability.

Evolution of PV modules, inverters, and requirements for connecting PV systems to the grid is constantly asking for new grid impact studies. According to a report of IEA [1], the installed PV system capacity in 22 analyzed countries was 103 MW in 1992, 678 MW in 2000, and 34953 MW in

2010. These numbers clearly show that PV systems are quickly becoming an important part of the electrical power system, and should be taken into account in system studies.

The literature is offering a number of models for power flow, stability, short-circuit, transient, and harmonic load flow studies, with details added or neglected for each specific study type. However, there is still a need for a generalized modeling approach to initiate the modeling process with the selection of the appropriate model which would emphasize the dominant effect of PVs on the system. The objective of this paper is to give an overview of available models of PV systems for different types of studies, and to explain their applications and limitations. Attention is also given to the aggregation of multiple units and their summated effect on grid operation.

An overview of characteristics of different PV models and studies is given in Table I. Each type of studies is elaborated further in a separate section.

II. MODEL FOR POWER FLOW CALCULATION

In normal steady state operation the control system of the converter determines how the solar generator must be represented. In the most common case, the generator will be operated as a PQ node. In this mode, the generator is assumed to produce constant active and reactive power. The active power contribution in reality depends on the solar irradiation, which is assumed to be constant for the point in time under investigation. The converter control system is set up to achieve a constant reactive power contribution as well, as modern converter systems can operate freely within a certain reactive power range. Converter control system modes of constant power factor or constant reactive power only correspond to different data input modes for the generation asset as a PQ node.

Due to their ability to adjust their reactive power contribution within a certain range, converter-based power plants can also be used for voltage control. When used in this function, the solar power plant must be treated as a PU node in the power flow calculation. At the PU node active power and voltage magnitude are known values, and reactive power and voltage angle are determined by the power flow calculation. As with all generation assets, the maximum currents have to be taken into account – the calculation procedure must ensure that the reactive power limits of the voltage-controlling converter are not exceeded.

Software packages usually achieve this by internally converting nodes from PU to PQ where needed.

A third variant is that setpoints can be given for both

This work is supported by Forschungszentrum Jülich – ETN, Energimyndigheten, and Energinet.dk as a part of the European project “Smart Modelling of Optimal Integration of High Penetration of PV” (Smooth PV). Project website: <http://www.smooth-pv.info/>

V. Čuk is with the Eindhoven University of Technology, p.o. box 513, 5600 MB Eindhoven, the Netherlands (e-mail: v.cuk@tue.nl).

P. F. Ribeiro is with the Eindhoven University of Technology, p.o. box 513, 5600 MB Eindhoven, the Netherlands (e-mail: p.f.ribeiro@tue.nl).

J. F. G. Cobben is with the Eindhoven University of Technology, p.o. box 513, 5600 MB Eindhoven, the Netherlands (e-mail: j.f.g.cobben@tue.nl).

W. L. Kling is with the Eindhoven University of Technology, p.o. box 513, 5600 MB Eindhoven, the Netherlands (e-mail: w.l.kling@tue.nl).

F. R. Isleifsson is with Risø, Technical University of Denmark, Frederiksborgvej 399, 4000 Roskilde, Denmark (e-mail: fris@risoe.dtu.dk).

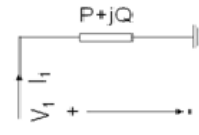
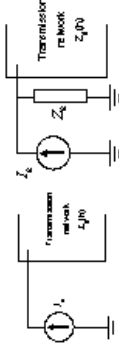
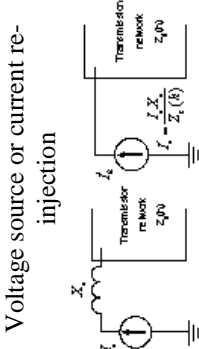
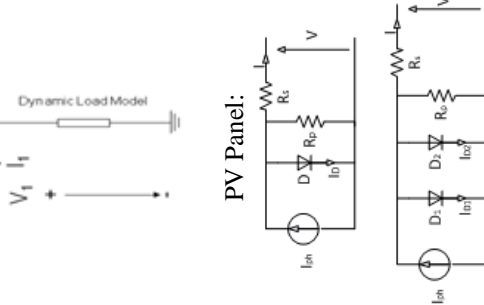
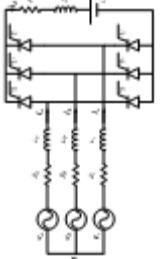

H. W. Bindner is with Risø, Technical University of Denmark, Frederiksborgvej 399, DK-4000 Roskilde, Denmark (e-mail: hwbi@risoe.dtu.dk).

N. Martensen is with Energynautics GmbH, Robert-Bosch-Strasse 7, 64293 Darmstadt, Germany (e-mail: n.martensen@energynautics.com).

A. Samadi is with the KTH Royal Institute of Technology, Teknikringen 33, SE-100 44 Stockholm, Sweden (e-mail: afshins@kth.se).

L. Söder is with the KTH Royal Institute of Technology, Teknikringen 33, SE-100 44 Stockholm, Sweden (e-mail: Lennart.Soder@ee.kth.se).

TABLE I
CHARACTERISTICS OF DIFFERENT TYPES OF MODELS AND STUDIES

| | | | | |
|--|---|--|--|--|
| Inverter model | | Harmonics | Electro-Mechanic stability | Electro-magnetic transients |
| | <p>PQ, PU, or DU node</p>  | <p>Ideal or non-ideal current source</p>  <p>Voltage source or current re-injection</p>  | <p>Dynamic profile – P and Q</p>  | <p>Detailed model of power electronics with controls</p>  |
| Aggregated model considerations | Arithmetic summation | <p>Summation coefficients</p> $I_{SUM} = \sqrt{\sum_t I_t^\beta}$ | No simplified models available | No simplified models available, use actual circuit |
| General model considerations | Steady state | <p>Frequency domain</p> <p>Frequency Scan of the point of connection is very important</p>  | Weather conditions and cloud formations are or significant importance for voltage level fluctuations | Time-Frequency domain |

voltage and reactive power at the same asset. Since it is impossible to perform voltage control and reactive power control at the same assets, the setpoint deviations of both are weighted against each other, using a weighting factor called droop. Higher droop settings shift the weight from a smaller voltage setpoint deviation towards a smaller reactive power setpoint deviation. This type of node is called a DU node, which references the resulting voltage setpoint deviation. Since neither voltage nor reactive power is known from the beginning, the power flow algorithm starts with the assumption of zero voltage setpoint deviation and then adjusts both voltage and reactive power in each iteration

step. This works because the correlation between voltage and reactive power at the node is known from the droop setting. Of course, reactive power limits must be taken into account in the same way as for a PU node.

III. MODEL FOR SHORT CIRCUIT CALCULATION

In the past, converter-based generation assets did not contribute a significant share of active power generation to the power system. Since their reactive current contribution to short circuit currents is also limited in comparison to the traditional synchronous machine based power plants, it was

common practice that they were immediately disconnected when a fault was detected. However, this practice is not feasible any longer with the increasing share of converter-based generation. Disconnecting large active power shares generated by such assets has a severe impact on system stability and can cause supra-regional blackouts.

New connection guidelines and regulations (grid codes) therefore require that new converter-based power generation assets of significant size be capable of “riding through faults”. They have to remain connected to the grid as long as the fault impact does not exceed certain specified limits. While they remain connected their control system has to respond to voltage changes by adjusting the reactive current contribution along a given characteristic, which mimics the contribution of a synchronous machine. The required control system response is fast enough to guarantee appropriate contribution to transient fault currents. As a result, short circuit calculations must include the contribution of converter-based assets for accurate results.

Short circuit calculations are carried out in network planning and network operation. In network planning, approximate solutions are acceptable, as there are often other factors that are not fully known yet, and the intention of the study is the appropriate dimensioning of circuit breakers. It is often acceptable to apply the synchronous machine model also for converter-based generators in this kind of study.

However, in network operation, more accurate results are required to determine whether the given equipment is capable of dealing with short circuit currents that can occur after switching the grid to a different configuration. The approach to use the synchronous machine model could be taken as well, but the results will not be very accurate. The problem is the limitation of the reactive current magnitude by the converter: power electronic converters are limited to produce current up to their rated current, which they produce at nominal apparent power. However, synchronous machines can provide transient short circuit contributions above their nominal current by a factor of up to eight. The representation of a converter by a synchronous machine model can therefore only be accurate to a certain degree (i.e., when certain conditions are met). When the synchronous machine model parameters are set correctly for a short circuit at the generator terminals, they will be incorrect for remote faults and vice versa. Due to the limitation of the converter contribution to the short circuit current, this contribution is in fact independent of the fault distance to some degree. Only if the voltage drop at the converter remains within certain limits, the fault current contribution will resemble a synchronous machine. This behavior is fundamentally non-linear, and cannot be represented in the traditional and standardized linear short circuit calculation methods.

An alternative approach is to run a dynamic simulation for each case. Unfortunately, this approach requires a much higher modeling effort and significantly more time for simulation and result evaluation. In fact the effort is so high that this approach must be considered infeasible for use in regular network operation.

A new approach has recently been developed by DIgSILENT GmbH [2]. The basic idea is to accept the non-linearity of the converter characteristic and use an iterative approach for the short circuit calculation in the transient time scale. In comparison to the traditional short circuit calculation methods, this leads to longer calculation times. However, sufficiently accurate results can be obtained while still avoiding the additional effort of time-domain modeling and simulation.

IV. MODELS OF PV PANELS AND MPP TRACKING

Describing solar array I-V characteristic according to irradiance and temperature is mainly analyzed by two lumped models in literature, namely single diode model (SDM) and double diode model (DDM). DDM considers more parameters and along with gives better precision particularly at low irradiance [3]. In SDM (Fig. 1), current-voltage characteristic function of the PV array is depicted as:

$$I = I_{ph} - I_0 \left[\exp\left(\frac{V + R_S I}{AV_t}\right) - 1 \right] - \frac{V + R_S I}{R_p} \quad (1)$$

In (1), I_0 is the dark saturation current, R_S is the cell series resistance, R_p is the cell parallel resistance, A is the diode quality (ideality) factor and V_t is the junction thermal voltage which is described by $V_t = kT_{stc}/q$, where k is the Boltzmann’s constant, q is the charge of the electron and T_{stc} is the temperature at standard test condition (STC).

I_{ph} is the photo-generated current which is a linear function of irradiance and a function of temperature [4]. I_{ph} , in short circuit condition, can be approximated to:

$$I_{ph}(G, T) = I_{sc,STC} \frac{G}{G_{STC}} [1 + K_I(T - T_{ref})] \quad (2)$$

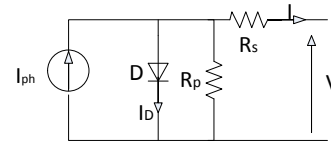


Fig. 1. Single diode scheme

where G is irradiance and G_{STC} is irradiance in STC ($1000\text{W}/\text{m}^2$), $I_{sc,STC}$ is the short circuit current at STC, T_{ref} is the reference temperature at STC (298°K) and K_I is the short-circuit current temperature coefficient ($\%/^\circ\text{K}$). Moreover, open circuit voltage can be expressed as a linear function of temperature [4].

$$V_{OC}(T) = V_{OC,STC} + K_V(T - T_{ref}) \quad (3)$$

where $V_{OC,STC}$ is the open circuit voltage in STC and K_V is the open-circuit voltage temperature coefficient ($\text{V}/^\circ\text{K}$).

For, DDM (Fig.2) V-I characteristic function is illustrated as [3]:

$$I = I_{ph} - I_{01} \left[\exp\left(\frac{V + R_S I}{V_t}\right) - 1 \right] - I_{02} \left[\exp\left(\frac{V + R_S I}{2V_t}\right) - 1 \right] - \frac{V + R_S I}{R_p} \quad (4)$$

Finding unknown parameters requires iterative process, in [4] was shown how to derive solar array parameters through datasheet values. However, by reducing the complexity of model, for instance neglecting parallel resistance and assuming some approximations it would be possible to reach a four-parameter model based on the analytical expressions.

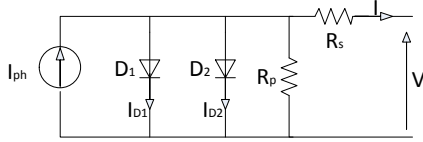


Fig. 2. Double diode scheme

The characteristic of PV array power-voltage for different irradiation levels has been illustrated in Fig. 3. As can be seen, by decreasing the irradiance level the output power decreases. Fig. 4 depicts that the output power of solar array is reduced when the temperature rises. It is desired that PV system operates at Maximum Power Point (MPP) then the desired operating point for each PV cell is I_{mp} and V_{mp} .

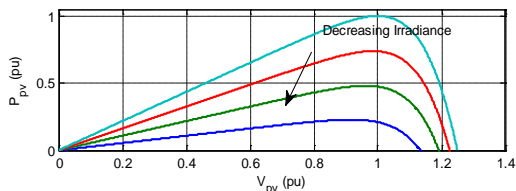


Fig. 3. Irradiance impact on power-voltage characteristic of a PV cell

Extracting maximum power from the PV array needs Maximum Power Point Tracking (MPPT), therefore MPPT is the essential part of PV system. MPPT function is to regulate output voltage and current of the PV system in such a fashion to get maximum power of the PV array according to weather conditions. Different MPPT algorithms have been proposed and implemented such as perturb and observe (P&O), incremental conductance (IncCond), fractional open-circuit voltage, fractional short-circuit current and etc. P&O method makes a perturbation in voltage and observes the consequent of this change on the output current and power of PV array, in doing so if the power increases, the perturbation is held in the same direction otherwise it is reversed [5], [6]. Once the MPP is reached, there would be an oscillation at output power of PV. Reducing perturbation step size decreases oscillation but in the meantime slows down the MPPT. Some methods have been proposed to get optimum perturbation step size by having variable step size [6]. Under fast environmental change within one MPPT perturbation, MPPT may fail to track the correct MPP and getting diverged. Some techniques like employing three-point weight comparison or optimizing sampling rate have been introduced to overcome this drawback [5]. Incremental conductance performance is based on this fact that the slope of power curve is zero at MPP. Via comparing instantaneous conductance (I/V) and incremental conductance ($\Delta I/\Delta V$), MPP is met when both of conductances are equal [4], [5].

The speed of MPPT is adjusted by the increment step size. By large increment step size, on the one hand fast MPP tracking can be obtained but on the other hand the system would oscillate around MPP. In order to minimize oscillation different procedures have been proposed [6]. Fractional open-circuit voltage and fractional short-circuit current are two similar approaches that are taking the advantage of close linear relationship between V_{MPP} and V_{OC} , $V_{MPP}=k_1 V_{OC}$, as well as I_{MPP} and I_{SC} , $I_{MPP}=k_2 I_{SC}$, for varying environmental conditions [6], [7]. Where k_1 and k_2 depend on PV array characteristic and must be calculated for different atmospheric conditions in advance. Once the k_i ($i=1,2$) values determined, V_{MPP} and I_{MPP} can be determined by measuring V_{OC} via shutting down the power converter which leads to temporarily loss of power. Moreover this approach is based on the linear approximation and increment step size, by doing so exact MPP might not be achieved. In fractional short-circuit current method measuring I_{SC} during operation of the system needs extra switch to periodically short the PV modules to get I_{SC} which brings about power reduction. Moreover as fractional open-circuit voltage, exact MPP is not finely matched. There are other types of MPPT algorithms available in literature. In [6], it is mentioned that there are at least nineteen distinct algorithms in literature. However, P&O and IncCond are widely employed in industry.

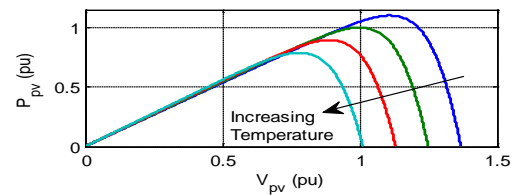


Fig. 4. Temperature impact on power-voltage characteristic of a PV cell

MPPT plays a key role in performance of the PV system to the extent that speed of the system is dominated by the MPPT, this issue has been addressed in [8] and according to it a dynamic model for the PV system based on the analyzing of experimental results was developed.

V. MODELS FOR VOLTAGE STABILITY STUDIES

A large fraction of the PV systems that are being installed are connected in the LV distribution system at the end customer's premises. The implication of that is that the operating conditions of the LV voltage grid are changed significantly. In particular often there will be bi-directional power with rapid changes which has an impact on the voltage level and the voltage fluctuations of the grid. It is thus necessary to have tools enabling analysis of the voltage issues and investigation of possible solutions. These tools should be able to assess the impact of the PV connected along a feeder i.e. they should be able to simulate the LV grid with consumption and realistically represent the PV input. Since many of the issues with integration of PV are associated with the fluctuations it is necessary to be able to do proper time series simulations to be able to assess the statistical properties of the voltage such as distribution of

voltage level and amount and size of voltage fluctuations.

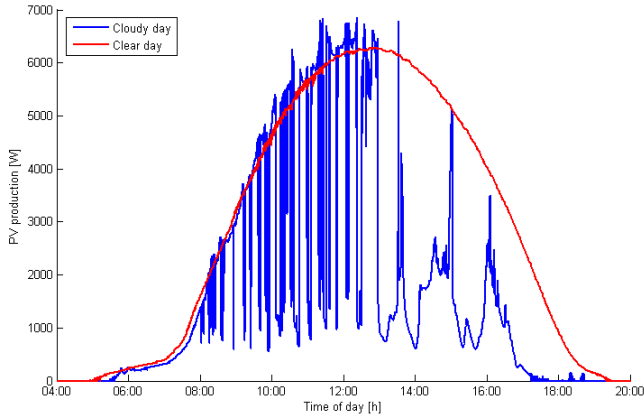


Fig. 5. Active power production from a PV plant showing two days with different cloud coverage

The electrical models to analyze the grid impact will be standard load flow models of the grid [9] implemented in simulations tools for power systems [10], [11]. The main problem is proper modeling of the input to represent the fluctuations of the PV production on the relevant timescales, seconds-hours but also representing the correct distribution between different types of days such as days without cloud cover, days with different types of partial cloud cover (large/small, fast/slow moving) and days with unbroken cloud cover. A related issue of importance is correlation between different PV installations connected to a feeder and correlation with consumption. Another important issue is the ability of the tools to represent the control of the active components of the system e.g. inverters, storage units and controllable loads.

To illustrate some of the issues the power fluctuations for the PV installation that is part of SYSLAB @ Risø DTU [12] have been analyzed. The power production from the PV plant is shown in Fig. 5 for the days analyzed. The data has been processed to show the fluctuations at different timescales. Fig. 6 shows the fluctuations on a day with clear sky while Fig. 7 illustrates the situation on a day with passing clouds. It is very clear from the figures that it is necessary to have a good description of the input i.e. the solar irradiation on both short on short timescales (intra-day) and longer timescales, day to day and over the year.

The solar power production will induce voltage variations in the grid due to the impedances of the grid. For traditional LV grids the voltage is highest at the bus bar and decreases along the feeder to have the maximum capacity without violating the voltage range. When solar power is introduced the picture gets slightly more complicated since the solar power is contributing to raising the voltage. The result is that situations could occur where the voltage is above the upper limit allowed due to the solar power production and the consumption. The situation for a feeder in SYSLAB is shown in Fig. 8. The maximum and minimum voltage curves are for situations with maximum solar power/minimum consumption resp. minimum solar power/maximum consumption while the two curves in between illustrates how the inverter on the PV installation

can be controlled to narrow the range of voltage level variation by consuming resp. producing reactive power.

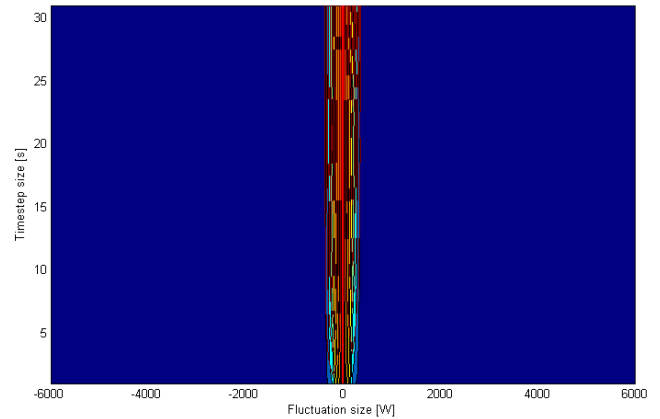


Fig. 6. Fluctuations of the power output of a PV plant on a cloudless day. The color map shows the number of fluctuations at different power levels against the length of time from the observation to the change in power output

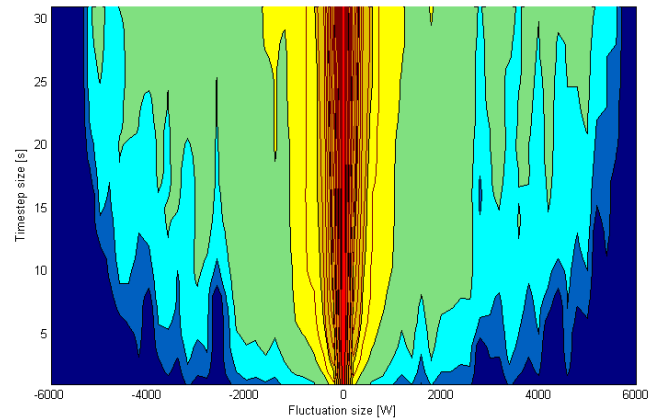


Fig. 7. Fluctuations of the power output of a PV plant on a cloudy day. The color map shows the number of fluctuations at different power levels against the length of time from the observation to the change in power output

The above figure illustrates one of the options that exist to mitigate the issue of voltage level variations. Other options exist such as on load tap changers or energy storage. This emphasizes the importance of being able to model the various options with realistic input and control of the active components.

VI. MODELS FOR HARMONIC INTERACTION STUDIES

Harmonic interaction studies can be done in the time domain, frequency domain, or as hybrid calculations [13], [14].

Time domain calculations use differential equations, and therefore require detailed models of power electronic devices, including the control algorithm of the PV inverter. With a detailed model of a device, they are known to be very accurate when predicting behavior in different conditions. Examples of studies done in the time domain are given in [15]-[18]. A restriction of time domain calculations is that they are difficult to do for systems with a large number of different units. Including the control algorithm of several different devices can be a problem or even

impossible, since their control algorithms are not always available.

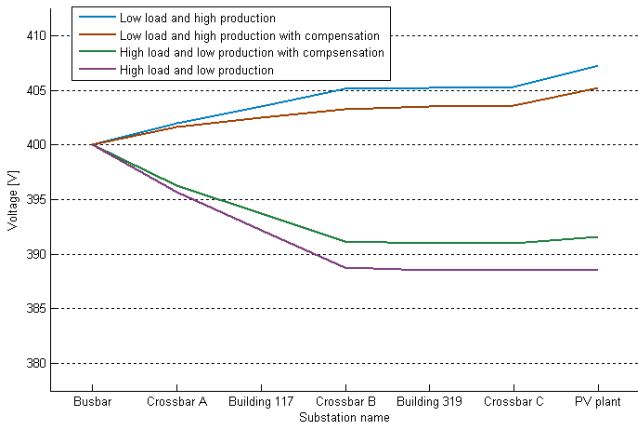


Fig. 8. Voltage levels along a feeder connected to a busbar at one end and a PV plant at the other. The figure shows four different states of production and consumption; a low load and high production state; a high load and low production state and then those two states with compensation from the PV plant

Calculations in the frequency domain are widely used for harmonic studies. Sources of harmonic currents are represented as ideal or non-ideal current sources, or the current is determined from a look-up table based on the voltage of the busbar. As [14] suggests, a harmonic source can also be represented as voltage source with a series impedance, or as a current source dependent on the system impedance (current re-injection), which emphasizes the effect of the system impedance on the current of the source.

Several types of calculations are proposed in the frequency domain [13], [14]: current source method, power flow method, and iterative harmonic analysis. Examples of studies in the frequency domain are given in [19]-[23].

Current source method solves the network equation:

$$[Z][I] = [U] \quad (5)$$

for each harmonic frequency. Harmonic currents are assumed to be independent of voltages which makes the calculation relatively simple, but also reduces the accuracy. Network elements that do not generate harmonics are modeled as linear impedances. Background harmonic voltages that originate from higher voltage levels can be modeled as voltage sources.

Harmonic power flow method uses a Newton-type algorithm to solve current and voltage equations at the same time for a single frequency. This allows the harmonic current sources and other elements to be voltage dependent, and gives more accuracy. On the other hand, the calculation becomes more complicated than the current source method. A number of software tools use this method for harmonic analysis of the system.

Iterative harmonic analysis is an advanced version of direct and power-flow calculations. The original methods are supplemented with voltage dependent current sources, and sometimes even the frequency coupling. The direct matrix or power-flow simulation is initially executed with assumed voltages on busbars of non-linear elements,

resulting in initial harmonic current values. These voltages are then compared with calculated voltages for those busbars, and if needed, the calculation is repeated with new values for current sources. This iterative procedure is repeated until the voltage changes on busbars are within the desired error margins. The accuracy of these methods is dependent on the complexity of models used. When detailed models of all elements are used very accurate results can be achieved, but on the other hand the models require a lot of parameters, which sometimes makes them difficult to implement for complex systems.

Hybrid calculations are a mixture of time and frequency domain methods. Currents of non-linear elements are calculated in the time domain, based on the voltages which are solved in the frequency domain, usually with iterations. This type of calculation was still not used for harmonic studies with photovoltaic systems.

Frequency dependent impedance of the system is important for harmonic interaction studies. Harmonic voltages are often increased due to a resonant or near-resonant condition, and therefore attention should be given to the effect of impedance of PV inverters. Other nearby equipment, such as power factor correction capacitors, should be taken into account.

In the case of multiple inverters connected to the system, an aggregated model can be used to substitute the effect of all units. Summated current can have a maximal value equal to the arithmetical sum of individual currents, but due to the phase angle diversity of individual currents the sum is usually lower than that. Technical reference [24] suggests using a generalized summation law for determining the total harmonic current of random loads:

$$I_{SUM} = \sqrt{\sum_i I_i^\beta} \quad (6)$$

where β is the summation coefficient with a value of 1 or greater, depending on the harmonic order. General considerations about the summation of random currents are given in [24]-[27]. Examples of aggregated models of PV inverters are given in [28], [29]. Reference [28] presents measurement result in which β had a value of approximately 1 (arithmetic summation) for harmonic orders up to 17, and a value of approximately 2 for higher orders.

VII. MODELS FOR ELECTRO-MAGNETIC TRANSIENT STUDIES

Behavior of PV inverters during electro-magnetic transients can be accurately modeled in the time domain. As mentioned in previous sections, this requires significant modeling effort. Converters control plays a key role during transients and has to be modeled accurately. This makes it difficult to model large systems with a great number of inverters. Examples of time domain studies are given in [30], [31].

Aggregation of PV inverters in electro-magnetic transient studies still needs to be explored. More work in this field is needed to obtain simplified models of a large number of inverters, because new regulations oblige even small

inverters to comply with certain low voltage ride-through requirements.

VIII. CONCLUSIONS

Considerations on Photovoltaic system modeling for grid interaction studies are presented in the paper. An overview of different PV models for different types of studies is given, with their applications and limitations.

For load flow calculations, they can be modeled as constant active and reactive power nodes, or voltage dependent, as described in section II.

PV systems and other converter-interfaced generators were often neglected in short-circuit studies, but new fault ride-through requirements are increasing their contribution in short-circuit currents. The approach for modeling them is described in chapter III.

PV modules are modeled with single diode or double diode circuits. Different MPP tracking algorithms are described in section IV.

For LV network voltage level studies it is important to take into account the effect of weather conditions, such as solar irradiance, temperature, and cloud formations. These effects are emphasized in section V.

Harmonic interaction studies are usually done in the frequency domain, using ideal or non-ideal current sources as models of PV systems. Simulations can also be done as iterative or in the time domain. It is important to estimate the effect of PV inverters on the frequency dependent impedance of the rest of the system. These effects are described in section VI.

Electro-magnetic transient studies are done in the time domain, using detailed models of power electronics and controls of inverters. At present, no simplified models are proposed for this type of studies.

Concerning the aggregation of multiple PV systems, for load flow studies they can be summated arithmetically, and for harmonic studies using summation coefficients. For stability and electro-magnetic transient studies more work is needed to obtain simplified summated models.

IX. REFERENCES

- [1] International Energy Agency (IEA): "Trends in Photovoltaic Applications, Survey report of selected IAE countries between 1992 and 2010" – Preliminary statistical data, Report IEA-PVPS T1-20:2011, 2011.
- [2] Pöller, M./DIGSILENT GmbH: "Modelling of Wind Generation for Fault Level Studies", In Proc. 1st Wind Integration Symposium, Frankfurt, 2011, <http://windintegrationsymposium.org/>
- [3] D. Chan and J. Phang, "Analytical methods for the extraction of solar cell single- and double-diode model parameters from i-v characteristics", *IEEE Trans. on Electron Devices*, vol. 34, no. 2, pp. 286–293, 1987.
- [4] Sera, R. Teodorescu, P. Rodriguez, "PV panel model based on datasheet values", In Proc. IEEE International Symposium on Industrial Electronics ISIE 07, June 4-7, 2007, pp.2392-2396.
- [5] D. P. Hohm and M. E. Ropp, "Comparative study of maximum power point tracking algorithms using an experimental, programmable, maximum power point tracking test bed", In Proc. IEEE Photovoltaic Specialist Conf., 2000, pp. 1699–1702.
- [6] T. ESRAM and P. L. Chapman, "Comparison of photovoltaic array maximum power point tracking techniques", *IEEE Trans. on Energy Conversion*, vol. 22, no. 2, pp. 439-49, June 2007.
- [7] M. A. S. Masoum, H. Dehbonei, and E. F. Fuchs, "Theoretical and experimental analyses of photovoltaic systems with voltage and current-based maximum power-point tracking", *IEEE Trans. on Energy Conversion*, vol. 17, no. 4, pp. 514–522, Dec. 2002.
- [8] Y.T. Tan, D.S. Kirschen, and N. Jenkins, "A Model of PV Generation Suitable for Stability Analysis", *IEEE Trans. on Energy Conversion*, V19.4, 2004.
- [9] P. Kundur: "Power System Stability and Control", McGraw-Hill Inc, New York, 1993.
- [10] DIGSILENT PowerFactory: Version 14.0. DIGSILENT GmbH, 2010
- [11] H. Bindner, O. Gehrke, P. Lundsager, J.C. Hansen, T. Cronin: "IPSYS - A simulation tool for performance assessment and controller development of integrated power system distributed renewable energy generated and storage", In Proc.2004 European Wind Energy Conference and Exhibition, London (GB), p.p. 128-130, Nov 2004.
- [12] O. Gehrke, H.W. Bindner: "Building a test platform for agents in power system control: Experience from SYSLAB", In Proc. International Conference on Intelligent Systems Applications to Power Systems 2007, IEEE, 2007.
- [13] A. Medina, "Harmonic simulation techniques (methods & algorithms)", In Proc. IEEE Power Engineering Society General Meeting, 2004.
- [14] A. Medina, N.R. Watson, P.F. Ribeiro, C.J. Hatziadoniu: Harmonic Analysis in Frequency and Time Domains, Harmonic Modeling Tutorial, Chapter 5, IEEE
- [15] I.T. Papaioannou, M.C. Alexiadis, C.S. Demoulias, D.P. Labridis, P.S. Dokopoulos: "Modeling and Field Measurements of Photovoltaic Units Connected to LV Grid. Study of Penetration Scenarios", *IEEE Trans. on Power Delivery*, vol. 26, no. 2, April 2011.
- [16] J.L. Agorreta, M. Borrega, J. Lopez, L. Marroyo: "Modeling and Control of N-Paralleled Grid-Connected Inverters With LCL Filter Coupled due to Grid Impedance in PV Plants", *IEEE Trans. on Power Electronics*, vol. 26, no. 3, March 2011.
- [17] C.M. Ong: "Operational Behavior of Line-Commutated Photovoltaic Systems on a Distributed Feeder", *IEEE Trans. on Power Apparatus and Systems*, vol. PAS-103, no. 8, August 1984.
- [18] M.C. Benhabib, J.M.A. Myrzik, J.L. Duarte: "Harmonic Effects Caused by Large Scale PV Installations in LV Network", In Proc. Electrical Power Quality and Utilization, October 2007.
- [19] G.L. Campen: "An Analysis of the Harmonics and Power Factor Effects at a Utility Intertied Photovoltaic System", *IEEE Trans. on Power Apparatus and Systems*, vol. PAS-101, no. 12, December 1982.
- [20] J.H.R. Enslin, P.J.M. Heskes: "Harmonic Interaction Between a Large Number of Distributed Power Inverters and the Distribution Network", *IEEE Trans. on Power Electronics*, vol. 19, no. 6, November 2004.
- [21] N. Jayasekara, P. Wolfs: "Analysis of Power Quality Impact of High Penetration PV in Residential Feeders", In Proc. Universities Power Engineering Conference AUPEC, 2010.
- [22] H. Oldenkamp, I. de Jong, P.J.M. Heskes, P.M. Rooij, H.H.C. de Moor: "Additional Requirements for PV Inverters Necessary to Maintain Utility Grid Quality in Case of High Penetration of PV Generators", In Proc. 19th European PV Solar Energy Conference and Exhibition, Paris, France, June 2004.
- [23] A.J. Bosman, J.F. Cobben, W.L. Kling, J.M. Myrzik: "Harmonic modeling of solar inverters and their interaction with distribution grid", In Proc. UPEC 2006, Newcastle, United Kingdom, September 2006.
- [24] *Electromagnetic Compatibility (EMC) part 3-14: Assessment of Emission Limits for the Connection of Disturbing Installations to LV Power Systems*, IEC Technical Report IEC/TR 61000-3-14, 2007.
- [25] W.G. Sherman, "Summation of Harmonics with Random Phase Angles", In Proc. IEE, vol. 119, no. 11, November 1972.
- [26] S.R. Kaprielian, A.E. Emanuel, R.V. Dwyer, H. Mehta: "Predicting Voltage Distortion in a System with Multiple Random Harmonic Sources", *IEEE Trans. on Power Delivery*, vol. 9, no. 3, July 1994.
- [27] Probabilistic Aspects Task Force of Harmonics Working Group: "Time-Varying Harmonics: Part II – Harmonic Summation and Propagation", *IEEE Trans. on Power Systems*, vol. 17, no. 1, January 2002.
- [28] G. Chicco, J. Schlabbach, F. Spertino: "Operation of Multiple Inverters in Grid-Connected Large-Size Photovoltaic Installations", In Proc. CIREP 2009, Prague, June 2009.
- [29] E. Vasanasong, E.D. Spooner: "The Effect of Net Harmonic Currents Produced by Numbers of the Sydney Olympic Village's PV Systems on the Power Quality of Local Electrical Network", In Proc. PowerCon 2000, 2000.

- [30] L. Wang, T. Lin: "Dynamic Stability and Transient Responses of Multiple Grid-Connected PV Systems", *In Proc. IEEE PES Transmission and Distribution Conference and Exposition 2008*, April 2008.
- [31] Y. Zhang, C. Mensah-Bonsu, P. Walke, S. Arora, J. Pierce: "Transient Over-Voltages in High Voltage Grid-Connected PV Solar Interconnection", *In Proc. IEEE PES General Meeting 2010*, July 2010.

Variability and smoothing effects of PV power production

A literature survey

J. Widén

This report is part of the Smooth PV project - KTH

The core part of this report is the literature overview that was performed to get an overview of the research field and the most recent findings. The results of the survey are presented below, divided on observations of variability and smoothing in monitored data for PV power production, observations of variability and smoothing in solar radiation data and theoretical and empirically based models. For a summary and brief overview of the most important findings in the studies described below, see Appendix A.

Observed variability and smoothing in monitored PV data

Three recent studies from the American company SunEdison show empirically how the variability of the power output from PV system ensembles depends on the sizes of individual systems and on the geographical dispersion of systems. In Golnas and Voss (2010) PV system fleets in three service territories in the United States were studied; two in California and one in New Jersey. In total 67 PV systems, continuously monitored with a 1-min resolution, were considered in the study, with seven days in May chosen for the analysis. The systems were grouped in ensembles with different total capacities and some different compositions of systems for each total capacity, and three different metrics were used to quantify the variability for these ensembles. The reported variability, evaluated over one single day, is therefore related to whether the ensembles consist of many small or a few large systems giving the same total capacity within roughly the same area. More systems imply a higher dispersion over the service territory (at maximum 48, 96 and 98 km, respectively, between systems in each area), but no explicit relation to the degree of dispersion was evaluated.

The obvious finding is that power production restricted to one or a few sites is more variable than production dispersed on a large number of smaller systems. Table 1 summarises some illustrative results from the study, in this case the difference in maximum (negative) step change between the least and most dispersed PV ensembles for each ensemble capacity. The differences are dependent not only on the number of systems aggregated, but also on the composition of the ensemble (whether a few systems are dominating in terms of capacity or if there is an even distribution), the exact area for dispersion, and the irradiation variability on the actual day. Nevertheless, the table shows what smoothing can be achievable through distribution of PV systems. Distributing capacity around 1 MW_p over smaller, widely spread systems could lower maximum daily step changes from around 40-50 % of capacity to around 5 % of capacity. Note, however, that since only one day was studied for each ensemble, the

observed maximum step change is probably lower than what would appear over a longer observation period.

Table 1. Maximum PV step changes during one observed day in Golnas and Voss (2010). Note that the degree of dispersion depends both on the number of systems *and* whether one or a few systems are dominating, which is why the least dispersed ensembles can contain quite a few systems.

| Ensemble size (kW _p) | Least dispersed ensemble | | Most dispersed ensemble | |
|-------------------------------------|----------------------------------|----------------------|----------------------------------|----------------------|
| | Maximum 1-min step change (%) | Number of systems | Maximum 1-min step change (%) | Number of systems |
| 440 | 37 | 1 | 6 | 11 |
| 1000 | 17 | 15 | 8 | 17 |
| 1200 | 50 | 1 | 17 | 8 |
| 1200 | 43 | 2 | 5 | 15 |
| 2300 | 36 | 2 | 18 | 11 |
| 2500 | 21 | 20 | 8 | 22 |

This is apparent in Golnas et al. (2011), where the output of distributed PV systems in one service area in New Jersey was analysed over the longer period of 11 months with the same approach; the systems, 31 in total, were grouped in differently composed ensembles spread over different distances, at maximum 155 km between systems. In the study an analysis was also made for different time resolutions. The main result is naturally that the variability metrics increase systematically with increasing aggregation of individual systems, while the dependence on the time resolution is less coherent. As an example of the former, the maximum 1-min step change for the largest and most widely spread ensemble (1000 kW_p) is around 20 % of rated capacity while for a single system (440 kW_p) it is around 70 %. These maximum step changes are higher than in the previous study. Since an observed maximum is dependent on the observation period, a more suitable metric is to use a percentile of the distribution of the step changes. Golnas et al. (2011) use the 95th and 99.7th percentiles. For the most dispersed ensemble in this study the 95th percentile is 5 % of rated capacity and the 99.7th percentile is 11 %. As can be seen from those figures, another result is that the distribution of the step change is rather long-tailed, meaning that there are large jumps between the upper percentiles.

In the third study, Golnas and Bryan (2011) investigated the output fluctuations from a centralized PV plant that was Europe's largest at the time of writing. This plant, located in Rovigo, Italy, has a capacity of 70 MW_p in total and consists of 60 individual arrays, covering a total area of 850 000 m². In addition to the previous two studies, the authors systematically

analysed the impact of dispersion on variability (over relatively short distances, at maximum 1200 m between systems), as compared to the impact from capacity increases within the same limited area. This was done by on the one hand grouping the arrays into differently sized ensembles within the same area, and on the other hand considering ensembles of the same size dispersed on circles with different radii. The result was, naturally, that increased ensemble size dispersed within the same area does not decrease variability, whereas wider dispersion of the same capacity does. Dispersion of capacity along circles with radii from 100 to 600 m made the maximum observed step change over 9 months decrease from almost 70 % to around 45 % of capacity at the 1-min resolution. Note the difference to the previous studies, where the wider dispersion (maximum distances between systems in the order of 100 times longer) gave considerably lower maximum step changes.

A limited study of observed impacts of clouds on variability is provided by Kankiewicz et al. (2010). The study concerns a large PV plant covering 728 000 m² (180 acres) of land with a rated capacity of 25 MW_p, located in Florida. The analysis is based on electricity production data monitored at the 17 subsystems of the plant. The results presented are restricted to one day in December, but the time resolution of 10 seconds is higher than in the studies above. The impact of dispersion over the area of the plant can be clearly seen. The maximum 10-second step change observed over this day with passing clouds is around 60 % of capacity for individual subsystems (sized 0.8-1.6 MW_p) and around 5 % for the whole 25 MW_p system. The same figures for the 1-min resolution are around 40 % and 20 %, respectively. If observed over a longer period of time, the figures would probably be more similar to those of the Rovigo plant.

Two studies by Marcos et al. (2011a,c) analyse the impacts on variability from increasing system size and from increasing geographical dispersion of up to eight Spanish PV systems in the capacity range of 48 kW_p to 9.5 MW_p, over distances of up to 60 km. The analysis is more detailed than most of the previous ones and covers time resolutions from 1 second up to 10 minutes. The studies show both the variability of differently sized individual systems and of different aggregates of systems on variability. As an example, in Marcos et al. (2011a) the maximum 1-s step change is around 55 % of capacity for the smallest system (48 kW_p) and merely around 5 % for the largest system (9.5 MW_p), from one-year observations. The corresponding figures for the 1-min resolution are around 100 % and 70 %. The authors also report the 90th percentile of the step changes, plotted in Figure 1 against the plant area. As can be seen, there is considerable smoothing on the shorter time scales. Combining six systems within distances of 60 km further reduces the total variability. In Marcos et al. (2011c) the

99th percentiles are reported for all possible combinations of up to six plants. These decrease from around 10 % of capacity for one system to around 2 % for six systems at the 1-s resolution. The corresponding drop for the 1-min resolution is from 85 % to 35 %.

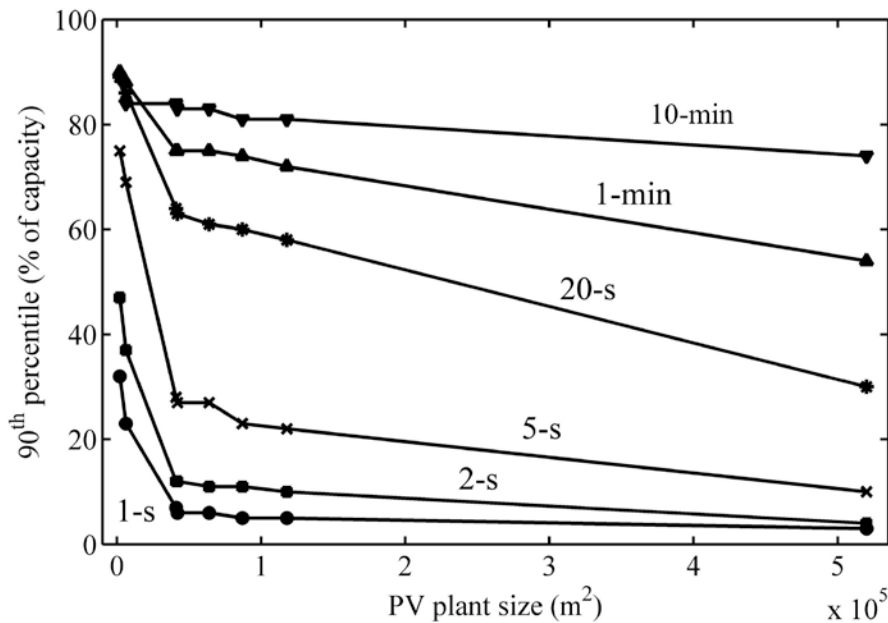


Figure 1. 90th percentile of step changes in the output from differently sized PV plants, based on values reported in Marcos et al. (2011a).

The latter study also uses these data to find empirical relations between the number of dispersed PV plants grouped, the 99th percentile of the step change, and the time resolution. The percentile decreases systematically with the dispersion and increases with the time resolution. For the extreme resolutions the decrease is from around 10 % of capacity to 2 % for the 1-s resolution, as mentioned, and from 90 % to 50 % for the 10-min resolution. In an attempt to generalize their findings the authors also fit their data to an empirical function relating the 99th percentile of the step change to the PV plant size and the number of dispersed systems (see below).

Two studies are also worth mentioning that consider the smoothing effect from dispersion over nation-wide distances. Murata et al. (2009) analysed electricity production data from 52 sites distributed over Japan. The main goal of the study was to relate the maximum step change to the standard deviation via empirically determined so-called fluctuation coefficients (see further discussion below). Wiemken et al. (2001) studied the electricity production from 100 PV systems spread over Germany, all monitored over one year with a 5-min resolution.

The main findings were that no step changes at this resolution were higher than 5 % of total capacity. Also, the aggregate power was never above 65 % of the total capacity.

Observed variability and smoothing in solar radiation data

Since PV variability depends directly on the variability in the irradiation on the solar cells, expected smoothing from geographical dispersion can also be determined from radiation data. An early study was made by Otani et al. (1997) using a Japanese radiation monitoring setup with 9 sites in a 4 x 4 km grid. The authors used a metric called the *fluctuation factor*, which is defined as the rms value of the fluctuations. With aggregation across the monitoring grid the authors could show that fluctuation factors based on 1-min data decreased by 40 % on average over one studied month and by 87 % at maximum. The same experimental setup was used by Kawasaki et al. (2006) to study the impact of different typical weather types on fluctuations and smoothing across the grid, showing distinctly different fluctuation patterns and degrees of smoothing on clear and rainy days and on days with moving clouds.

In a more recent study, Lave and Kleissl (2010) used measurements of global radiation on the horizontal plane at four sites in Colorado, located between 19 and 197 km apart, to study the smoothing effect. The maximum ramp rate, observed in 5-min data covering one whole year, was between 161 and 189 $\text{Wm}^{-2}\text{min}^{-1}$ for individual sites and 112 $\text{Wm}^{-2}\text{min}^{-1}$ for the four sites combined. As ramp rates in Wm^{-2} depend both on the sun's deterministic position in the sky and on cloud movements, it is customary to analyse the clearness index (actual radiation divided by the clear-sky radiation) rather than the absolute irradiance. Mills and Wisser (2010) used the clearness index determined from 1-min global horizontal radiation data covering one whole year to quantify the smoothing from dispersion of 23 PV sites over distances from 20 to 440 km. For example, the authors found that the 99.7th percentile dropped from 0.58 for one site to 0.19 for five sites, and to 0.09 for all 23 sites. Since the clearness index and the PV output relative to rated capacity are related, it is not surprising that these figures are comparable in size to the 99.7th percentile values for the PV output in Golnas et al. (2011) mentioned above.

Lave et al. (2011) used a one-month series of 1-s data for the clearness index at six sites, separated by less than 3 km, in San Diego, USA, to determine fluctuations on different time scales with a spectral analysis. Two metrics were used to characterize the variability; the *fluctuation power index* (fpi) and the *variability ratio* (VR). The fpi describes the power content in the fluctuations at each timescale. The VR is the fpi for one site divided by the fpi

for a set of aggregated sites. Thus, it shows the reduction in variability with aggregation. One of the results from the study is that the VR is around 6 (the number of sites) for short timescales and approaches 1 for longer timescales. This is analogous with the reduction in variability being equal to the number of sites for short timescales, for which the clearness indices are virtually uncorrelated, and with a slight or no reduction for longer timescales, for which the clearness indices are strongly correlated. The same thing can be seen in Figure 1 above where the plant size has less impact on the variability for longer times scales.

Theoretical and empirical models

Since widespread distributed PV has been extensively integrated in distribution systems just over the past one and a half decade, early studies used modeling techniques to determine the impact of moving clouds on aggregate PV generation. An early study was made by Jewell and Ramakumar (1987) who simulated clear-sky radiation and cloud movements to study the time to loss of all PV capacity in a service area due to movement of a squall line. Different service areas with uniformly distributed PV systems were considered. For example, the authors concluded that time for loss of all PV capacity during such an event was 1.8 min for a 10 km² area and 176 min for a 100 000 km² area.

Another early study on ramp rates in aggregate PV production was made by Kern et al. (1989). They used monitored PV production data from four individual systems combined with cloud models to find the aggregate power production from 28 PV systems and their total ramps during cloud passages. In total, 62 kW_p rated capacity was considered, spread over an area of 202 000 m² (50 acres). Over a whole cloud passage event, the average ramps were found to be 75 % of total capacity for a single system and 60 % for 28 systems. This corresponded to a ramp rate of 10 % per second for the single system and 3 % per second for 28 systems. Although hard to compare directly to the observed variability above, it is in the same order of magnitude observed e.g. for the systems in Figure 1.

More recent modeling efforts have tried to find generalized methods that can be used to determine the output variability in an arbitrarily large and arbitrarily distributed fleet of PV systems. Murata et al. (2009) suggested a partly empirical method to determine the maximum power fluctuation for an arbitrary aggregate of PV sites and implemented it, as mentioned, for Japanese nation-wide radiation data. In short, the model requires empirical data for the so-called *output fluctuation coefficient*, which is the ratio of the maximum step change to the standard deviation, and for the correlation coefficients between a representative number of

sites. By using the correlation data the standard deviation of an arbitrary set of sites can be determined, and the maximum step change can be found by multiplying this extrapolated standard deviation with the empirical output fluctuation coefficient. A percentile of the step changes for an arbitrary aggregate can be determined in the same way. The drawback of this method is of course the extensive data requirement.

A more elegant model based only on theoretical considerations was proposed by Hoff and Perez (2010) and is worth discussing in detail. The model is based on a variability metric called the *relative output variability*, which is the standard deviation of the Δt time step changes for the aggregate output from a fleet of N distributed PV systems ($\sigma_{\Delta t}^N$), divided by the standard deviation for the same fleet concentrated in one single location ($\sigma_{\Delta t}^1$). Another central concept is the dispersion factor, defined as

$$D = \frac{L}{V\Delta t}$$

where L is the extension of the PV fleet in the direction of cloud movement, V is the transit rate of clouds and Δt is the time resolution. The dispersion factor is thus the number of time intervals required for a cloud disturbance to pass over the whole PV fleet. The variability for this fleet of systems is dependent on the relative magnitudes of N and D . Four different cases can be defined:

1. The *spacious region*, $N \ll D$, where the output variability is independent between systems. The relative output variability in this region is inversely proportional to the square root of the number of systems:

$$\frac{\sigma_{\Delta t}^N}{\sigma_{\Delta t}^1} = \frac{1}{\sqrt{N}}$$

2. The *optimal point*, $N = D$, where a cloud shading one system will shade the next one in exactly one time step. At this point the relative output variability is

$$\frac{\sigma_{\Delta t}^N}{\sigma_{\Delta t}^1} = \frac{\sigma_{N\Delta t}^1}{\sigma_{\Delta t}^1} \frac{1}{N}$$

3. The *crowded region*, $N > D$, where a cloud affects more than one system of the fleet in one time interval. The relative output variability is then

$$\frac{\sigma_{\Delta t}^N}{\sigma_{\Delta t}^1} = \frac{\sigma_{D\Delta t}^1}{\sigma_{\Delta t}^1} \frac{1}{D}$$

4. Finally, the *limited region*, $N < D$, where a cloud disturbance does not reach the next PV system before the next time interval. For this region, no explicit expression for the relative output variability can be found, but a limiting value as D increases is the same as for the spacious region, i.e.

$$\frac{\sigma_{\Delta t}^N}{\sigma_{\Delta t}^1} = \frac{1}{\sqrt{N}}$$

A schematic outline of the relative output variability in these different regions is given in Figure 2.

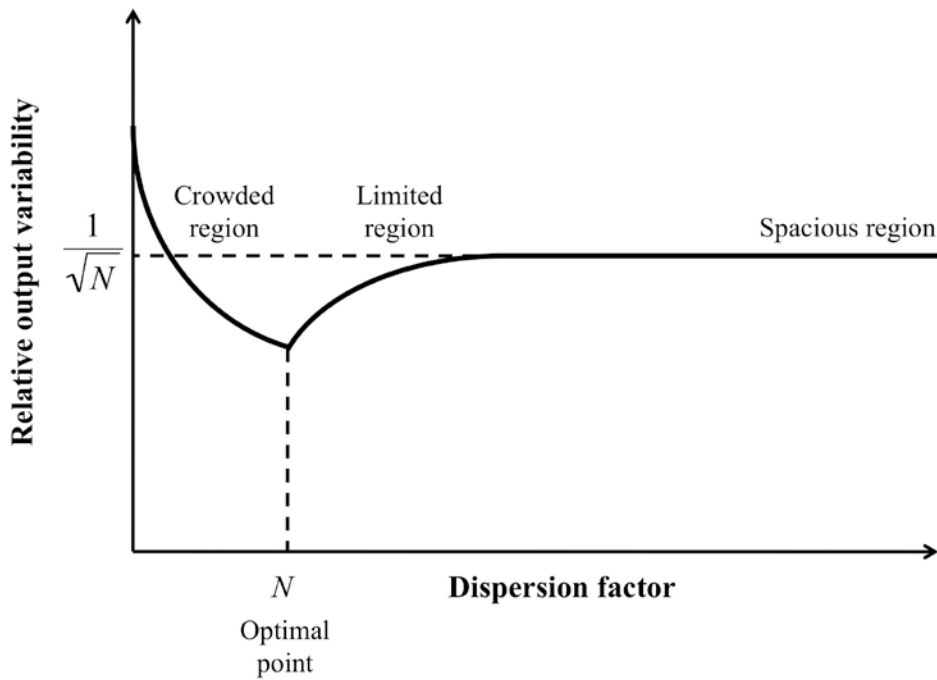


Figure 2. Schematic outline of the relative output variability as a function of the dispersion factor, with the different regions in the Hoff and Perez model indicated. Based on a similar outline in Hoff and Perez (2010).

Hoff and Perez use the theoretical model to determine the relative output variability in three scenarios where 100 MW_p PV capacity is distributed in different ways: one central power plant, 100 plants of 100 MW_p each and 20 000 plants of 5 kW_p each. The relative output

variability in these three scenarios was 18 %, 10 % and less than 1 %, respectively. An important observation is that the variability from the central power plant depends on the cloud transit rate and thus on the dispersion factor, while the variability from distributed systems depends on the number of systems.

These theoretical results are yet to be compared to data for real systems. Already, however, there have been attempts to test the validity of the model by some other authors. In an empirical model proposed by Marcos et al. (2011a,c) and fitted to the monitoring data already summarized above, the models for the crowded and spacious regions were reproduced. Already in Marcos et al. (2011a) it was noted that the curves shown in Figure 1 above could be fitted to exponential functions for the 90th percentile of the step change. Following the notation of Marcos et al., these functions are on the form:

$$90^{\text{th}}(\Delta P_{\Delta t, N}) = mS^{-c}$$

where S is the plant area, m is some proportionality constant and c is, for short time steps, equal to 0.5. This means that for high time resolutions the percentile decreases in proportion to $1/\sqrt{S}$. Noting that the square root of the plant area is the extension of the plant in one direction, this appears to correspond to the expression for the crowded region, where the output variability is inversely proportional to the dispersion factor D , which in turn is proportional to the plant extension L . For lower resolutions c approaches zero. This is also in line with the crowded region model, where the relative output variability approaches one for lower dispersion factors. This means that plant size does not influence the fluctuations on longer time scales, since clouds have time to pass over the whole plant within single time steps.

Marcos et al. (2011c) extend their empirical model to the 99th percentile of the step change for an arbitrary set of N sufficiently uncorrelated plants with plant areas S :

$$99^{\text{th}}(\Delta P_{\Delta t, N}) = 99^{\text{th}}(\Delta P_{600,1}) \left(1 - e^{-0.24\Delta t}\right)^{-c} N^{-a}$$

where $\Delta P_{600,1}$ is the hourly step change for one individual system. To obtain the parameters c and a the expression is fitted to data describing the smoothing with plant size and to data for the smoothing with site aggregation. As previously, for small Δt the c parameter turns out to

be close to 0.5 and for large Δt close to zero, analogous to the crowded region. For large Δt the a parameter is close to 0.5 and increases for shorter time scales. For the longer time scales this apparently corresponds to the Hoff and Perez model for the spacious region, because of the proportionality to $1/\sqrt{N}$. However, as the authors point out, the correlations between all considered sites was close to zero for all time scales, which suggests that the spacious region model should hold for all considered Δt . It is not entirely clear why the a parameter increases, but it might be an effect of the increasing total plant area, which provides further smoothing for high resolutions.

As Hoff and Perez, the authors use the model to extrapolate the 99th percentile of step changes for 100 MW_p PV capacity distributed in different ways. Some selected results are shown in Table 2. The value for the 1-min step changes can be compared to the empirical findings from the Rovigo system as reported by Golnas and Bryan (2011). The value estimated here for the centralized system is 70.9 % of capacity, whereas the maximum step change observed over 9 months for the Italian 70 MW_p plant apparently was around 45 %. One reason for the difference may be that the model, as admitted in the study, overestimates the percentile for larger areas and in particular for longer timescales (1-min and 10-min). Another reason could also be differences in local weather conditions and cloud movements.

Table 2. Calculated variability of 100 MW_p PV on different time scales (Marcos et al. 2011c).

| N | S (Ha) | 99 th percentile (% of total capacity) | | |
|--------|----------|---|-------|--------|
| | | 1-s | 1-min | 10-min |
| 1 | 651 | 0.9 | 70.9 | 86.1 |
| 10 | 65.1 | 0.5 | 18.6 | 31.3 |
| 100 | 6.51 | 0.2 | 4.9 | 11.3 |
| 1 000 | 0.651 | 0.1 | 1.3 | 4.1 |
| 10 000 | 0.0651 | 0.1 | 0.3 | 1.5 |

Appendix A

| Studies | Methodology (monitoring, simulation, etc.) | Data (time resolution, time period covered, number of systems, etc.) | Variability metrics (ramps, standard deviation, etc.) | PV system size / dispersion | Most important findings |
|----------------------------|--|---|--|--|--|
| Golnas and Voss (2010) | Statistical analysis of monitored electricity production | <ul style="list-style-type: none"> ▪ Electricity production from 67 systems in three service areas ▪ 1-min resolution ▪ 4 observed hours per day on 7 days in May 2010 | <ul style="list-style-type: none"> ▪ Standard deviation of step change ▪ Maximum power drop between time steps ▪ Fraction of step changes above 10 % of capacity | <ul style="list-style-type: none"> ▪ Differently sized ensembles of up to 22 systems ▪ Total capacities from 440 to 2500 kW_p ▪ Maximum distance between systems 98 km | <ul style="list-style-type: none"> ▪ Variability depends on ensemble size and composition ▪ Most power changes within 10 % of capacity ▪ For 2/3 of the ensembles more than 90 % of step changes below 10 % of capacity |
| Golnas et al. (2011) | Statistical analysis of monitored electricity production | <ul style="list-style-type: none"> ▪ Electricity production from 31 systems in one service area ▪ 1-, 10- and 60-min resolution ▪ 4 observed hours per day over 11 months, September 2010 – July 2011 | <ul style="list-style-type: none"> ▪ Maximum step change ▪ Distribution of step changes ▪ 95th and 99.7th percentiles of step changes | <ul style="list-style-type: none"> ▪ Differently sized ensembles of up to 23 systems ▪ Total capacities from 440 to 1000 kW_p ▪ Maximum distance between systems 155 km | <ul style="list-style-type: none"> ▪ Variability depends on ensemble size and composition ▪ For most distributed fleets 95 % of 1- and 10-min step changes below 10 % of capacity |
| Golnas and Bryan (2011) | Statistical analysis of monitored electricity production | <ul style="list-style-type: none"> ▪ Electricity production from 60 separate arrays of one large system ▪ 1-min to 60-min resolution ▪ 4 observed hours per day over 9 months, December 2010 – August 2011 | <ul style="list-style-type: none"> ▪ Standard deviation of step changes ▪ Maximum step change over monitoring period ▪ Step changes exceeding a certain magnitude | <ul style="list-style-type: none"> ▪ Differently sized ensembles of up to 60 arrays ▪ Total capacities from 6 MW_p to 70 MW_p ▪ Dispersion within a radius of up to 600 m | <ul style="list-style-type: none"> ▪ Variability depends on dispersion and not on total capacity ▪ Maximum step change 40-60 % of total capacity depending on time resolution ▪ Probability of step changes above 50 % of total capacity below 0.02 % for time steps between 1 min and 30 min |

| | | | | | |
|-----------------------------|--|--|---|--|---|
| Hoff and Perez (2010) | Modelling / simulation | Theoretically derived model relating PV output variability on different time scales to the so-called dispersion factor (number of time steps required for a cloud to pass the PV fleet) | Relative output variability: ratio of the standard deviation of step changes for a distributed PV fleet to the standard deviation for a single point location | Modelling of 100 MW PV capacity in three scenarios: <ul style="list-style-type: none"> • One central power plant • 100 plants, each 100 MW • 20 000 plants, each 5 kW | <ul style="list-style-type: none"> • Analytical formulas for the relative output variability for four different sizes of the dispersion factor in relation to the number of PV systems • In the three modelled scenarios, relative output variability is 18 %, 10 % and less than 1 %, respectively |
| Jewell and Ramakumar (1987) | Modelling / simulation | <ul style="list-style-type: none"> • Simulated clear-sky radiation and cloud movements • Time resolution from 6 seconds to 5 minutes | <ul style="list-style-type: none"> • Time to loss of all PV generation in a service area • Maximum loss of PV within a certain time frame | <ul style="list-style-type: none"> • Uniform distribution of PV systems within a service area (no exact capacity given) • Service areas from 10 km² to 100 000 km² | <ul style="list-style-type: none"> • Time for loss of all PV capacity due to a squall line range is 1.8 min for a 10 km² area and 176 min for a 100 000 km² area • During a 1 min interval 15.9 % of total PV capacity may be lost for a 10 km² area and 2.7 % for a 100 000 km² area |
| Kankiewicz et al. (2010) | Statistical analysis of monitored electricity production | <ul style="list-style-type: none"> • Electricity production from 17 subsystems within one large system • Time resolution from 10 seconds to 60 minutes • Analyzed data from one day (December 13, 2009) | Power step changes | <ul style="list-style-type: none"> • 17 containers (array groupings) of 0.8-1.6 MW_p within one system • Total capacity 25 MW_p • Covers 180 acres of land | <ul style="list-style-type: none"> • 10-sec maximum step changes around 60 % for individual containers, around 5 % for whole 25 MW_p site • 1-min step changes within 40 % of capacity for 1.6 MW_p, within 20 % for 25 MW_p • 10-min and 60-min step changes similar for 1.6 MW_p and 25 MW_p (within 40 %) |
| Kawasaki et al. (2006) | Statistical analysis of monitored radiation data | <ul style="list-style-type: none"> ▪ Global horizontal radiation from 9 sites ▪ 1-min resolution • Four days with different weather types (July and August 1997) | <ul style="list-style-type: none"> • Frequency distribution of fluctuations (Fourier transform) • Magnitude of fluctuations (Wavelet transform) | <ul style="list-style-type: none"> • 9 sites within a 4 × 4 km grid | <ul style="list-style-type: none"> • The largest fluctuations and the largest smoothing naturally appear on days with moving clouds • Clear and rainy days have the lowest fluctuations and the smallest smoothing |

| | | | | | |
|-------------------------|--|---|---|--|---|
| Kern et al. (1989) | Modelling / simulation | <ul style="list-style-type: none"> • Modelled electricity production of 28 aggregated systems, extrapolated with cloud models from 4 monitored systems • 1-s resolution • 10 minutes on one day (September 25, 1987) studied | <ul style="list-style-type: none"> • Average ramps during cloud passage events • Ramp rates per second during these events | <ul style="list-style-type: none"> • 28 systems, each with 2.2 kW_p rated power • Total rated capacity 61.6 kW_p • Spread over a 50 acre area | <ul style="list-style-type: none"> • Average ramps during cloud passage 75 % of total capacity for a single system, 60 % for 28 systems • Average ramp rates during cloud passages 10 % per second for a single system, 3 % per second for 28 systems |
| Lave and Kleissl (2010) | Statistical analysis of monitored radiation data | <ul style="list-style-type: none"> • Global horizontal radiation data of four sites • 5-min resolution • One whole year (2008) | <ul style="list-style-type: none"> • Statistical ramp rate metrics (maximum, mean, standard deviation) • Probability distribution of ramp rates | <ul style="list-style-type: none"> • Four sites • Distances between the sites range from 19 to 197 km | <ul style="list-style-type: none"> • Mean ramp rates are between 6.2 and 9.9 Wm⁻²min⁻¹ for single sites, 5.6 Wm⁻²min⁻¹ for the four sites combined • Maximum ramp rate is between 160.8 and 188.6 Wm⁻²min⁻¹ for single sites, 111.8 Wm⁻²min⁻¹ for the four sites combined |
| Lave et al. (2011) | Statistical analysis of monitored radiation data | <ul style="list-style-type: none"> • Clearness index at six sites • 1-s resolution • Almost one month (July 31 – August 25) | <ul style="list-style-type: none"> • Coherence spectra • Fluctuation power index (power content in fluctuations at each timescale) • Variability ratio for different time scales (reduction in variability with aggregation) | <ul style="list-style-type: none"> • Six sites • Distances between sites up to 3 km | <ul style="list-style-type: none"> • Variability ratio close to the number of sites for timescales shorter than about 4-min • Variability ratio nearly one for timescales longer than 1-h |
| Marcos et al. (2011a) | Statistical analysis of monitored electricity production | <ul style="list-style-type: none"> • Electricity production from 8 individual systems • 1-sec to 10-min resolution considered • One year, May 2008 – April 2009 | <ul style="list-style-type: none"> • Maximum power step changes • 90th percentile of step changes • Distributions of power step changes • Fitted empirical expression for 90th percentile step change as a function of plant size | <ul style="list-style-type: none"> • 8 separate systems with capacities ranging from 48 kW_p to 9.5 MW_p • Land area covered from 0.21 to 52 hectares • Distances between systems from 6 to 60 km | <ul style="list-style-type: none"> • Maximum 1-sec power step change is around 55 % for the smallest system and around 5 % for the largest system • Maximum 10-min step change is between 90 and 100 % for all systems • 90th percentile step change can be described by an exponential decay function with parameters dependent on the time resolution |

| | | | | | |
|-------------------------|---|---|--|--|--|
| Marcos et al. (2011c) | Statistical analysis of monitored electricity production | <ul style="list-style-type: none"> ▪ Electricity production from 7 individual systems ▪ 1-sec to 10-min resolution considered ▪ One year (2009) | <ul style="list-style-type: none"> ▪ Maximum power step changes ▪ 99th percentile of step changes ▪ Distributions of power step changes ▪ Fitted empirical expression for 99th percentile step changes as a function of plant size and number of sufficiently dispersed (uncorrelated) systems | <ul style="list-style-type: none"> ▪ Different combinations of 7 separate systems with capacities from 1 to 9.5 MW_p, 20 MW_p in total ▪ Land areas covered by system from 4.1 to 52 hectares ▪ Distances between 6 of the sites from 6 to 60 km, 7th site 320 km away | <ul style="list-style-type: none"> ▪ Maximum power fluctuations decrease from around 10 % for one system to around 2 % for 6 systems at 1-s time resolution, from 90 % to 50 % at 1-hour resolution ▪ Maximum power fluctuation for individual sites vary with system size from around 70 % for 1 MW_p to 30 % for 9.5 MW_p at 10-s resolution, from around 85 % to 70 % at 60-s ▪ 99th percentile step change can be empirically related to inverse powers of the system size and the number of dispersed systems |
| Mills and Wisser (2010) | Statistical analysis of monitored radiation data | <ul style="list-style-type: none"> ▪ Clear-sky index for 23 sites calculated from global horizontal radiation ▪ 1-min resolution ▪ One year (2004) | <ul style="list-style-type: none"> ▪ Cumulative distribution functions for step changes ▪ Statistical metrics of step changes (maximum, standard deviation, 99.7th percentile) | <ul style="list-style-type: none"> ▪ 23 sites ▪ Distance between sites from 20 to 440 km | <ul style="list-style-type: none"> ▪ Decrease in all statistical metrics with increasing aggregates, e.g. 99.7th percentile drops from 0.58 for one site to 0.19 for 5 sites, and to 0.09 for 23 sites at 1-min resolution ▪ The empirical distribution of step changes is more fat-tailed than a normal distribution but the similarity increases with aggregation |
| Murata et al. (2009) | Statistical analysis of monitored electricity production and radiation data | <ul style="list-style-type: none"> ▪ Electricity production and global horizontal radiation from 52 sites ▪ 1-min resolution ▪ 3 months (May, August, October) | <p>Two fluctuation coefficients based on step changes with different resolutions:</p> <ul style="list-style-type: none"> ▪ Ratio of maximum to standard deviation ▪ Ratio of 99.75th percentile to standard deviation | <ul style="list-style-type: none"> ▪ 52 sites spread over Japan ▪ Rated PV systems capacities from 0.12 to 5.6 kW, 3.2 kW on average | <ul style="list-style-type: none"> ▪ Extrapolated fluctuation coefficients for an infinite number of PV systems in a given region decrease with time resolution, e.g. the ratio of maximum to standard deviation is around 6-7 for 1-min and around 3 for 20-min ▪ The maximum step change from an arbitrary set of systems can be derived from the fluctuation coefficients and an analytical expression of the standard deviation |

| | | | | | |
|--------------------------|--|---|--|---|--|
| Otani et al. (1997) | Statistical analysis of monitored radiation data | <ul style="list-style-type: none"> ▪ Global horizontal radiation from 9 sites ▪ 1-min resolution ▪ One month (October 1996) / one day (May 16, 1996) | <ul style="list-style-type: none"> ▪ Fluctuation factor (rms value of the fluctuations) ▪ Power spectral density | <ul style="list-style-type: none"> ▪ 9 sites within a 4 × 4 km grid | <ul style="list-style-type: none"> ▪ Daily fluctuation factors decrease by 40 % on average over one month and by 87 % at maximum ▪ Power spectral density peaks and average values decrease with aggregation |
| Wiemken et al. (2001) | Statistical analysis of monitored electricity production | <ul style="list-style-type: none"> ▪ Electricity production from 100 systems ▪ 5-min resolution ▪ One year (1995) | <ul style="list-style-type: none"> ▪ Frequency distribution of ramps ▪ Output power distribution | <ul style="list-style-type: none"> ▪ 100 individual 1-5 kW_p systems ▪ 243 kW_p in total ▪ Spread out over Germany, 600 × 750 km² | <ul style="list-style-type: none"> ▪ No ramps above 5 % of total capacity ▪ Power levels below 65 % of total capacity |

